GEOLOGY AND ALTERATION ASSOCIATED WITH THE HAMLIN LAKE VMS SYSTEM, SHEBANDOWAN GREENSTONE BELT, NORTHWESTERN ONTARIO, CANADA

By

Amy Lynn Shute

A thesis submitted in partial fulfillment of
the requirements for the degree of:

Master of Science in Geology

2008
Lakehead University
955 Oliver Road
Thunder Bay, ON
P7B 5E1

ABSTRACT

The Hamlin Lake area is located approximately 120 km southwest of the City of Thunder Bay, Ontario within the Shebandowan greenstone belt of the Wawa Subprovince, Superior Province. The purpose of this study was to understand the relationship between an extensive felsic volcanic rock package and the hydrothermal alteration.

Mapping of the area exposed five major lithologies consisting of mafic metavolcanic rocks, intermediate metavolcanic rocks, felsic metavolcanic rocks, felsic intrusive rocks and iron formation. The felsic metavolcanic rocks vary from rhyolites and banded ash to lapilli tuffs and debris flows, whereas the intermediate metavolcanic rocks are made up of dacites and andesites. The only mafic metavolcanic rocks are the debris flows. The felsic intrusive rocks consist of a quartz-eye porphyry and pink breccia. Primary textures, such as fiamme, can still be observed and which are indicative of a subaqueous environment.

Major and trace element geochemical analyses were undertaken on 200 samples of andesitic to rhyolitic volcanic and volcaniclastic rocks. The major elements have become mobile, whereas the trace elements have remained relatively immobile. Hydrothermal alteration affected the primary textures of the Hamlin Lake area so it was necessary to use trace elements to correctly classify the volcanic rocks. Primitive mantle-normalized (PM) and Zr versus Ti plots were used to separate major suites of rocks and also to determine the tectonic setting. The PM plots showed negative anomalies of the Nb and Ti elements, an indication of a supra-subduction zone setting.

A plot of Zr versus Y was used to establish that the rhyolites and andesites are both of a mildly calc-alkaline affinity and the dacites are strongly calc-alkaline. The VMS classifications of Lesher et al. (1986) and Hart et al. (2004) were used to classify the rhyolites and andesites as FII felsic volcanic rocks, whereas the dacites were classified as FI felsic volcanic rocks. FI felsic volcanic rocks are thought to have originated from a deeper source than the FII felsic volcanic rocks suggesting that the Hamlin Lake volcanic rocks were produced in a mature arc-setting.

Mapping and geochemistry was further supported by analysis of Sm-Nd and oxygen isotopes. Nine samples were analyzed for Sm-Nd isotopes and yielded εNd_{2700} values from -6.59 to +2.62 suggesting some samples had undergone contamination by older material. Several of the samples were close to the value for 2.7 Ga depleted mantle, but one particular sample with a ε_{Nd} value of -6.59 showed that it had been affected by contamination that could only be explained by a contaminant that was much older than the surrounding 2.7 Ga rocks. The source of the contamination is likely the result of continentally derived sediments being subducted into the mantle wedge, because oceanic arcs are not underlain by older continental crust.

Thirty-seven samples were analyzed for O isotopes to recognize alteration patterns in the Hamlin Lake area. The area mapped at Hamlin Lake was not large enough to clearly show an alteration halo, but it does show that the samples at Hamlin Lake have elevated $\delta^{18}O$ values, the result of interaction with low temperature hydrothermal fluids.

ACKNOWLEDGMENTS

<div align="center">

TABLE OF CONTENTS
</div>

List of Appendices

CHAPTER 1

INTRODUCTION

1.1 Introduction

The Hamlin Lake area has been the focus of geological work; including prospecting, exploration and detailed mapping beginning in the early 1950's. MacLeod-Cockshutt Mines discovered several showings in the Shebandowan area in the 1950's, which lead to an increase in prospecting and eventually a revival of exploration in the lower Shebandowan Lake area (Hodgkinson, 1968). Mapping projects have been carried out by Giblin (1964), Hodgkinson (1968), Harris (1970), Osmani (1997) and most recently by Hart (2007). This is the first study of the alteration of any part of the Shebandowan belt using a combination of geochemistry, Sm-Nd isotopes and oxygen isotopes.

1.2 Objective

The purpose of this study was to use field mapping, petrography, whole rock geochemistry, Sm-Nd isotopes and oxygen isotopes to understand the geology, alteration, and tectonic processes that have affected the Hamlin Lake area. A study of the alteration was necessary in order to distinguish the intensely altered volcanic rocks from the least altered volcanic rocks. Although the whole area has undergone alteration and even locally intense alteration, the whole rock geochemistry can be used to determine the original lithologies of the felsic volcanic pile and related rocks. Geochemical patterns of the trace elements can be used to determine the tectonic setting of the area, differentiating between suites of rocks and classifying the units and the VMS system type. With the use of whole rock geochemistry, the least altered and most altered rocks can be distinguished and the field relationships better understood. Sm-Nd radiogenic isotopes have been used to provide a clearer picture of the tectonic and depositional environment in which the felsic volcanic rocks were formed. The final step of this project was to utilize oxygen isotope data to identify alteration boundaries and patterns that exist in the Hamlin Lake area. The overall objective

1

was to produce an alteration model of the study area using field and analytical evidence. This will help guide exploration companies working in the Shebandowan belt to find the next VMS deposit.

1.3 Volcanogenic Massive Sulfide Mineralization

Volcanogenic massive sulfide (VMS) deposits have been an area of intense research during the last 50 years (*see* Hutchinson, 1973; Franklin et al., 1981; Ohmoto, 1996; Franklin et al., 2005). Volcanogenic massive sulfide deposits are described by Franklin et al. (2005) as strata-bound accumulations of sulfide minerals that precipitated at or near the sea-floor in spatial, temporal, and genetic association with contemporaneous volcanism. A VMS deposit can be separated into two main parts: a concordant massive sulfide lens, containing greater than 60% sulfide minerals; and a discordant vein-type sulfide mineralization, commonly called the stringer or stockwork zone (Franklin et al., 2005; Fig. 1.1).

A number of classification schemes have been proposed for VMS deposits. These can be based upon composition (Franklin et al., 1981; Hannington et al., 1999b), geologic setting (Eremin et al., 2000), or host rock composition (Lesher et al., 1986; Barrie et al., 1993; Barrie and Hannington, 1999; Hart et al., 2007). However, in practice each VMS system is unique and often requires a combination of two or more classification schemes.

The discovery of black smokers on the seafloor has not only helped us to understand how metals are precipitated, but also how hydrothermal fluid processes work. New factors have been found to play an important role in the precipitation and deposition of sediments and metals around VMS systems, including the biological life that thrives around these active vent systems (Franklin et al., 2005). With the discovery of active black smokers on the ocean floor, came intense interest from researchers and an increase in the potential for future exploration and metal reserves (Franklin et al., 2005). VMS mining districts lead base metal production, with countless deposits found on almost every continent (*see* Franklin et al., 2005 for a comprehensive summary). Among the best studied deposits are Mount Read, Tasmania (Large et al., 2001;

Crawford et al., 1992), Kidd Creek, Ontario (Beaty and Taylor, 1982; Prior et al., 1999a,b; Hannington et al., 1999) and Bathurst, New Brunswick (Van Staal et al., 1992; Lentz, 1999; Goodfellow et al., 2003). Recently deposits have also been found in Peru and Mexico in Cretaceous settings where VMS deposits are rare (Sherlock and Michaud, 2000; Winter et al., 2004).

The components of a VMS system have been discussed by Ohmoto (1996) and more recently by Franklin et al. (2005). The six elements of a VMS system (Fig. 1.1) are: (1) a heat source to drive the hydrothermal convective system and contribute some metals; (2) a high temperature reaction zone that serves as a reservoir where metals are leached from the surrounding volcanic and
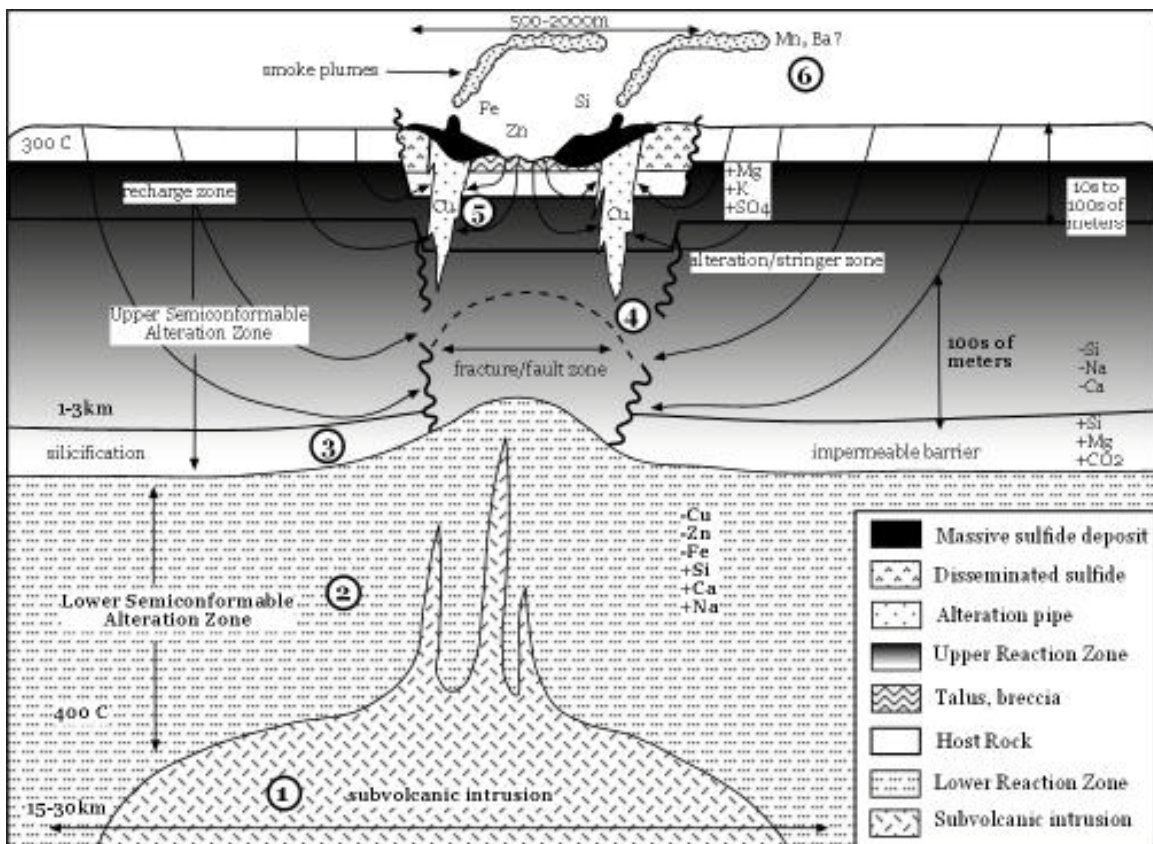
FIGURE 1.1 – A general model of the formation of VMS deposits and how a VMS system works (after Franklin et al., 2005). (1) a heat source to drive the hydrothermal system, (2) a high-temperature reaction zone, (3) synvolcanic faults or fissures to permit discharge of hydrothermal fluids, (4) footwall, and hanging wall alteration zones, (5) the massive sulfide deposit and (6) distal products.

sedimentary rocks via interaction with modified seawater; (3) synvolcanic faults or fissures that allow focused discharge of hydrothermal fluid from the reservoir; (4) footwall and sometimes hanging-wall alteration zones produced by high temperature fluid-rock reaction involving ascending hydrothermal fluids and locally heated seawater; (5) the massive sulfide deposit, formed at or near the sea-floor; (6) distal products, which represent a hydrothermal contribution to background sedimentation.

1.4 Structure of Thesis

The thesis is organized into eight chapters consisting of: (1) introduction, (2) methodology, (3) regional geology, (4) mapping and petrography, (5) whole rock geochemistry, (6) Sm-Nd isotopes, (7) oxygen isotopes and (8) conclusions. The methodology chapter discusses the location and access to the study area and summarizes the sampling procedures and the methods used to analyze the samples. The third chapter briefly discusses the geology of the Superior Province and Wawa Subprovince, and covers the regional geology of the Shebandowan belt. The mapping and petrography chapter outlines the units mapped in the Hamlin Lake area and presents the field observations, followed by petrographic characteristics. The fifth chapter summarizes the whole rock geochemistry and the classification of volcanic units using major and trace element geochemistry. The Sm-Nd isotope data was interpreted to identify the tectonic environment in which the Hamlin Lake volcanic sequence was formed, whereas the oxygen isotopic data was used to identify the regional alteration patterns. The conclusion discusses the overall relationships seen between field mapping, geochemistry and isotopes and presents a model for a supra-subduction arc formation in the Hamlin Lake area.

CHAPTER 2

METHODOLOGY

2.1 Location and Access

The study area is located approximately 160 km west of the City of Thunder Bay, Ontario (Fig. 2.1). Road access from Thunder Bay begins with a 110 km drive west on Hwy 11 to the community of Kashabowie, followed by a 50 km drive south on Swamp Road, where the study area can then be accessed by ATV or on foot. The study area is approximately 6 km² with the majority of the outcrops located in a previously logged area, making access and exposure ideal.

The well-exposed felsic to intermediate metavolcanic rocks of the Hamlin Lake area are elongated in a northwest-southeast fashion with an overall oval shape and low-lying topography. The outcrops are low-lying with the mafic debris flows forming the highest ridges in the area. The majority of the trees have been logged, exposing the outcrops. The low lying swampy areas were originally filled with black spruce stands, but were the focus of logging in the 90's leaving only small groupings of black spruce remaining. Areas that escaped being cut host trembling aspen, white birch, balsam spruce, and white and red pine, which are sparse. Grasses and saplings now cover the cut areas, however jack pine have been planted within the last ten years by a reforestation company, with the trees currently at about waist height. Black bears frequent the area, as well as red fox and a variety of song birds.

2.2 Sampling Procedures and Locations

The main objective when sampling was to collect a set of samples that represented the lithologies of the exposed outcrops. Weathered surfaces were removed in the field, 50% of the sample was sent for geochemical analysis and the remainder kept for future reference.

FIGURE 2.1 – Map showing the Shebandowan area relative to the City of Thunder Bay.

All 200 samples collected in the field were submitted for whole rock geochemical analysis. This was carried out in Thunder Bay, Ontario at the ALS Chemex Labs. Hand specimens that were of either textural or geochemical significance were brought to the Lakehead University lapidary facility to make petrographic thin sections. Sixty samples were thin sectioned in all. A representative subset of samples was chosen for Sm-Nd and oxygen isotopes on the basis of their location in the field and geochemistry. The Sm-Nd isotopic work was undertaken at the Isotope Geochemistry and Geochronology Research Centre (IGGRC) in Ottawa, Ontario, while the oxygen isotope samples were sent to the Queen's Facility for Isotope Research in Kingston, Ontario.

2.3 Analytical Methods
2.3.1 ICP-MS and XRF

The whole rock analysis of all 200 samples used during this study was performed at the ALS Chemex Lab located in Thunder Bay, Ontario. The sample was first weighed, dried and finely crushed to better than 70% passing a 2.0 mm

screen. A split of 250g was taken from this and then pulverized in a tungsten carbide ring pulverizer to better than 85% passing a 75 micron screen (www.alsglobal.com). Quality control was very important during the process and samples were prepared using a comprehensive dust control collection system while crushing and grinding to prevent cross contamination (www.alsglobal.com). Glass disks were prepared for each sample before using Wavelength Dispersive X-Ray Fluorescence Spectroscopy (XRF) to determine the major elements to an error of 0.01% expressed as oxides. The glass disks were prepared by first fusing the sample using lithium borate fusion in an automated fashion using a Claisse-type fluxer, and then the melt was poured into a mould and cooled to yield a solid glass disk (www.alsglobal.com). The disks were then analyzed using XRF and the elements determined by comparison with standard reference materials. The standards and blanks used during analysis by ALS Chemex were regulated and quality control samples become part of a separate database that was used for quality assessment by ALS Chemex. In each set of samples submitted every tenth analysis was duplicated for accuracy and precision. Standard deviations are within 5%, loss on ignition (LOI) ranged from 0.27 to 7.83% and totals for all samples did not vary more than 1.85% from 100%.

The trace elements were analyzed using lithium meta-borate fusion, after they underwent nitric acid digestion. Samples later underwent Inductively Coupled Plasma-Mass Spectroscopy (ICP-MS) to determine their concentrations. The same quality control and processes were used for the ICP-MS as the XRF analyses. The detection limits vary for different trace elements, but are between 0.5-5 ppm.

2.3.2 Sm-Nd Procedure

Least altered samples were chosen for Sm-Nd isotope analysis in order to cover a representative suite of rocks for the sample area. The nine samples were crushed at the Lakehead University Lapidary Facility until they were 2 to 3 mm in diameter using a tungsten carbide mallet. The crushing area and devices were thoroughly cleaned between each sample. The crushed sample was then further pulverized in an agate rotary mill which reduces the sample to approximately

75μm in diameter. Analyses were carried out at Carleton University in Ottawa, Ontario at the Isotope Geochemistry and Geochronology Research Centre (IGGRC) using a ThermoFinnigan TRITON T1 Thermal Ionization Mass Spectrometer (TIMS) and a Finnigan MAT 261 Thermal Ionization Mass Spectrometer. Between 100 and 300 mg of sample powder were weighed into a screw-cap Teflon vial and a ^{148}Nd-^{149}Sm spike was added. This mixture was then dissolved in HNO_3-HF and then in HNO_3 and HCl until absolutely no residue was left. Samarium and neodymium were then separated using a standard cation exchange technique (Cousens, 1996). The REE-bearing residue was dissolved in 0.26N HCl and loaded into a 10 ml borosilicate glass chromatographic column containing a 2 cm high bed of Teflon powder coated with HDEHP di(2-ethylhexyl) orthophosphoric acid (Richards et al., 1976). Samples were loaded with 0.3N H_3PO_4 on one side of a Re filament assembly, and then run at temperatures of 1750-1800°C in a 9-cup ThermoFinnigan TRITON T1 multicollector mass spectrometer.

Total procedural blanks for Nd are <200 pg and concentrations are precise to ± 1%. The La Jolla standard was run by the IGGRC regularly to ensure accuracy and precision of the preparation process. The ratios were then normalized to ^{146}Nd/^{144}Nd = 0.72190 (Cousens, 1996). Initial ε_{Nd}^T values for volcanic rocks were calculated at 2700 Ma. The 2σ uncertainty in the ^{146}Nd/^{144}Nd values is ±0.000002 to 0.000008. Epsilon values at time T were calculated using the following relation:

$$\varepsilon_{Nd}^T = [(^{143}Nd/^{144}Nd_{sample}^T/^{143}Nd/^{144}Nd_{CHUR}^T)-1]*10000$$

where CHUR is the Chrondrite Uniform Reservoir and T is generally the time the rock was formed. Depleted mantle model ages were calculated assuming a modern upper mantle with ^{148}Sm/^{144}Nd = 0.214 and ^{143}Nd/^{144}Nd = 0.513115.

2.3.3 Oxygen Isotopes

The 37 oxygen isotope samples were analyzed at the Queen's Facility for Isotope Research (QFIR) in Kingston, Ontario. Samples were chosen based on

their field locations and lithology. Whole rock samples were pulverized to 75μm following the same procedure as for the Sm-Nd samples at the Lakehead University Lapidary Facility. Oxygen was then extracted from bulk rock powder using bromine pentafluoride (BrF_5) following the methods of Clayton and Mayeda (1963) at Queen's University. Fluorination of both oxides and silicates was carried out at 600-650°C for 15 hours. Oxygen was converted to CO_2 by reaction with a hot graphite rod. The CO_2 gas was analyzed with a Finnigan MAT 252 gas source mass spectrometer.

Isotopic compositions were reported in δ-notation, as deviations in per mil (‰) relative to Vienna Standard Mean Ocean Water (V-SMOW). Replicate analyses of the White Crystal in house standard (accepted value of 16.7 μmoles of CO_2/mg with a $\delta^{18}O$ (V-SMOW) value of 9.7‰) was calibrated to the international standards. Reproducibility of values based on replicate analyses of the White Crystal standard is ±0.2‰ (1σ).

CHAPTER 3

REGIONAL GEOLOGY

3.1 Superior Province

The Superior Province is the largest and most studied Archean craton in the world with an area of 1 572 000 km^2 (Thurston, 1991; Fig. 3.1). Often called the Canadian Shield, the Superior Province has been described as being a dome-like structure of Precambrian age bedrock with a gently undulating surface which dips to the north and south (Bally, 1989), isolated from other neighbouring Archean cratons by the Proterozoic orogens that surrounded it (Fig. 3.1). Card and Ciesielski (1986) proposed the subdivision of the Superior Province into provinces and since then the subdivisions have been widely accepted (Fig. 3.2). Recently, with an increasing understanding that the tectonic assembly of the Superior Province took place through a progression of orogenies, supported by geochronological and isotopic data, Stott et al. (2007) has proposed that new boundaries, individual terranes and associated domains can be identified.

The Superior Province is subdivided into subprovinces which are fault-bounded, medium-to-large scale regions characterized by similar rock types, structural style, isotopic age, metamorphic grade, geophysics and mineral deposits (Thurston, 1991). The subprovinces are separated not only by plutonic, volcanic and sedimentary sequences, but also by age boundaries and strong structural differences. The subprovinces include plutonic, volcanic-plutonic, high-grade gneissic and metasedimentary rocks ranging in age from 3.0-2.65 Ga (Thurston et al., 1991; Fig. 3.1) and it is thought that the assembly of the subprovinces was diachronous from north to south (Card and Ciesielski, 1986; Williams, 1990). Stott et al. (2007) have combined some subprovinces such as the Wawa-Abitibi belts into one terrane. A terrane is a fault-bounded package of stata that is allochthonous to, and has a geological history distinct from, the adjoining geologic units (Howell, 1986). The Wawa and Abitibi belts have been proposed to have once been one continuous belt (Williams et al., 1991). Lithologies found in the subprovinces can
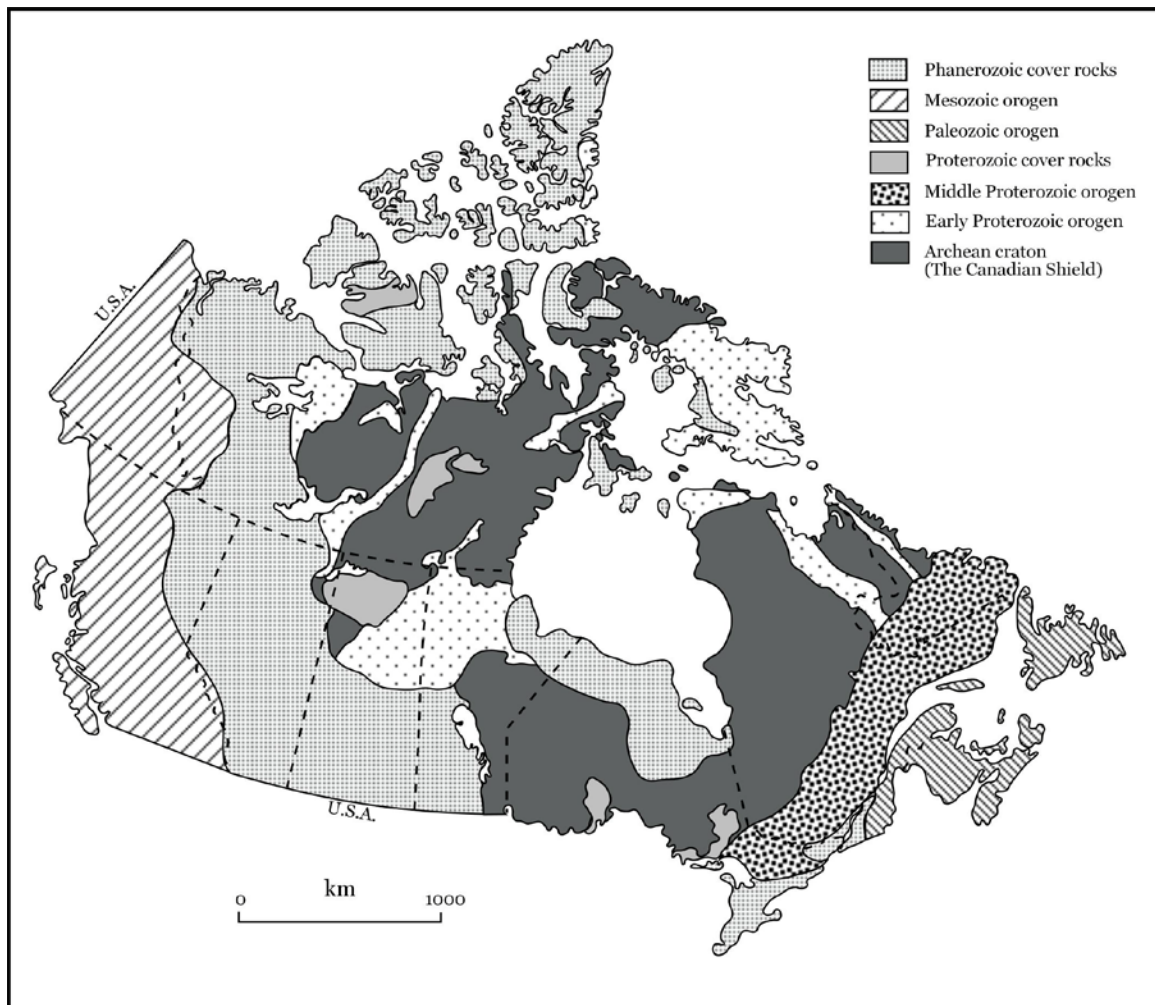
FIGURE 3.1 – A geological map of Canada showing the orogens, the Archean craton known as the Canadian Shield and the cover rocks (*modified after* Williams et al., 1991).

vary from granites, tonalite-trondhjemite-granodiorite (TTG) suites, to komatiites, basalts, rhyolites and iron formations with tectonic environments ranging from volcanic arcs, continental arcs, back arcs, plateau basalts and ocean-island basalts (Thurston et al., 1991; Hollings et al., 1999; Whalen et al., 2002; Polat and Kerrich, 2001).

Archean greenstone belts of the Superior Province are thought to have amalgamated through subduction-accretion processes comparable to those of Phanerozoic convergent margin tectonics (Hoffman, 1991). Many Archean granite-greenstone terranes are interpreted as juvenile island arc sequences that
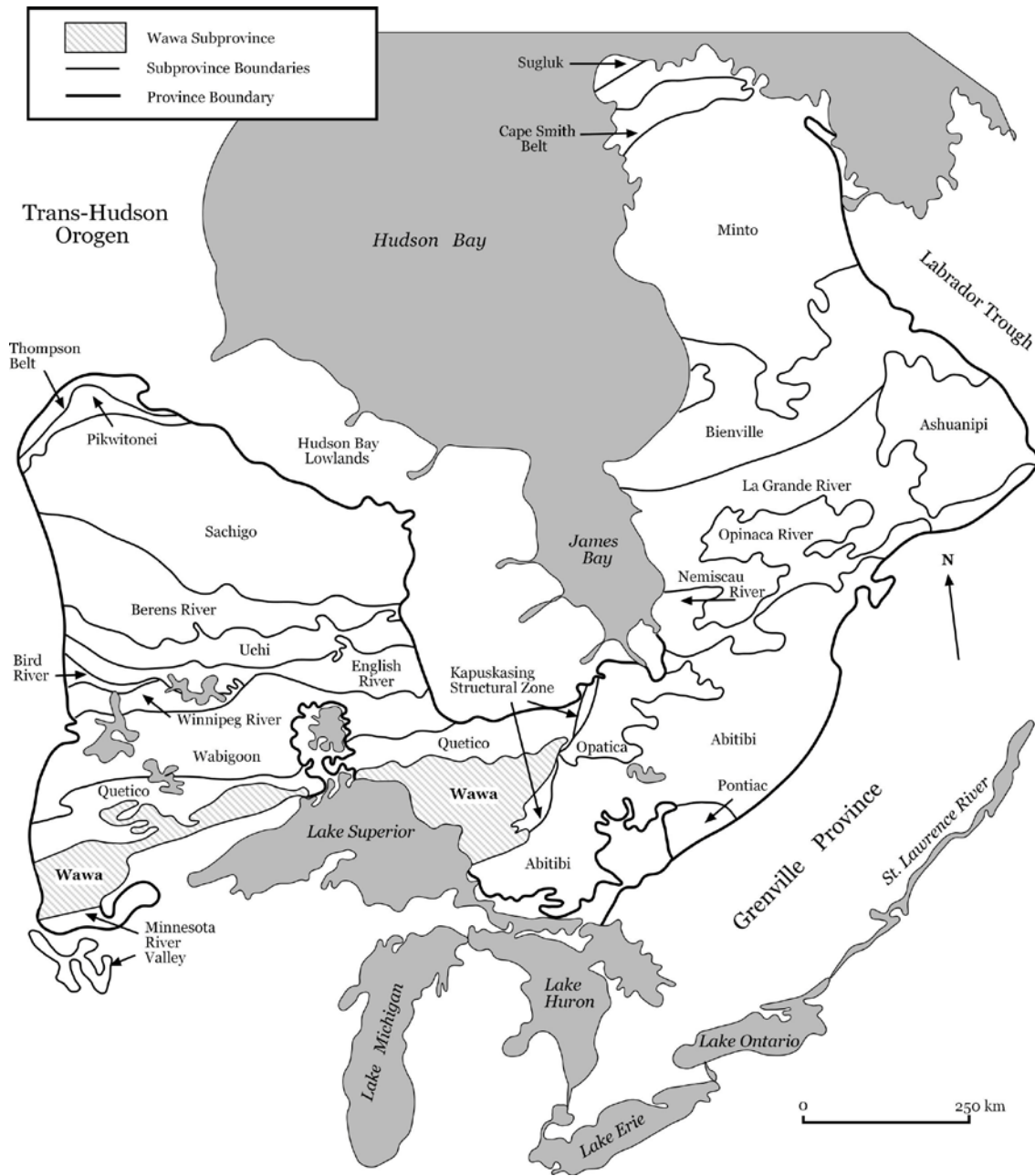
FIGURE 3.2 – A map of the Superior Province showing the subprovinces (*after* Card and Ciesielski, 1986).

grew above subduction zones, matured, then amalgamated during collisional orogenesis forming new continental crust of oceanic arcs and plateaux (Kusky and Polat, 1999; Percival et al., 2001). However, new evidence has been introduced supporting a vertical tectonic model (Bédard et al., 2003). Vertical tectonic models were introduced because of the overall lack of structural repetitions in accretionary sequences (Bédard et al., 2003), but the debate continues.

3.2 Wawa Subprovince

The Wawa Subprovince comprises Archean greenstone belts and granitoid plutons. The subprovince boundary to the north is in contact with the Quetico Subprovince, whereas the southern boundary is separated from the Marquette greenstone belt and Minnesota River Valley gneiss terrane by the Great Lakes Structural Zone in the east (Williams et al., 1991). In the west, the Wawa Subprovince is in contact with the Montreal River fault and is hidden beneath Lake Superior and the Animikie Basin in the central portion of the subprovince. The Wawa Subprovince as a whole extends from the Kapuskasing Structural Zone in the east to the Proterozoic Trans-Hudson Orogen in the west (Williams et al., 1991, Fig. 3.1).

The Wawa Subprovince and neighbouring Abitibi Subprovince are thought to have once been continuous (Williams et al., 1991). The greenstones belts which they contain are composed of metamorphosed volcanic and sedimentary rocks and are separated by belt-like domains of tonalite-trondhjemite-granodiorite (TTG) plutons (Williams et al., 1991). The relationships between the volcanic and sedimentary rocks are usually unclear and interrupted by shearing (Williams et al., 1991). The Wawa Subprovince is composed of two linear concentrations of greenstone belts separated by belt-like domains of plutonic rocks. The first is located in the northern part along the Quetico Subprovince border and includes the Shebandowan greenstone belt, while the second is the Mishibishu-Michipicoten-Gamitagama area (Fig. 3.3). Williams et al. (1991) proposed that the last three stages of supracrustal development took place in the Wawa Subprovince characterized by bimodal magmatism at approximately 2.90,

2.75 and 2.70 Ga, suggesting that there must have been numerous geodynamic events involved in the evolution of the Subprovince. The granitoid plutonic rocks surround the greenstone belts and also occur as intrusions within them. They are not well studied, but Williams et al. (1991) proposed that the tonalitic rocks may be synvolcanic to the greenstone assemblages of the Wawa Subprovince. Most stratigraphic relations have been disrupted, but in general komatiites and associated tholeiitic basalts occur at the base of the volcanic sequences therefore tholeiitic and calc-alkaline basalts, andesites, dacites and rhyolites are more often found at the upper stratigraphic levels (Williams et al., 1991). Relationships between assemblages and greenstone belts suggest that the greenstone belts within the Wawa Subprovince were assembled prior to the assemblage of the subprovinces of the Superior Province (Williams et al., 1991).

3.3 Shebandowan Greenstone Belt

The greenstone belts of the western most part of the Wawa Subprovince extend from Lake Superior to Minnesota. Two greenstone belts make up the western portion of the Wawa Subprovince; the Shebandowan and Saganagons greenstone belts (Fig. 3.3). The Shebandowan greenstone belt is located in the southwest portion of the Wawa Subprovince with the Saganagons greenstone belt connecting to the northeast (Fig. 3.3). It has been proposed that these two
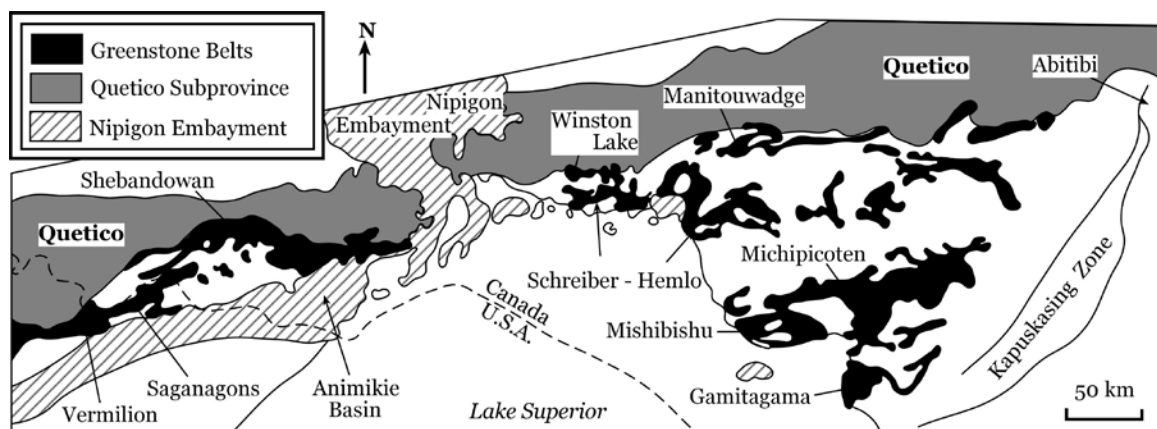
FIGURE 3.3 – A map showing the distribution of greenstone belts within the Wawa Subprovince (*after* Corfu and Stott, 1998).
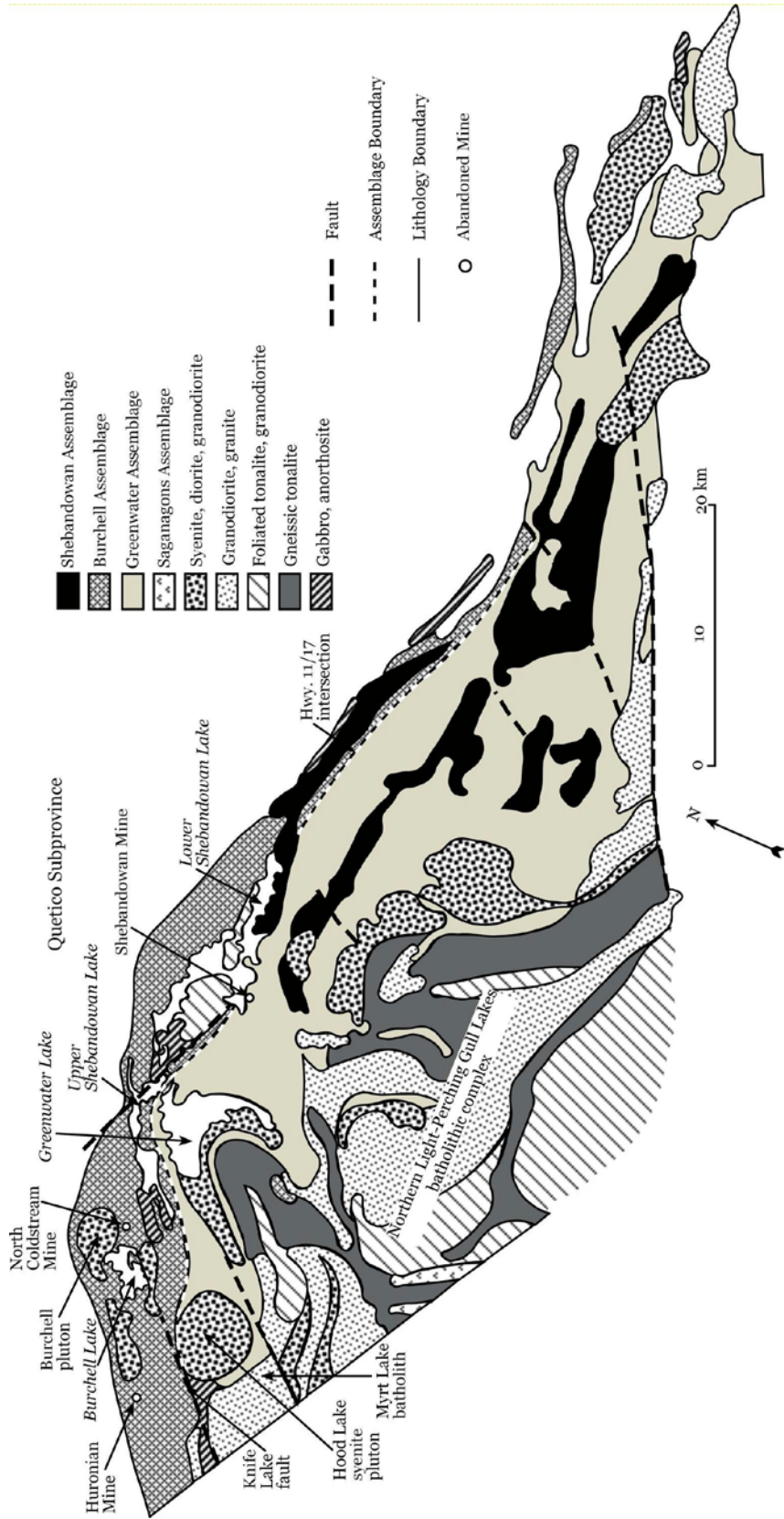
FIGURE 3.4 – A geological map showing the different lithologies, faults and abandoned mine sites of the eastern part of the Shebandowan Greenstone Belt. The Shebandowan assemblage consists of metasedimentary and lesser metavolcanic rocks, whereas the Saganagons assemblage consists dominantly of basaltic metavolcanic rocks. The Greenwater and Burchell assemblages both consist of arc-type metavolcanic rocks (*modified from* Williams et al., 1991).

15

greenstone belts may have been continuous at one point (Williams et al., 1991). The Shebandowan belt (Fig. 3.4) borders the Quetico Subprovince to the north and the Northern Light-Perching Gull Lakes batholitic complex (NLPG) to the south and is a 2.77 to 2.75 Ga metavolcanic assemblage with metasedimentary packages and numerous intrusions; including the Hood Lake pluton, Myrt Lake batholith and Burchell pluton (Williams et al., 1991).

Williams et al. (1991) divided the Shebandowan greenstone belt into three assemblages (Williams et al., 1991). The older Greenwater and Burchell assemblages, which oppositely face each other, are thought by Williams et al. (1991) to be separated by a fault, and the younger Shebandowan assemblage overlaps the other two older assemblages (Fig. 3.5). The contact between the Burchell and Greenwater assemblages can be found immediately south of Upper and Lower Shebandowan Lakes (Fig. 3.4). The older metavolcanic Burchell assemblage to the north consists of three northward younging cycles; the Greenwater assemblage has three southward facing cycles; and the Shebandowan assemblage straddles the two older assemblages and consists of volcanic and sedimentary rocks (Williams et al., 1991; Fig. 3.3). Each of the volcanic cycles typically consists of a lower sequence of tholeiitic basalt flows and an uppermost sequence of calc-alkaline andesite, dacite and rhyolite. Some of the stratigraphically lower sequences only preserve the basaltic portion (Williams et al., 1991). More recently, Corfu and Stott (1998) reevaluated the Shebandowan greenstone belt and reclassified the assemblages into three new subdivisions. The first subdivision incorporates the Burchell and the Greenwater assemblages because they are indistinguishable in terms of age (2720 Ma) and are consistent in younging directions. However, the northern part of the Burchell assemblage is separated into the Kashabowie assemblage (2695 Ma) and includes the 'Timiskaming-type' rocks that Williams et al. (1991) first described as being in the overlying Shebandowan assemblage. The third youngest subdivision is the Auto Road assemblage, a small sedimentary basin in the northeastern part of the area.

Corfu and Stott (1986) described two main deformation events in the Shebandowan greenstone belt. The D_1 deformation produced a vertical schistosity with west-southwest plunging mineral lineations, upright folds and

apparently affected the entire Shebandowan greenstone belt. The D_2 deformation only affected the northern half of the belt and crosses into the Quetico Subprovince. Corfu and Stott (1986) proposed that the D_2 deformation was caused by a major, oblique, subhorizontal compression along a northwest-southeast axis and is thought to be related to the closing of the Quetico sedimentary basin. More recently, Williams et al. (1991) recognized three deformational episodes in the Shebandowan greenstone belt. The D_1 deformation is preserved over the majority of the belt and consists of a westerly plunging lineation with a vertical northward dipping schistosity; while the second deformation, D_2, overprints the first deformation in parts of the belt. The first two deformations share a common schistosity, but D_1 lineations plunge to the west, whereas D_2 lineations plunge to the east. The D_2 deformation also produced brittle-ductile shear zones, which are seen in most areas across the belt and are thought to be related to the gold mineralization in the area (Stott and Schnieders, 1983). The third and last deformation, D_3, generated steeply plunging kink folds and is more commonly seen in the northern portion of the belt (Williams et al., 1991).

The belt is cut by several major faults that have affected parts of the Shebandowan greenstone belt. The faults are northeast and northwest striking and are interpreted to be the result of crustal shortening (Williams et al., 1991). The closest major fault affecting the study area is the Knife Lake Fault, which strikes northeast (Fig. 3.6). Harris (1970) observed that the 60 mile long fault follows the contact between the granite and the metavolcanic rocks north and south of the fault in the Hamlin Lake area.

The metamorphic events that affected that area have resulted in metamorphic grades from greenschist to lower amphibolite facies (Williams et al., 1991). Greenschist facies metamorphism is found throughout the belt with zones of amphibolite facies associated with the late to post-tectonic felsic plutons (Williams et al., 1991).

The Hamlin Lake area is located south-southwest of Moss Lake (Fig. 3.6). Hamlin Lake is the defining landmark in the area and is surrounded by mafic to

felsic metavolcanic rocks to the north and the Powell Lake granite and Myrt Lake batholith in the south.

3.4 *Previous Work*

Hodgkinson (1968) noted that the Shebandowan area first received attention when people using the Old Dawson route to western Canada, which passed through Shebandowan and Kashabowie Lakes, recognized the unique geology of the area. The earliest geological report was written by W. McInnes (1897) in a report for the Geological Survey of Canada. Soon after, gold and iron
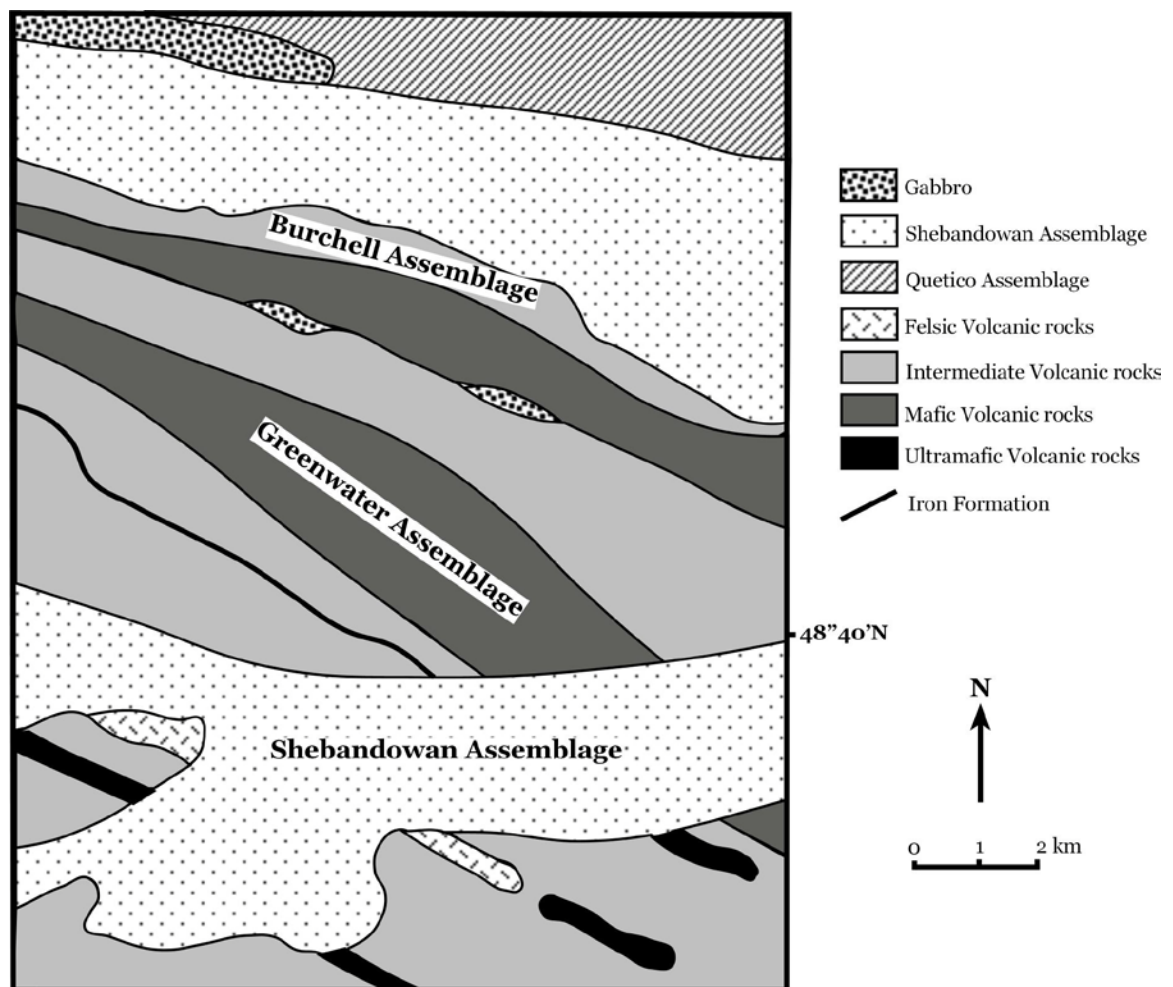
FIGURE 3.5 – A geological map showing the intertwining relationships between the Burchell and Greenwater assemblages in a small area of the Shebandowan greenstone belt and how the Shebandowan assemblage overlies parts of the Greenwater Assemblage (*modified after* Williams et al., 1991).

deposits were reported by prospectors and the Shebandowan area became an area of even more geological interest.

Giblin (1964) mapped the Burchell Lake Area and produced the Burchell Lake Area map (map 2036) (Fig. 3.7). The greywacke and arkose metasediment rocks mapped in the north belong to the Quetico Subprovince and mark the boundary between the Quetico Subprovince to the north and the Wawa leucogranite, biotite granite, hornblende granite and muscovite granite (Giblin, 1964). A few smaller intrusions of syenite were also recognized including leucosyenite, biotite syenite and hornblende syenite. There are mafic intrusions in the area including gabbro, diorite and lamprophyre dikes.
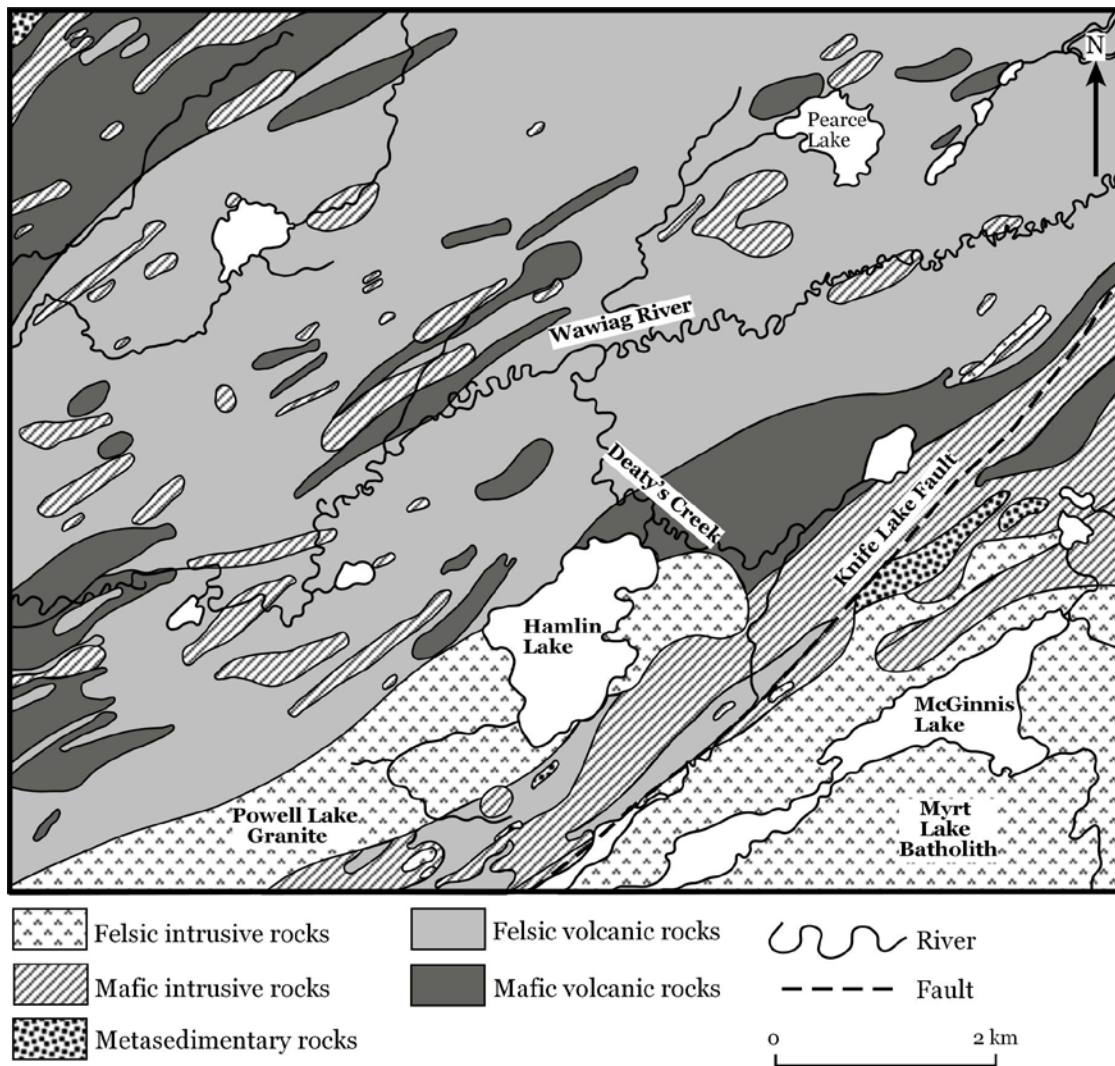
FIGURE 3.6 – A portion of Harris's (1970) geological map of the area surrounding Hamlin Lake.

The suite of northwest striking metavolcanic rocks present in Giblin's (1964) mapping area strike northwest from the Wawiag River through Burchell Lake and northwest beyond the mapping area (Fig. 3.7). The area contains felsic and mafic metavolcanic rocks, but rhyolite is the most common rock found in the area, with lesser amounts of rhyolitic breccia, sericite schist, porphyritic rhyolite and rhyolite tuff also found (Giblin, 1964). Giblin (1964) observed that the rhyolites were aphanitic with some containing quartz and feldspar phenocrysts. Giblin (1964) observed varying colours in the rhyolites from light beige, grey and even shades of pink and green.

The mafic metavolcanic rocks are described as an assortment of amphibolite schists, chlorite schists, agglomerates, tuffs and pillow lavas (Giblin, 1964). The mafic rocks crop out mostly as chlorite schists as a result of greenschist metamorphism. Giblin (1964) also noted an agglomerate unit found near Hwy. 11 on the north shore of the Upper Shebandowan Lake which contained felsic and mafic fragments in a schistose matrix, but it was noted that felsic fragments dominated. These fragments are lenticular and exhibited a "pinch and swell" structure with a maximum length of 20 inches. Giblin (1964) observed deformed and sheared pillow lavas while mapping as well, but it was impossible to determine way-up directions on all the pillow lavas observed.

Giblin (1964) recognized some folding in the area, but regional metamorphism obscured most of the fold patterns causing a lack of field structures. He suggested that the main rhyolite band running from the southwest to the northeast is the core of an anticline. However, there are problems with this interpretation as although there are several outcrops of pillow lavas with north facing exposure, there is only one outcrop of south facing exposure.

Hodgkinson (1968) mapped the Kashabowie area and produced two maps, the Greenwater Lake Sheet (map 2127) and Kashabowie Sheet (map 2128; Fig. 3.7). The Greenwater Lake map covers a lot of the granite around Greenwater Lake, whereas to the east is a mix of amphibolite and amphibolite schist intruded by long, narrow dikes of gabbro. The Kashabowie Sheet covers the Upper and Middle Shebandowan Lakes area encompassing similar geology to Giblin (1964). The map overlaps Giblin's (1964) work and extends to the northeast of his
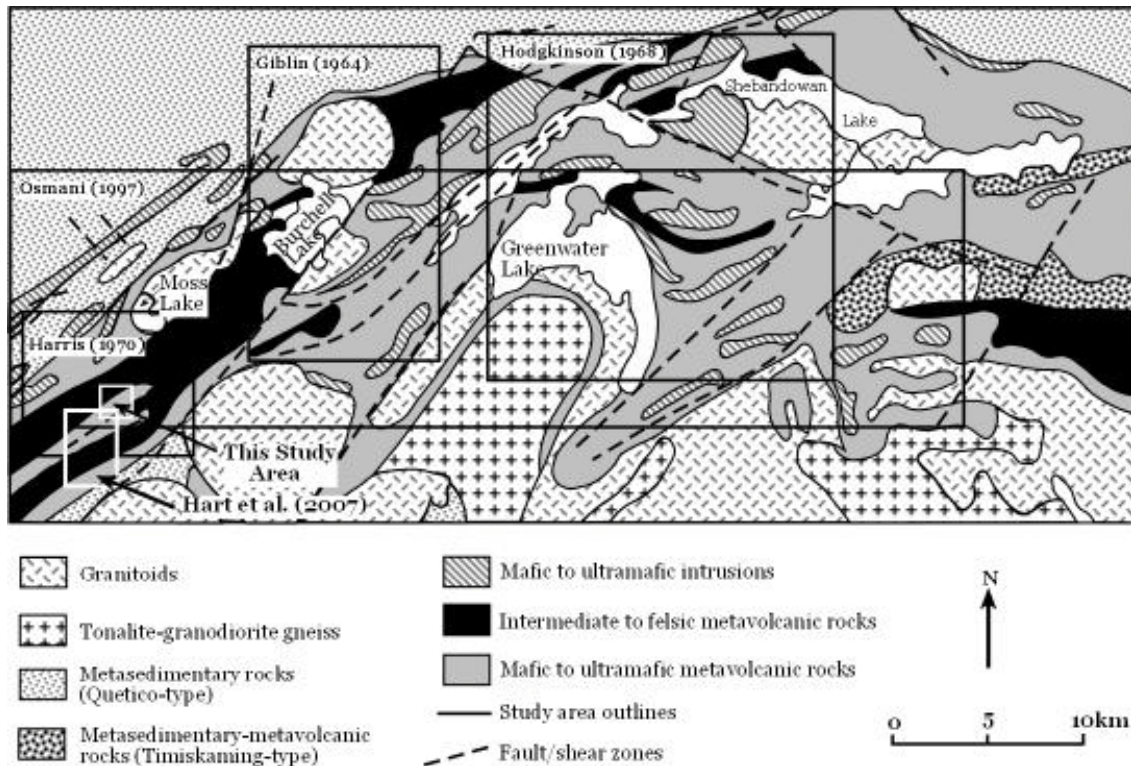
FIGURE 3.7 – A geological map showing locations of previous mapping efforts in the Shebandowan area (*after* Osmani, 1997).

mapping area where the felsic and mafic metavolcanic package continues (Fig. 3.7). The felsic and mafic units are similar to those in Giblin's (1964) mapping area with the only difference being that there are more mafic volcanic rocks in Hodgkinson's mapping area. The metavolcanic rocks are also intruded by mafic and felsic intrusive rocks and the thick belt of metasedimentary rocks from Giblin (1964) continues into this mapping area as well. The Greenwater Lake sheet is geologically similar to the Kashabowie Sheet excluding the biotite granite that surrounds Greenwater Lake and the long, slender gabbro and peridotite intrusions present in the area.

Hodgkinson (1968) mapped several felsic volcanic units including: rhyolite, sericite schist, dacite, tuff, agglomerate and even pillow lavas. Sericite schist is common where the pillowed lavas are found. The colour of the felsic volcanic rocks weathered surfaces are white to light-cream with fresh surfaces being grey, green, pink, or light-cream (Hodgkinson, 1968). The agglomerate and tuff were frequently observed and were well exposed on the shores of Middle

Shebandowan Lake (Hodgkinson, 1968). The fragments of the agglomerate are elongated with lengths of up to 20 cm and have a matrix almost entirely of sericite. The rhyolite is altered to sericite schist in most exposures and Hodgkinson (1968) observed that some of the rhyolites have a SiO_2 content of only 60 wt.%, causing him to reclassify them as andesites. Hodgkinson (1968) concluded that the felsic volcanic rocks in the area are found as long and narrow pyroclastic bands that he interpreted to be Pelean-type avalanche deposits.

Mafic volcanic rocks consist of amphibolite schist, chlorite schist, porphyritic mafic flows, agglomerate, pillow lavas and tuffs. Amphibolite schists dominated the mapping area of Hodgkinson (1968) and metamorphism affected the rocks with changes in metamorphic grade visible over the mapping area (Hodgkinson, 1968). In the southeast of the mapping area the mafic volcanic rocks contain chlorite and pale amphibole, but to the north they are richer in hornblende possibly because of the granite intrusion in the northern portion of the mapping area (Hodgkinson, 1968). The amphibolites in the southeast are distinctive because they are medium-grained and greenish in colour. The darker the green, the more hornblende-rich the rock, while the paler the green the more chlorite-rich the rock (Hodgkinson, 1968). The mafic flows are fine-grained and porphyritic and some have well-developed pillow structures still preserved at surface. Mafic tuff and agglomerate units were found in the mapping area; the agglomerate contains pink, intermediate fragments in a mafic matrix. Hodgkinson (1968) interpreted the brecciated agglomerate to be the result of different magma types extruding simultaneously from the same volcanic centres.

Metasedimentary rocks mapped by Hodgkinson (1968) consist of greywacke and arkose similar to those mapped by Giblin (1964) and are altered to schist (Hodgkinson, 1968). Banded iron formation was mapped in many places amongst the metavolcanic rocks in zones up to 30m wide and 910m long (Hodgkinson, 1968).

The main structural feature in Hodgkinson's (1968) map area is the Postans Fault, which separates the metasedimentary rocks of the Quetico Subprovince from the metavolcanic rocks of the Wawa Subprovince. The

schistosity of the area is approximately N65°E and the few top determinations indicate a south facing sequence.

Harris (1970) mapped part of the Shebandowan Belt overlapping this study area, and produced the Tilly Lake (map 2203) and Powell Lake Sheets (map 2204; Fig. 3.7). The Tilly Lake Sheet covers granite and syenite intrusions, along with a metavolcanic belt separating the two and a small portion of the metavolcanic rocks in the southeast. The Powell Lake map (2204) extends from Moss Lake in the north to Greenwood Lake in the south, and from Clay Lake in the west to east of McGinnis Lake (Fig. 3.7). In the northwest corner of the Powell Lake map, the same metasedimentary rocks mapped by Giblin (1964) and Hodgkinson (1968) are present and the large Myrt Lake Batholith covers the southeast portion of the mapping area. The Myrt Lake Batholith and the metasedimentary rocks are separated by the northeast striking unit of mafic and felsic volcanic rocks that pass through Moss Lake and Snodgrass Lake and are part of the same metavolcanic package of rocks that Giblin (1964) and Hodgkinson (1968) mapped. This same package of metavolcanic rocks is intruded by the Powell Lake Granite (Fig. 3.6), which is thought to have provided the heat and energy for the mineralization found in the area (Harris, 1970). Harris (1970) describes the felsic metavolcanic unit as being concentrated in the central region of the belt and includes massive rhyolite, porphyritic rhyolite, banded rhyolite, tuff, agglomerate, breccia and sericite schist. Harris (1970) observed that the most abundant unit is a dacitic crystal tuff, which contains 20-50% white, subhedral plagioclase crystals and 5-10% rounded quartz crystals. The quartz phenocrysts vary in abundance and size throughout the metavolcanic rock. The matrix is aphanitic and light grey to dark grey on fresh surfaces, but white to light grey on weathered surfaces. The felsic agglomerate that Harris (1970) observed is different than Giblin's (1964) and Hodgkinson's (1968) mapping observations because it is associated with the dacitic crystal tuff and the agglomerate displays considerable variation of fragment size and an aphanitic matrix. Thin sections were reported to have quartz and altered plagioclase phenocrysts with the groundmass being a mixture of quartz, white mica, chlorite and small amounts of biotite (Harris, 1970). Harris (1970) also noted that

besides a well formed foliation, there are also lenses of coarser grained groundmass thought to represent rock fragments or devitrified pumice fragments. The more massive rhyolite is very hard with colours ranging from white to light green, with aphanitic sericite schist and grey-green schist with chlorite concentrated along the foliation (Harris, 1970).

The mafic metavolcanic rocks are composed of massive lava, tuff, agglomerate, pillowed lava, vesicular to amygdaloidal lava, chlorite schist, and plagioclase-hornblende schist (Harris, 1970). These are located mostly along contacts with the intrusions (Fig. 3.6). The most abundant unit is aphanitic basalt to dacite (Harris, 1970). The massive basalt is soft and green to brown on surface. On average the basalts contain up to 10% chlorite, are foliated and even contain up to 10% blue quartz eyes, interpreted to be the result of silicification (Harris, 1970). In thin section, chlorite, epidote, amphibole, altered plagioclase, calcite and quartz are the most common minerals recognized (Harris, 1970). The second most abundant unit is the agglomerate. Harris (1970) describes this unit as containing felsic fragments of irregular shape set in a mafic matrix. On the weathered surface the clasts are white and stand out from the much darker matrix, the fragments can be as long as 30 cm and make up 15-25% of the rock (Harris, 1970). Harris (1970) also describes some of the fragments as being rhyolitic.

The mafic intrusive units mapped by Harris (1970) consist of peridotite, diorite, gabbro and amphibolite. The mafic intrusive rocks are located along the borders of the granitic intrusions, and are also found sporadically intruding the metavolcanic rocks throughout the mapping area (Harris, 1970; Fig. 3.6). The contact between the mafic intrusions and the granitic Myrt Lake Batholith (MLB) falls on the Knife Lake Fault. The MLB is massive biotite granite and is medium to fine-grained, while the Powell Lake Granite is exposed in the centre of the metavolcanic rocks and is also medium-grained, pink and contains biotite and chlorite (Harris, 1970). The metasedimentary rocks range from greywacke to migmatites and are part of the same metasedimentary rock package mapped by Giblin (1964) and Hodgkinson (1968).

A more recent mapping project involving the Shebandowan greenstone belt was undertaken by Osmani in 1997 (Fig. 3.7). Osmani's (1997) work ended approximately 2 km north of this mapping project. The volcanic rocks mapped by Osmani (1997) are important to this study because they are part of the same volcanic package that was mapped in the Hamlin Lake area for this study. Osmani (1997) published the Burchell-Greenwater Lakes Area (West Half; map 2622) and Moss Township (map 2624). Osmani (1997) mapped a large portion of the volcanic sequence located near Moss Lake (Fig. 3.7). The Burchell-Greenwater Lakes area covers parts of the same mapping project that Giblin (1964) mapped, but it also extends from Burchell Lake in the west to Upper Shebandowan Lake in the east and south to Squeers Lake. The Moss Township map consists of metasedimentary rocks and metavolcanic rocks, from northeast of Moss Lake to the Hood Lake Batholith to the south and finally to the west of Pearce Lake (Fig. 3.6). This area has also been previously mapped by Harris (1970), but Osmani (1997) mapped at smaller scale and therefore, greater detail.

Osmani (1997) described the ultramafic metavolcanic rocks as generally massive and sometimes showing polygonal jointing, but lacking spinifex texture or pillows. The mafic to intermediate metavolcanic rocks are the most abundant and form three northeast to east striking volcanic belts. They consist of massive (fine to coarse-grained), plagioclase-phyric, variolitic, pillowed flows and flow-top breccia. There are mafic to intermediate fragmental volcanic rocks consisting of tuffs, lapilli tuffs and tuff breccia that are abundant throughout the belt. High strain zones contain chlorite schists that are derived from mafic protoliths, and amphibole schists and gneisses that are interpreted to be related to the larger granite bodies (Osmani, 1997). Osmani (1997) also noted that there are garnet-bearing mafic schists/gneisses found adjacent to stocks in the area formed by amphibolite-grade contact metamorphism. The pillow lavas are the most abundant mafic metavolcanic rocks found in the area, whereas the massive to pillowed variolitic flows are the next most abundant. The other types of mafic volcanic rocks are found sporadically within the belts.

The intermediate metavolcanic rocks are mostly found northwest of Burchell Lake and can be up to 600m thick (Fig. 3.7) and can occur as narrow

bands that grade into mafic or felsic volcanic rocks (Osmani, 1997). The metavolcanic rocks are composed of tuffs, lapilli tuffs, monolithic and heterolithic tuff breccia, and minor amounts of massive, feldspar-phyric and amygdaloidal or vesicular flows (Osmani, 1997). These units weather a greyish-brown or greyish-white and grey to greenish-grey on the fresh surface. They can be distinguished from the mafic units by their slightly higher hardness and higher colour indices (Osmani, 1997). Osmani (1997) also mentioned a coarse pyroclastic and debris flow unit. He described it as subangular to ovoid, with intermediate, felsic and less commonly mafic clasts set in a fine-grained, well-foliated matrix of intermediate composition. The clasts can sometimes make up 20-80% of the unit and in highly sheared areas the matrix is typically sericitized and chloritized. A fine- to medium-grained tuff is also abundant in the area and can be found intercalated with felsic and mafic tuffs and clastic and chemical metasedimentary rocks (Osmani, 1997). The intermediate to felsic volcanic rocks are predominantly dacite to rhyodacite and occur mostly as massive (aphanitic) and porphyritic flows. They weather white to beige and are greenish grey on fresh surfaces (Osmani, 1997). The intermediate to felsic metavolcanic rocks can also crop out as pyroclastic rocks and can appear as lapilli tuffs and tuff breccias, which are angular to subangular in shape.

The felsic volcanic rocks consist of tuff, lapilli tuff, tuff breccia, pyroclastic breccia and massive to porphyritic flows (Osmani, 1997). They are generally aphanitic, but massive and porphyritic in some cases, and form thick pyroclastic felsic piles. They can weather cream white, white and grey and typically light grey on the fresh surface. In high strain zones, the units become sericite schists (Osmani, 1997).

The most recent mapping project was conducted by Hart (2007) of the Ontario Geological Survey (OGS) during the summers of 2005 and 2006. Hart (2007) mapped the metavolcanic rock package from Wye Lake north to Hamlin Lake (Fig. 3.7). Preliminary interpretations of the Hamlin Lake area, which was part of Hart's (2007) mapping project showed near identical ages of 2720 Ma for two samples taken from the northern and southern metavolcanic arms of the volcanic package (Hart, 2007; personal communication). The northern arm

sample was taken from within the mapping area of this study. The similar age of the Hamlin Lake-Wye Lake samples with the Greenwater Lake Assemblage of the eastern Shebandowan belt was interpreted by Hart (2007) to indicate that they are part of the same volcanic rock package.

3.5 *Mineral Deposits of the Shebandowan Area*

Over one hundred years of exploration has resulted in the discovery of several mineral deposits in the Shebandowan greenstone belt. The biggest in size was the INCO Shebandowan Mine, a nickel-copper sulfide deposit found in 1913, hosted in a komatiitic flow unit (Lavigne et al., 1990). This deposit was discovered on the south shore of Lower Shebandowan Lake, known as Discovery Point, and began production in 1972 (Osmani, 1997; Fig. 3.4). The mine shut down in 1992, but reopened in 1996 for two years before closing again in 1998 (Osmani, 1997).

The Huronian Mine, also known as the Jackfish Lake, Moss and Ardeen mine, is located in Moss Township and was discovered in 1871 (Fig. 3.4). This was the first gold discovery in northwestern Ontario and operated from 1884-1885 (Hodgkinson, 1968). It was reopened from 1932-1936 and again in 1942 with gold mostly being mined, but silver was extracted as a by-product as well (Harris, 1970). A total of 29,948 ounces of gold and 172,376 ounces of silver were mined from 1932-1942 (Harris, 1970).

The North Coldstream Mine (Fig. 3.4) is another deposit of the Shebandowan area and was first mined from 1958-1964, when it was known as the Tip Top deposit (Hodgkinson, 1968). Copper was discovered at the North Coldstream Mine in the 1870's and produced sporadically in 1903, 1906, 1916-1917, 1957-1958 and 1960-1964 (Giblin, 1964). Over this time, the mine produced 31,493,699 ounces of copper, 6,224 ounces of gold and 139,505 ounces of silver (Giblin, 1964). The orebodies are hosted by very siliceous, brecciated chert (Giblin, 1964). The ore is contained in massive sulfide bodies and disseminated sulfide with some stringers and contains chalcopyrite and pyrite with minor pyrrhotite, which have replaced and filled fractures in the host rocks

(Giblin, 1964). The chert which hosts the deposit extends approximately 20 km southwest to the vicinity of the Quetico Provincial Park boundary (Giblin, 1964).

Mineralization was first found near Hamlin Lake in 1956 when a copper showing was discovered. The first occurrence was reported near Hamlin Lake by Ray Smith in 1967 on the northwestern corner of Hamlin Lake, then known as Discovery Lake (Harris, 1970). The mineralization was said to be hosted in an altered zone of rhyolite and andesite, the alteration being due to the granite intrusion exposed to the south, part of the Powell Lake granitic intrusion (Harris, 1970). Harris (1970) suggested that the mineralization found in the Hamlin Lake area, was related to the Powell Lake intrusion. He noted that if this intrusion did not supply the metals that it at least supplied the energy to concentrate the sulfide minerals found in the metavolcanic rocks and this is why it has become a favourable zone for prospecting.

3.6 Exploration History of Hamlin Lake

Geological interest in the Shebandowan area started in the late 1800's. Poor access kept prospectors from the area until 1956, when Ray Smith and his partner Red Sanderson found copper mineralization northwest of Hamlin Lake (Harris, 1970; Fig. 3.8). The same year Noranda Mines Limited and Prospector Airways Company Limited optioned 31 claims north of Hamlin Lake, then known as Discovery Lake, from Ray Smith, opened up seven trenches and surveyed the claims by electromagnetic (EM) methods. Several conductors were recognized and tested with seven drill holes, but only minor mineralization was found (Harris, 1970). The first copper showing, still referred to today as the Ray Smith showing, lies only 200m north of the west side of Hamlin Lake with pyrite and chalcopyrite still exposed (Fig. 3.8). Following the initial discovery of the Ray Smith showing, several different companies optioned the Hamlin Lake claims sequentially. In the same year as Noranda's exploration program, MacLeod-Cockshutt Gold Mines Limited optioned the claims north and northeast of Hamlin Lake and again carried out an EM survey and drilled holes discovering two important showings in the areas, now called the MacLeod Cockshutt occurrences (Fig. 3.8). In the following years, copper and gold mineralization has

been found sporadically in the Hamlin Lake area, but never enough to be economically feasible for mining (Fig. 3.8).

Several companies performed new surveys and tested new conductors in the following 20 years after Ray Smith's discovery. After more attention was brought to the central Shebandowan greenstone belt, several mapping projects covered parts of the large, unmapped areas (Giblin, 1964; Hodgkinson, 1968; Harris, 1970; Osmani, 1997; Fig. 3.7). These geological mapping projects laid the foundation for prospectors to finally target areas of geological significance, and increased the potential for mineral deposit discoveries.
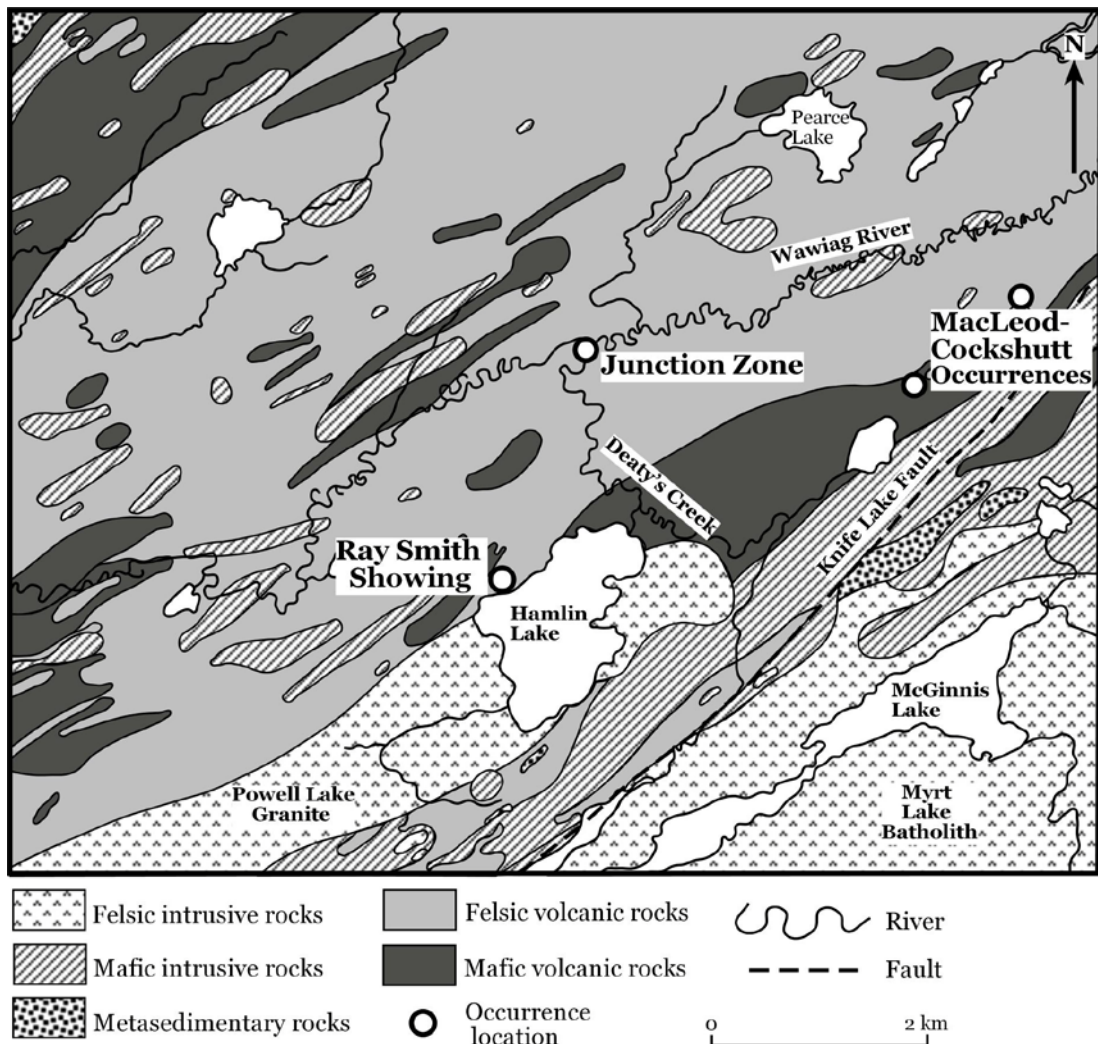
FIGURE 3.8 – Geological map showing the location of mineralized areas in the Hamlin Lake area (*after* Harris, 1970).

In the 1980's, Kennco Explorations (Canada) Ltd. performed ground magnetometer and VLF-EM surveys on the claims surrounding Hamlin Lake, as well as geological mapping and major element geochemistry. In 1987, Grande Portage Resources Ltd. conducted an induced polarization (IP) survey on the same area followed by trenching and sampling. This further exposed the mineralization discovered by Kennco Explorations Ltd., known as the Junction Zone, and the Ray Smith Showing (Fig. 3.8). Noranda Mines Ltd. returned to the property performing an EM survey and a total field magnetic survey. In 1989, Grande Portage Resources Ltd. drilled eight holes approximately 2.5 km north-northeast of Hamlin Lake and eight more holes in the vicinity of the Wawiag River and Deaty's Creek intersection near the Junction Zone (Fig. 3.8).

Recently East West Resource Corp. and Mega Uranium Ltd. have undertaken a number of geophysical and geological surveys in the Hamlin Lake area. The geophysical surveys found numerous new targets warranting further investigation. The targets were investigated with prospecting, trenching, geological mapping, sampling and drilling. No deposit has yet been found in relation to the felsic volcanic rocks, but the pink breccia unit located directly north of Hamlin Lake, has received the most attention and drilling from East West Resource Corp. after copper mineralization was recognized.

CHAPTER 4

MAPPING AND PETROGRAPHY

4.1 Introduction

Field work was undertaken during the summers of 2005 and 2006 in the Hamlin Lake area. A portion of each summer was devoted to mapping and sampling in order to generate a geological map of the area (Fig. 4.1). There are several lithologies present on the Hamlin Lake property; mafic metavolcanic rocks, felsic metavolcanic rocks, intermediate metavolcanic rocks, felsic intrusive rocks and iron formation. The most extensive units are the volcanic rocks, with the rhyolites and andesites being nearly equal in abundance. The felsic metavolcanic rocks vary from rhyolites and quartz-eye rhyolites, through banded ash and lapilli tuffs, to debris flows. The intermediate metavolcanic rocks consist of dacites and andesites, although distinguishing them in the field from the felsic volcanic rocks was difficult without the use of wholerock geochemistry and thin section work; and most of the intermediate volcanic rocks were mapped as felsic during field work. The mafic metavolcanic rocks were primarily debris flows. The felsic-to-intermediate intrusive rocks consisted of quartz-eye feldspar porphyry and the felsic pink breccia. Lenses of iron formation were also observed on the Hamlin Lake property. All of the lithologies observed on the property have been sheared in a northeast-southwest direction (~234°) and have an average dip of 86°N, but the dips range from 65° to 90°N.

4.2 Felsic to Intermediate Metavolcanic Rocks

The felsic to intermediate metavolcanic rocks were the most extensive unit observed while mapping the Hamlin Lake area. The prefix "meta" will not be used throughout the remainder of the chapters, but it is implied that the volcanic rocks at Hamlin Lake have been metamorphosed to lower greenschist facies by the presence of chlorite and actinolite. All the rocks have been altered to some degree and for the purpose of this discussion slight alteration involves 10-30%
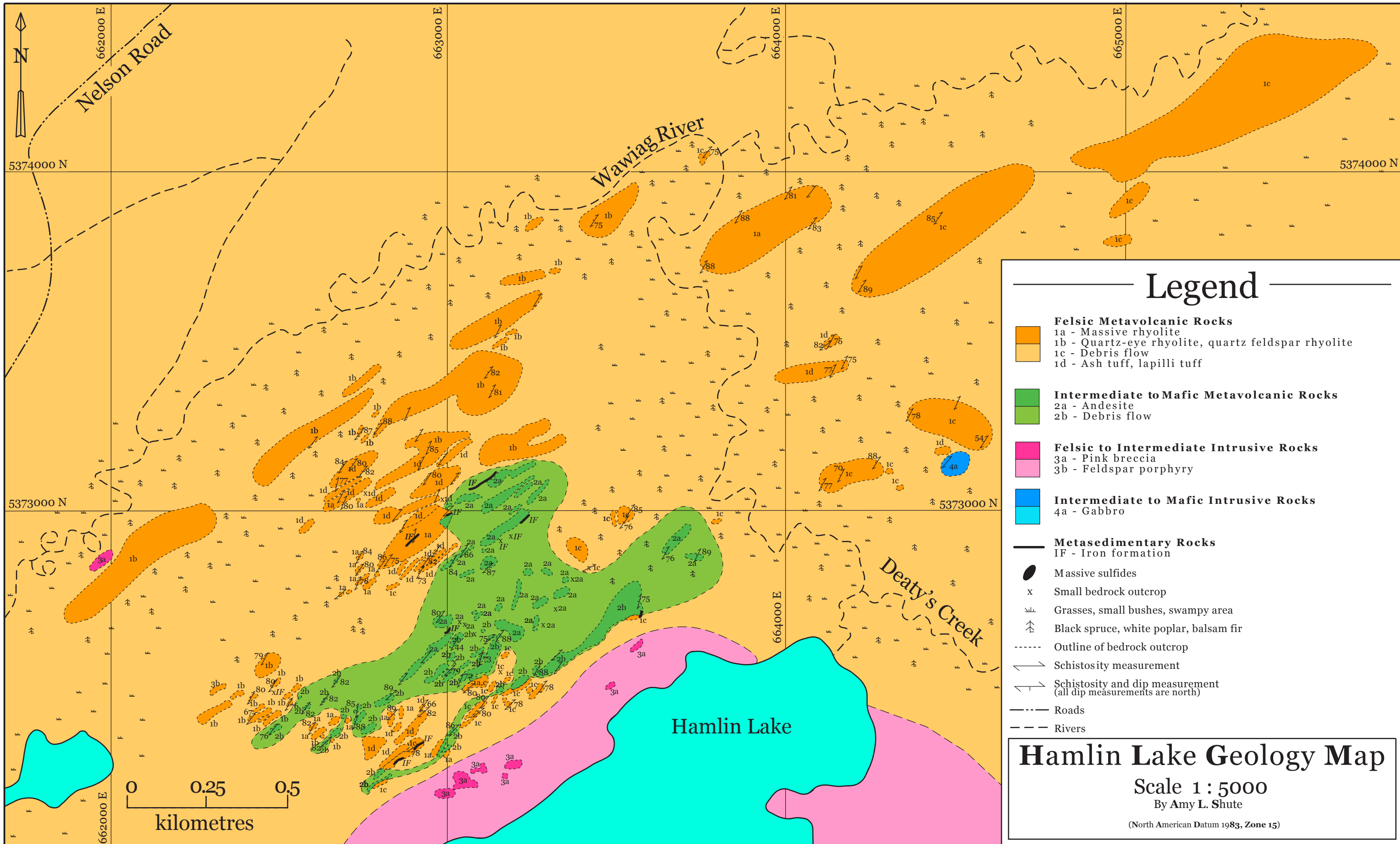
FIGURE 4.1 - Geological map of the Hamlin Lake area.

Legend

Felsic Metavolcanic Rocks
1a - Massive rhyolite
1b - Quartz-eye rhyolite, quartz feldspar rhyolite
1c - Debris flow
1d - Ash tuff, lapilli tuff

Intermediate to Mafic Metavolcanic Rocks
2a - Andesite
2b - Debris flow

Felsic to Intermediate Intrusive Rocks
3a - Pink breccia
3b - Feldspar porphyry

Intermediate to Mafic Intrusive Rocks
4a - Gabbro

Metasedimentary Rocks
IF - Iron formation

Massive sulfides
x   Small bedrock outcrop
Grasses, small bushes, swampy area
Black spruce, white poplar, balsam fir
Outline of bedrock outcrop
Schistosity measurement
Schistosity and dip measurement
(all dip measurements are north)
Roads
Rivers

Hamlin Lake Geology Map

Scale 1 : 5000

By Amy L. Shute

(North American Datum 1983, Zone 15)

Nelson Road

Wawiag River

Deaty's Creek

Hamlin Lake

kilometres

0   0.25   0.5

32

alteration minerals in the sample, moderate alteration 30-60%, strong alteration 60-80% and very strong or intense alteration would be >80% alteration minerals. The volcanic rocks crop out as round to oval mounds, generally striking in the same direction as the cleavage (~234°).

4.2.1 Rhyolitic Tuff

The rhyolites range from massive flows containing phenocrysts, to pyroclastic units with chert fragments. All rhyolite units have undergone slight to very strong alteration, from chloritization to sericitization. The weathered surfaces of the rhyolites vary considerably from green and white, to a pinky-orange and brown-maroon. On fresh surfaces, colours can vary from light brown to yellowish white, grey-tan, dark grey and black-green and as a result of the presence of different alteration minerals. The light green colours are a result of sericitization; the pink-orange is a combination of iron staining and hematization; and the darker grey-green varieties are from chloritization (Fig. 4.2 a-d). Gradual colour changes and contacts observed in other outcrops are related to different alteration intensities, but in general primary textures, colours and field relationships have been overwritten by hydrothermal alteration. The rhyolite unit contains quartz amygdules in some outcrops, which are round in appearance, white in colour and can vary in size from 0.5cm to 3.0cm (Fig. 4.2 b-c). One outcrop contains large amygdules that show a distinct tear drop shape and were difficult to distinguish from volcaniclastic fragments because the amygdule size was bigger than previously observed; however, the same outcrop also contained smaller amygdules helping to distinguish them from fragments (Fig. 4.2b). Other outcrops containing amygdules also contained vesicles within a fine-grained matrix and an overall tan colour. The quartz-eye rhyolites contain the same alteration features as the massive rhyolites with quartz-eyes varying in colour from clear to grey to blue and ranging in size from 1.0mm to 5.0mm. Some outcrops were noted to contain from 10-20% quartz-eyes, but the average abundance of quartz-eyes was 2-5%.
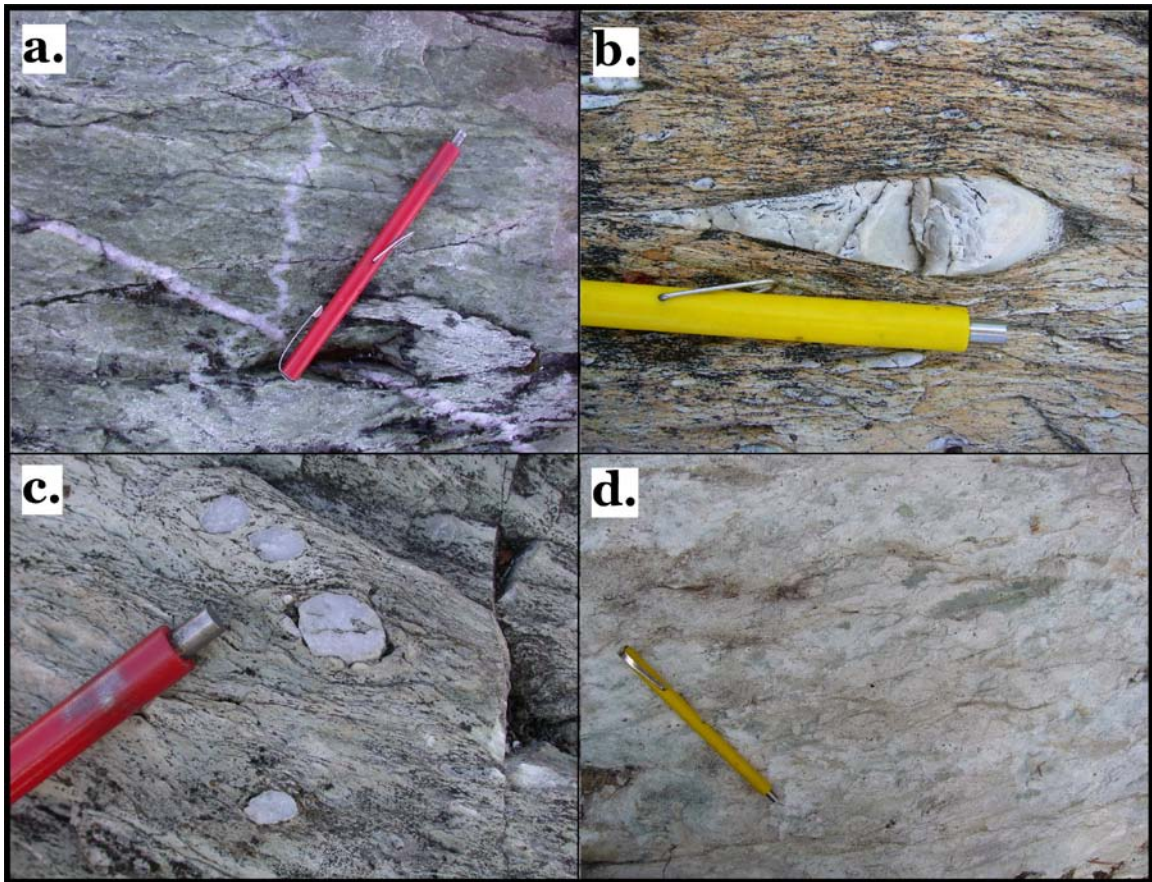
FIGURE 4.2 – Field photographs of rhyolite samples. (a-d) shows the varieties of colours that the rhyolite rocks were altered to, (b) shows the large amygdules, (c) shows the smaller round amygdules and (d) shows the bleached colour of a rhyolite.

In hand sample, alteration is recognized by colour changes and mottled textures. Chlorite alteration is found smeared along sheared surfaces. When rhyolite outcrops have been highly sericitized, the rock displays a distinct light green colour (Fig. 4.2d). The difference between the green colours of the chlorite and sericite alteration is the deeper green observed in the chlorite (Fig. 4.2a) and the much brighter lime green seen as a result of sericite alteration (Fig. 4.2d). In the rhyolites, silicification is not always as apparent in the field, because of the original high concentration of quartz in felsic volcanic rocks, but where present it does cause the silicified rock to become much harder.

In the 21 rhyolite thin sections, samples are fine-grained to very fine-grained. The sample with the least amount of quartz contained only 35% quartz and was mostly sericite (AS-05-046b), whereas the highest quartz content found in a sample was 90% (AS-05-042); however, the average quartz content is 70-

80%. Sericite is the second most abundant mineral found in the rhyolites in thin section, with a range of 15-60% and an average of 30%. Accessory minerals include calcite, ranging from 5-40% and chlorite ranging from 5-20%, although neither mineral is frequently seen in the rhyolite samples. Plagioclase crystals are found in only a few of the thin sections, and only appear as relict structures showing faint twinning, almost entirely replaced by sericite. The replacement of feldspar by sericite crystals leaves behind black patches. The most common texture found within the rhyolite samples is porphyritic quartz and feldspar, although there are few plagioclase feldspar crystals. The quartz and feldspar phenocrysts look like they were sutured within sericite and are interpreted to be the result of rapidly growing crystals enclosing groundmass material leaving embayments along the perimeter of the phenocrysts (Fig. 4.3; c-e).

Thin sections, which contained high amounts of sericite alteration, comprise preferred dimensional orientation of lath-shaped sericite crystals (Fig. 4.3a). The alignment of the crystals foliation is a result not only of hydrothermal fluids, but also deformation (Fig. 4.3; a-b). In thin sections containing veins, a high concentration of sericite adjacent to the veins was common, with sericite content decreasing away from the vein. The decreasing abundance of sericite away from the vein suggests that the hydrothermal fluids entered the rock through the vein systems, therefore altering the minerals which are closest to the veins.

In thin section, it is common to see veins containing quartz crystals and minor calcite crystals running through samples (Fig. 4.3f). The thin sections show that the primary quartz crystals closest to the veins have been the most altered and also, the degree of sericite alteration in the feldspar crystals decreases away from the veins. Samples with calcite veins show similar sericite alteration as the samples with quartz veins, with the alteration most intense closest to the veins and diminishing away from the vein.
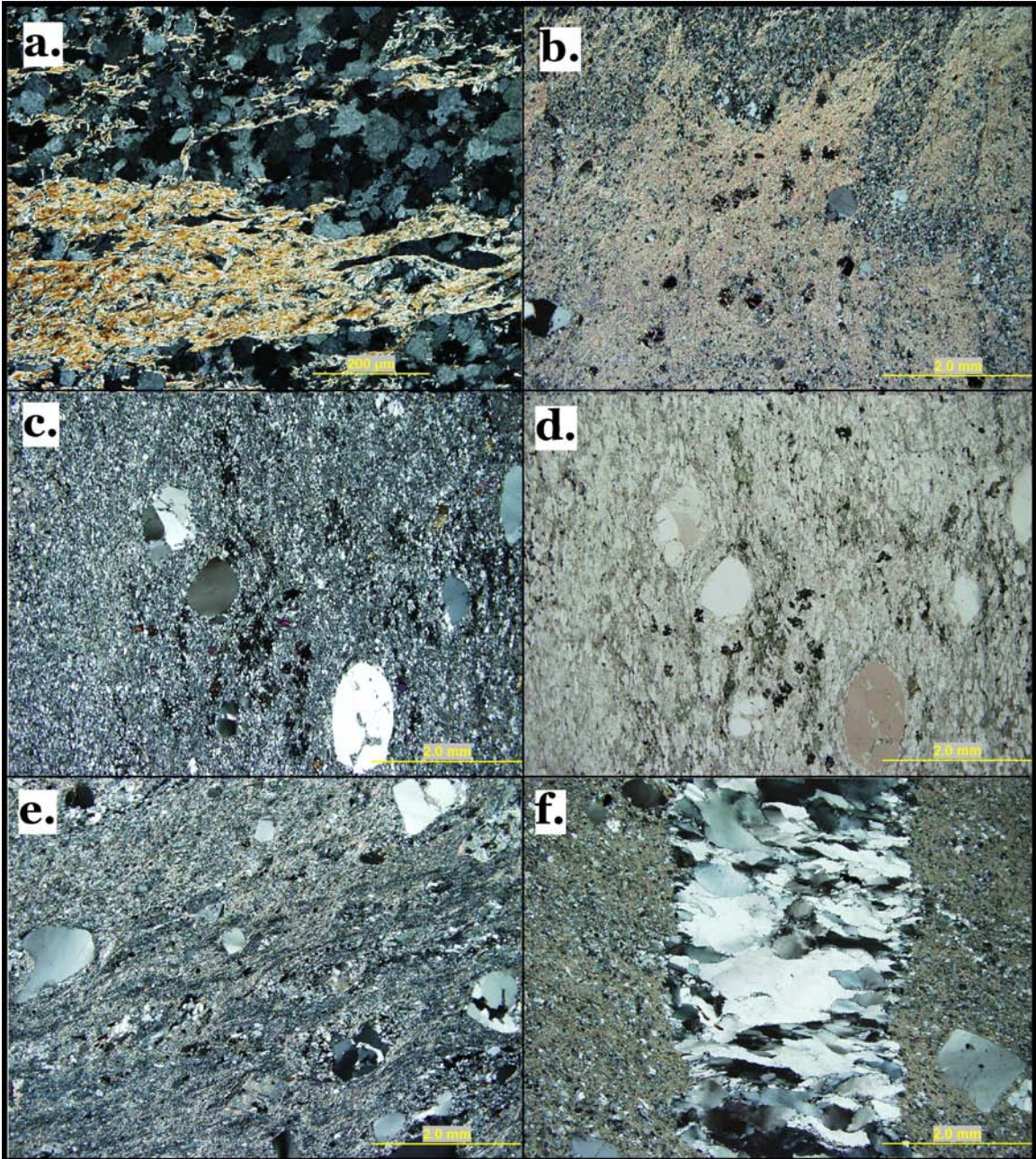
FIGURE 4.3 – Rhyolite photomicrographs in plane polarized light (ppl) and cross polarized light (cpl) showing; (a) sericite alteration in rhyolite (AS-05-012; cpl), (b) fine-grained sericite alteration encompassing the majority of the sample (AS-05-046; ppl), (c) and (d) show feldspar and quartz phenocrysts with embayments in cpl and ppl, respectively (AS-05-045), (e) shows similar embayments in phenocrysts and fine-grained crystals of sericite and quartz (AS-06-011; cpl), while (f) shows a quartz vein with minor calcite (AS-05-049; cpl).

4.2.2 Dacite Lapilli Tuff

The dacite unit is the least abundant unit found in the mapping area (Fig. 4.1). Only one dacite flow was recognized in the mapping area, otherwise the dacite samples are found as ash and lapilli tuffs and pyroclastic agglomerates

scattered around the mapping area in smaller showings (Figs. 4.1; 4.4 a-f). The dacites are typically very fine-grained with some outcrops containing lapilli-sized grains amongst fine ash grains and in a few outcrops large angular bomb size pyroclastic fragments are found (Fig. 4.4 a-f). One diagnostic feature of the ash and lapilli units are the alternating 1.0 cm to 2.0 cm thick layers (Fig. 4.4 a-b,d,f). The alternating colours and sharp contacts of the ash layers helped to determine that they were in fact a result of ash deposition and not alteration, which can also change the colour of the rock (Fig. 4.4 b,f). The weathered surfaces on the non-banded dacite outcrops are a light tan-brown to green-white colour, while the fresh surfaces are a light yellowish-green to brown grey colour. Some of the dacitic crystal tuffs have distinct feldspar crystals within the matrix and rarely quartz-eyes as well. The quartz-eyes are round, 1.0 mm to 3.0 mm in size and are clear to white in colour. Overall, because of the thinness and fine-grained ash layers, it is thought that the dacite units are part of a different volcanic system than the rhyolites and andesites and the ash layers are the distal products of that volcanic centre.

In hand sample and in outcrop, the ash and lapilli tuffs are difficult to distinguish from massive flows, because although there are size differences between ash and lapilli, it is not always apparent in the field or hand sample that it was a pyroclastic rock because the ash tuffs are so fine-grained. Some of the lapilli fragments are angular, fractured and shard-like in appearance helping to distinguish their pyroclastic origin. When examining the rocks closely, grains and crystals can often be distinguished, but when heavily altered it is difficult to identify the pyroclastic material even when using a hand lens.

In the field, alteration is not easily recognized within the dacite unit. Colour differences between dacite outcrops are the only signs of alteration observed in the field, with the outcrops showing a distinct yellow-green colour on surface, diagnostic of sericite alteration, as opposed to grey to light grey in an unaltered to weakly altered sample.

Seven samples of dacite were thin sectioned, the most abundant mineral present is quartz, ranging from 5-90% and averaging 50%. Sericite is the second most abundant mineral in the dacite samples ranging from 15-85%, averaging
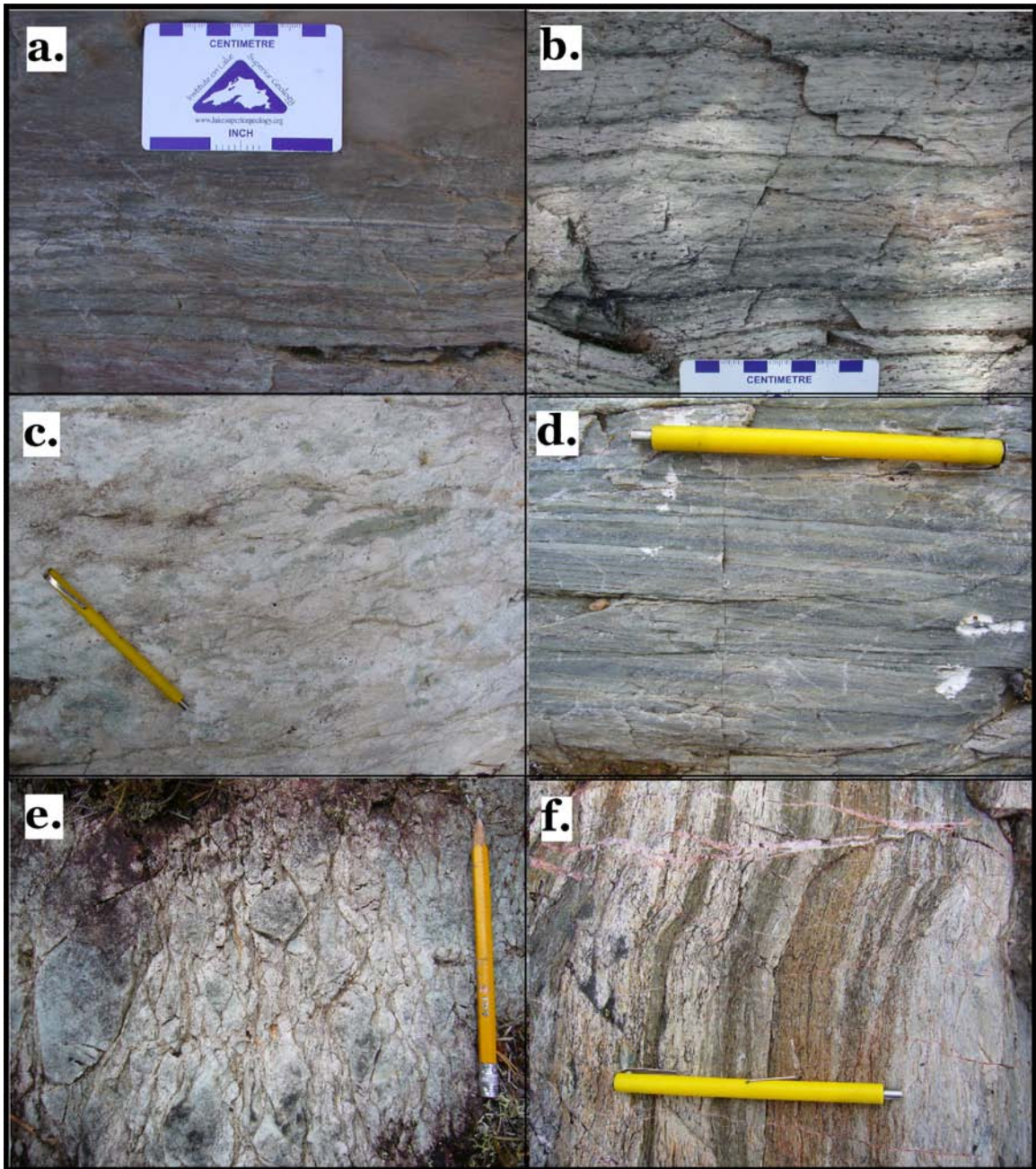
Figure 4.4 – Photographs of outcrops (a), (b), (d), (f) show the ash layers that are evident in the different coloured layers; (c) showing fine-grained ash tuffs that are very light in colour; (e) a dacite unit showing large fragments that vary from bomb sized to coarse ash sized fragments.
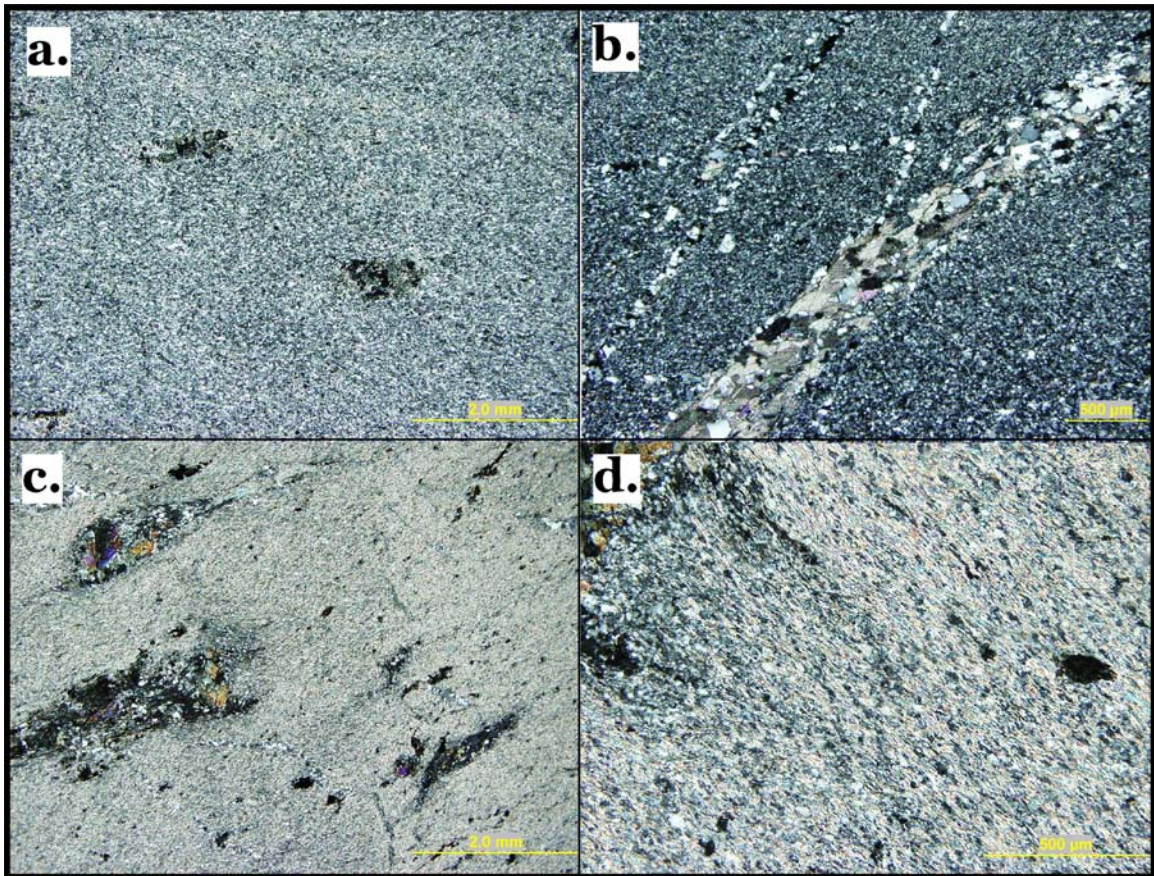
FIGURE 4.5 – Photomicrographs displaying very fine-grained dacites. In the field the dacites often display fine-grained layers, but in thin section the layers are not as evident. (a) OC-327; cpl, (b) OC-335; cpl, (c) AS-05-021; cpl, (d) AS-05-021; cpl.

40%, and showing lath-shaped, aligned crystals (Fig. 4.5a-d). Feldspar crystals are not as prevalent as quartz and sericite and range from 15-35% with an average of 25%. The feldspar crystals are difficult to identify without the occurrence of faint twinning still present in a few of the crystals. Accessory minerals include calcite and chlorite and can range from 5-15%. The calcite crystals occur as single crystals between the fine-grained sericite crystals and the chlorite crystals occur in clusters surrounded by a fine-grained matrix of quartz and sericite.

Chlorite found within the dacite samples is found in clusters and also within the matrix (Fig. 4.5c). It is common to find the chlorite crystals replacing pyroclastic clasts. Sericite is also found as very fine, lath shaped grains making up the majority of the rock, depending on the degree of alteration in the sample. The samples which have undergone moderate sericite alteration show alignment

39

of the sericite crystals, especially around feldspar phenocrysts. The feldspar crystals in the dacite are similar to those found in the rhyolite samples, in that they now occur as relict structures with faint twinning and are almost entirely replaced by sericite crystals.

4.2.3 Andesitic Lapilli Tuff

The intermediate metavolcanic rocks observed in the mapping area consist of andesites, which are present throughout the area (Fig. 4.1). During field mapping most andesites were mapped as felsic to intermediate metavolcanic rocks, however, after interpreting the whole rock geochemistry (Chapter Five), it was apparent that the felsic to intermediate units could be separated into rhyolitic, dacitic and andesitic volcanic suites. The andesites are similar in appearance to the rhyolites, with similar grain size and colour, but only slight variations in silica contents, making it difficult to distinguish between the two units in the field. The andesites exhibit medium grey-green colours on fresh surfaces and are fine-grained to very fine-grained. The pyroclastic material observed varies from lapilli tuffs, with distinct lapilli, to coarse and angular pyroclastic material (Fig. 4.6 a-d). The fragments are more apparent on the weathered surfaces where the matrix has undergone recessive weathering. Sericite alteration is not commonly observed in the andesite hand samples, but it is petrographically.

In the field, the andesitic lapilli tuff units show similar alteration to the rhyolitic and dacitic units. Chlorite can be observed on surface, with smears of black chlorite on the sheared planes and sometimes a darker grey colour on the fresh surfaces.

Petrographically, the andesitic rocks are similar to the rhyolitic rocks. They consist mostly of quartz and are fine-grained to very fine-grained. The primary pyroclastic material found in the andesite volcanic rocks has been replaced with chlorite, preserving the clast textures. The pumice fragments appear as wispy and lenticular chloritic clusters, with the faint appearance of collapsed pumice and in a thin section of sample OC-202, round lapilli are recognized (Fig. 4.7 b-e). The thin sections provide a clearer picture of the
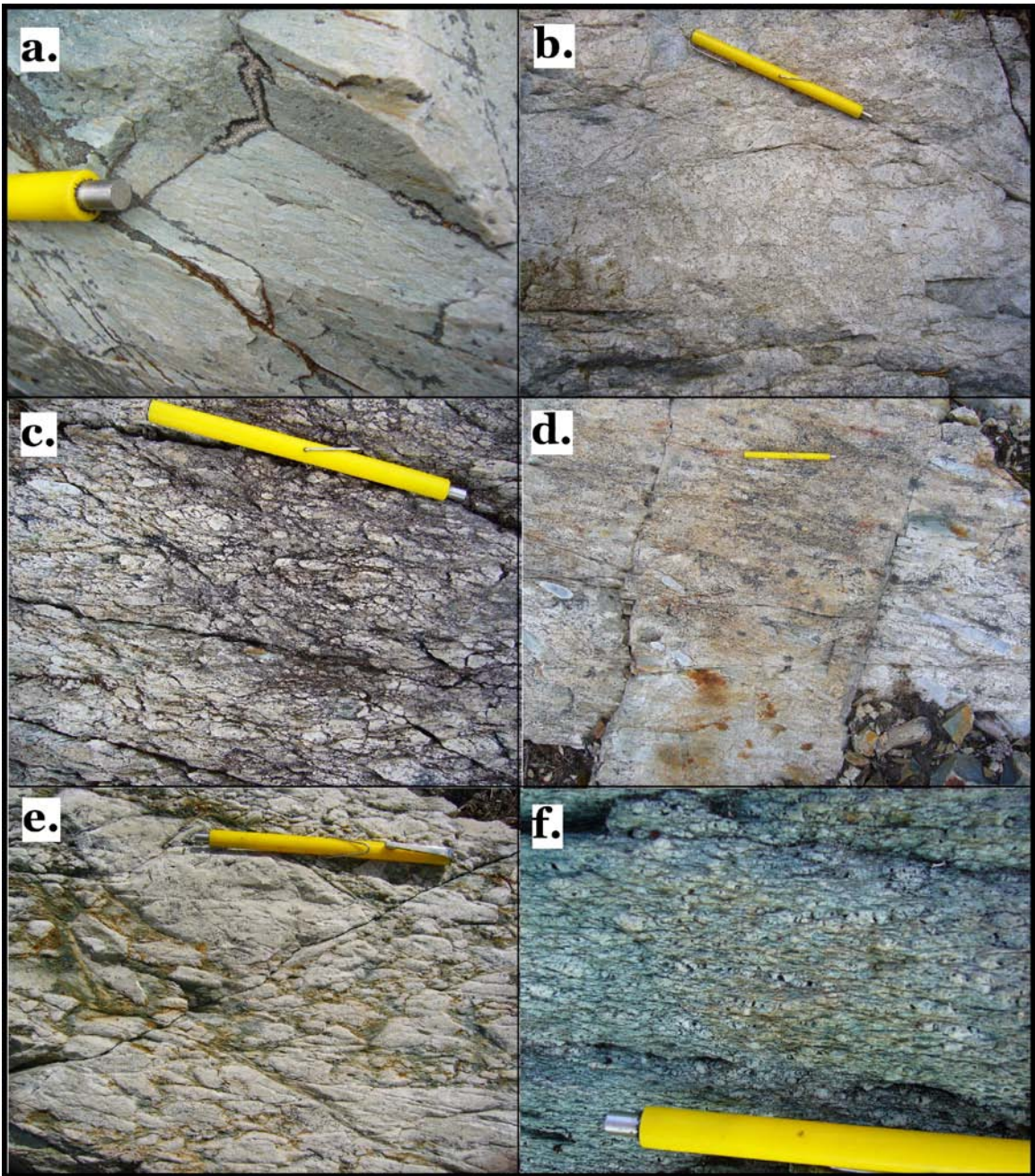
FIGURE 4.6 – Photographs of selected field samples: (a) layered beds of lapilli in a highly siliceous matrix; (b) andesitic pyroclastic breccia with the angular blocks still showing vesicles; (c) outcrop of lapilli tephra showing distinct fragments; (d) a block and ash flow with a fine-grained matrix and angular blocks of different sizes and shapes; (e) an agglomerate of subangular fragments of varying from bomb to lapilli in size; (f) a lapilli tuff that covers a large part of the lower stratigraphy of the Hamlin Lake area.

pyroclastic material, with lapilli varying in size from 0.5 mm to 1.0 mm. Feldspar crystals are rarely recognized in thin section both because of the fine grain size and the sericite alteration

41
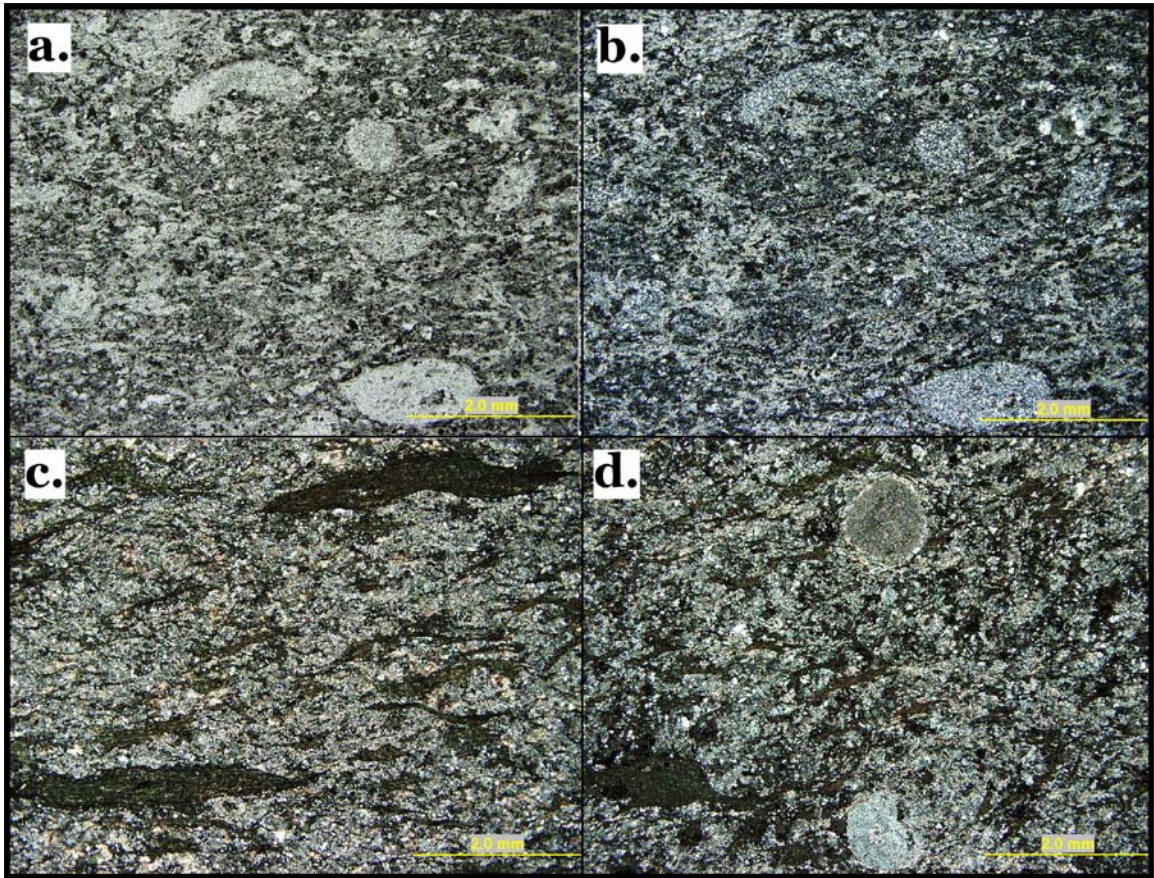
FIGURE 4.7 – Photomicrographs (a) and (b) are of pyroclastic sample AS-05-039 in (a) ppl and (b) cpl showing lapilli and ash in a quartz and chloritic matrix; (c) and (d) are of pyroclastic sample OC-202 showing collapsed chloritic pumice clasts and lapilli both in cpl. Some of the accretionary lapilli still preserve their round shape.

replacing the feldspars. Sericite alteration affected these samples considerably by replacing the feldspars, whereas fine-grained quartz phenocrysts are still abundant and mixed with sericite crystals. In the highly sericitized samples, the pyroclastic material and their textures have been destroyed by sericitization.

4.2.4 Felsic Debris Flow

The felsic debris flows found at Hamlin Lake are not as common as the rhyolite units, but they are critical to understanding the volcanic environment in which the rock was erupted (Fig. 4.1). The unit is composed of matrix-supported chert clasts, white to grey in colour and varying in size from 1 cm to 20 cm (Fig. 4.8; a-b). Size differences between chert clasts can be observed more easily
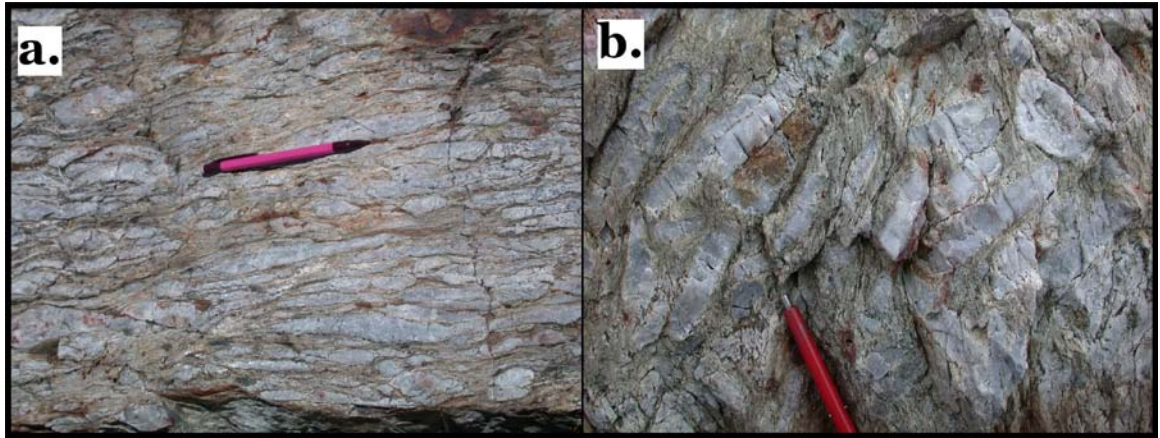
FIGURE 4.8 – Photographs of felsic debris flows showing a light coloured felsic matrix with lenticular and enlongate chert clasts comprising the majority of the units. Photograph (a) shows a clast supported debris flow, whereas (b) shows a matrix supported debris flow.

between outcrops, than within outcrops. The felsic debris flows do not show grading, characteristic of turbidites, but some outcrops do show a greater clast density than others, signifying different concentrations of coarse- versus fine-grained sediment representing different flows. The differing clast concentrations help to distinguish different debris flow events. The majority of the clasts are lenticular in shape, but round and semi-rounded clasts can also be observed (Fig. 4.2 d-f). The differences in shape are a result of deposition and the degree of roundness depends on the amount of reworking the clasts experienced before and during deposition along with tectonic flattening. In the field, the type of debris flow can quickly change, over a distance of 5.0m, from a felsic debris flow to a mafic debris flow. The overall lenticular shape of the outcrops and sharp contacts between flows observed in the field, suggests that these units are preserved channels of debris flow events and the changes in lithology are a result of the original matrix composition. The more felsic units likely originally contained a greater proportion of volcanic ash in the matrix, whereas the more mafic flows contained muddy sediment in the matrix. The matrix could be muddier in some flows than others because of sediment that was incorporated into the flow, while it was being deposited or if there was substantial time between events, muddier sediment may have settled on top of the pyroclastic units.

In thin section, the felsic debris flows show a fine-grained, quartz-rich matrix with sharp contacts with the chert clasts. The chert clasts are a mass of fine- to medium-grained quartz grains that have been recrystallized. The matrix shows sericite alteration similar to the rhyolite and dacite units, and low amounts of chlorite.

4.3 Mafic Rocks

The mafic metavolcanic rocks observed on the property consist of debris flow units (Fig. 4.1). The mafic debris flow units are similar to the felsic debris flow units, varying only in the composition of the matrix. The matrix of the mafic debris flow units are highly chloritized and are locally magnetic. In places magnetite fragments can be found in the unit. These units also contain minor amounts (2-3%) of cubed or disseminated pyrite and as a result the weathered surfaces of the debris flow units have a rusty appearance in places (Fig. 4.8 a-f). The highly chloritized matrix is blue-green in colour on the weathered and fresh surfaces, and the fresh surface of the matrix is strongly schistose in appearance as a result of deformation. The debris flows contain chert clasts similar to the chert clasts found in the felsic debris flow units, as they also have a lenticular and/or round shape (Fig. 4.8 a-f). The chert clasts can vary from 2.0 cm up to 15.0 cm in length and are matrix supported.

4.4 Felsic Intrusive Rocks
4.4.1 Quartz-Feldspar Porphyry

Only one quartz-feldspar porphyry outcrop was mapped during this study, in the northwestern portion of the mapping area (Fig. 4.1). The porphyry is fine-grained with round phenocrysts ranging in length from 1 to 2 mm. The weathered surface is a grey-white colour and the fresh surface is a dark-grey to green. Feldspar phenocrysts have been slightly altered, with only small patches of feldspars replaced by sericite crystals. The quartz phenocrysts show embayments against the groundmass, the result of rapidly growing crystals enclosing the groundmass material (MacKenzie and Guilford, 1980), similar to the feldspar phenocrysts found in the rhyolites.
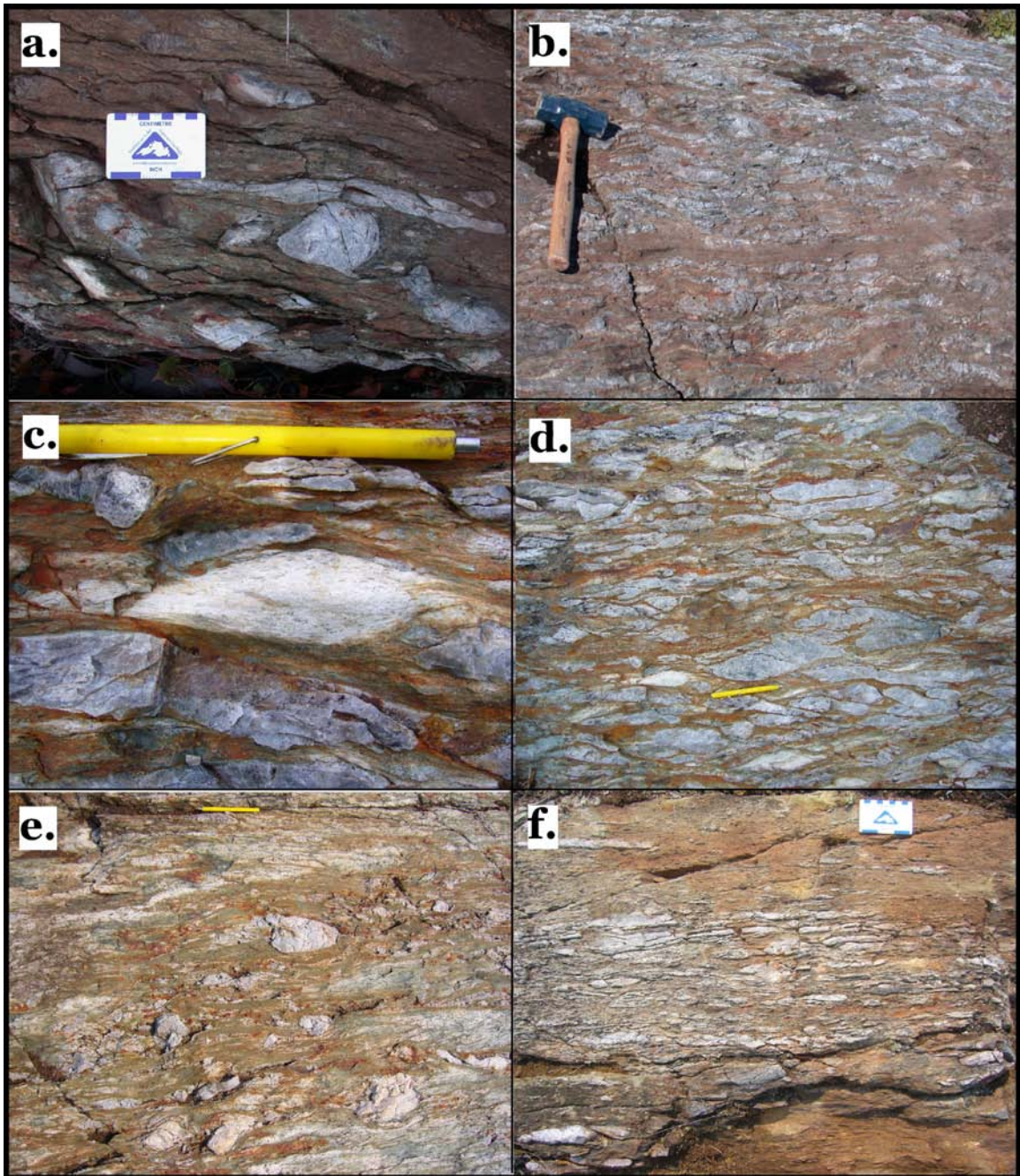
FIGURE 4.9 – Photographs (a) to (f) show the differences and similarities between the mafic debris flows. (a) shows how the clasts can vary in size from rounded to elongate in one unit; (b) shows a more typical mafic debris flow at Hamlin Lake with a high concentration of clasts and patches of more matrix in one outcrop; (c) shows a rhyolite clast set in an outcrop that consists almost completely of chert clasts (d); photograph (e) also shows a variety of clast shapes and sizes; and (f) shows the different clast concentrations within units.

4.4.2 Granite

        The granite crops out on the southern and eastern edges of Hamlin Lake and is part of the Powell Lake Granite (Fig. 4.1). The fresh and weathered surfaces of the granite are light pink in colour and medium-grained.

        In thin section, grains are equigranular with twinned plagioclase and quartz making up the majority of the samples, with minor amounts of fine-grained sericite altering the plagioclase. The crystal length varies from 0.5mm to 2.0mm and are shades of grey, white and black.

4.4.3 Pink Breccia

        The pink breccia found on the property was not recorded by Harris (1970). No contacts are exposed at surface; therefore, the relationship with the surrounding rock units remained unclear until a drill program in 2005 by East West Resource Corp. It was determined after drilling that the breccia underlies the volcanic rocks to the north (Fig. 4.1) and is the result of an intrusion. The breccia is polymictic and contains clasts of rhyolite, quartz/feldspar porphyry, diorite, gabbro, chert and magnetite (Fig. 4.10a). The clasts vary in size from 1.0 to 15 cm in length and are angular to subangular in shape (Fig. 4.10b). Sulfide mineralization is found sporadically throughout the unit. One area contains visible chalcopyrite and pyrite. Epidote, hematite and chlorite alteration affect the breccia unit, with some areas containing greater amounts of alteration than others. The colour can range from a distinct bright pink to dull pink, mixed with areas of light green to a creamy green. The matrix consists of small clasts, but mostly it is very fine-grained quartz and epidote and is hard to identify in hand specimen. The rhyolite clasts are fine-grained and appear to be the pinkest of all the lithologies along with the quartz-feldspar porphyry, which are both fine-grained overall. The diorite and gabbro clasts are larger than the rhyolite and porphyry clasts overall and are more affected by epidote alteration than hematite alteration. There are no patterns observed in the breccias to suggest clast sorting or grading; overall, the clasts appear to be chaotic. Locally the breccia can be distinctly pink as a result of the hematization and in other areas distinctly green from epidotization, however, some areas only show minor epidote and hematite
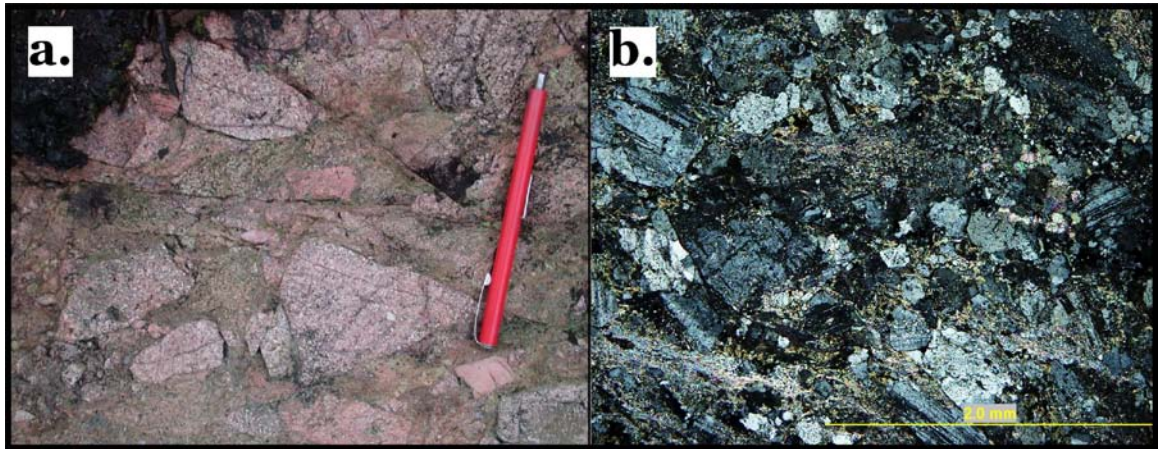
Figure 4.10 – Photographs of pink breccia showing (a) polymictic clast lithologies and angular shaped clasts in the field. Photomicrograph (b) of AS-05-001 showing coarse grained crystals in cpl.

alteration. Only one area on surface shows obvious chlorite alteration and that is near the Ray Smith showing (Fig. 3.8).

4.5 Mafic Intrusive Rocks

The gabbro observed in the area is located on the east side of Deaty's Creek and is magnetic and brecciated in places. This gabbro is also medium to coarse-grained and is dark grey-black in colour on the weathered and fresh surfaces. There was only one outcrop of gabbro mapped during this study, but the unit does continue east into the Deaty's Creek area (Fig. 4.1).

On surface, the gabbro is fine- to medium-grained with feldspar crystals making up the majority of the matrix. The mafic minerals consist of hornblende and pyroxene with minor biotite.

4.6 Metasedimentary Rocks

The only metasedimentary rock found in the mapping area is iron formation, and it is located sporadically throughout the mapping area (Fig. 4.1). The iron formation consists of banded chert and magnetite layers (Fig. 4.11b). One outcrop of iron formation, in the central part of the property, is larger than the other occurrences at approximately 10m in length, whereas, the smaller more common lenses located throughout the area are on average 1 to 2 m in length.

In thin section, the iron formations show the same banded magnetite-chert patterns as in hand specimen on surface. The magnetite and quartz crystals

are both fine-grained forming laminated, 1 to 10 cm thick beds. In general, the chert layers are thicker than the magnetite layers because the magnetite layers can vary from 1 mm in thickness to 10 mm, while the chert layers can be several centimeters thick (Fig. 4.11b). The chert layers show only fine equigranular quartz grains with no accessory minerals present, while the magnetite beds do not always occur in defined beds and can be found as thin wispy layers between the chert layers. In thin section, different layers of chert can be recognized, even when not separated by a magnetite layer, because the grain size can differ between layers (Fig. 4.11b).

4.7 Mineralization

The sulfides found on line seven (LN7) of the geophysical cut lines were one of the first indications that the mineralization in the Hamlin Lake area was VMS related (Fig. 4.1). The LN7 sulfides contain 1.49% copper and 4.0g gold/tonne and can be traced for approximately 200m (eastwestres.com; Sept.7/05 news release). Drilling showed no depth to the exposed sulfides and the copper and gold numbers are inconsistent, so it was concluded that the LN7 sulfides did not warrant further exploration. On surface, the sulfides appear as lenses of massive pyrite in a fine-grained matrix. Closer examination shows small chert lenses making up part of the matrix with very small traces of
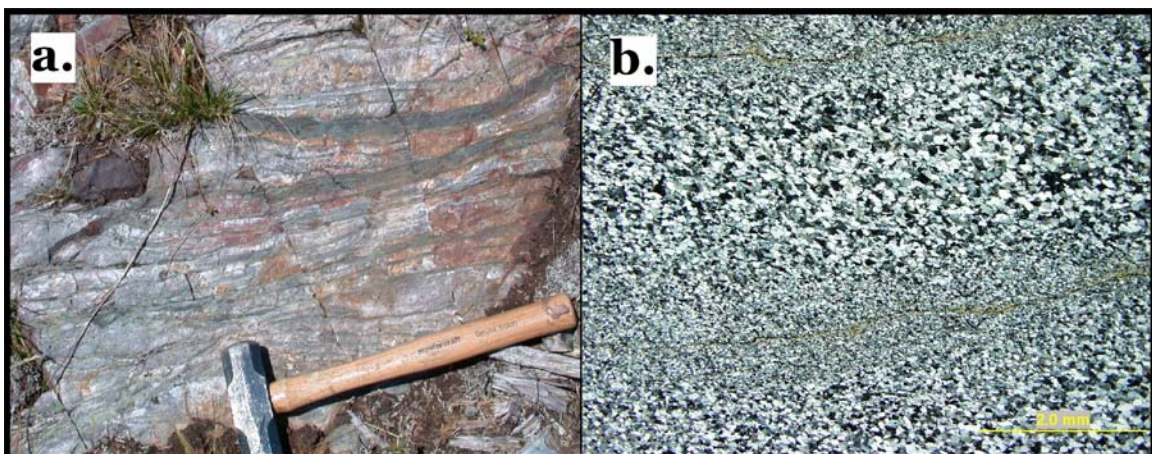
FIGURE 4.11 – Photograph of an iron formation located within the debris flows. This iron formation could be a rafted piece of an iron fragment that was caught up in a debris flow episode. Photomicrograph (b) is a sample of iron formation (AS-05-024b) in plane polarized light showing thinly banded layers and the differences between grain sizes in layers.

chalcopyrite located on the exterior portion of the lenses, but it was difficult to locate the chalcopyrite without polishing the sample. The lenticular shape of the pyrite lenses and the fine-grained matrix resembles the debris flows except instead of chert clasts, there are sulfide clasts. The matrix of the LN7 sulfides is dark grey in colour, containing chlorite with minor amounts of quartz and chert clasts. On the weathered surface, the mineralized area is red and rusty. The pyrite and trace amounts of chalcopyrite found on LN7 occur in 2 to 6 cm long lenses that are similar to the chert lenses found in the debris flow units, but are composed of sulfides instead of chert. It is possible that these pyrite 'lenses' may have been continuous beds at one point and after deposition, the beds broke up as a result of the weight of overlying units and now appear as lensoid shapes. However, after detailed observation it was concluded that the pyrite lenses were formed in the same way as the debris flows because of their many similarities, except instead of chert clasts being included in the flow it was pyrite clasts.

In polished hand sample and polished thin section, chalcopyrite mineralization can be seen only in trace amounts, although it is more visible in polished thin section. This indicates that the chalcopyrite that is present is disseminated and very fine-grained. The chalcopyrite is found on the outside of the pyrite lenses, but not interstitially with the pyrite, suggesting it formed after the pyrite.

The most economically viable unit located in the Hamlin Lake area is the pink breccia, which contains low grade copper in the form of chalcopyrite, located in the matrix of the breccia. The initial grades from trenching showed values ranging from 7.78% to 0.1% copper, 6.44 to 0.3 g/t of gold, 1635 to 3ppm of molybdenum and 81 to 1 g/t of silver (eastwestres.com; Oct.18/05 news release).
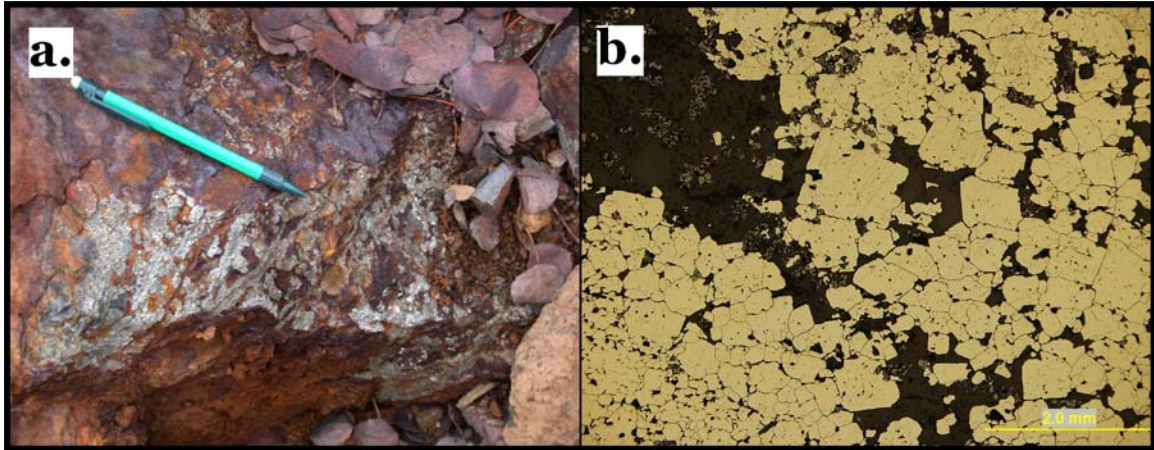
FIGURE 4.12 – Photograph (a) is of mineralization from the LN7 area showing the massive nature of the sulfides in the field. Photomicrograph (b) of the LN7 sulfides (AS-05-072), showing pyrite under reflected light.

4.8 Discussion

4.8.1 Mapping

The most common rocks present in the area are intermediate to felsic metavolcanic rocks that are similar in colour, because of alteration, and textures making it difficult to differentiate between lithologies in the field. Hodgkinson (1968) encountered these same difficulties, while mapping nearby areas. Textures, colours and field relationships are overprinted by metamorphism and alteration. Apart from the BIF, the only other easily recognizable units in the mapping area were the mafic debris flows because of the contrast between the dark chloritic matrix and the white chert clasts. Recognizable textures in the field are amygdules, lapilli and ash layers; all diagnostic of volcanic deposits. In thin section, primary pyroclastic textures, such as fiamme and accretionary lapilli are recognized. Contacts between volcanic units were overprinted by alteration making it difficult to separate flows. Separation of lithologies was initially carried out in the field and eventually re-evaluated for accuracy using thin section work and geochemistry.

Shearing of the area was in a southwest-northeast direction, broadly in the same direction as the strike of the outcrops, which was on average 234° (Fig. 4.12). All the units show shearing in the same orientation. Many of the outcrops in the Hamlin Lake area have a lenticular shape, which may be caused by the

combination of channel-like flows and deformation, however, Osterberg et al. (1987) recognized lens or wedge shapes to the outcrops of the Onaman Area of Northwestern Ontario and concluded the cause of the lensoid shape was a result of shearing deformation. At Hamlin Lake, it was determined that the cause of the lenticular-shaped outcrops was because of channel-like flows. Approximately 150 structural measurements were taken yielding an average cleavage dip of 86°S. Previous mapping projects have concluded that the area is part of a larger anticlinal fold, but measurements taken in the field showed very little variation and dips fell between 64° and 90° north. If the structural measurements evolved from facing south to north, then this would have been consistent with folding, however, field observations show that the way-up direction is south, although this conclusion is based on pillow lavas to the north of the mapping area. The only unit with obvious foliation is the mafic debris flow because of the highly concentrated incompetent chlorite matrix that resulted in a schistose fabric.

The pink breccia and the banded iron formation were the only two units that did not show prominent metamorphism or shearing. The absence of structural remnants, such as foliation, in the pink breccia suggests emplacement after peak metamorphism; this is supported by the presence of rhyolite and gabbro clasts that still show angular shapes. The banded iron formation is observed as small outcrops scattered around the Hamlin Lake area and because of the minerals present, may have been more resistant to metamorphism and consequently deformed in a brittle fashion, preserving the original layering. Originally the iron formation may have been in one continuous layer, but deformation and shearing may have caused fracturing, breaking the iron formation into larger pieces, but not destroying the original layering.

Active volcanic terranes combine volcanic and sedimentary processes, whether subaerial or subaqueous, as well as volcaniclastic processes that involve clast formation, transport and deposition (McPhie et al., 1993). At Hamlin Lake, there are massive flows, pyroclastic and volcaniclastic units, and banded iron formations. The pyroclastic rocks were generated by explosive magmatic eruptions, such as fallout deposits and redeposited pyroclastic units. All of these types of eruptions are capable of creating pyroclastic material that varies from

fine ash to blocks. The combination of these processes has created a very complex mapping area.

The rhyolitic, dacitic and andesitic units exposed at Hamlin Lake are difficult to distinguish because of similar texture and colours. The aphanitic and porphyritic textures are commonly seen in the massive silicic flows, but the matrix and composition of most of the pyroclastic units are also aphanitic because of the fine ash composition and interstitial sediment/ash mixture in the fluids that were part of the debris flows making petrography essential.

With the interfingering of the massive, pyroclastic and volcaniclastic units and poor continuous exposure, it was difficult to trace any particular unit. No specific unit or lithology is confined to any one area nor are they continuous over the mapping area, reflecting unstable depositional environments and reworked deposits. What appeared to be similar lithologies and units in the field were reclassified using geochemistry (Chapter 5) and consequently recognized not to be part of the same flows or volcanic events. The multiple lithologies in a confined area likely reflect multiple volcanic centres.

4.8.2 *Pyroclastic Flows*

Over the years, the term 'pyroclastic flow' has been misused. Pyroclastic flows are defined as hot, variably fluidized, gas-rich, high particle concentration mass-flow of pyroclastic debris (Cas and Wright, 1991). Basically, a flow must be welded to be classified as a pyroclastic flow, and geologists have been incorrectly classifying water-supported mass-flows as pyroclastic flows for years without supporting evidence of hot deposition (Cas and Wright, 1991). In general, deposits in volcanic environments that display accumulation of clasts, whether pumice or other lithologies, were loosely labeled 'pyroclastic flow(s)' without field or microscopic proof of (1) the presence of pyroclastically fragmented debris, (2) facies characteristics of pyroclastic flows or (3) evidence for a hot state of emplacement (Cas and Wright, 1991). At Hamlin Lake, many of the volcaniclastic units were initially mapped as pyroclastic flows. This was because the volcaniclastic flows consist of explosively fragmented debris, such as pumice, but really the majority of the volcaniclastic units at Hamlin Lake are redeposited,

subaqueous, pyroclastic debris flows, not primary volcanic flows. There was only one outcrop that clearly showed evidence of hot emplacement or welding, OC-202. Sample OC-202 showed fiamme (eutaxitic texture) and accretionary lapilli, supporting a hot emplacement most likely the result of an explosive magmatic eruption and fallout (Fig. 4.7). Eutaxitic texture is seen in welded tuffs and displays flattened glassy discs (fiamme) in an ashy matrix (Kearey, 2001). There are other units at Hamlin Lake that do contain volcaniclastics and pumice clasts, but do not show evidence of hot emplacement, and therefore cannot be classified as primary pyroclastic flows. Clasts that were originally formed by volcanic processes can be eroded or reworked by non-volcanic processes and then redeposited by volcanogenic-sedimentary processes (McPhie et al., 1993).

In the lower portion of the stratigraphy at Hamlin Lake, there are other outcrops that show unique textures. One outcrop shows silica nodules (Fig. 4.13b), but is relatively small, approximately 2 x 6m, and contains very round, dark-grey, 1 to 3cm in diameter silica nodules set in a white matrix. These nodules do not resemble amygdules, nor do they look like redeposited clasts. The nodules have the appearance of having fallen into the matrix because they are round and appear as if they are just sitting in the matrix. McPhie et al. (1993,

Pyroclastic flows are hot, ground-hugging and generated by volcanic eruptions. When pyroclastic flows are produced in association with the extrusion of lava flows, the flows are called block and ash flow deposits or avalanche deposits. These deposits are poorly sorted and contain lapilli- to block-sized pyroclasts that are supported in an ash matrix and can be weakly to distinctly graded. Sometimes larger fragments can be sub-angular to round because of abrasion during flow (McPhie et al., 1993). Since there are primary pyroclastic deposits at Hamlin Lake, it is thought that they were formed in a shallow water setting. There are only primary pyroclastic flows documented in shallow subaqueous settings, deep aqueous examples have yet to be demonstrated (McPhie et al., 1993). Explosive eruptions capable of generating primary pyroclastic flows are restricted to vents in subaerial and shallow subaqueous settings McPhie et al. (1993).

FIGURE 4.13 – Field photographs of two separate pyroclastic units. Photo (a) shows a pumice rich unit, while (b) shows a silica nodule rich unit thought to be formed by explosive eruption.

p.139) described similar silica nodules deposited in a shallow water environment that may have originally been steam bubbles that formed in an ignimbrite. The outcrop at Hamlin Lake displays a vug-like appearance to the nodules and a pumice clast amongst the nodules (Fig. 4.13b). Silicic nodules are diagnostic of hot, gas-supported deposition, although welding and baking of underlying deposits are also common observations seen in a hot, gas-supported deposition according to McPhie et al. (1993).

Another unique outcrop in the Hamlin Lake area is one that shows block sag, the result of a fallout deposit (Fig. 4.14). The sag structure is caused by the impact of a ballistic block which deformed the underlying ash beds. Similar structures were reported by McPhie et al. (1993; p.159) in the Tertiary Tower Hill maar rim beds of western Victoria. The larger clast has an altered rim on the outside of clast that is most likely related to hydrothermal alteration after deposition because fluids were affecting the clast from the outside in (Fig. 4.14). The clast also displays internal fracturing, which might be the result of the impact because there is no fracturing in any of the surrounding rock and the fracturing is only seen inside of the clast. This suggests that the clast was cool upon deposition, as otherwise it would have deformed plastically. This outcrop at Hamlin Lake is close to the outcrops that contain fiamme and silica nodules and is probably part of the same volcanic centre and possibly the same volcanic eruption because the textures they contain are produced by primary pyroclastic
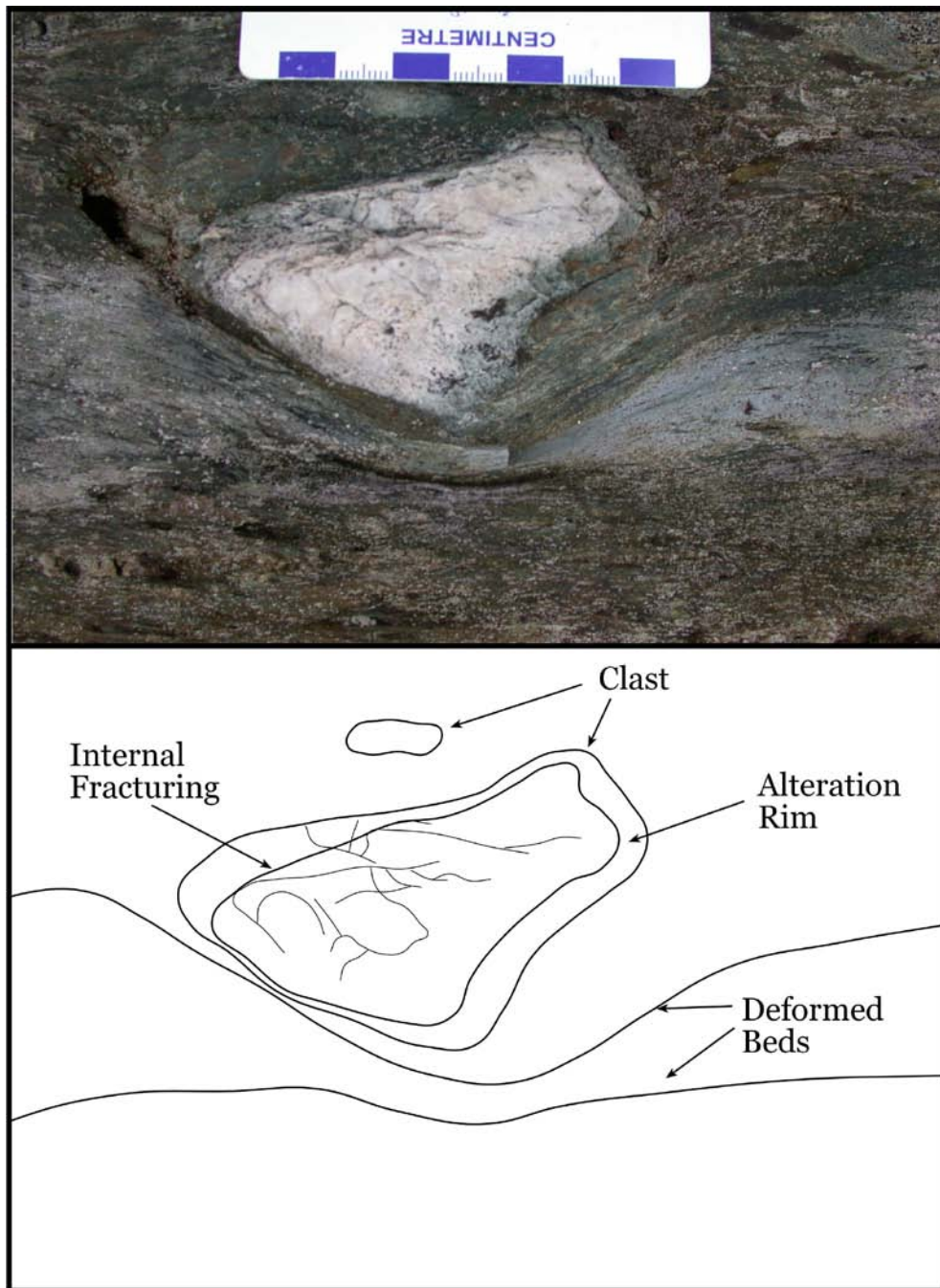
FIGURE 4.14 – A field photograph of a block sag structure (near sample AS-05-038) caused by an explosive volcanic episode. Upon impact, the block caused the underlying layers to deform and 'sag,' as well as causing internal fracturing of the clast. The field observations also show an alteration rim affecting the outer portion of the clast.

eruptions and are only found in one area. In this part of the Hamlin Lake area (Fig. 4.1), the lowest portion of the stratigraphy, there are significant quantities of tuffs and then stratigraphically above these tuffs are the fiamme and silica nodules, which then grade into the debris flows. There is also one large banded iron formation outcrop found within these pyroclastic units. At this point in the stratigraphy the debris flows begin and then increase in abundance as one moves up stratigraphy (south). The fact that the banded iron formations are located amongst the pyroclastic fallout deposits suggests that they were deposited not too far away from the hydrothermal vent. The depositional environment must have been below the wave base because waves did not disrupt the layering in the banded iron formation, nor did it disrupt the eutaxitic texture of the welded tuff that contained preserved fiamme.

4.8.3 Iron Formation

There are two common types of iron formations: Superior-type and Algoma-type. Superior-type iron formations are found in shelf-type sedimentary rocks such as dolomite, quartzite, arkose, black shale and conglomerate; volcanic rocks are minor components (Peter, 2003). Algoma-type iron formations are found within turbidites and volcanic or volcaniclastic rocks and are thought to have formed in volcanic arcs or back arcs, spreading ridges and rifts (Peter, 2003). The iron formations that are located at Hamlin Lake are Algoma-type iron formations because they occur in an area dominated by volcanic rocks. Algoma-type iron formations are precipitated from hydrothermal fluids that are contemporaneous with volcanism and are located near the site of venting fluid (Peter, 2003).

Iron formations are related to subaqueous sedimentary, specifically Superior-type iron formations (Raymond, 1995). Gross (1995) stated that, although there are many chert-magnetite iron formations associated with VMS deposits, these are generally products of distal or widespread unfocused low-temperature hydrothermal discharge (Fig. 4.15).

Peter (2003) stated that there are spatial relationships between chemical sedimentary rocks (iron formations) and volcanic-hosted sulfide deposits. These

chemical sedimentary rocks typically occur in the immediate vicinity of mineralization and can occur at the same stratigraphic horizon or slightly lower or higher (Peter, 2003). In the Bathurst Mining Camp, the iron formation covers the massive sulfide deposit and can be traced for up to 12km as a marker unit (Peter, 2003), as well as in the Finlayson Lake base metal district of the Yukon (Bradshaw et al., 2001). This is because the hydrothermal component generally makes up between 40-70% of the iron formation (Peter, 2003).

The presence of sub-angular to round, pumiceous, volcaniclastic outcrops suggests that these were subaqueous in origin. After studying the hydroclastic deposits of the Wawa and Wabigoon greenstone belts of the Superior Province, Osterberg et al. (1987) determined that the grain size, number of fragments within beds and vesicularity of fragments can be used to distinguish explosive hydroclastic from magmatic eruptions and submergent from emergent deposits, because there is an abundance of ash-sized material and low lithic content of the beds and they are very fine-grained.

4.8.4 Massive Flows

The massive, coherent lava flows are porphyritic with quartz and feldspar phenocrysts. In the vicinity of the lava flows, there are also showings of very angular clasts set in a fine-grained matrix, which is interpreted to be preserved hyaloclastite. Hyaloclastite enclosing lava lobes and pods of the Archean Abitibi Belt is documented by Yamagishi and Dimroth (1985). McPhie et al. (1993) stated that in the Ushikiri Formation of SW Japan that erupted in 200-1000m water depth, the units are composed of lobes of lava, enclosed by masses of angular fragmented breccia, interpreted to be *in situ* hyaloclastite. Similarly, in small volume rhyolitic extrusions of the Archean Abitibi Belt, lava lobes propagating from master dykes are surrounded by hyaloclastite (Yamagishi, 1987). It is common for silicic lavas to be encased or overlain by hyaloclastite (McPhie et al., 1993), so the observations of angular clasts near the massive flows could be related to the deposition of the lava flows, instead of the deposition of pyroclastic material. In order to determine if the clasts are hyaloclastite or pyroclastic it is necessary to look for either jigsaw-fit or welded textures. The

only observation not seen at Hamlin Lake that would solidify that the angular clasts are hyaloclastite or pyroclastic is if they were distinctly jigsaw-fit or welded, respectively. Although the clasts are of the same lithology, they are not jigsaw-fit, although alteration and metamorphism has destroyed many of the primary features and could be disguising important textures. Although the lava flows at Hamlin Lake are not 10's or 100's of metres thick, they do suggest a depth of deposition. At a deeper water depth, the confining pressure would be greater, therefore the lava could retain more volatiles and lower viscosity and maintain greater mobility than subaerial flows of equivalent compositions (De Rosen-Spence et al., 1980). This would produce thinner more spread out lava flows (<1m), whereas at Hamlin Lake, they are short lobes of felsic lava that are not thick units (100m), traceable or widespread.

Overall, the units are thin (~2 to 10m), the outcrop size small, the outcrops appear as low relief lobes and there is a diversity of lithologies in a relatively small area. This is interpreted as being the product of many small overlapping and coalescing volcanic flows. The overlapping and coalescing volcanic flows are interpreted as being originally deposited on unstable, sloped surfaces causing the flows to become interfingering, channel-like and lenticular in shape. This is consistent with Hart (2007) who interpreted the small lobe-like outcrops in the surrounding area to Hamlin Lake as high viscosity flows. De Rosen-Spence et al. (1980) reported that subaqueous silicic lavas can form lobes and are commonly seen in Canadian Archean rhyolites.

4.8.5 Amygdules

The amygdules that are found in some of the massive flows vary in size considerably and are evidence of water depth during emplacement. The sizes of the amygdules at Hamlin Lake vary considerably which likely reflects different eruptive environments and pressures. Most outcrops containing amygdules show sizes <0.5 to 1.0 cm, but there is one outcrop that consists of large tear-shaped amygdules that are larger than any other amygdule in the Hamlin Lake area with the largest being ~9.0cm long. The larger the amygdule, the less pressure the flow must have been under during emplacement, suggesting a shallower

emplacement. McPhie et al. (1993) proposed that in flows with large amygdules, the flows were emplaced in shallow water depth because of the low confining pressure of the surrounding water. Although amygdules are still affected by the original magma volatile content and viscosity, vesicle size and abundance is directly affected by the confining pressure (McPhie et al., 1993).

4.8.6 Debris Flows

The many units showing sub-angular to sub-rounded clasts at Hamlin Lake can be classified as redeposited pyroclastic debris units according to Cas and Wright (1991) or as resedimented syn-eruptive volcaniclastic rocks according to McPhie et al. (1993). Redeposited pyroclastic debris can be produced by debris avalanches, debris flows or turbidity currents (Cas and Wright, 1991). Debris avalanches are a rapid form of mass movement in a narrow channel down a steep slope, whereas debris flows are a sediment gravity flow process in which particles up to boulder size are supported principally by their buoyancy in, and the cohesive strength of the sediment-water slurry. Finally, a turbidity flow is a turbulent, subaqueous density current of suspended sediment driven by gravity and can occur in marine or non-marine, or shallow or deep environments (Kearey, 2001). At Hamlin Lake, the redeposited pyroclastic debris are observed as small, channel-like units that are monolithic and can be rhyolitic, dacitic or andesitic in composition. One outcrop consists of only pumice clasts. There are also a lot of channel-like outcrops that consist of redeposited chert clasts. These debris flows are probably the result of chert layers that were built up on sloped surfaces and then when becoming unstable, flowed down slope in a mud matrix. The slopes can become unstable as a result of increasing the depositional angles on the slopes or from earthquakes.

Debris flows are resedimented syn-eruptive volcaniclastic deposits that are either water-supported volcaniclastic mass flows or gravity-driven volcaniclastic mass flows that occur temporary with eruptions. Mass-flows transport clasts with air, water or volcanic gas as the interstitial fluid. At Hamlin Lake, the debris flows are matrix supported and the amount of clasts and matrix can vary between outcrops. The water supported volcaniclastic mass flows can include debris flows

to mud flows, while the gravity-driven volcaniclastic mass flows can produce volcaniclastic slides to debris avalanches. Debris avalanches are due largely to gravity acting on unstable deposits. It is unclear at Hamlin Lake exactly what type of mass flows created the debris flows, but because there is clast-dominant and matrix-dominant debris flows at Hamlin Lake it is interpreted that a combination of the two occurred.

Cohesive debris flows involve high concentration, poorly sorted, sediment-water mixtures. Fine particles totally suspended in the water create a muddy water or watery mud cohesive slurry that has enough strength to support very large clasts during 'flowage' (Lowe, 1976). These can also be called mud flows. These flows both have clast-and matrix-supported fabrics with sharp contacts and can vary from <1m to 100m. They can be polymictic or dominated by one clast type. McPhie et al. (1993) stated that in ancient sequences, establishing a primary origin for, ungraded, pyroclast-rich, monomictic mass-flow deposits that lack evidence of hot emplacement is very difficult, and hydrothermal alteration can make identifying these even more difficult. The difference between slides and debris flows is that slides are driven by gravity, and debris flows are dependent on interstitial fluids (McPhie et al., 1993). In the field it is difficult to distinguish between the two, but since the debris flows at Hamlin Lake are monomictic, with the exception of the odd clast, this supports debris flow origin because a gravity flow could pick up more clast types than a debris flow.

4.8.7 Pink Breccia

Approximately 100m north of Hamlin Lake the pink breccia unit is exposed at surface. Drilling performed on the pink breccia shows that the unit intrudes into the exposed ridge of volcanic rocks (www.eastwestres.com). The pink breccia is interpreted to be a roof pendant breccia because of the incorporation of the surrounding lithologies in the breccia. The emplacement of the Powell Lake granite to the east and south is interpreted to be the cause of the uplift and brecciation of the overlying volcanic rocks and parts of the granite. When the granite was intruding and being emplaced, the overlying volcanic rocks

and gabbro were fragmented and incorporated into the top of the granite intrusion.

4.9 Petrography

When considering all the petrographic thin sections from the Hamlin Lake area, there are common characteristics. Quartz was the most prevalent mineral found, except in a few samples where sericite alteration had been intense and made up approximately 85% of the rock. Sericite alteration is present in all the samples that were studied, some more than others. There appears to be no relationship between the area the sample was taken from and the degree of alteration. A sample taken at one outcrop could be only weakly altered by sericite or chlorite, while at the outcrop only meters away there was strong sericite or chlorite alteration present. The patchy alteration is interpreted as being controlled by the porosity and lithology of the units. Units with a higher porosity, such as the pyroclastic ones, are likely to be more susceptible to alteration. Some of the volcaniclastic units, such as the debris flows with high concentrations of pumice clasts would have a higher porosity than the debris flows with rhyolite clasts. Outcrops with a higher porosity allow hydrothermal fluids to flow through the rocks more readily. Large et al. (2001b) also recognized this pattern in the volcaniclastic rocks of the Rosebery-Hercules deposit of Australia where the very high permeability and porosity led to widespread and variable intensities of alteration. Chlorite alteration is not present in every sample, but it is prevalent in the mafic debris flows. The mafic debris flows are heavily chloritized, while the rhyolite samples only showed patches of chlorite. The heavy chlorite concentration seen in the mafic debris flows is thought to be the result of the primary composition of the matrix, which is thought to have been muddy sediment. Calcite was not regularly seen in thin section. Only a handful of samples show up to 15% calcite; seen in veinlets along with quartz, sericite and chlorite. The presence of sericite and chlorite in the Hamlin Lake area is typical of VMS alteration.

One important petrographic discovery found within the andesitic rocks was the presence of true pyroclastic material. Sample OC-202 consists of fiamme

and accretionary lapilli (Fig. 4.7c-f). The pyroclasts seen in thin section are collapsed pumice clasts which have been flattened. The wispy-shaped ends of the chloritic material suggest that they could have reacted with hot seawater causing a quick reaction with sea-water when released from the active volcanic centre into seawater and also shows fine ash material interstitially.

4.10 Alteration

Alteration occurs when existing components become unstable under changing physical and chemical conditions and alter to more stable minerals (Gifkins et al., 2005). In a volcanogenic massive sulfide (VMS) system, two main kinds of alteration can affect the surrounding area; diagenetic, caused by seawater interactions or hydrothermal, caused by hydrothermal fluid interactions (Large et al., 2001). Hydrothermal alteration related to VMS systems principally involves the breakdown of plagioclase and volcanic glass in the primary volcanic host rocks and their replacement by sericite, chlorite, carbonate, pyrite and quartz in varying proportions, depending on the zonal pattern of the individual hydrothermal system under study (Large et al., 2001).

Sericite is a white mica (muscovite) and in the field sericite alteration appears as a light greenish colour. Sericite alteration is a pervasive, replacement mineral found in the footwall of VMS systems. The sericite is concentrated in stockwork feeder zones but can found deeper in the footwall and extending into the hanging wall in some deposits (Thompson and Thompson, 1996). Sericite commonly replaces primary minerals in intermediate to felsic rocks and can be found in the Hamlin Lake area, giving the rocks an overall bleached appearance. Quartz alteration is usually closely associated with sericite alteration (Thompson and Thompson, 1996). Textures include replacement of feldspars, micas and in volcanic rocks, it can replace volcanic glass (Thompson and Thompson, 1996). Samples with higher concentrations of sericite crystals in the Hamlin Lake samples also show greater alignment. This could be the result of hydrothermal fluids flowing through the rock which has aligned the sericite crystals. The surrounding minerals do not appear to be as aligned, such as the quartz grains, suggesting that the alignment of sericite crystals is the result of hydrothermal

fluids flowing through the rock and not from pervasive regional metamorphism (Thompson and Thompson, 1996).

Chlorite alteration is most prominent in the mafic debris flow samples. Chlorite alteration is a pervasive alteration and is commonly found in the footwall of VMS systems (Thompson and Thompson, 1996). Mg-chlorite, commonly found spread around the periphery or upper part of stockwork zones, is considered to be the result of the interaction of cold seawater and hot hydrothermal fluids. The chlorite minerals are also aligned in some samples. It is suggested that this alignment is the result of dynamic metamorphism (deformation). Petrographically, the chlorite grains appear in both deep green and deep blue varieties, suggesting that there is both Mg- and Fe-chlorite occurring in the Hamlin Lake area and neither is more prevalent in samples than the other. SEM-EDS work was attempted on the samples of Hamlin Lake, but because of the fine-grained crystals, accurate analytical results could not be achieved.

Silicic alteration is not evident in the field because intermediate and felsic volcanic rocks are the most common lithology and they are originally highly siliceous, however, silicic alteration makes the hand samples look sugary in appearance. The most common appearance of rocks which had undergone silicic alteration in the Hamlin Lake area was a sugary texture and an increase in hardness.

Carbonate alteration is only recognizable in the field in veinlets and with the use of HCl, but in thin section it is not only found in veins, but also appears as single crystals. Thompson and Thompson (1996) state that carbonate alteration can occur as disseminated alteration in footwall sequences, commonly over extensive lateral and stratigraphic areas. The type of carbonate varies from siderite to dolomite depending on the host rocks, proximity to feeder zones and interaction with seawater.

4.11 Mineralization

Overall there is insufficient data to fully understand the potential of the mineralization related to the VMS system at Hamlin Lake. The LN7 sulfide lenses are thought to be the result of the same process that created the debris flows, except instead of having chert, rhyolite or pumice clasts, the debris flow incorporated massive sulfide clasts. The sulfide clasts may have originated from a larger massive sulfide deposit that was destroyed during the eruption. A second possibility for the occurrence of the pyrite clasts is that there was interbedding between shale and pyritiferous bands and over time the pyrite and shale beds were metamorphosed into the pyrite lenses that is observed today. This second idea is not as likely as the first because of the extreme resemblance of the debris flows to the LN7 sulfides it is likely the pyrite lenses originated the same way. The LN7 outcrop should be treated as a sign that the hydrothermal vent was not far away. The scenario involving the massive sulfide clasts being picked up during a mass flow and incorporated into the mass-flow deposit is the most likely of scenerios causing the unique LN7 sulfides. The massive sulfide clasts could be derived from a massive sulfide deposit during emplacement along the flow path. This is further supported by the thin sections that show the chalcopyrite located on the outside of the pyrite and never interstitially, meaning the chalcopyrite was deposited after the pyrite.

4.12 Historical Mapping Projects

Previous mapping projects by Giblin (1964), Hodgkinson (1968) and Harris (1970) uncovered similar features to those observed during this project at Hamlin Lake (Fig. 3.7). Harris (1970) mapped around the Hamlin Lake area and identified similar geological units to those recognized during this study, but at a broader scale. The felsic to intermediate rocks that were mapped by Harris (1970) are concentrated in the same volcanic belt as Hamlin Lake and run southwest-northeast across the Shebandowan belt. A dacite tuff was described as having quartz phenocrysts and being closely related to the felsic agglomerate units. The dacitic agglomerates Harris (1970) described are closely related to the dacitic ash layers observed in the Hamlin Lake area. The dacite units of Hamlin

Lake consist mostly of quartz, white mica (sericite), chlorite and minor amounts of biotite, similar to the intermediate to felsic units described by Harris (1970).

Hodgkinson (1968) mapped a variety of felsic volcanic units as agglomerates and their descriptions, fragments elongated with schistosity, are extremely similar to the debris flow units found in the Hamlin Lake area. Although Hodgkinson (1968) describes the agglomerates vaguely, pictures of these outcrops are similar to the mafic and felsic debris flows observed in the Hamlin Lake area (Hodgkinson, 1968). Based on the Hamlin Lake work, these can be reinterpreted as debris flows, a common occurrence amongst volcanogenic massive sulfide deposit host rocks (Hodgkinson, 1968). Hodgkinson (1968) commented that a lot of the agglomerate underwent sericite alteration and some rhyolites were completely sericite schist. Another similar characteristic between the Hamlin Lake and Hodgkinson's (1968) mapping project is that the rhyolite packages are generally long and narrow, which Hodgkinson (1968) ascribes to the high viscosity of felsic lavas and that the long and narrow bands are pyroclastic layers.

An agglomerate "fragmental" was also described by Giblin (1964) when mapping the Burchell Lake area to the north of Hamlin Lake. He observed the same lenticular shape to the felsic fragments that are set within a schistose mafic matrix, similar to the description of the debris flows described at Hamlin Lake. The debris flows mapped at Hamlin Lake change rapidly from debris flows with high concentrations of clasts, to debris flows with half the concentration of clasts, and then within metres there will be a felsic to intermediate volcanic unit suggesting multiple eruptions in an unstable area by the amount of small flows. This is consistent with the earlier observations at Hamlin Lake that the debris flows were deposited on a sloped surface.

Debris flows are not uncommon in VMS deposits. The Myra Falls and Kutcho Creek deposit of British Columbia both have debris flows in the vicinity of the VMS mineralization (Barrett and MacLean, 1999; Bridge et al., 1986). Bridge et al. (1986) interpreted the rapid facies change of the rhyolitic pyroclastic rocks and the debris flows of the Kutcho Creek deposit to suggest that hydrothermal activity and fissure-related felsic eruptions occurred in close proximity in an
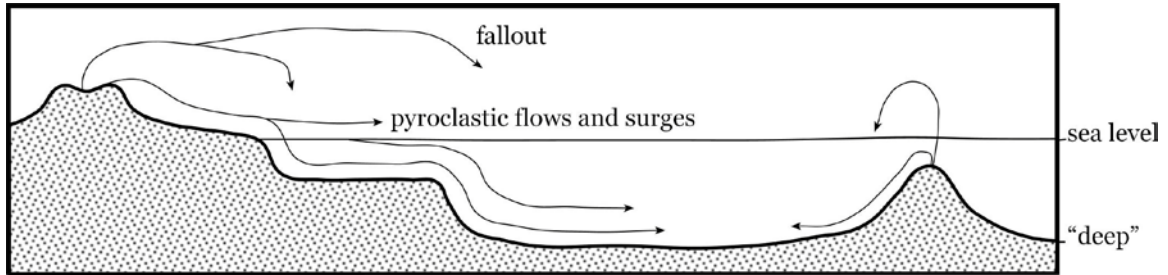
Figure 4.15 – A cartoon image of the possible environments in which pyroclastic units form (*modified from* McPhie et al., 1993).

extensional setting with significant sea-floor relief. This further supports the interpretation of an increase in explosive activity at Hamlin Lake as one moves up in stratigraphy (south). The debris flows and rapid facies change suggests a high relief in stratigraphy.

The redeposited pyroclastic material observed at Hamlin Lake is frequently angular to subangular. It can be interpreted that the larger and more angular the clasts the closer to a volcanic centre, however Lesher et al. (1986) recognized that felsic clasts can be transported considerable distances during explosive eruptions and highly angular pyroclastic material is sometimes incorrectly interpreted as being close to the volcanic centre, but it is not an accurate method for estimating the center of volcanic activity. At Hamlin Lake, the lenticular-shaped outcrops consist of redeposited pyroclastic material in various sizes, shapes, lithologies and concentrations over the scale of the mapping area. Some outcrops have a high concentration of clasts because of a clast supported deposition, while others have very few clasts suggesting a matrix supported deposition. The variation seen in pyroclastic clasts and lithologies at Hamlin Lake are interpreted as the contribution of more than one volcanic centre, while the lenticular shape of the outcrops is thought by the author to represent deposits that were formed close to the volcanic centre because of their high relief. This is consistent with the work of McPhie et al. (1993) who stated that when a volcanic area contains both pyroclastic flows and layered ash falls it can be interpreted as being created by several eruptions. Subaqueous silicic lava flows do not extend more than a few kilometres from the source and are a good indication of proximity to a vent, within a few kilometres for a flow (McPhie et al.,

1993). Some Archean subaqueous rhyolites extend up to 10km from the source, suggesting that the lavas erupted in deep water because the deeper the water, the higher the pressure which lowers the viscosity and allowing lavas to flow long distances (McPhie et al., 1993). When studying the Timiskaming area of Kirkland Lake, Cooke and Moorhouse (1969) interpreted the lenticular form and interfingering of the volcanic flows as the result of their closeness to the center of volcanic activity. The presence of flows, tuffs and volcanic breccias was also an indication of a volcanic centre for Cooke and Moorhouse (1969), who stated that the actual volcanic structure may have been destroyed by the intrusion of a stock. At Hamlin Lake, the Powell Lake intrusion is located approximately a hundred metres from the volcanic rocks on surface (Fig. 4.1). Hamlin Lake has the combination of flows, pyroclastic flows, tuffs and volcanic breccias in a small area (~6km²), along with lenticular-shaped flows and interfingering of lithologies, all signs of being near a volcanic centre. The presence of the pink breccia, which is the combination of pink granite, rhyolite, gabbro and feldspar porphyry clasts, all lithologies derived from the surrounding area, supports the observation that the Powell Lake intrusion may have destroyed additional evidence of the volcanic center.

It is clear from the pyroclastic debris, tuffaceous material and lenticular-shaped flows that are interfingering at Hamlin Lake, that more than one volcanic centre contributed to the deposits located there. As one moves up in the stratigraphic column (north to south), the deposits and depositional environments change drastically. The lower stratigraphy displays thicker units of ash and lapilli tuff and one outcrop clearly displays petrographic evidence of fiamme structures and accretionary lapilli. As one moves up stratigraphy, it is clear that the eruption products change from a finer-grained ash to larger lapilli and then to clastic fragments and eventually silicic nodules. This could be a sign that the eruptive environment became more explosive. It is at this point in the stratigraphy that the cohesive debris flows are found as well. This could represent the point at which the eruptive column collapsed from stronger explosions and the debris flows began in response to larger amounts of volcaniclastic debris being deposited during explosive eruptions. At the same

stratigraphic level, but in the western portion of the mapping area, the massive lava flows begin and the debris flows become abundant.

4.13 Summary

Overall, the majority of the outcrops at Hamlin Lake are pyroclastic in texture. The pyroclastic texture can be difficult to distinguish because of similar colour and alteration between the clasts and the matrix. When closely examined, many of the clasts have a pumiceous texture (Fig. 4.13a) and because of the differing clast sizes and lack of exposed contacts, it is difficult to interpret exactly what processes deposited these pyroclastic units and in what depositional environment. Along with the pyroclastic units showing varying depositional processes and clast types, there is also ash layering, massive flows, debris flows (which are closely related to the pyroclastic deposits) and banded iron formations.   These units suggest a subaqueous environment, however, determining the depth of deposition is difficult. McPhie et al. (1993) stated that in ancient settings, establishing whether the environment is subaqueous or subaerial for silicic lava flows was based on the close spatial association of coherent lavas, *in situ* hyaloclastite and resedimented hyaloclastite along with the presence of lobes. At Hamlin Lake, hyaloclastite is thought to be present, and some of the outcrops that are labeled volcaniclastic could be resedimented hyaloclastites, and all outcrops are lobe shaped.

The geology is complex at Hamlin Lake because of the numerous small outcrops, and differing textures/concentrations of clasts from one outcrop to the next. The presence of massive rhyolite flows and perhaps hyaloclastite, along with pyroclastic flows all in a small area suggests that this area was affected by more than one volcanic centre, but because of the alteration that has camouflaged the majority of the primary textures it is difficult to interpret.   The primary pyroclastic textures seen in thin section were generated by explosive magmatic eruptions, while the channel-like shapes to the units and lenticular outcrop shapes reflect an unstable depositional environment. The presence of the hot emplacement of the pyroclastic flows especially the silica nodules are diagnostic of a shallow environment. The iron formations are also a good indication of

depth of deposition. Since the iron formations are a product of hydrothermal discharge they had to be produced at a depth of 2-3km. If the volcanic rocks were emplaced in a deep environment, then the confining pressure of the water column would cause the flows to be thin and widespread, whereas at Hamlin Lake, the flows are lobe-shaped and are not <1m or widespread suggesting a shallower environment. The occurrence of large amygdules also provides further proof that the confining pressure was low, allowing the vesicles to remain large. In conclusion, the field evidence suggests multiple eruptive centres erupting in 1-2 km water depths in the vicinity of a VMS system.

CHAPTER 5

GEOCHEMISTRY

5.1 Introduction

Major and trace element analyses were undertaken on 200 samples of andesitic to rhyolitic volcanic and volcaniclastic rocks of the Hamlin Lake area. Weak to intense hydrothermal alteration is seen in hand sample and in thin section, so geochemical analyses can be used to help quantify the intensity of the alteration. Unraveling a volcanic sequence in Archean greenstone belts is complicated because mineralogical, textural and chemical characteristics of rocks are often overwritten by hydrothermal alteration and metamorphism, leading to incorrect classification of field identifications and rock affinities (MacLean and Barrett, 1993).

Large et al. (2001) stressed that lithogeochemistry is used mostly to try to answer a series of questions relating to a deposit. In this study, the main questions to be answered by the geochemistry are: (1) What samples are the least altered and what are their field relationships if there are any? (2) What does the geochemistry show us about the tectonic setting? and (3) is the alteration related to a hydrothermal system and if so, how is this alteration related to the mineralization? These questions will be answered in the following section.

5.2 Major Element Mobility

When examining an area that is suspected to have undergone alteration related to hydrothermal fluids, such as that associated with a volcanogenic massive sulfide (VMS) system, it is important to first study the major elements to determine the extent of the elemental mobility before classifying the suite of rocks. Element mobility describes the chemical changes which take place in a rock after its formation (Rollinson, 1993). In the case of the Hamlin Lake suite, element mobility took place during interaction with hydrothermal fluids and/or metamorphism. Element mobility is dependent upon the stability and composition of the minerals in the unaltered rock, the stability and composition of the minerals in the alteration product and the composition, temperature and
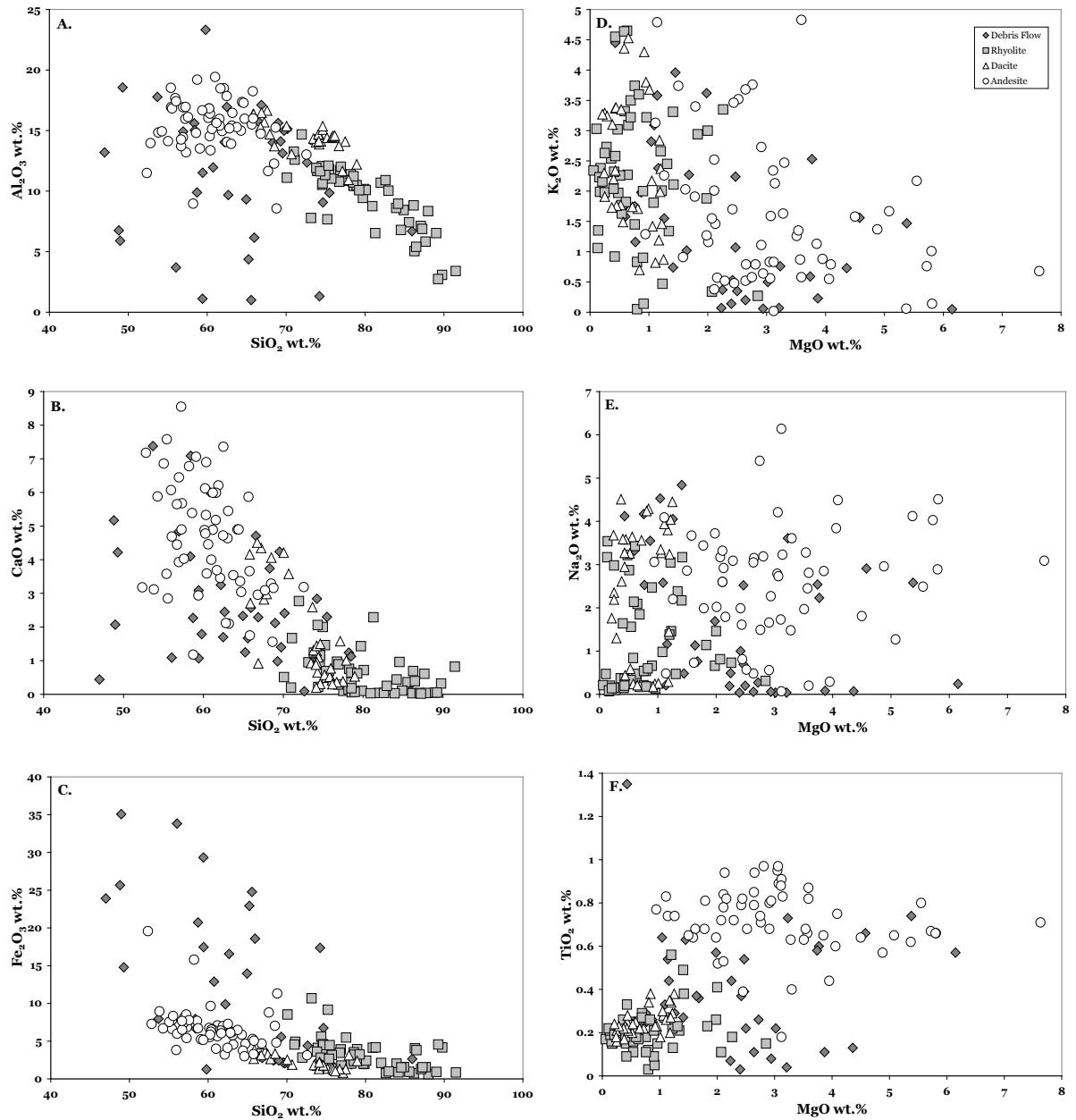
FIGURE 5.1 – Variation plots of (A) SiO$_2$ versus Al$_2$O$_3$ wt.%, (B) SiO$_2$ versus CaO wt.%, (C) SiO$_2$ versus Fe$_2$O$_3$ wt.%, (D) MgO versus K$_2$O wt.%, (E) MgO versus NaO$_2$ wt.% and (F) MgO versus TiO$_2$ wt.%. Plots D, E and F show considerable scatter for the andesite samples, while plots D and E show the most scatter of the rhyolite samples, and finally the dacite samples show the most scattering in plots A, B, D and E. The debris flow samples show scattering in all plots because of the difficulty in separating the matrix from the chert clasts, leading to compositional differences and reflecting their non-igneous nature. Legend in plot D can be applied to each plot.

volume of the altering fluids (Rollinson, 1993). Elemental mobility can be determined by scattered trends on variation diagrams, a result of mass and volume changes arising from the removal or addition of elements (Rollinson, 1993). Rollinson (1993) noted that under hydrothermal conditions the elements Ti, Al and P are generally immobile, whereas the elements Ca and Na are almost always mobile. In Figure 5.1, the elements Al, Ca and Fe appear to be the most immobile because they show the least scatter, whereas the elements K and Na appear to be the most mobile because of the scatter of data points. Campbell et al. (1984) showed that the major, large ion lithophile (LIL) and transition elements are mobile in pervasively silicified, sericitized and chloritized low-grade areas surrounding alteration pipes in VMS systems. A deposit has not yet been recognized at Hamlin Lake, but it does host silicic, sericite and chlorite alteration. The scatter of data points in Figures 5.1 and 5.2 show that there is mobility of some of the major elements, however, the tight clusters seen in some elements (e.g. Al_2O_3, Fe_2O_3, TiO_2) prove that not all the major elements were mobile indicating that hydrothermal alteration may not have been completely destructive.

A very common way to classify volcanic rocks is with the total alkalis-silica diagram (TAS). This diagram plots SiO_2 wt.% versus K_2O + Na_2O wt.% and classifies data into several areas from ultramafic to high silica felsic rocks (Fig. 5.3). The mobility of silica, alkaline and alkaline earth elements within felsic and intermediate-felsic volcanic rocks during hydrothermal processes precludes their use as a definitive petrogenetic indicator (Lentz, 1999). Barrett et al. (1993) also supported the idea that classification diagrams comparing alkalis and silica content were not reliable due to the mobile nature of these elements. Until recently, SiO_2 wt.% was the basis of many of the original classification schemes, however, the importance of classification schemes using immobile and rare earth elements (REE) is now recognized (Barrett and MacLean, 1993; Hart et al., 2004). Initially during this study the rocks of the Hamlin Lake area were plotted on a TAS diagram to get a general understanding of the lithologies making up the Hamlin Lake suite, but because of the mobility of major elements during hydrothermal alteration, the TAS classification is not reliable or accurate for
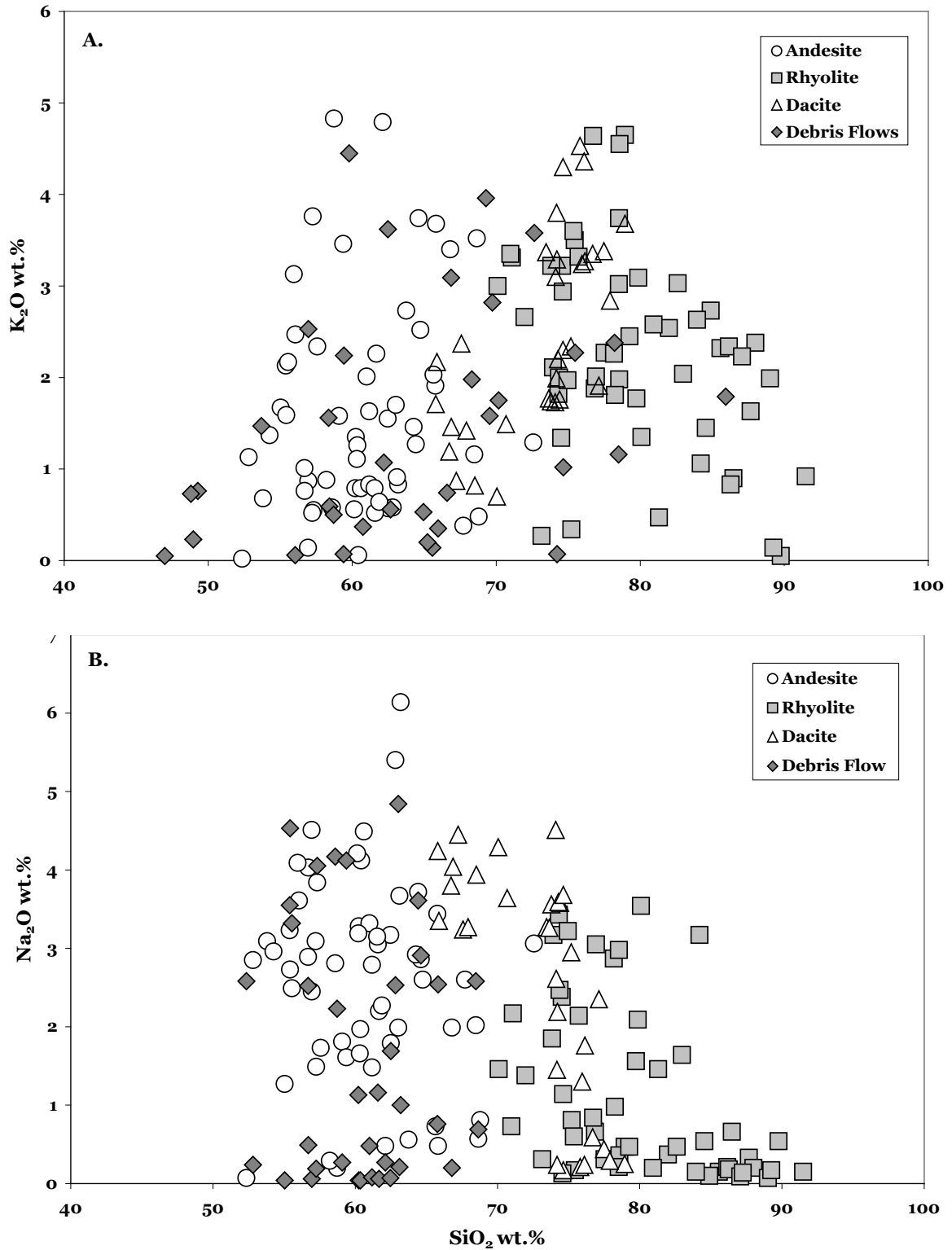
FIGURE 5.2 – Plots of (A) SiO$_2$ versus K$_2$O wt.% and (B) SiO$_2$ versus Na$_2$O wt.%. The scatter of the data for all lithologies shows the mobility of Na and K, and that this rock suite was affected by alteration. Note: samples were classified using a combination of Zr vs. Ti classification and PM spidergram plots, explained later in the chapter.

distinguishing between different lithologies (Fig. 5.3). The Hamlin Lake samples were initially classified using the combination of a Zr versus Ti plot and spidergram plots, as these elements are considered to be immobile even in hydrothermally altered suites of rocks.

In Figure 5.2, the rhyolite samples range from approximately 70% to 90% SiO_2 wt.%, the dacite samples from approximately 67% to 77%, while the andesites range from approximately 52% to 68% SiO_2 wt.%. The evidence of silicification recognized in hand sample and thin section suggests that these silica contents do not represent primary compositions.

Even though major element compositions are not a reliable way to classify hydrothermally altered rocks into different lithologies, one use for them is to estimate the degree of alteration in a given sample. Barrett and MacLean (1993;
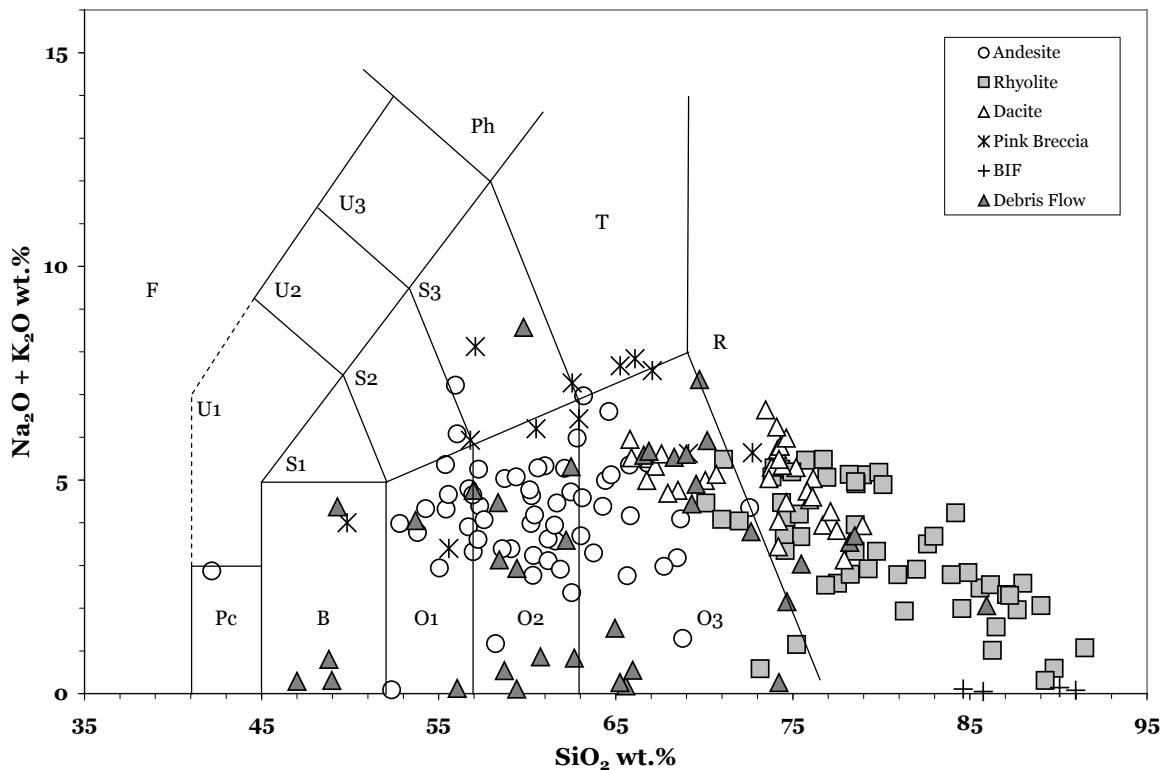
FIGURE 5.3 - A silica vs. total alkalis diagram showing classification of the Hamlin Lake samples. (Symbols: B-Basalt, O1-Basaltic Andesite, O2-Andesite, O3-Dacite, R-Rhyolite, T-Trachyte or Trachydacite, Ph-Phonolite, S1-Trachybasalt, S2-Basaltic trachyandesite, S3-Trachyandesite, Pc-Picrobasalt, U1-Basanite or Tephrite, U2-Phonotephrite, U3-Tephriphonolite, F-Foidite). Source of fields after Le Maitre et al. (2002). The six lithologies shown in the legend were classified using other methods (later in this chapter), not the TAS method.

74

1991) use Na$_2$O wt.% to separate the least-altered rocks from the moderately to intensely altered rocks in felsic volcanic suites related to VMS deposits. Barrett et al. (1993) found that to determine the samples with the least alteration in intermediate to felsic volcanic suites it is necessary to look at samples with Na$_2$O wt.% ranging between 3-5%. Figure 5.2 shows that more than half of the 200 samples are below 3 wt.% Na$_2$O, and one-quarter lie below 1%. These low levels suggest that Na depletion has occurred as a result of hydrothermal alteration. With sericite alteration, there is a loss of Na$_2$O and a gain of K$_2$O, because of the breakdown of feldspars (Lentz and McCutcheon, 2006). The samples that lie below the 1% mark have undergone intense hydrothermal alteration. This is confirmed in thin section where samples showing <1% Na$_2$O wt.% also show intense sericite alteration. Samples lying above 3 wt.% and up to 6 wt.% are considered weakly altered, which is consistent with thin section observations.

5.3 Trace Element Immobility

As major elements show element mobility in Hamlin Lake rocks, it is necessary to determine and demonstrate that hydrothermal alteration did not affect the normally immobile elements. Campbell et al. (1984) demonstrated that rare earth elements (REE), which are typically immobile, can become mobile in alteration pipes below massive sulfide deposits. Low-grade alteration does not commonly mobilize the REE's, but in large and intensely altered VMS systems, such as Kidd Creek, the light rare earth elements (LREE), middle rare earth elements (MREE) and Y have been shown to be mobile and depleted beneath ore zones (Campbell, 1984). The high field strength elements (HFSE) were the only elements that remained immobile during the alteration at Kidd Creek. Campbell et al. (1984) also noted that the degree of REE mobility is a useful indicator for distinguishing between small and large massive sulfide deposits.

Trace element mobility can result from either, ionic exchange between a mineral and the metasomatic fluid or by dissolution of a mineral containing a significant concentration of the element, although it is noted by Campbell et al. (1984) that the former is not as likely as the latter. Campbell et al. (1984) did note that to demonstrate if the trace elements have become mobile in a system,

one must know the range of trace element concentrations in the rock before and after alteration as if the trace elements have in fact become mobile, then the ratios should vary between the altered and unaltered rocks. When studying the geochemistry of the Hamlin Lake rocks, the least-altered rhyolite samples were compared to sericite-chlorite altered rhyolites and there appears to be no difference between the overall REE abundance of the two categories of rocks. This suggests that even though the Hamlin Lake area underwent intense alteration in places, the REE abundances were not affected and therefore can be trusted for classification and interpretation.
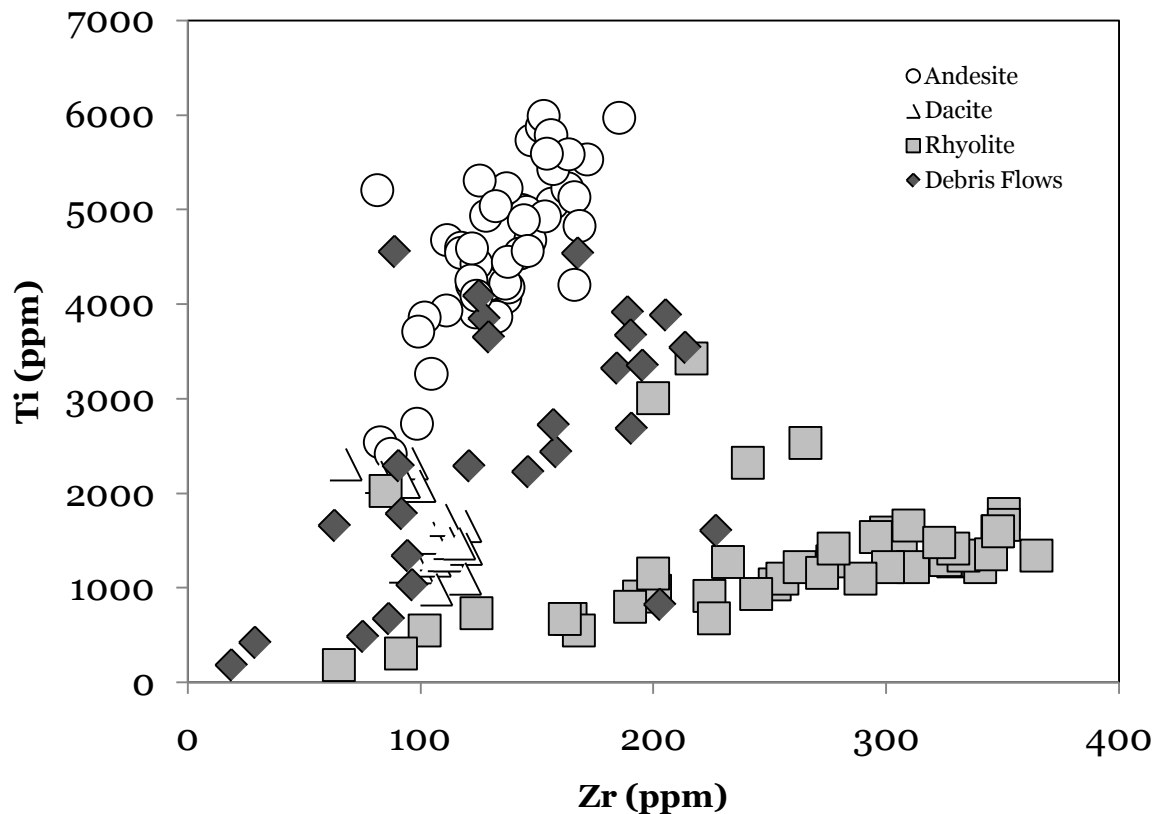
FIGURE 5.4 – A plot of Zr (ppm) versus Ti (ppm) showing all the samples of the Hamlin Lake area. Hydrothermal alteration in the area prevents the use of only mobile elements in classifying volcanic suites, so it is necessary to incorporate immobile elements as well.

5.3.1 Zr versus Ti

Using a combination of major elements and immobile elements is the best way to classify hydrothermally altered rocks and truly understand the lithologies of an altered suite of rocks. Barrett et al. (1991; 1993 a,b) have used Zr versus Ti in numerous studies involving highly altered rocks associated with massive sulfide deposits and hydrothermal alteration. Zr is useful because it is immobile, highly incompatible and sufficiently abundant in volcanic rocks for analysis, while Ti has been proven in numerous studies to be immobile in alteration zones surrounding VMS systems in greenstone belts (MacLean and Barrett, 1993).

When the volcanic rocks of Hamlin Lake are plotted on a Zr versus Ti diagram (Fig. 5.4) distinct groups of samples are recognized. In the field the volcanic units are the most difficult to classify because alteration has changed their appearance, whereas the BIF, debris flows and pink breccia were easier to classify because of their distinct appearance. In the field it was nearly impossible
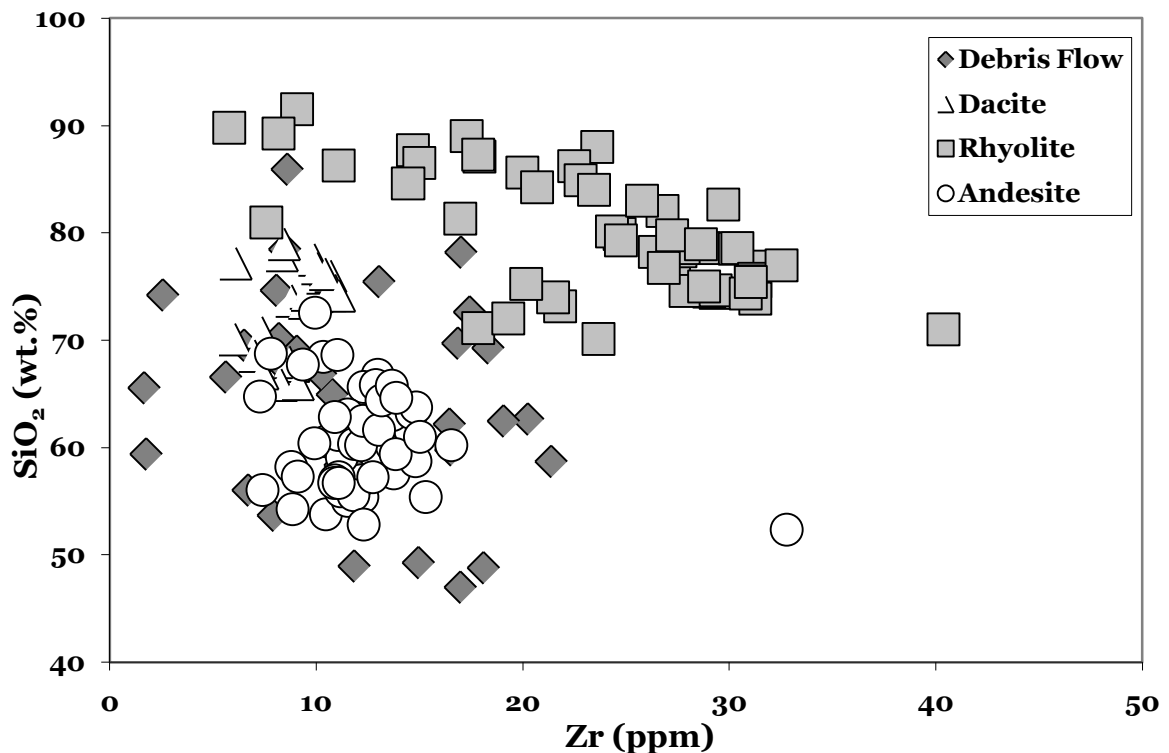
FIGURE 5.5 – A plot of Zr versus SiO$_2$ wt.% showing the clustering of the andesite and dacite volcanic rocks and the mobility of the rhyolite samples.

to distinguish the different volcanic lithologies because of the lack of primary textures and minerals, and the overprinting of alteration minerals. On the Zr versus Ti plot the rhyolites, dacites and andesites plot along distinct trends. To clarify the reason for the larger spread of data points, Zr versus SiO_2 (wt.%) was plotted to determine if Zr was mobile. Figure 5.5 shows that while the andesite and dacite volcanic rocks remain in a cluster, the rhyolite volcanic rocks do show some mobility, especially in the Zr. The samples that are furthest away from the main clusters in Figure 5.5 show low Na_2O (wt.%) values and high LOI values as well, indicating that they were more altered than others.

5.3.2 TiO_2 and Al_2O_3

Rock types can also be identified using immobile-element ratios involving Al_2O_3 (wt.%), TiO_2 (wt.%) and Zr (ppm) as discussed by Barrett et al. (2005). Plotting Zr versus TiO_2 does show the main subdivisions between the andesite, dacite and rhyolite volcanic rocks, but it is necessary to use other immobile elements to determine whether there were more subdivisions to be made within the units that may represent different magmas.
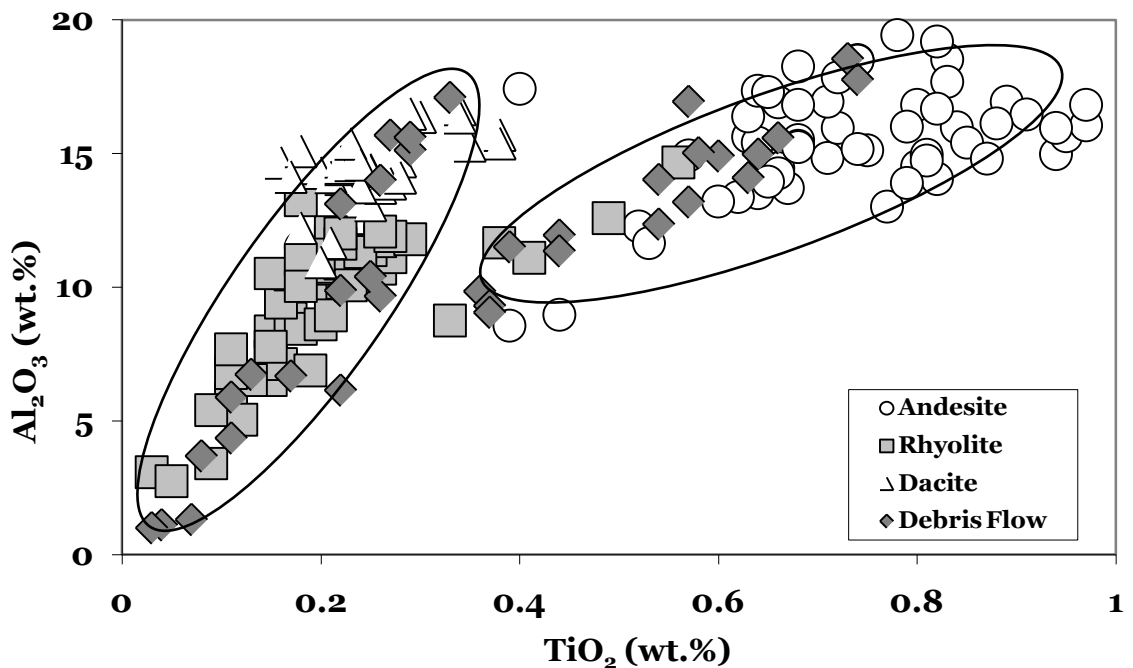
FIGURE 5.6 – A plot of TiO_2 vs. Al_2O_3 wt.% shows that there is distinct suites of rocks. Difficulty in separating out the matrix from the chert clasts in the debris flow samples led to mixed compositions and therefore those samples do not conform with the two suites.

If alteration had affected Zr, Al or Ti, then there would be less clustering of samples and the samples would be more spread out. Even though Al and Ti are major elements, they are typically considered to be immobile in hydrothermal systems (Barrett et al., 1999). Proof of their immobility is important when using classification schemes because in some cases, immobile elements can become mobile. Figure 5.6 is a plot of TiO_2 wt.% versus Al_2O_3 wt.%, showing a clustering of data points. Clustering of data points proves that the elements did not become mobile during alteration. If the elements had become mobile, then the data points would become scattered because the elemental concentrations had changed. Figure 5.6 shows that there are distinct differences between the andesites, rhyolites and dacites and even further supports the Zr vs. TiO_2 plot distinguishing between the main lithologies and can be used to help distinguish between flows in different units. Figure 5.6 shows two distinct rhyolite units, but does not show any variances in the andesite and dacite groups. The five rhyolite samples that plot away from the main cluster show intense alteration in thin section and when studying their geochemistry. Figure 5.6 shows that there is a distinct separation between the majority of the rhyolites and dacites and between the andesites. This could mean that there were two separate magma batches causing the separation of sample clusters.

5.3.3 Alteration Indices

To determine the least-altered rocks in this study, the alteration box plot (Large et al., 2001a) was used. When dealing with an altered suite of rocks, it is important to separate the least-altered samples, from the moderately or intensely altered samples. A simple approach to distinguishing between the least and most altered samples is by plotting them on a graph that uses alteration indices. Alteration box plots are a useful tool for relating lithogeochemical data to mineral assemblages and alteration intensity in VMS systems, but should always be used in conjunction with hand sample and field observations.

The alteration index was first developed by Ishikawa et al. (1976) for use on the plagioclase-destructive hydrothermal alteration systems of the Kuroko VMS deposit (Japan). The alteration index (AI) is a combination of the ratio

between the main rock-forming elements gained during chlorite and sericite alteration ($MgO + K_2O$) over the elements lost ($Na_2O + CaO + MgO + K_2O$) during the breakdown of Na-plagioclase and volcanic glass (eqn.1; Ishikawa, 1976). The AI usually reaches maximum values (100) in the proximal hydrothermal zone beneath massive sulfides (Gifkins et al., 2005). The range of AI numbers can vary considerably for unaltered (20-60) and altered rocks (50-100), but the ranges can vary depending on each individual suite of rocks. High AI values (>60) reflect high MgO and K_2O contents relative to CaO and Na_2O and may be related to intense hydrothermal sericite and chlorite alteration, but does not differentiate between the two (Gifkins et al., 2005). However, low AI values (<30) signify high CaO and Na_2O contents, the result of albite or calcite alteration. The direct relationship between Na_2O depletion and AI value means that the closer to 100 a sample gets on the AI index, the more replacement of feldspars and glass by sericite or chlorite there was (Large et al., 2001a).

(eqn.1)
$$AI = \frac{100(K_2O + MgO)}{(K_2O + MgO + Na_2O + CaO)}$$

The two biggest limitations of this classification scheme are: (1) it does not take into account carbonate alteration; and (2) when used by itself, it does not allow for the separation between chlorite and sericite alteration (Large et al., 2001a).

Figure 5.7a shows the relationship between Na_2O wt.% and AI for the Hamlin Lake volcanic rocks and demonstrates that there is a direct relationship between Na depletion and an increase in AI. Samples found in the lower right corner with the highest AI are the most altered and have become mostly chlorite and/or sericite; this is further supported by thin section observations. Figure 5.7b shows the opposite trend, with K_2O wt.% increasing with the AI. From looking at Figure 5.7, the Hamlin Lake rocks clearly show that not all samples have been intensely altered because of their location away from a value of 100 on the AI and through petrographic work. Gifkins et al. (2005) stated that AI ranges
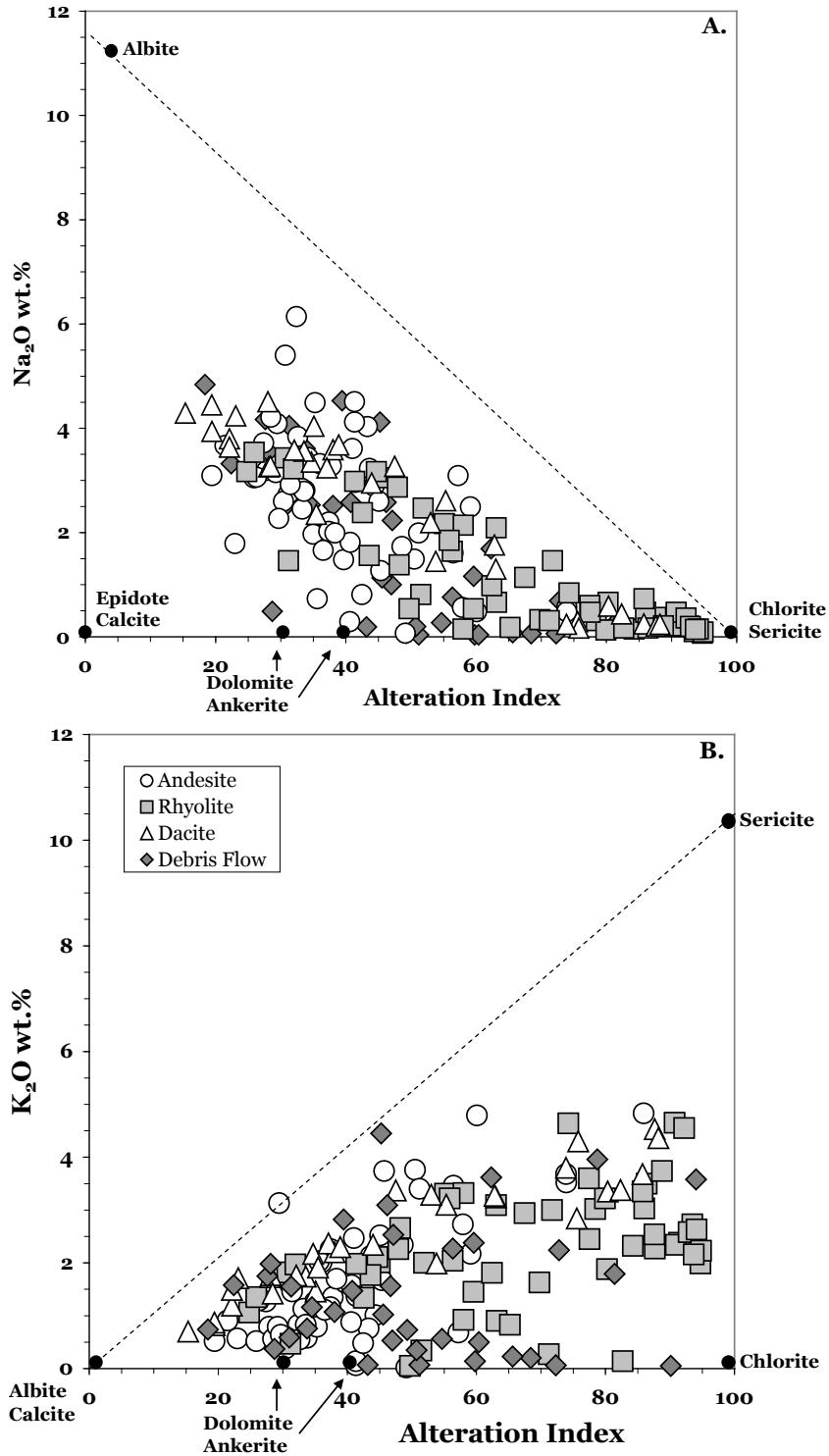
FIGURE 5.7 – Trends of AI with (A) Na₂O wt.% and (B) K₂O wt.% for the Hamlin Lake rocks. Samples with an AI >60 are considered to be affected by alteration due to hydrothermal alteration (*after* Large et al., 2001). Black dots represent the alteration mineral compositions that plot around the margins of the alteration box plot. The dashed line signifies between diagenetic and hydrothermal alteration. Samples that plot below the dashed line represent hydrothermally altered rocks.

81
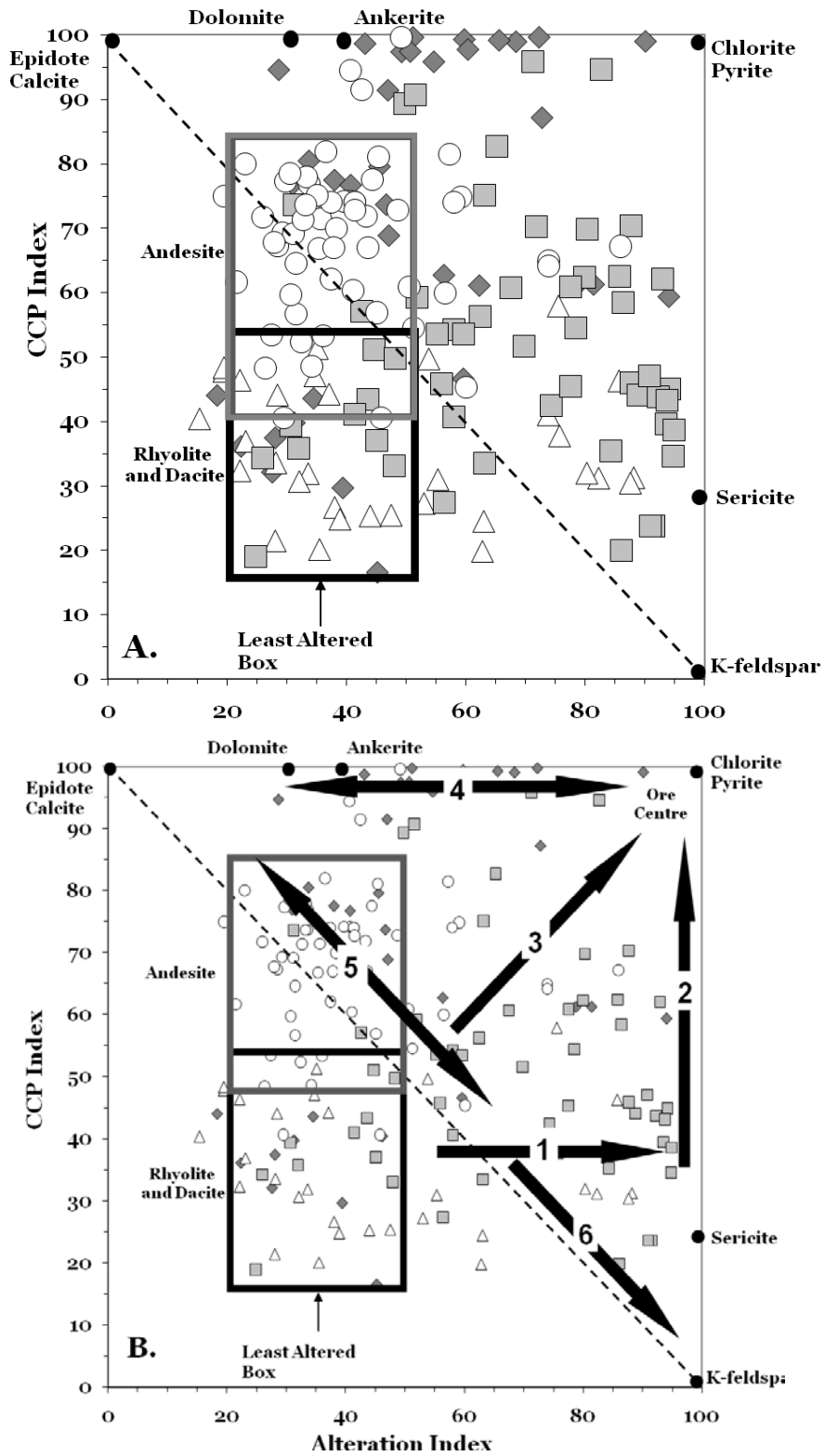
FIGURE 5.8 - An alteration box plot of the Hamlin Lake samples showing distinct hydrothermal alteration, especially in the rhyolitic samples. See text for discussion of alteration patterns.

for subtly, weakly, moderately, strongly or intensely altered rhyolites, dacites, andesites and basalts are similar.

To correct the limitations of the AI index, Large et al. (2001a) created the chlorite-carbonate-pyrite index (CCPI; eqn.2) which when plotted against AI (Fig. 5.8) helps overcome the limitations of the AI and allows for a better understanding of which type of alteration is affecting the chosen samples and which alteration minerals are the most prevalent.

$$\text{(eqn.2)} \qquad \qquad CCPI = \frac{100(MgO + FeO)}{(MgO + FeO + Na_2O + K_2O)}$$

The CCP index was modified from Lentz's (1996, 1999) alteration index so it could be compared to the Ishikawa AI (Large et al., 2001a). High values of the CCPI indicate high FeO and MgO contents, suggesting intense alteration to Fe- or Mg-rich minerals such as chlorite, Fe-Mg-bearing carbonates, pyrite, magnetite or hematite. The CCPI is better suited for felsic rocks because it is sensitive to MgO and FeO contents that make up mafic rocks, and because CCPI is influenced by primary composition, more evolved felsic rocks have lower CCPI values (10-50).

A limitation of the CCP index is that it is affected by magmatic fractionation (Fig. 5.9a). Figure 5.9a shows that when the CCPI is plotted against SiO_2 wt.% there is a distinct fractionation trend from the andesite samples to the dacite samples, and some of the rhyolite samples. When plotting these same samples against AI (Fig. 5.9b), alteration trends are shown by the scatter of data points, instead of being influenced by following a fractionation trend, seen in Figure 5.9a, where the data points show a linear trend. Another limitation is that even the slightest trace of chlorite will result in the CPPI value equaling 100. A further limitation of both the AI and the CCP index is that neither of these plots includes SiO_2 and therefore does not provide a direct measure of intensity of quartz or silica alteration (Large et al., 2005).

The advantage of using alteration box plots is that only major elements are required the equations used are simple; and the data is easy to interpret. When

using the alteration box plot, the least-altered volcanic rocks plot towards the centre of the diagram, whereas the more hydrothermally altered rocks plot away from the least-altered box towards the alteration minerals indices that are located towards the edges of the plots (Fig. 5.8b). The least-altered box for the Hamlin Lake volcanic rocks was defined by the samples which have undergone the least-alteration. In most hydrothermally altered systems, all rocks have undergone some alteration so it is unrealistic to define unaltered samples. An important step before plotting samples on the alteration box plot is to identify the least altered rocks in the suite of rocks. Large et al. (2001a) used a combination of sodium content ($2<Na_2O$ wt.%<5) and petrographic studies to distinguish the least-altered rocks from the more intensely altered ones. Although in other studies such as Barrett et al. (1993), a range of $3<Na_2O$ wt.%<5 was used to distinguish least-altered rocks along with petrography. The samples with the least alteration were defined by Na_2O contents and petrographic thin section observations. The least-altered rocks of Hamlin Lake were separated by the Na_2O wt.% range of Barrett et al. (1993) because after looking at this range of samples and thin sections, these samples contained the least alteration. Another technique used by Large et al. (2005) was to look at the Ti/Zr ratio, where rhyolites have Ti/Zr<10, dacites 10-20, and andesites and basalts are >20. The rocks in this study were classified using a combination of Zr versus Ti plots and primitive mantle-normalized spidergram plots, but the samples generally fall within the classification schemes of Large et al. (2001a, 2005). Samples that had a Na_2O wt.% content greater than 3 wt.% were considered the least altered. Samples with less than 3 wt.% Na_2O were considered altered and the greater the Na_2O wt.% value below 3 wt.%, the greater the hydrothermal alteration. This was based on observations of modern arc calc-alkaline rhyolites by Barrett et al. (1993) and has been applied to altered hydrothermal systems of the Mount Read volcanic rocks and the Rosebery and Hercules VMS deposits all of western Tasmania by Gifkins and Allen (2001) and Large et al. (2001b), respectively.
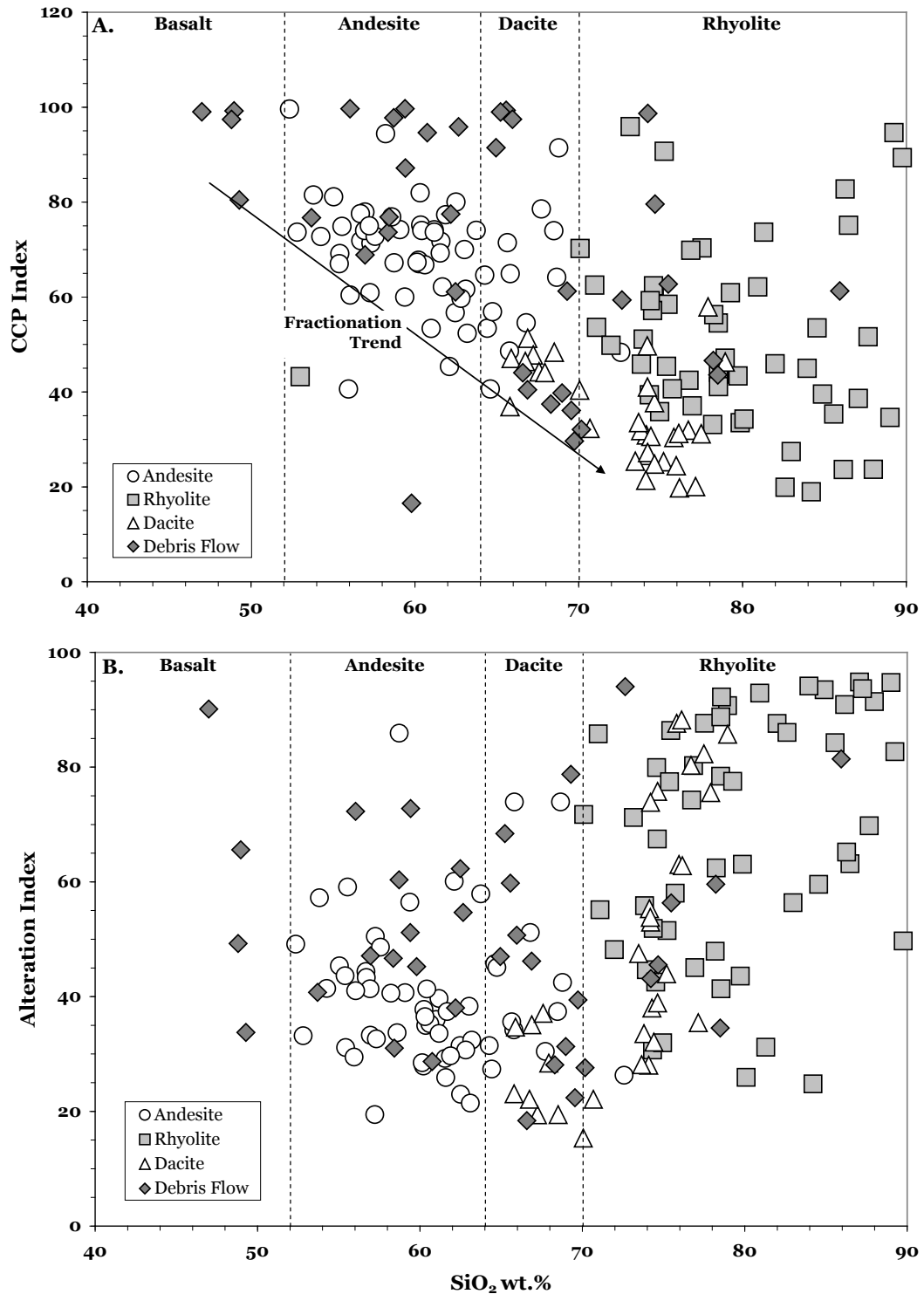
FIGURE 5.9 – The differences seen between plotting (A) SiO₂ wt.% versus CCPI and (B) SiO₂ wt.% versus AI. One of the downfalls of using just the CCPI (A) is that magmatic fractionation trends affect the distribution (B) shows the true scatter of points as a result of alteration (*after* Large et al., 2001).

The benefit of plotting samples on an alteration box plot, such as the one created by Large et al. (2001a), is that it can show the main hydrothermal alteration trends. The trend from subtly to intensely hydrothermally altered rocks associated with VMS deposits is characterized by increases in both CCPI and AI values and also decreases in Na_2O wt.% (Gifkins et al., 2005). Figure 5.8b shows the hydrothermal trends that are defined by Large et al. (2001a). Large et al. (2001a) defined trend one as reflecting an influence from weak sericite alteration at the margins of a hydrothermal system in felsic volcanic host rocks (Large et al., 2001a). Trend II shows the effect of a stronger sericite-chlorite-pyrite mineral assemblage found in the proximal footwall alteration system of a VMS system (Large et al., 2001a). Trend III is similar to trend III, except chlorite and pyrite is more prevalent than sericite, a common trend of chlorite-dominated footwall alteration. Trend IV only develops immediately adjacent to a massive sulfide lens and is chlorite-carbonate alteration. The sericite-carbonate alteration of trend V is found in the immediate hanging wall to the massive sulfide unit, while trend VI is an uncommon K-feldspar-sericite alteration found developed locally within felsic footwall volcanic rocks. The data from Hamlin Lake mostly lays along trends I and II. This suggests that the most common types of alterations are sericite and sericite-chlorite alteration, which is consistent with petrographic thin sections. In a typical VMS system the zones of sericite and sericite-chlorite are located on the outside of the alteration zone, so the Hamlin Lake area could represent the external zone of the alteration package that was produced by a VMS system.

When plotting the samples from Hamlin Lake on an alteration box plot it is evident that the rhyolites were affected the most by hydrothermal alteration because they scatter to the top-right, whereas if they scattered to the bottom-left then it would be indicative of diagenetic alteration rather than hydrothermal. The andesite and dacite units are not nearly as altered as the rhyolite volcanic rocks because there are not as many rhyolite samples that have a Na_2O wt.% greater than 3 wt%.

The majority of the rhyolites are scattered away from the least-altered rhyolite box and therefore have been affected by hydrothermal fluids (Fig. 5.8).

The dashed diagonal line running across the plot can be used to determine what type of alteration affected the samples. If the samples scatter towards the top right, then this indicates that rocks that have been hydrothermally altered, whereas a scatter towards the bottom left represents alteration during diagenetic processes (Large et al., 2001a). The volcanic rocks of the Hamlin Lake suite have been affected by hydrothermal alteration, which resulted in movement towards the right and top right portions of the plot (Fig. 5.8a). The rhyolites, more than the mafic/intermediate samples, plot to the left of the altered box lying between the chlorite and sericite alteration fields (Fig. 5.8a). This is also seen in thin section with the rhyolite samples showing the most alteration, mostly fine-grained sericite and some samples containing clumps of chlorite. Only eight dacite and andesite samples have moved from their least altered area towards the sericite minerals. In thin section, the amount of sericite and chlorite in the andesites and dacites is not strong especially when compared to the rhyolite volcanic rocks. When looking at the debris flow samples, the majority of the samples lie in the chloritized area and the rest can be found in the least-altered box and near sericite alteration. In the field and in thin section, the mafic debris flow samples are highly chloritized, while the felsic debris flow samples are less so, explaining why so many of the debris flow samples plot in the chlorite alteration area but others scatter away from that field.

The mobility of silica, alkaline and alkaline earth elements within felsic volcanic rocks during hydrothermal processes prevents the use of these elements during classification, but the separation and use of the least-altered suite is representative of the primary composition of the volcanic rocks. The most important piece of information that can be attained from alteration box plots is the least-altered samples. This is important for determining the initial lithologies and to determine how much the area has been affected by hydrothermal alteration. When looking at a map of where the least-altered rhyolitic volcanic rocks are located within the mapping area (Fig. 5.10a), it is apparent that there is no defined pattern to the sample locations. The samples that fall into the least-altered area also have Na_2O wt.% higher than three, along with lower LOI values suggesting less alteration. This provides further evidence that the samples are

indeed weakly altered. In thin section, the least-altered samples are very fine-grained and show weak sericite alteration.

The other major groups that could be recognized from the alteration box plots were samples that were strongly chloritized (Fig. 5.12a) and samples that were strongly sericitized (Fig. 5.12b). When looking at Figure 5.10, the least altered rhyolites and the moderately sericitized and chloritized rhyolites are also found in these same areas, therefore there is no strong correlation to specific units with the weakly and strongly altered samples. The absence of a clear pattern of altered samples could be a result of the relatively small sample area compared to the size of area that a hydrothermal system could affect. If more samples were taken over a larger area, than perhaps a more defined alteration pattern could be recognized, with areas showing weakly altered samples and areas showing concentrations of strongly altered samples, but that was beyond the scope of this study. Figure 5.11 shows the least-altered rhyolite samples plotted on a TAS diagram. The samples plot in the rhyolite and rhyodacite fields, supporting the interpretation that these samples are in fact the least-altered and the alteration box plot can be used with confidence with this suite of rocks.

Alteration systems can vary in size depending on the amount of time, pressure and temperature that the system occurred at. Alteration haloes around VMS systems depend on the host rock composition, timing of the hydrothermal alteration relative to the emplacement or deposition of facies, structures, fluid pathways, distribution patterns of the ore, and chemical and physical conditions of the hydrothermal fluids (Large, 1992). This can result in considerable variations in size, shape, composition and intensities of the haloes. Reactions between the volcanic successions and modified seawater have involved Na-Si-Ca-Fe-K-or Mg-metasomatism in samples and leached ore metals. If alteration haloes can be found by mapping alteration types, (e.g., sodium depletions) then this can be beneficial in finding the centre of hydrothermal activity and in turn finding mineralization associated with this. After plotting samples that have undergone considerable chlorite and sericite alteration, zoned alteration is not evident at Hamlin Lake. This may be because metamorphism in the area has masked any original alteration or possibly because the hydrothermal system
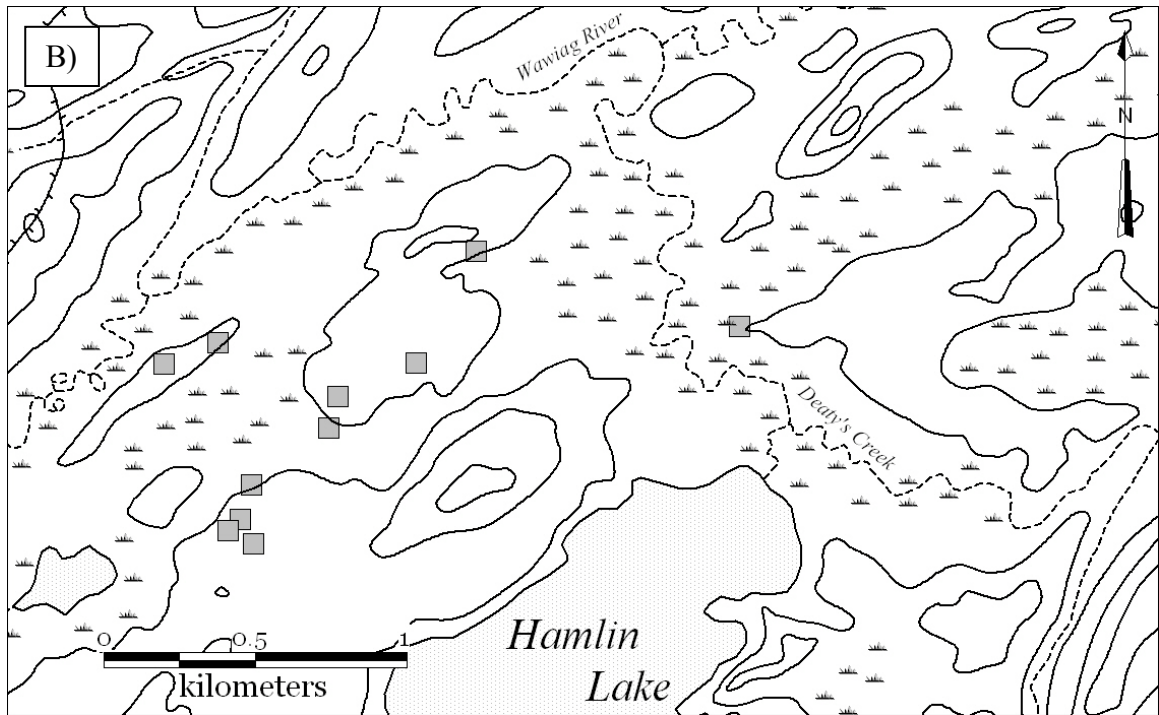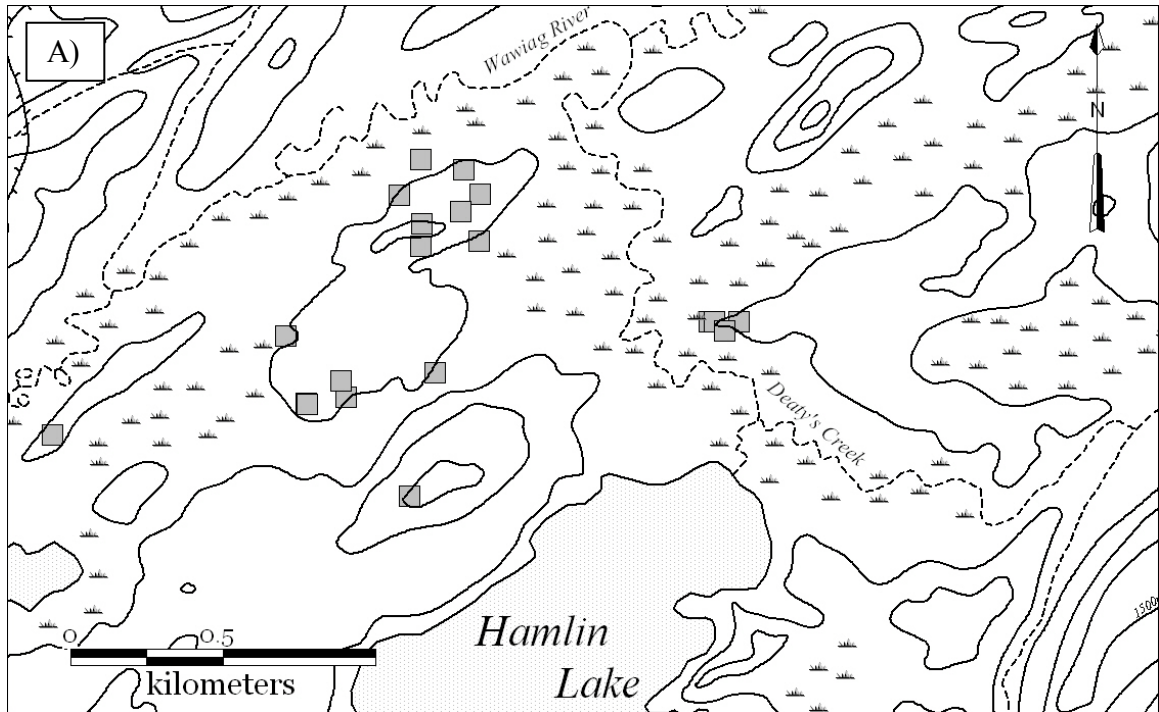
FIGURE 5.10 – Topographic maps showing relationships between (a) least-altered rhyolites, and (b) moderately sericitized and chloritized rhyolites.
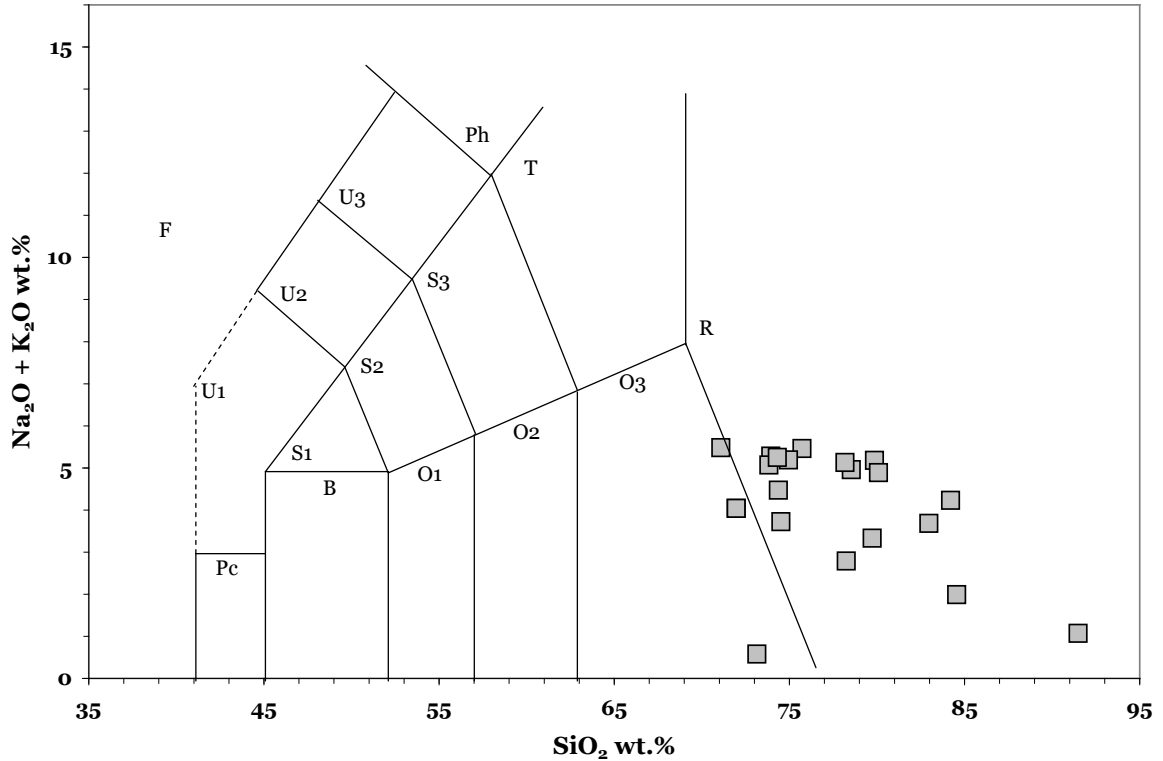
FIGURE 5.11 – This plot of the least altered rhyolite samples shows that they do in fact fall dominantly within the rhyolite field (refer to Figure 5.3 for fields).

did not run for a long enough period of time to produce defined zones of alteration. Alternatively, the hydrothermal system could have affected a much larger area than was mapped and sampled and the Hamlin Lake area only represents the distal product of the alteration system.

5.4 Lithological Classification

5.4.1 Primitive Mantle Plots

A Zr versus Ti plot was used in conjunction with primitive mantle (PM) normalized spidergram plots of trace elements to help distinguish between different suites of volcanic rocks at Hamlin Lake. The PM plot is used as further support for the Zr versus Ti plot and distinguishes patterns in enrichments and depletions between light rare earth elements (LREE) and heavy rare earth elements (HREE). These patterns can help to differentiate between different tectonic settings and certain elements show positive and negative anomalies,

90

distinguishing between each of the lithological groups found in the Hamlin Lake area. The use of multi-element diagrams also becomes useful in showing the difference in behaviour between elements, which are mobile and which are not (Rollinson, 1993).

Originally Lesher et al. (1986) separated the magmas into three different groups: FI, FII, FIIIa and FIIIb magmas, but Hart et al. (2004) further categorized felsic volcanic rocks into one more group, adding FIV magmas. The groups are meant to help geochemists separate felsic magmas, based on their differences in petrogenesis, specifically their formation or degree of modification in high-level magma chambers. Further details can be found in the VMS classification section (5.5) later in this chapter.

The rhyolite samples in Figure 5.13a and b show that the LREE's have higher abundances than the HREE's. The gentle slope between La and Lu is only slightly negative. The ratio of $[La/Sm]_n$ for the rhyolites is 2.44, while the ratio for $[Gd/Yb]_n$ is 1.18. Nb has a distinct negative anomaly; Zr and Hf have positive anomalies; Eu and Ti have negative anomalies as well as Al. The presence of negative Eu anomalies confirms fractionation of plagioclase while the magma was en route to the surface according to Lesher et al. (1986). However, the most distinct feature of the rhyolites is that the HREE's are flat. There are slight inconsistencies between the rhyolite patterns, with some samples showing minor variances in the HREE because of alteration and four samples showing negative La anomalies because of alteration. The LREE's have not been preferentially mobilized in the leached rhyolites, because the slope of the LREE patterns do not change and all of the samples in the Hamlin Lake area have depleted Nb and Ti anomalies, which are characteristic of arc settings. The rhyolites have Eu/Eu^* ratios of 0.41-0.88 and the Zr/Y ratio is on average ~7.5 which makes it transitional to mildly calc-alkaline according to the classifications of Barrett and MacLean (1994). Table 5.1 shows the range of values for $[La/Yb]_n$, Eu/Eu^*, and Zr/Y for the different classifications of rhyolites. According to Lesher et al. (1986), the gently sloping REE patterns, moderate Zr/Y ratios and Eu ratios seen at Hamlin Lake are linked with FII rhyolites (Table 5.1).
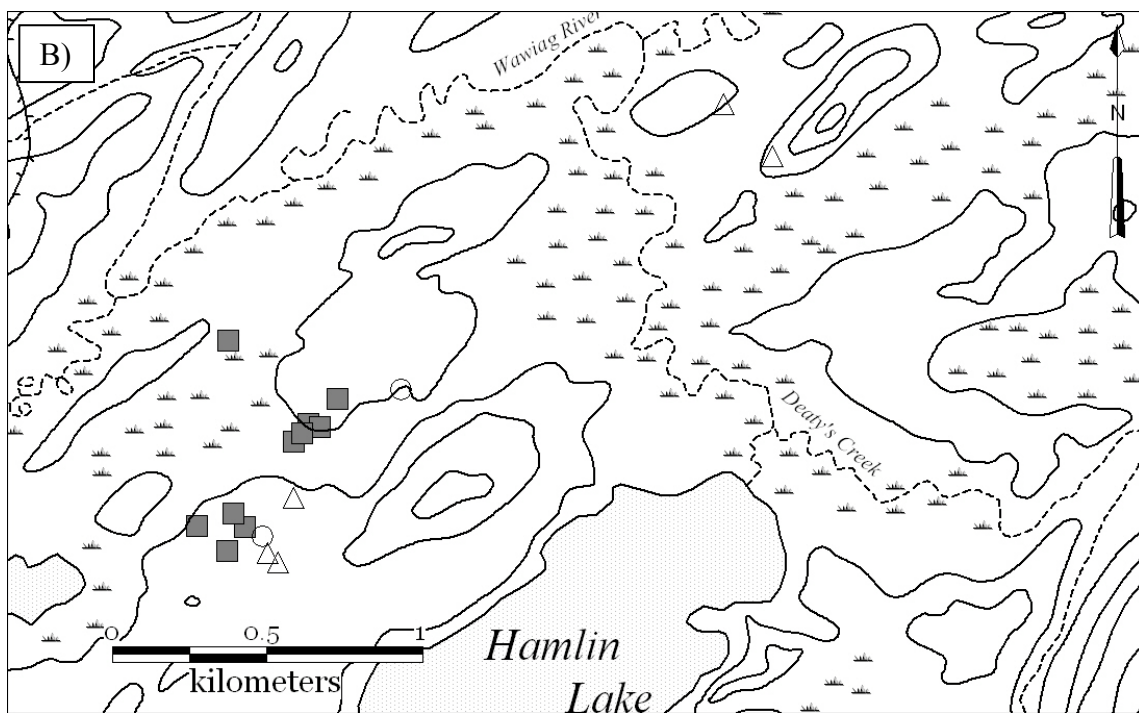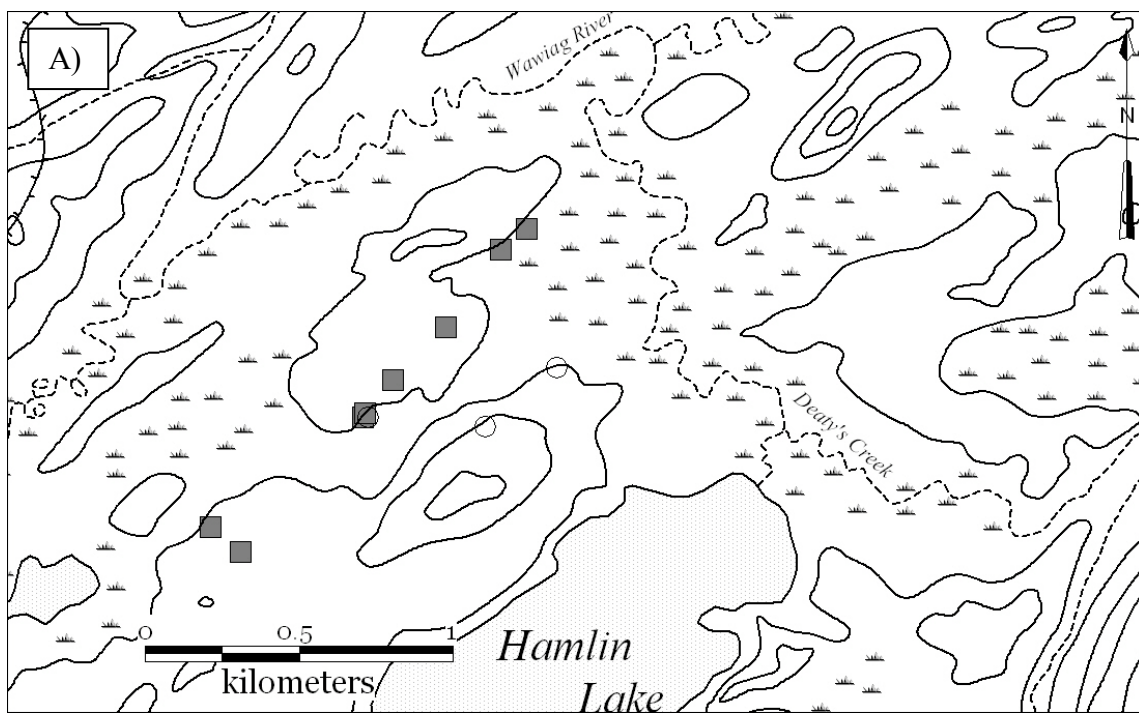
FIGURE 5.12– Topographic plots of samples that are (a) strongly chloritized, and (b) strongly sericitized.

The dacites shown in Figure 5.14 also display negative Nb anomalies with positive Zr and Hf anomalies. There is a weak negative Ti anomaly and a weak positive Eu anomaly. The HREE's are not flat and do not show the smooth patterns characteristic of unaltered rocks, rather there is evidence of HREE mobility. The $[La/Sm]_n$ ratio is 4.83 and the $[Gd/Yb]_n$ ratio is 3.17 showing that the slope of the dacites are a lot steeper than the rhyolites. There is variation seen within the HREE's meaning that some of the elements may have become mobile during hydrothermal alteration. The Eu/Eu^* ratio is 0.54-1.34 falling within the FI category of Lesher et al. (1986; Table 5.1). The slope of the samples show $[La/Yb]_n$ ratios of 10-36, which is significantly higher than the rhyolite and andesite samples. Also, there is no Eu anomaly and the Zr/Y ratio is on average ~32 all of which are consistent with FI rocks and fall within the strongly calc-alkaline category. FI lavas, according to Lesher et al. (1986), are low degree partial melts of a basic source region at high pressures with minimal fractionation during ascent and probably did not evolve in a high-level magma chamber.

Figure 5.17 shows primitive mantle-normalized REE plots for the andesite volcanic rocks. The andesitic volcanic rocks show negative Nb anomalies with very slight positive Zr and Hf anomalies. There is also a slight negative Ti anomaly and no Eu anomaly. Initially, the HREE's look flat, but closer investigation reveals a slightly negative slope ($[La/Sm]_n = 2.68$, $[Gd/Yb]_n = 1.4$). The Eu/Eu^* ratio ranges from 0.5-1.12 which falls within FII classification by Lesher et al. (1986; Table 5.1). The La/Yb_n ratio ranges from 2-12 and the Zr/Y ratio is ~7.10, making the andesite volcanic rocks transitional to mildly calc-alkaline (Barrett and MacLean, 1994).

TABLE 5.1 – A summary of ratios for rhyolite volcanic rocks (after *Lesher et al., 1986*).

	FI	FII	FIIIa	FIIIb	FIV
$[La/Yb]_n$	6-34	2-6	1-4	1-4	0.2-2
Eu/Eu^*	0.87-2.0	0.35-1.4	0.37-0.94	0.2-0.61	~~~
Zr/Y	9-31	6-11	4-7	2-6	0.67-4.8
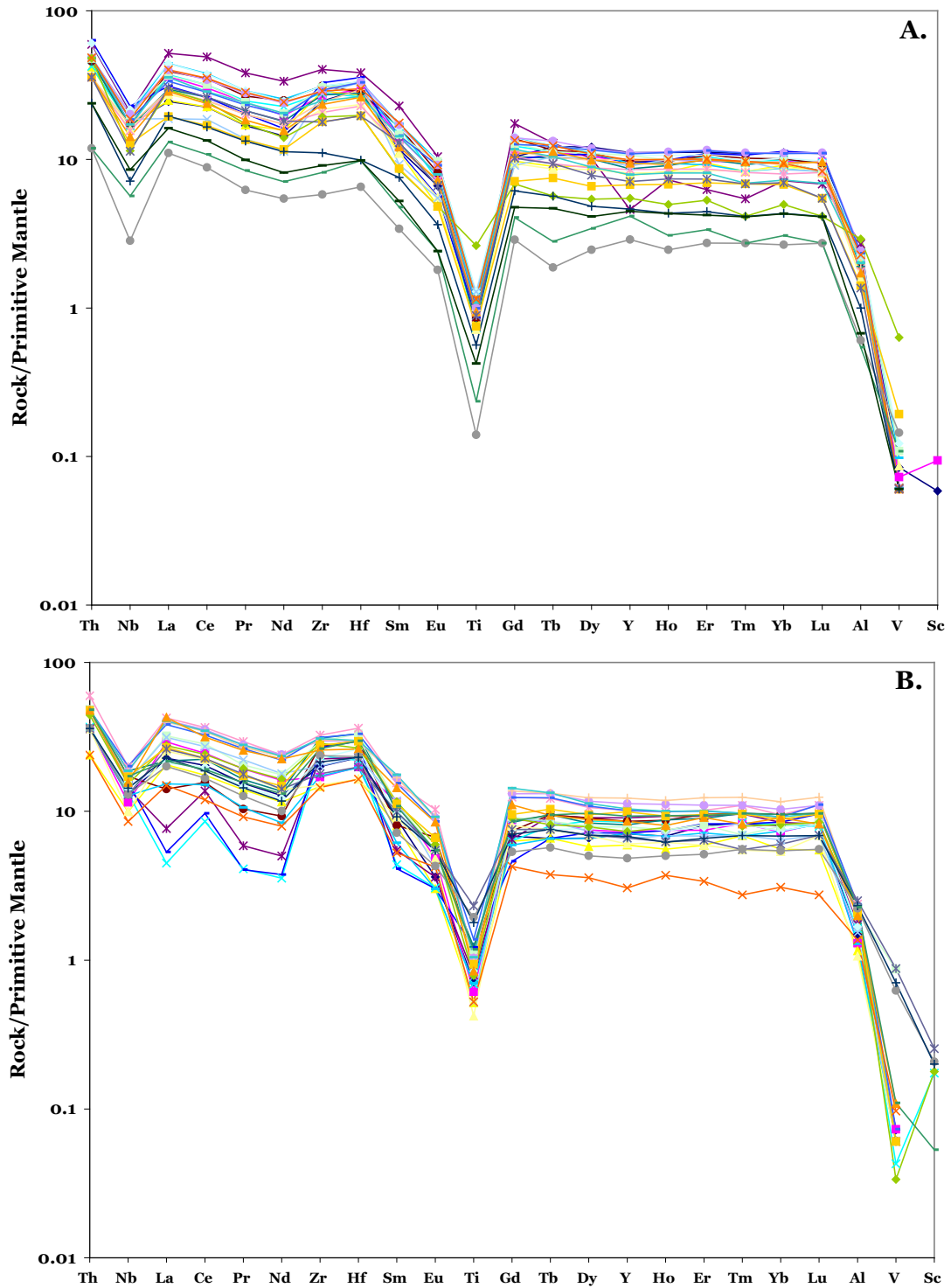
FIGURE 5.13 – Representative primitive mantle-normalized spidergrams for all the rhyolite samples showing a very uniform pattern amongst all the samples. There is a gentle slope from the LREE to the HREE and very prominent Nb and Ti negative anomalies. The Zr and Hf elements show positive anomalies (All spidergram plots are normalized to values of Sun and McDonough, 1989).
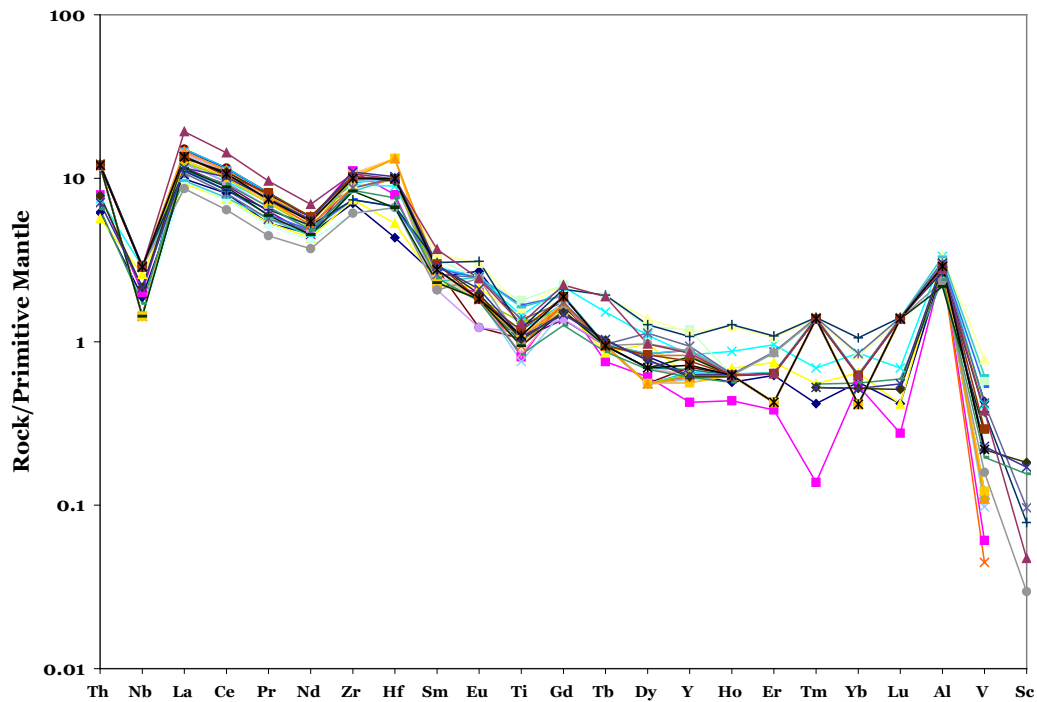
FIGURE 5.14 – A primitive mantle-normalized spidergram plot showing all of the dacite samples of the Hamlin Lake area. The same negative Nb anomaly that is present in all the lava flows at Hamlin Lake is recognized here along with a positive Zr and Hf anomaly and a slightly negative Ti anomaly. The positive Al anomalies are distinct to this unit.

Overall, primitive mantle-normalized spidergram plots for the andesites and rhyolites show that the andesitic samples have a more negative slope than the rhyolites. Even though at first glance they look quite similar, the La/Yb ratios representing the slope of the andesites are steeper than the rhyolites, but still overall only displaying a weak negative slope.

When the debris flow samples are plotted on a primitive mantle-normalized spidergram plot (Fig. 5.16), there is a resemblance between the debris flows and the rhyolite and andesite volcanic rocks. The REE patterns show very similar outlines likely because the debris flows consist of material produced by the same event that produced the rhyolites and andesites.
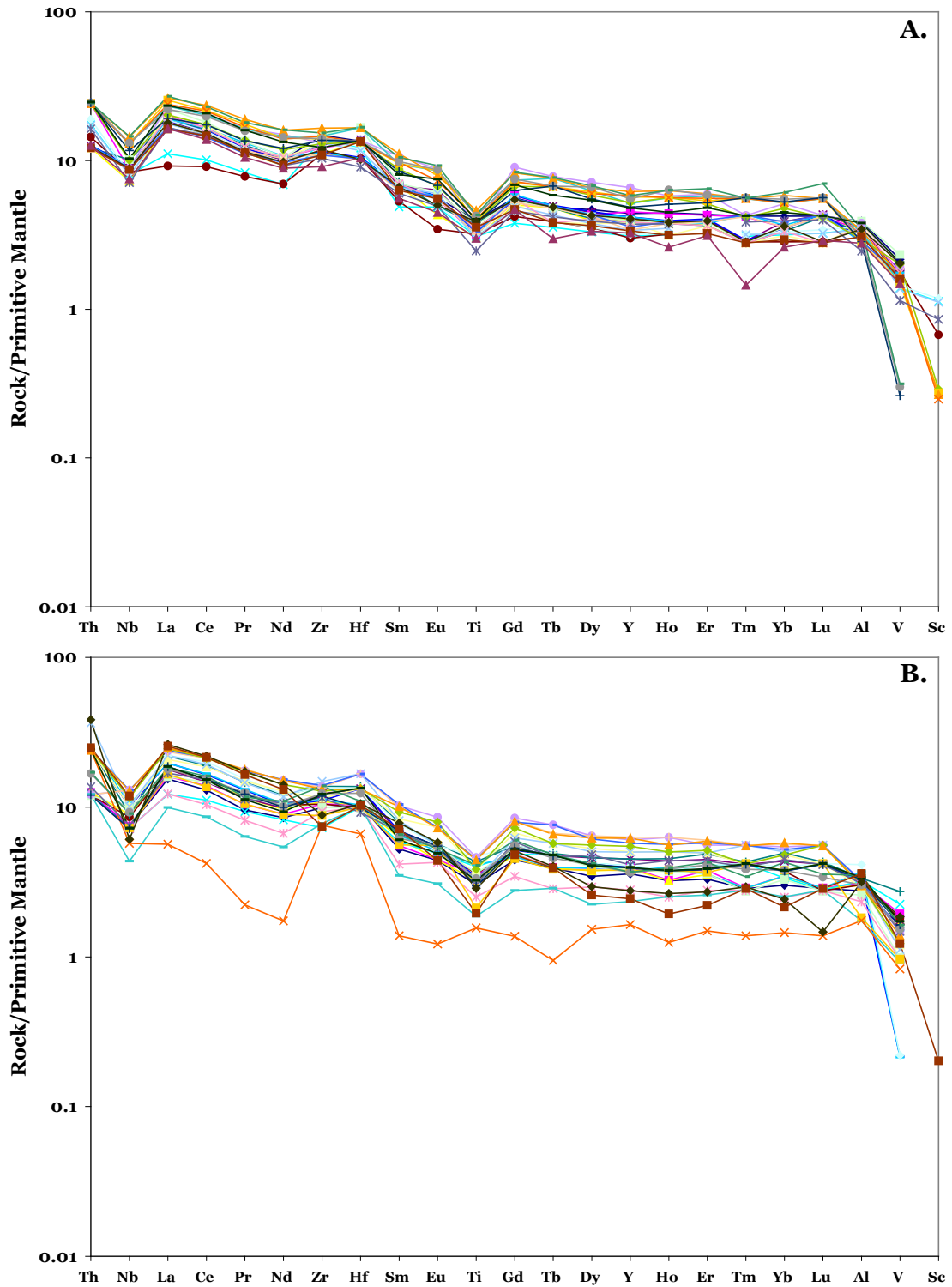
FIGURE 5.15 – Primitive mantle-normalized spidergram plots for all andesite samples. There is a gentle slope to the patterns with negative Nb anomalies and slight positive Zr and Hf anomalies and negative Ti anomalies.
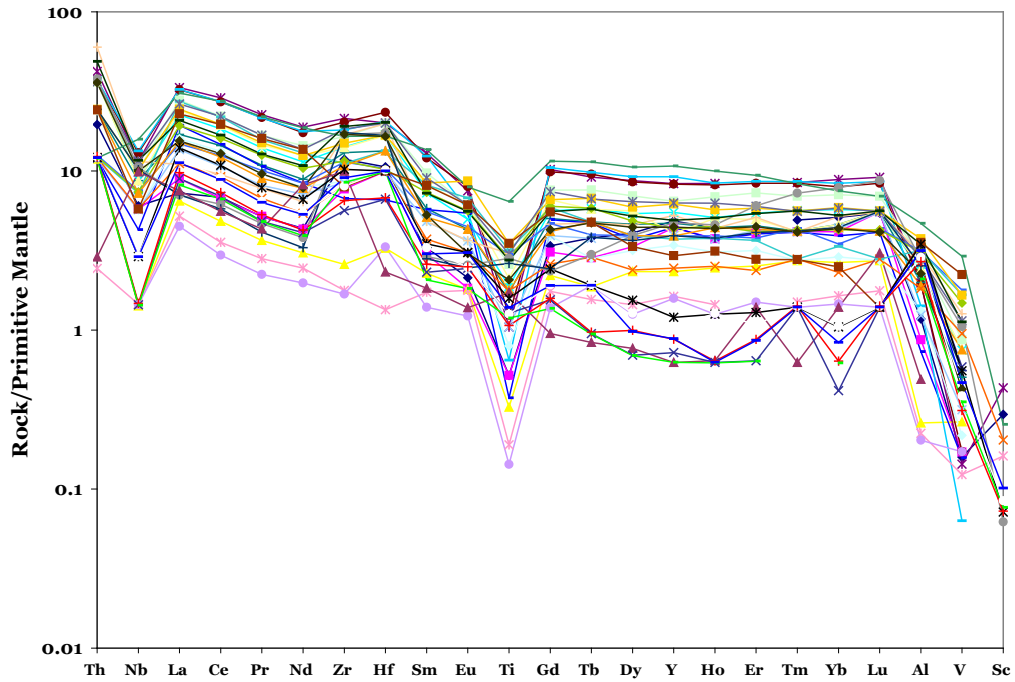
FIGURE 5.16 – A primitive mantle-normalized spidergram plot of the debris flow samples. It is apparent that the debris flow samples have a great resemblance to the rhyolite and andesite volcanic rocks when plotted on a primitive mantle-normalized spidergram.

The debris flow samples consisted of mud and pieces of various rocks that were in the path of these flows, so they show variable PM plots, but most can be related to either the rhyolite or andesite flows. Figure 5.17 shows this well with all four main lithology outlines plotted together. The negative Nb and Ti anomalies and the positive Zr and Hf anomalies are similar to the rhyolites, dacites and andesites. The debris flow outline falls within the rhyolite and andesite fields with similarities to both. Although the individual elemental patterns are similar to the rhyolites, the sharp negative Nb and Ti anomalies, and overall abundance of elements is more similar to the andesite samples. Even when looking back at Figure 5.6, the samples can be divided into two suites, one hosting the rhyolite and dacite samples with half of the debris flow samples located with this group and the other suite hosting the andesite samples with the other half of the debris flow samples.

5.4.2 Magmatic Affinity

The most commonly incompatible and immobile elements used for magmatic affinity classifications are Nb, Y, Yb and Zr (Barrett et al., 1993). On plots of incompatible-immobile elements, fractionation lines and alteration lines will both pass through the origin; therefore, alteration does not affect the slopes of the fractionation lines, but simply displaces sample points along this line (Barrett et al., 1993). Consequently, each fractionation line with a different slope represents magmas of a different chemical affinity (MacLean and Barrett, 1993). This means that the altered and unaltered samples can both be examined for magmatic affinity. Barrett and MacLean (1994) stated that Zr/Y ratios for magmatic affinities vary from <2 – 4.5 for tholeiitic affinities, 4.5 – 7 for transitional, and 7 - >25 for calc-alkaline rocks. A plot of Zr versus Y indicates that the Hamlin Lake rocks have affinities ranging from mildly calc-alkaline to strongly calc-alkaline (Fig. 5.18). Zr/Y ratio for the andesitic volcanic rocks is 7.1; 7.5 for the rhyolitic volcanic rocks; and 32.0 for the dacitic volcanic rocks. When looking at Figure 5.18 it is clear that there are two distinct magmas of different affinities. It is difficult to separate the andesitic and rhyolitic magmas from each other because of their similar slope and therefore, similar magmatic origin, but the dacite magma definitely originated from a different magma than the andesitic and rhyolite magmas. The dacites also show a very tight cluster of points because of their narrow range of Zr. The andesitic and rhyolitic volcanic rocks of Hamlin Lake are mildly calc-alkaline in affinity and lie along the same slope, while the dacites are strongly calc-alkaline in affinity and have a much shallower slope. The andesite and rhyolite samples most likely originated from the same magmatic event, whereas the dacite samples are from a different event. One differing graph is Figure 5.6, TiO_2 wt.% versus Al_2O_3 wt.%, where the rhyolites and dacites are likely from the same suite, while it is the andesites that are different. It is important to remember that the TiO_2 wt.% versus Al_2O_3 wt.% plot is used mainly to distinguish elements which have become mobile from elements which have not, therefore helping with alteration of suites more than magmatic affinities.
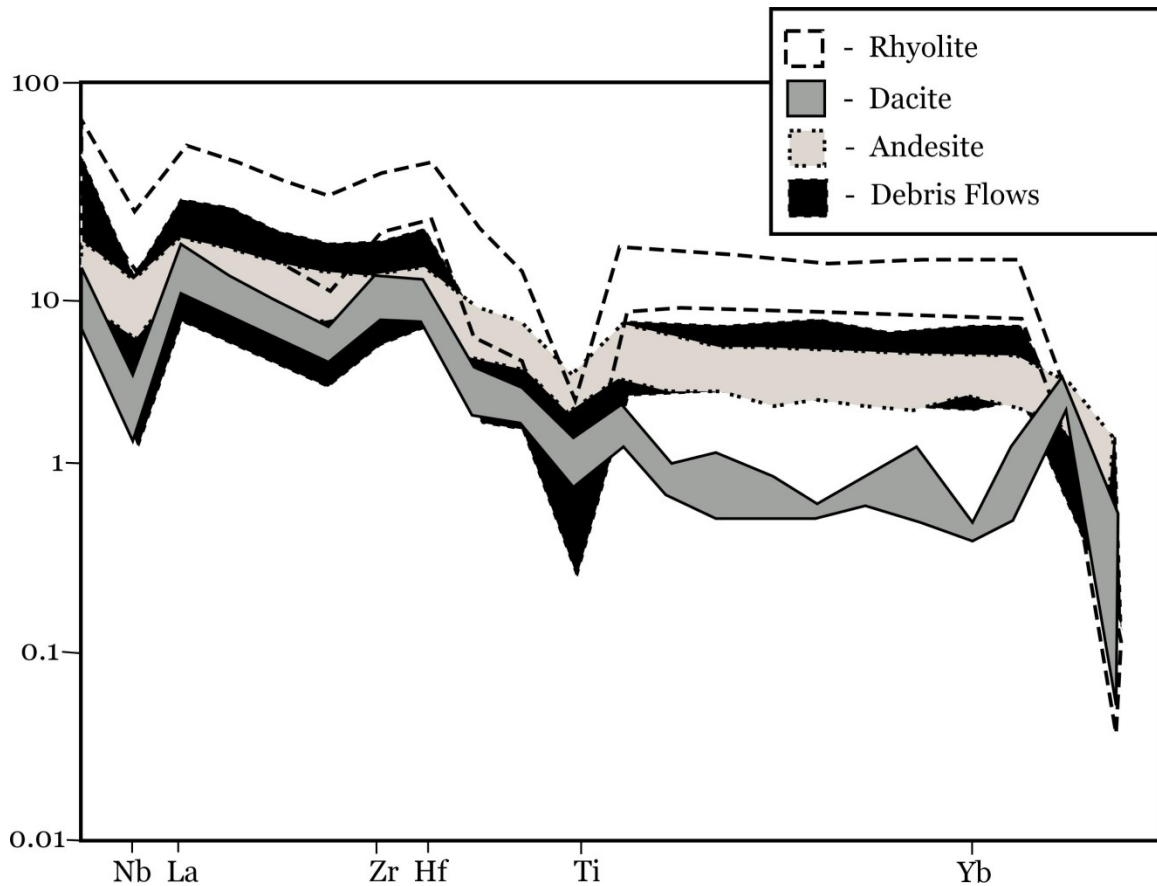
FIGURE 5.17 – A primitive mantle normalized spidergram plot which shows different patterns for the main lithologies.

The element Nb has the same characteristics as Y because they are both HFSE, so a plot of Zr versus Nb (Fig. 5.19) shows similar trends to Figure 5.18, in which the andesites and rhyolites have the same slope and are separated from the dacitic volcanic rocks, which show a much shallower slope. The separation of volcanic data shown by Zr/Y ratios shows a mildly calc-alkaline affinity in the andesite and rhyolite volcanic rocks, and a strong calc-alkaline affinity for the dacite volcanic rocks. These trace element characteristics thus serve to distinguish felsic rocks of mildly calc-alkaline affinity from those of a much stronger calc-alkaline affinity. The contrasting affinities of the mildly calc-alkaline and the strongly calc-alkaline rocks reflect derivation from different source areas, or a lot of contamination of a mildly calc-alkaline magma by a crustal component. Barrie et al. (1993) proposed that FI lavas could be the result of crustal contamination of arc-derived lavas. The andesitic and rhyolitic units
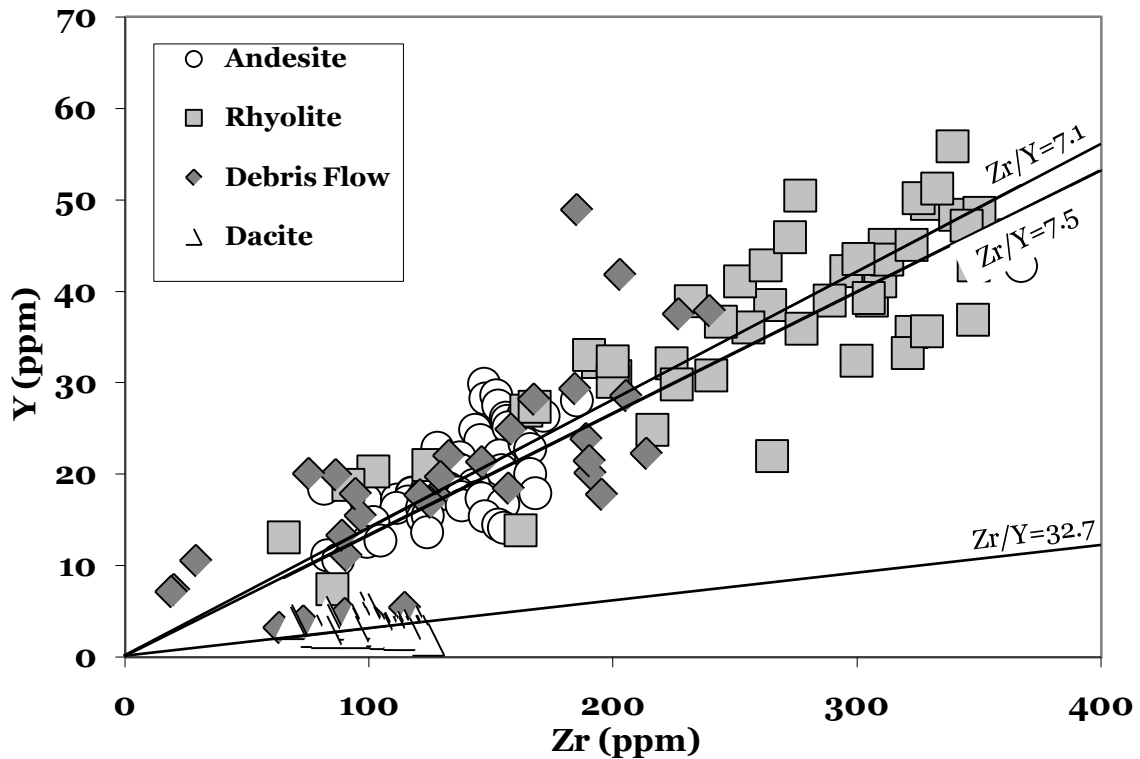
FIGURE 5.18 - A plot of Zr (ppm) vs. Y (ppm) provides an estimate of the magmatic affinity of the rocks which ranges from mildly calc-alkaline for the andesites and rhyolites to strongly calc-alkaline for the dacites.

have similar Zr/Y and Zr/Nb ratios, so it is suspected they originate from the same mantle source. MacLean and Barrett (1993) use Zr/Nb ratios to confirm magmatic affinity. The Zr/Nb ratio is said to be higher in anorogenic (rift-related) than in orogenic (subduction-related) alkaline rocks, and is thought to provide a reliable discriminate for magmatic suites and tectonic setting (Hawkesworth et al., 1993). The Hamlin Lake rocks show different Zr/Nb ratios with the dacites showing a ratio of 69.5, which is much higher than the ratio for the andesites and rhyolites, which are 20.5 and 24.7, respectively. The dacites show a much higher Zr/Nb number than the andesites and rhyolites, but it is unlikely that the dacites are anorogenic in origin because of the occurrence of andesites and rhyolites which show island arc affinities. The dacites are found interspersed with the andesites and rhyolites and are not confined to one area. Previously it was noted that the dacites are FI in origin and the rhyolites and andesites are mostly FII in origin. Barrie et al. (1993) stated that FI rocks are

from arc-related lavas derived from a metasomatized wedge with variable amounts of crust contamination, while FII lavas are found in extensional environments (Lentz, 1998). With the dacites showing different Zr/Y ratios and Zr/Nb ratios compared to the rhyolites and andesites, it is clear that they are separate suites of rocks and derived from distinct sources.

Barrett et al. (2005) showed that the effects of alteration can be eliminated using an immobile-element ratio plot. Plots of Al_2O_3/TiO_2 versus Zr/Al_2O_3 (Fig. 5.20a) and Al_2O_3/TiO_2 versus Zr/TiO_2 (Fig. 5.20b) of the Hamlin Lake rocks show a positive trend from the andesitic samples to the rhyolitic samples. It is necessary to plot both to reduce the effect of using the same denominators which can affect the trends. Barrett et al. (2005) maintain that a positive trend
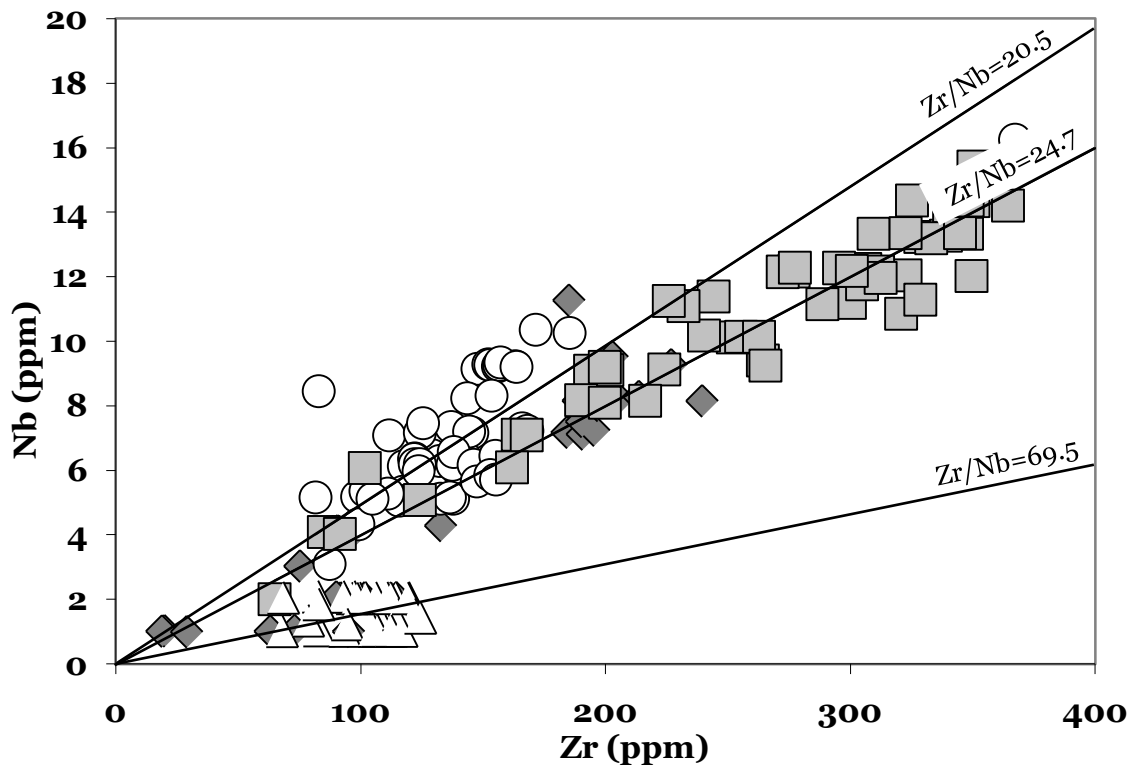
FIGURE 5.19 – Plot of Zr versus Nb indicating that the andesite and rhyolite samples have similar magmatic affinities. The dacite samples plot in a distinct field suggesting that they have a different magmatic affinity. Legend is the same as Figure 5.18.
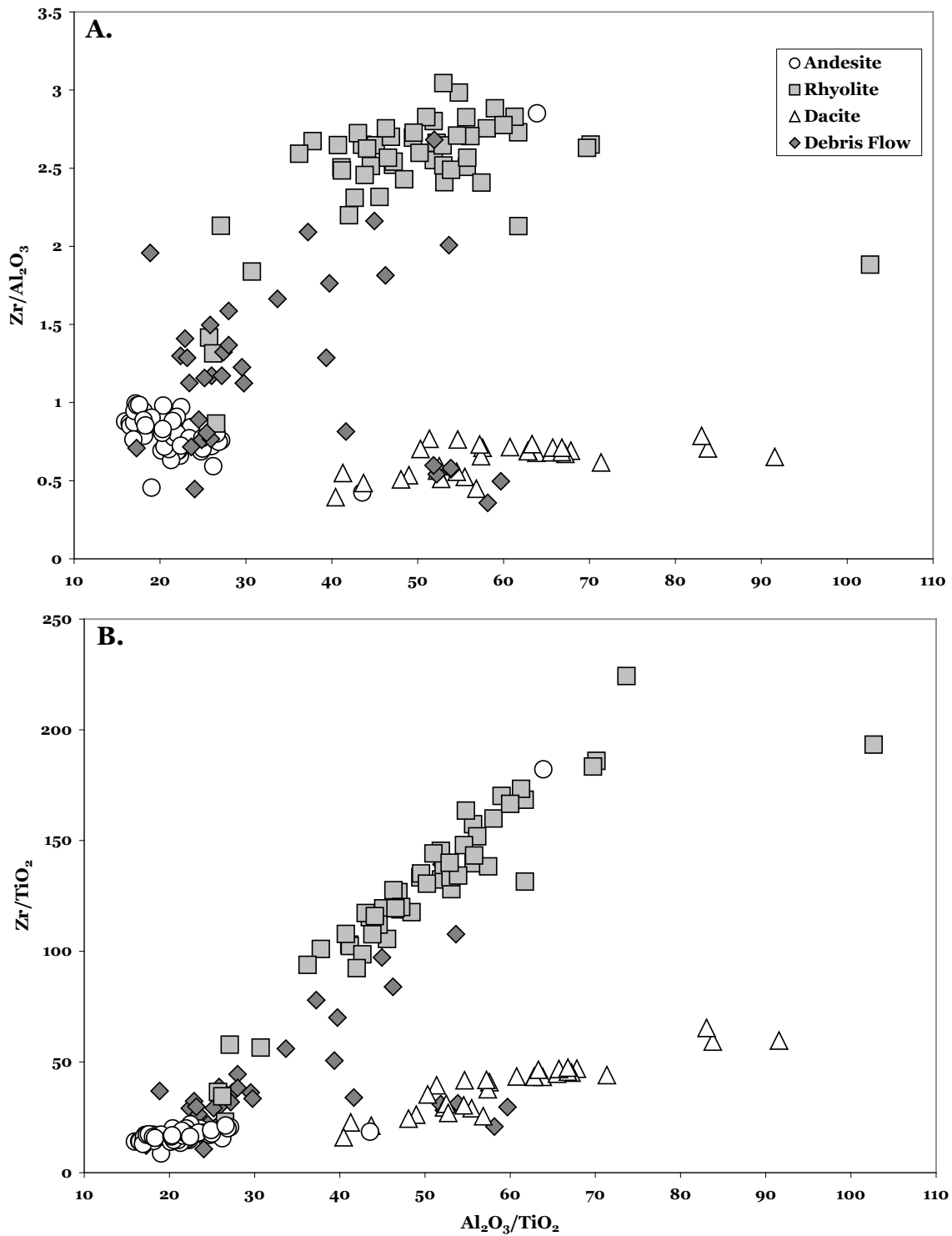
FIGURE 5.20 – Plots of Al_2O_3/TiO_2 vs. Zr/Al_2O_3 and Al_2O_3/TiO_2 vs. Zr/TiO_2 for andesite, rhyolite and dacite samples. There is a positive trend from the andesite samples to the rhyolite samples showing the magmatic fractionation trend. The dacite samples lie off the main trend showing a different compositional trend and different magmatic affinity.

like this reflects the fractionation trend for the magma as a whole. Figure 5.21 shows that there is a positive trend in the data and that the magma evolves from andesitic to rhyolitic in composition. The dacitic samples show an obvious compositional offset from the main trend of the other volcanic rocks suggesting a different magma source. Figure 5.20a shows the andesites and rhyolites with similar trends, however Figure 5.20b shows the dacites and rhyolites having similar trends, suggesting that the similar suites are fractionating from the same source.

Looking at a plot of Zr/Y versus La/Yb (Fig. 5.21) for the volcanic rocks, it shows that the andesite and rhyolite samples plot in overlapping fields, however, the dacite samples form a distinct field. Even though previous alteration plots (Fig. 5.9a) show only weak alteration of the dacites, Y can become slightly mobile in some VMS systems according to Barrett and MacLean (1993); therefore the scatter of the dacite samples must be the result of Y mobility as a result of alteration.

5.5 VMS Classification

Igneous rocks can be classified using major and large ion lithophile elements (LILE), but these values are often unreliable in altered areas because of their mobility during alteration. Lesher et al. (1986) found that by looking at the REE geochemistry of felsic volcanic units, one can make reliable estimates of whether or not a felsic package contains mineralization related to a VMS system or whether the rocks are barren of a deposit. Lesher et al. (1986) proposed a classification scheme in which felsic volcanic rocks can be classified according to their VMS deposit potential. The method of Lesher et al. (1986) has become one of the most useful and popular methods to classify felsic volcanic rocks and a powerful exploration tool (e.g, Hart et al., 2004), but other classification schemes have also been created, such as Barrie et al. (1993). During this study, the classification scheme of Lesher et al. (1986) was used because it is more commonly used in other studies, however, Lentz (1998) disagreed with the basis of Lesher et al (1986) classification. There are few differences between the two classification schemes except for the names of the groups, for example Lesher et

al. (1986) and Hart et al. (2004) uses the names FI, FII, FIII, FIV with FI felsic volcanic rocks containing the least amount of deposits with increasing potential with increasing numbers, whereas Barrie et al. (1993) uses group IV, III, II and I with group IV felsic volcanic rocks containing the least VMS deposits and increasing economic potential with decreasing numbers.

Lesher et al. (1986) defined three distinct groups of felsic volcanic rocks related to a VMS system. The first group is FI felsic metavolcanic rocks which consist of alkaline to calc-alkaline dacites and rhyodacites characterized by steep chondrite-normalized REE patterns ($[La/Yb]_n$=6-34) with weakly negative to moderately positive Eu anomalies (Eu/Eu*=0.87-2.0), high Zr/Y ratios (Zr/Y=9-31), low abundances of HFSE such as HREE, Y, Zr and Hf and also high abundances of Sr. FII felsic metavolcanic rocks include calc-alkaline rhyodacites and rhyolites characterized by lower REE patterns ($[La/Yb]_n$=2-6) with variable Eu anomalies (Eu/Eu*=0.35-1.4), moderate Zr/Y (Zr/Y=6-11), and intermediate
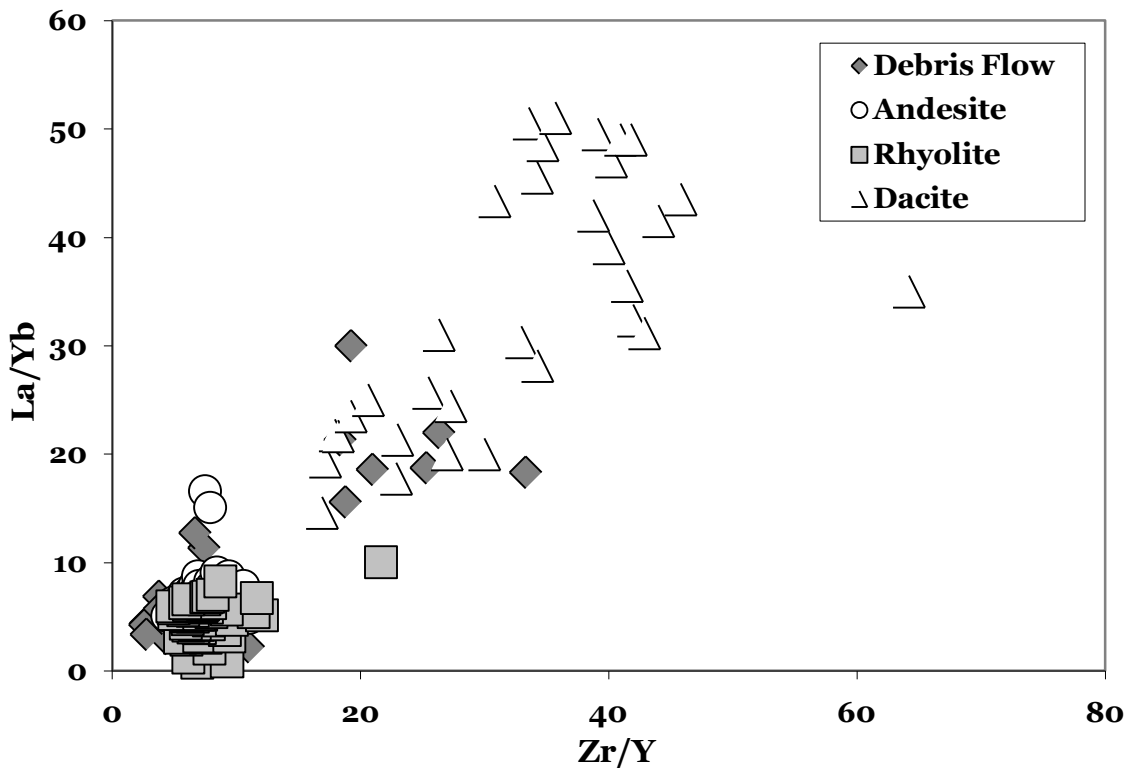
FIGURE 5.21 – A plot of Zr/Y versus La/Yb which shows tight clusters of the andesite and rhyolite samples.

abundances of HFSE and Sr. FIII felsic metavolcanic rocks consist of tholeiitic rhyolites and high silica rhyolites characterized by relatively flat REE patterns ($[La/Yb]_n$=1-4). The FIII felsic metavolcanic rocks can be divided into two separate classifications, FIIIa and FIIIb. FIIIa felsic metavolcanic rocks have variable negative Eu anomalies (Eu/Eu*=0.37-0.94), low Zr/Y ratios (Zr/Y=4-7) and intermediate abundances of HFSE and Sr, while the FIIIb felsic metavolcanic rocks have pronounced negative Eu anomalies (Eu/Eu*=0.20-0.61), low Zr/Y ratios (Zr/Y=2-6) and high abundances of HFSE with low Sr values. There is a less commonly found class of felsic volcanic rocks which Hart et al. (2004) mentions briefly consisting of rhyolites and high silica rhyolites of tholeiitic origin called FIV felsic volcanic rocks. The FIV felsic volcanic rocks consist of $[La/Yb]_n$ ratios of 0.22-2.1 and low Zr/Y ratios of 0.67 to 4.8.

FIII felsic metavolcanic rocks are most commonly associated with base metal VMS deposits, while the FI volcanic rocks rarely contain mineralization and FII felsic volcanic rocks can host deposits, but not as often as FIII felsic volcanic rocks. One problem with the Lesher et al. (1986) classification scheme is that it only classifies felsic metavolcanic rocks and not the intermediate to mafic metavolcanic rocks that are commonly related to many VMS systems; however, since there is no classification scheme for intermediate to mafic rocks related to VMS systems, it was applied to all of the volcanic rocks of Hamlin Lake, although the andesites must be treated with caution.

The majority of the volcanic rocks at Hamlin Lake fall within the FI and FII group. The dacites at Hamlin Lake fall within the FI category of the Lesher et al. (1986) classification. Their magmatic affinity is calc-alkaline with a $[La/Yb]_n$ ratio of 10-36 and Eu/Eu*=0.54-1.34 and high Zr/Y ratios of 16-45. The rhyolites and andesites found at Hamlin Lake have transitional to calc-alkaline affinity. The rhyolites show $[La/Yb]_n$=0.5-7, Eu/Eu* ratios of 0.41-0.88, and Zr/Y ratios of 4-21. The andesites have $[La/Yb]_n$ ratios of 2-12, Eu/Eu* ratios of 0.52-1.12, and Zr/Y ratios of 4-11. There are four samples which fall within the FIV category with $[La/Yb]n$ ratios of 0.55-1.48, Eu/Eu* ratios of 0.57-0.86, and a Zr/Y ratio of 6-9 with a transitional to calc-alkaline affinity.

The Lesher et al. (1986) classification scheme was based on the fractionation of LREE's and HREE's during magmatic processes by looking at the La/Yb$_n$ ratios, the abundance of Yb and variations of Eu (Lesher et al., 1986). On Figure 5.22 it can be seen that all of the dacite samples fall within the FI category, while the rhyolites fall within the FII category, however, there is overlap between the FII and FIIIa felsic volcanic rocks and four of the rhyolite samples fall within the FIV category.

The dacitic volcanic rocks of Hamlin Lake have less potential for hosting a VMS deposit, but the rhyolitic volcanic rocks do fall within the FII category and overlap with the FIIIa category, which does have the potential to host a VMS deposit. Figure 5.22 is based upon the plots of Lesher et al. (1986), which was updated by Hart et al. (2004) who elaborated on the fifth category for VMS deposits, FIV, defined by very flat to slightly LREE-depleted patterns and low total REE and HFSE abundances.

The FI felsic volcanic rocks, represented by the dacites in the Hamlin Lake area, constitute a minor component (<10%) of the mafic-felsic volcanic sequence. Even though the FI geochemistry is strongly calc-alkaline their geochemistry is consistent with a low-degree partial melting of a basic source at a high pressure. FI magmas are interpreted to have been derived from a deeper source and to have escaped significant high-level modification, which may be the cause for their lack of mineralization (Lesher et al., 1986).

The importance of FII volcanic rocks is that they are known to sometimes host VMS deposits (Lesher et al., 1986). FII magmas constitute the upper parts of a mafic-felsic sequence and are similar to modern calc-alkaline rocks and are consistent with a high-degree partial melt of a crustal source or fractional crystallization of an intermediate parent (Lesher et al., 1986). The Eu anomalies confirm some fractionation when en route to the surface because Eu is a compatible element with plagioclase fractionation. The andesites of this study fall within the FII field, but since Lesher et al. (1986) did not take into account intermediate to mafic samples; it is hard to compare the andesites even though they appear to perfectly fit within the FII group. FIII magmas are documented as being tholeiitic in affinity (Hart et al., 2004), whereas the Hamlin Lake volcanic

106

rocks are mildly calc-alkaline to strongly calc-alkaline in affinity, however, four of the rhyolite samples fall within the FIV group. These four samples have not been intensely altered and all lie near each other in the field in the most western portion of the mapping area. Unfortunately, mapping was not carried out past this point, so it is not known if they do in fact continue to the west. In the field and petrographically, there is no difference between these four samples and the other rhyolitic volcanic rocks seen in the Hamlin Lake area. Deposits which are associated with FIV felsic volcanic rocks include Snow Lake and Flin Flon of Manitoba and Kutcho Creek of British Columbia and are not as common as deposits associated with FIII felsic volcanic rocks (Hart et al., 2004).

FIIIa felsic metavolcanic rocks in the Superior Province show negative Eu anomalies and flat HREE patterns which are, according to Lesher et al. (1986), a result of plagioclase fractionation related to a high-level magma chamber processes and in turn, are most likely associated with massive sulfide deposits.
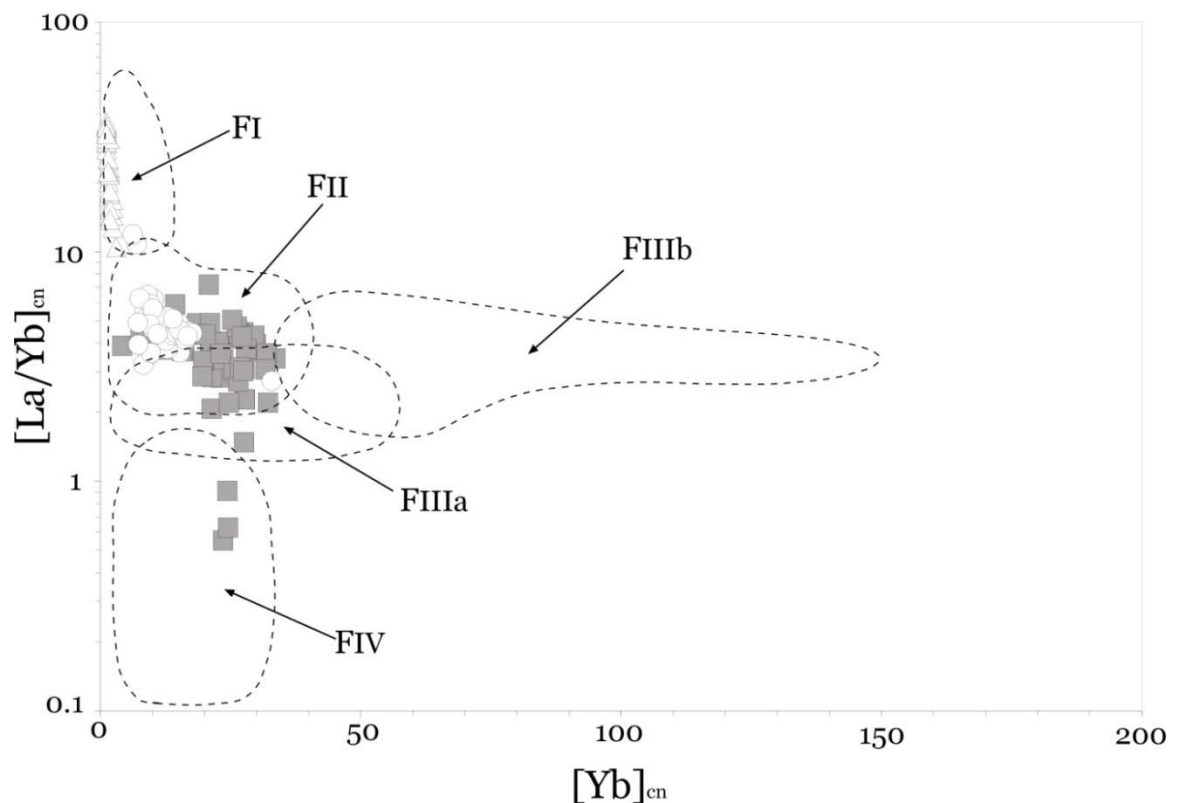
FIGURE 5.22 – A plot of [Yb]$_{cn}$ versus [La/Yb]$_{cn}$ for the rhyolites, dacites and andesites of the Hamlin Lake area. The plot is used to discriminate between the FI, FII, FIIIa and FIIIb and FIV classification scheme for VMS-related felsic volcanic rocks (*after* Lesher et al., 1986; Hart et al., 2004).

High-level magma chambers are interpreted to have supplied the heat to drive ore-forming hydrothermal systems and are considered important when looking for a VMS deposit. FIII volcanic rocks are common in the Superior Province's massive sulfide deposits and are associated with high-level magma chambers, which is why they are sought after in exploration for VMS deposits (e.g., Noranda, Kidd Creek, Kamiskotia; Lesher et al., 1986).

Franklin et al. (2005) distinguished five separate lithostratigraphic types of rocks related to VMS deposits, they include: (1) bimodal-mafic, (2) mafic, (3) pelitic-mafic, (4) bimodal-felsic and (5) siliciclastic-felsic. Bimodal-mafic occur in incipient-rifted suprasubduction oceanic arcs typically with flows and <25% felsic strata, mafic settings occur in primitive oceanic backarcs with ophiolite sequences and with <10% sediment, pelite-mafic settings occur in mature oceanic backarcs and have subequal amounts of pelite and basalt, whereas bimodal-felsic settings occur in incipient-rifted suprasubduction epicontinental arcs and can have 35-70% felsic volcaniclastic strata and siliciclastic-felsic settings occur in mature epicontinental backarcs with continent derived sedimentary and volcaniclastic strata. It was difficult to determine whether the Hamlin Lake volcanic suite of rocks were related to a bimodal-mafic or a bimodal-felsic stratigraphy because although there is only intermediate to felsic volcanic rocks found in the Hamlin Lake mapping area, there are pillow basalts found lower in the stratigraphy. However, as intermediate to felsic rocks make up the majority of rocks at Hamlin Lake. It is suggested that the Hamlin Lake volcanic rocks are a bimodal-mafic sequence not only because of the basalt-andesite-dacite-rhyolite sequence of rocks that are present, but also because the samples show subduction patterns when plotted on spidergram plots with enrichments of LREE and depletions of HREE. The felsic to intermediate volcanic rocks of the area are dominantly volcaniclastic rocks with debris flows containing lenses of chert, which would classify it as being bimodal-felsic, but the majority of bimodal-felsic rocks are Phanerozoic in age according to Franklin et al. (2005) whereas the Hamlin Lake area is Archean in age. Franklin et al. (2005) suggested that bimodal-mafic sequences are a result of ocean-ocean subduction and represents an evolution from arc-rifting to mature back-arc development.

5.6 Tectonic Setting

Wyman et al. (2002) stated that typical Archean arc volcanic sequences consist of (1) transitional tholeiite to calc-alkaline basalt and andesite and (2) later dacite-rhyolite magmas. After geochemically classifying the Hamlin Lake suite according to Lesher et al. (1986), Barrie et al. (1993) and Franklin et al. (2005) and studying the overall geochemistry, the tectonic setting can be further defined. The negative Nb and Ti anomalies seen in the andesite, rhyolite and dacites are consistent with a suprasubduction setting. The negative Ti anomaly is due to the fractionation of Fe-Ti oxides, while the negative Nb anomaly is indicative of subduction environments, and commonly found in arc derived rocks (Cousens, 2000). The enrichment of the LREE's compared to HREE's and depletion of the Nb relative to La, seen in the Hamlin Lake volcanic rocks, is diagnostic of arc environments (Cousens, 2000).

Subduction-related island arcs formed on oceanic crust show strongly depleted HFSE with low Zr/Y ratios and overall low levels of REE (Barrett and MacLean, 1999). Intraoceanic arc magmas are derived from primitive melts of depleted mantle. The Hamlin Lake volcanic rocks share characteristics observed by Barrett and MacLean (1999) but show positive Zr and Hf anomalies instead of the more commonly seen negative anomalies.

Most arc rocks crystallized from parental magmas generated in the mantle wedge with melting taking place in the presence of water (Hawkesworth et al., 1993). This water was released from the subducted oceanic crust and the more mobile major elements were transported via these fluids (Hawkesworth et al., 1993). Unlike mid-ocean ridge basalts (MORB) and ocean island basalt (OIB), intraoceanic arc volcanic rocks have distinctly lower HFSE abundances when compared to the REE and LILE elements, the basis to distinguish subduction-related magmas from magmas produced in other tectonic settings (Hawkesworth et al., 1993). The most distinct elemental pattern is the negative Nb and Ti anomalies seen in subduction-related settings. Low abundances of HFSE are the result of being left behind in the subducted slab, either because it contains a HFSE-bearing phase, or because the fluids released from the subducted slab do not mobilize the HFSE enough (Hawkesworth et al., 1993). In the Hamlin Lake

volcanic rocks, both Nb and Ti show negative anomalies. Pronounced Eu anomalies can also be formed with the combination of partial melting and plagioclase fractionation at crustal levels (Lentz, 1998), and the Hamlin Lake volcanic rocks show weak to moderate Eu anomalies.

The enrichments and depletions of REE and HFSE depend on the degree to which the underlying mantle wedge experienced previous subduction related LILE enrichment, the depth and extent of partial melting, and whether it was produced from enriched or depleted mantle (Barrett and MacLean, 1999). The age of the arc should be taken into consideration, because a mature arc may be underlain by more metasomatized mantle or thicker sequences of subducted oceanic crust and marine sediments, which may become involved in melt generation. In some cases, the felsic volcanic rocks may contain enrichment of the LREE compared to the mafic rocks, which are interpreted to be a result of crystal fractionation.

Hamlin Lake volcanic rocks are similar to the Noranda volcanic rocks, which are also dominated by an andesite-rhyolite sequence of transitional affinity and are interpreted to be representative of volcanic rocks produced in a mature island-arc terrane (Barrett and MacLean, 1999). In mature island-arc settings and their immediate back-arc settings, moderate enrichments in LREE and moderate depletions in HFSE commonly occur throughout the mafic to felsic volcanic suite (Barrett and MacLean, 1999). Back-arc basins make up the submarine portion of the arc system, and a typical assemblage would contain mafic to felsic volcanic rocks with volcaniclastic debris and may occur at depths of 2-3 kms (Franklin et al., 2005). Similarly, the Hamlin Lake volcanic rocks show an andesite-rhyolite volcanic sequence with enrichments in the LREE suggesting a mature arc-setting, similar to the Noranda volcanic rocks (Figs. 5.13; 5.14; 5.15). The rhyolites and andesites at Hamlin Lake could be classified as transitional in affinity because they are so close to the transitional-calc-alkaline boundary as defined by trace element signatures. Barrett and MacLean (1999) also noted that fractionated calc-alkaline lavas are generally depleted in Zr, Y, Nb, and the HREE's, but not Th, U or LREE's, the result of material undergoing partial melting, depth, pressure of fractionation or contamination by continental

crust. Hamilton (1995) suggests that mixing of mafic and felsic components, combined with assimilation and fractional crystallization, are responsible for the calc-alkaline compositional continuum seen in arc systems.

As an arc matures, the lavas evolve from tholeiitic to calc-alkaline in affinity of intermediate to felsic composition forming smaller isolated volcanic centers of intertwined lavas and volcaniclastic debris flows (Scott et al., 2002). An arc evolves from a proto-arc to arc building to arc rifting over time (Scott et al., 2002). The Hamlin Lake arc rocks likely represent the later stages of the arc-building processes because they are composed of rhyolites and andesites which suggests that the arc was beginning to mature. However, although the Hamlin Lake area resembles a mature arc-setting, bimodal volcanic rocks are typical of extensional settings. This may indicate that the Hamlin Lake rocks were formed in the back-arc area of the mature rifted arc setting because the Hamlin Lake rocks are fractionated.

5.7 Summary

Overall, within the Hamlin Lake volcanic suite of rocks, the major elements showed mobility, while the trace elements are generally immobile. The andesites, rhyolites and dacites all show consistent primitive mantle normalized patterns within each lithology with the exception of a few altered samples that show variation in their patterns. Average abundances of trace elements between the volcanic units are varied, with the rhyolites showing the overall highest average, which is higher than the andesites and significantly higher than the dacites average trace element abundances.

When classifying the rocks at Hamlin Lake, it was necessary to classify them using the REE, which are generally immobile in hydrothermal systems. In general the LREE were enriched compared to the HREE in all of the volcanic units. LREE enrichment is thought to be derived from a metasomatized mantle. In mature arc settings, LREE and LILE are enriched and HFSE are depleted, a result of subduction-related metasomatism of the mantle wedge below an island arc (Barrett and MacLean, 1999). Even though the overall abundances of elements show variation in the Hamlin Lake rocks, the slopes of the PM patterns

for the andesites and rhyolites stay almost the same indicating that suites are chemically related, probably by fractionation. The dacites show more variation, another indication that they belong to a separate magma source or were contaminated during emplacement.

The area mapped at Hamlin Lake is an andesite-rhyolite sequence with a dacite unit that varies considerably from the andesites and rhyolites with regards to magmatic affinity and overall elemental abundances. In nearly all of the plots, the dacites stand out as being very different from the rest of the lithologies. The observation of the elemental abundances being so different from the rhyolites and andesites suggests that it was generated from a distinct source. If the lithologies were related by fractionation, then one should see a progression from the andesites to dacites to rhyolites with regards to elemental abundances and this is not the case. The andesite and rhyolite volcanic rocks show a mildly calc-alkaline magmatic affinity (Zr/Y =~7.1 and ~7.5, respectively), while the dacite unit is strongly calc-alkaline (Zr/Y=~32). These differences suggest that the dacite volcanic unit is derived from a different magma. The dacites show a negative Nb anomaly, but not as strong a negative Ti anomaly as the rhyolites. There are several possibilities for the differences between the dacites and the rhyolites and andesites. Some of these include: different material undergoing partial melting, different depths of origin, pressure of fractionation and contamination by continental crust (Barrett and MacLean, 1999).

The dacites fall within the FI category by Lesher et al. (1986), which is thought to be derived from a deeper source than FII and FIII magmas. If the dacites of Hamlin Lake were from a deeper source, then this would explain their elemental differences, which could be the result of contamination on their ascent. Barrett and MacLean (1999) found that identifying an ancient tectonic setting may become complicated if an intraoceanic arc is surrounded by oceanic crust, but is underlain by continental crust. Remnant slivers of continental crust can underlie some modern intraoceanic arcs (i.e., Japan) and could affect the compositions of arc and back-arc magmas (Barrett and MacLean, 1999). Overall, the Hamlin Lake area shows a supra-subduction arc setting.

CHAPTER 6

SM-ND ISOTOPES

6.1 Introduction

Sm-Nd isotopic analyses were carried out on nine samples from the Hamlin Lake suite; five rhyolites, three debris flows and one andesite. The Sm-Nd isotopes were analyzed to distinguish the tectonic setting of the rocks in the area, the source of the magmatism and to investigate if crustal contamination affected the rocks. The Sm-Nd analyses are shown in Table 6.1.

The geochemistry and isotope systematics of Archean greenstone belts provide important constraints on the origin of the volcanic rocks and tectonic models for the evolution of Archean cratons (Cousens, 2000). Radiogenic isotopic data, combined with field observations and whole rock geochemistry has the potential to distinguish between different tectonic scenarios for the origin of volcanic rocks (Cousens, 2000).

TABLE 6.1 - Results of Sm-Nd isotopes analyses

Sample	Nd (ppm)	Sm (ppm)	$^{147}Sm/^{144}Nd$	$^{143}Nd/^{144}Nd$	T_{dm}	ε_{Nd2700} (CHUR)T
AS-05-081 Rhyolite	27.06	11.64	0.1654	0.511745 ± .000005	4251	-6.59
AS-05-036 Andesite	11.88	7.20	0.1332	0.511555 ± .000006	2925	+0.93
OC-159 Rhyolite	8.96	8.66	0.1446	0.511726 ± .000007	3028	+0.34
AS-05-059 Debris Flow	18.78	9.71	0.1333	0.511560 ± .000002	2919	+1.01
AS-05-034b Debris Flow	25.26	12.07	0.1381	0.511664 ± .000003	2895	+1.38
AS-05-010b Rhyolite	23.97	11.50	0.1380	0.511669 ± .000004	2881	+1.52
G05-19 Rhyolite	27.39	14.44	0.1424	0.511756 ± .000008	2878	+1.65
AS-05-042 Rhyolite	16.91	5.25	0.1383	0.511652 ± .000003	2851	+1.78
AS-05-032 Debris Flow	18.78	7.29	0.1257	0.511506 ± .000008	2761	+2.62
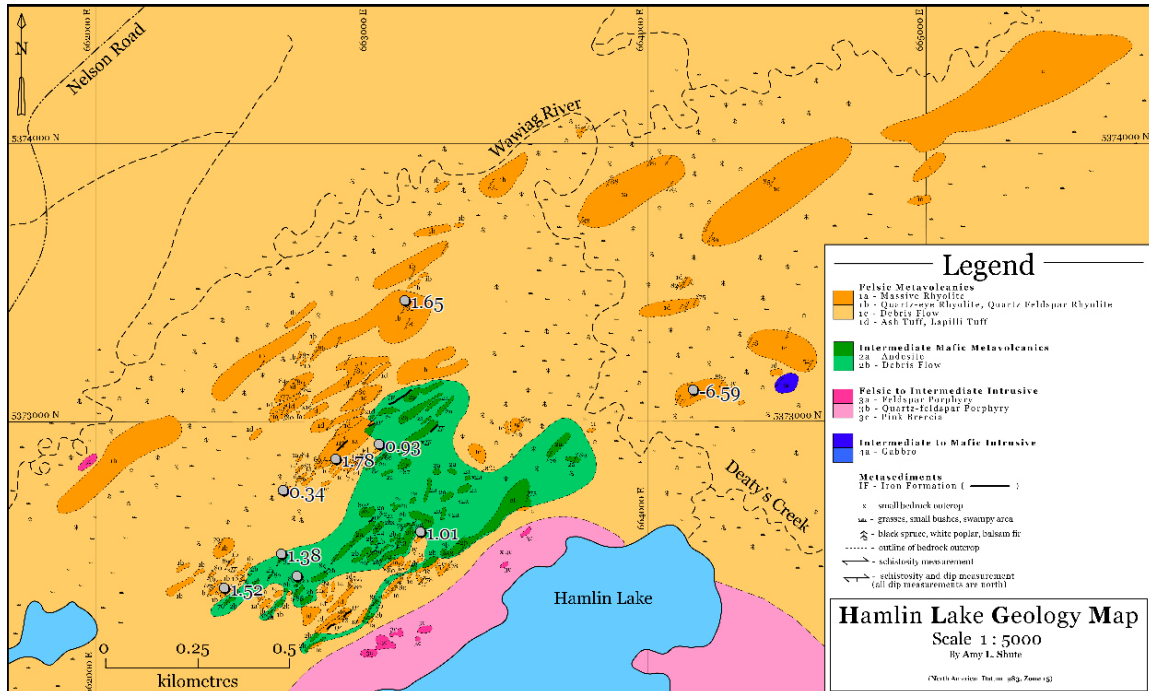
FIGURE 6.1 – Map showing the locations of the nine Sm-Nd samples and their ε_{Nd} values relative to the mineralization. Refer to Figure 4.1 for a detailed map and legend.

6.2 Results

The ε_{Nd} has been calculated using an age of 2700 Ma, which is the approximate age of volcanism at Hamlin Lake based on the U-Pb age of nearby rocks in the Wawa Subprovince (Tomlinson et al., 2002). Near identical ages (2720 Ma) for two samples, one from the northern and one from the southern metavolcanic areas surrounding the Hamlin Lake area, were found from Hart (2007) mapping project (Fig. 3.7). The ε_{Nd} values range from -6.59 to 2.62 with no systematic relationship towards the mineralization. When looking at samples of the same lithology there is no relationship seen, whether moving towards or away from the mineralization nor moving up or down in stratigraphy, nor is there a relationship recognized between lithologies (Fig. 6.1).

In order to utilize Sm-Nd data to interpret the tectonic setting of Hamlin Lake, it is necessary to show that the mineralizing fluids at Hamlin Lake did not affect the Sm-Nd values as Campbell et al. (1984) had noted REE mobility in the intensely altered rocks of the Kidd Creek deposit of the Abitibi greenstone belt. Campbell et al. (1984) showed that a large range in the Sm or Nd values could be

caused by high REE mobility as a result of intense hydrothermal alteration. It was also suggested by Prior et al. (1999) that negative ε_{Nd} values could reflect a disturbance in the isotopic system by metamorphic and/or metasomatic activity. This could occur when the Sm-Nd isotope system was reset, followed by leaching of Nd relative to Sm, which occurs in intensely altered rocks and reflects preferential migration of late fluids through the permeable, phyllosilicate-rich zones (Prior et al., 1999). The Hamlin Lake rocks have undergone alteration but it was not intense enough to reset the Sm-Nd system according to petrography and geochemistry (see Chapter 5). This is supported by the trace-element data discussed in Chapter five, which show that the REE are relatively immobile in most Hamlin Lake rocks.

Petrographic thin sections were also studied to ensure that alteration had not significantly affected the samples, and in turn the ε_{Nd} values. Of the nine samples analyzed for Sm-Nd isotopes, four have accompanying thin sections. A highly siliceous sample, AS-05-042 is very fine-grained and made up almost entirely of quartz (~90%) with minor amounts of calcite and chlorite (~5% of each). Samples AS-05-032 and AS-05-034b are debris flows: fine-grained and containing bands of magnetite and chert clasts. The matrix of AS-05-032 and AS-05-034b contains chlorite (45-55%) and a very fine-grained material that is unidentifiable in thin section, very dark in colour and most likely magnetite. The fourth thin section is of sample AS-05-081. Sample AS-05-081 is unique because it is the only sample of the nine samples analyzed for Sm-Nd isotope work that has a significantly different ε_{Nd} value. Geochemically, AS-05-081 is a rhyolite with 79% SiO_2 wt.% and a low LOI value (1.33), which is generally considered low by Barrett et al. (1993) and indicative of minimal alteration, however, in thin section this sample shows alteration. The thin section contains ~50% sericite, is very fine-grained making it difficult to distinguish and identify crystals, and contains approximately 40% quartz and 10% calcite, although the calcite is found in a vein. Any original textures have been overwritten by sericite alteration, leaving behind fine-grained, equigranular crystals. In some areas the crystals are so fine-grained and altered that only a black mass of sericite is left, but this

alteration is patchy and some areas are more altered than others. There is an apparent contradiction in the fact that a sample which appears moderately altered in thin section has such a low LOI. Even when plotted on an alteration box plot, sample AS-05-081 plots in the least-altered area for the rhyolites. When plotted on a primitive mantle-normalized plot, sample AS-05-081 does not differ in REE pattern shape or REE abundance confirming that even though the sample may have been altered it has not affected the REE. Even though geochemically this sample appears to have undergone limited alteration, the thin section showing sericite alteration, but this can be explained if the thin section happened to be taken from a section of the hand sample that was high in sericite. Regardless of the degree of alteration in the thin section for AS-05-081, the geochemical data indicated that the Sm and Nd have not been disturbed.

The Sm-Nd model ages range from 2761 to 4251 Ma, however the 4251 Ma value belongs to AS-05-081, which has a more negative ε_{Nd} value than the other samples. If sample AS-05-081 is excluded from the data set, then the range of model ages would be 2761 to 3028 Ma, a significantly narrower range. The model ages range from 2761 to 3028 Ma is similar to the range of other published ages for both the Wawa subprovince and the Superior province (e.g., Tomlinson et al., 2002; 2004; Corfu and Stott, 1998), whereas sample AS-05-081 which has a model age of 4251 Ga creates a problem, as it is older than reported ages for the Isua gneisses of Greenland (3770 ± 42 Ma; Hamilton et al., 1978) and close to the age of the formation of the earth.

6.3 Discussion

Even though the Hamlin Lake rocks have undergone hydrothermal alteration, it has not mobilized the REE in the samples analysed or their radiogenic isotopes. The Nd concentrations in the samples range from 8.96 to 27.39 ppm, and the Sm contents vary from 5.24 to 14.43 ppm. Prior et al. (1999) interprets Nd and Sm content variations as being a result of either magmatic variability, or light REE mobility. As the Hamlin Lake samples do not show

evidence of alteration induced mobility, magmatic processes are likely the cause of the variability.

The majority of the Hamlin Lake samples have $\varepsilon_{Nd\,(2700\,Ma)}$ values ranging from +0.34 to +2.62, with one outlier value of -6.59. The five rhyolite samples range from -6.59 to +1.78, the debris flow samples range from +1.01 to +2.62 and the andesite sample has a value of +0.93. The ε_{Nd} value of depleted mantle at 2700 Ma is calculated to be approximately +3.0 (Cousens, 2000; Tomlinson et al., 2002). Sample AS-05-032 of the Hamlin Lake suite shows a value of +2.62, a value close to the Archean depleted mantle estimate representing a nearly uncontaminated sample from the depleted mantle (Fig. 6.2). This suggests that the clasts or matrix material that make up the debris flow were derived from a mafic source with an isotopic composition similar to that of depleted mantle. The samples show a range of increasingly negative values implying that they have been contaminated by older material.

In order to quantify the amount of contamination required to generate the spread in ε_{Nd} values seen at Hamlin lake modeling of the data was undertaken using the values for 2.7 Ga depleted mantle of Cousens (2000) as a starting point and 3.0 and 2.7 Ga granites from the Wabigoon Subprovince as possible contaminants (Tomlinson and Percival, 2000). The modeling demonstrated that assimilation of between 1-5% of the 3 Ga granite can generate the spread in isotope data seen in the majority of Hamlin Lake samples (with the exception of AS-05-081). In contrast mixing with 2.7 Ga granites requires assimilation of 10 to 30% older material in order to generate the spread of data, which is not geologically reasonable given the geochemical characteristics of the Hamlin Lake rocks. Also, it would be difficult to assimilate 10% granite and yield a rock of andesitic composition. The model ages for the Hamlin Lake samples are broadly supportive of a ~3 Ga contaminant (Table 6.1). The linear relationship between ε_{Nd} values and model ages on Figure 6.3 is consistent with the variation in the ε_{Nd} signature being caused by varying proportions of the same contaminant rather than by isotopically distinct source regions. The ε_{Nd} of -6.59 for AS-05-081

would require assimilation of approximately 70% of the ~3 Ga contaminant, which is not geologically feasible and suggests that a significantly older contaminant was involved.

When ε_{Nd} values are low or have a considerable range in values, Stern et al. (1992) suggests that the parental magmas may have interacted with older lithosphere which had strongly negative ε_{Nd} values. The tectonic setting of the Hamlin Lake area is reviewed in Chapter Five, but overall the rhyolite and andesite volcanic rocks are consistent with a mature oceanic arc setting rather than a continental arc which would allow for contamination by continental crust. Barrett and MacLean (1999) found that some island arcs surrounded by oceanic crust can have a partly continental basement (i.e., Kuroko, Japan; Bathurst, Canada) and it is possible that a similar mechanism occurred in the Hamlin Lake area. Alternatively, when magma chambers are deep enough, parts of the underlying ocean crust can become incorporated into the magma, giving oceanic arc magmas "inherited"
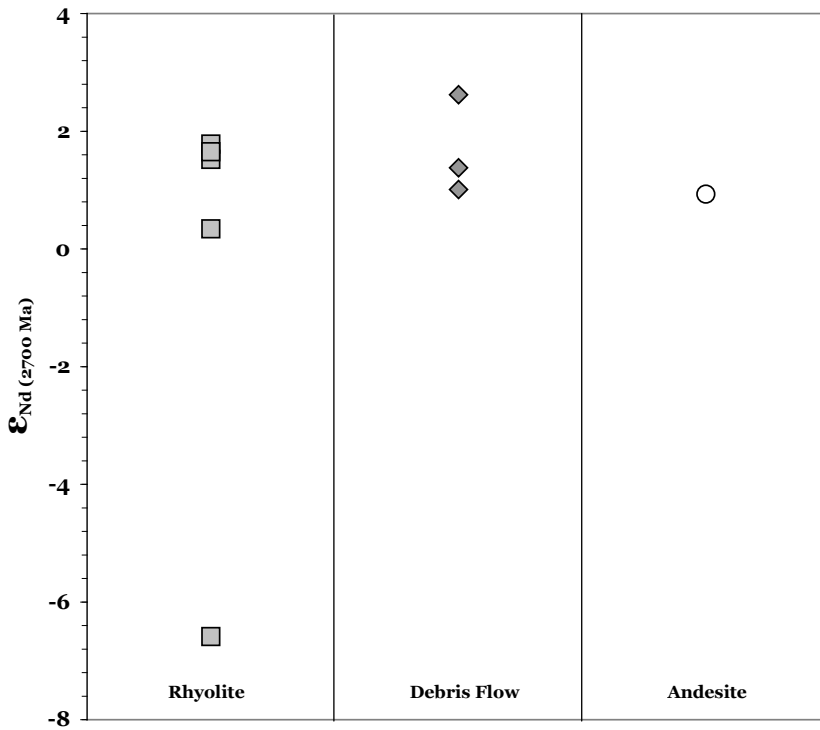
FIGURE 6.2 – A plot showing the range of ε_{Nd} values compared to their lithologies.

continental signatures. Rifting of such an intraoceanic arc could lead to volcanism that would be difficult to distinguish from that formed during rifting of a continental margin behind a volcanic arc (Barrett and MacLean, 1999). A crustal contamination signature could also be introduced into intraoceanic arc magmas by the subduction of marine sediments, causing an increase in radiogenic Nd and in turn producing much older model ages and implying older components were involved, such as continental crust (Tomlinson and Percival, 2000). Also, if older continental sediments are weathered off the continents and become part of the subducted material, then this too could give the impression that older continental material contaminated the magmas, but with no direct involvement of continental basement.

Sediment subduction in modern arcs is difficult to prove because if sediment was subducted in a present day environment, then a geochemical analysis of fresh sediment should show similar patterns to the erupting lavas, which is not always the case (Davidson, 1987). Sediment could be derived from multiple sources, including weathering off of the adjacent arcs, or it could be sediment carried across the ocean floor while the plates are moving (Davidson, 1987). The thin layer of sediment that collects on the ocean floor is derived from the continental crust for the most part, so the sediment subducted with the oceanic crust is basically continental crust recycled into the mantle (Othman et al., 1989).

The rhyolite and andesite volcanic rocks of Hamlin Lake show a mildly calc-alkaline affinity and are interpreted as being mature arc volcanic rocks. Lentz (1998) proposed that compositions between tholeiitic and calc-alkaline (arc) volcanic rocks are typical of back-arc environments and could be interpreted as a transition from arc to non-arc rocks. This could explain why the Sm-Nd data shows contamination when the tectonic setting is interpreted as being a mature oceanic arc-setting and should not have continental crust involved in the lavas.
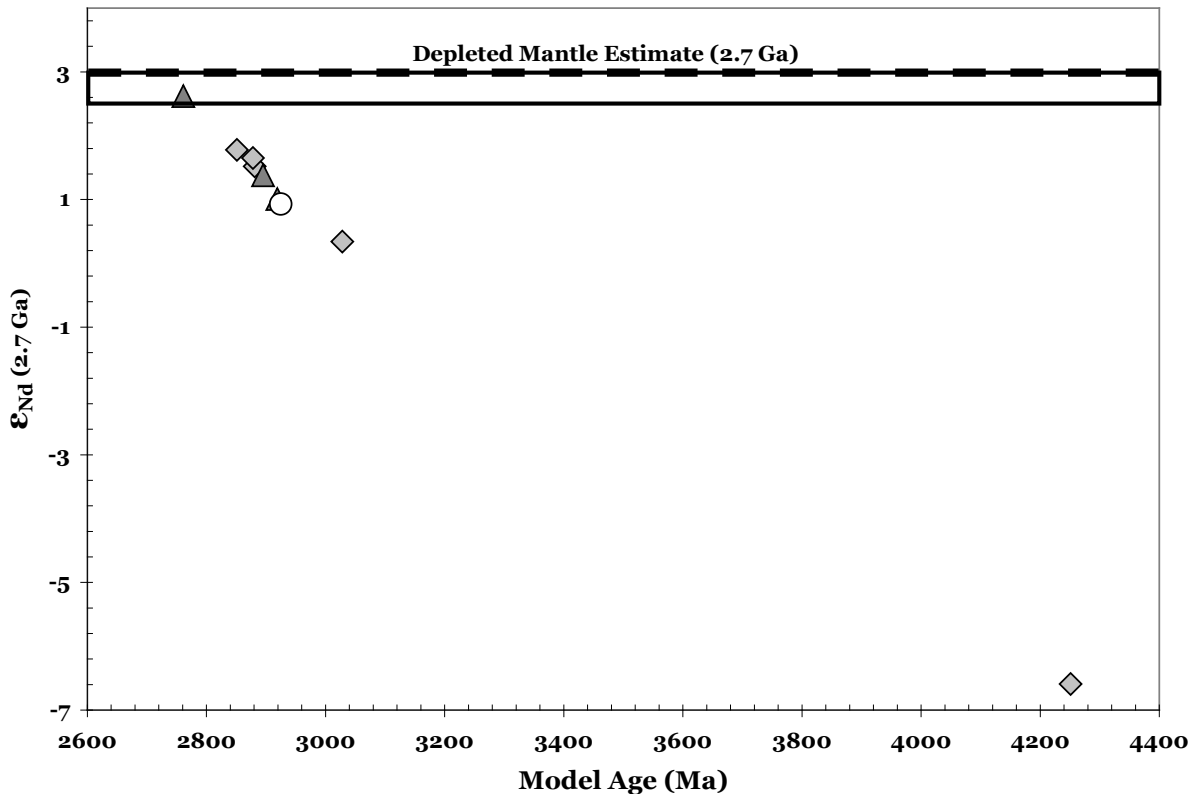
FIGURE 6.3 – A plot of model age versus ε_{Nd} values showing the Hamlin Lake samples relative to the depleted mantle estimate. Thick dashed line represents the depleted mantle estimate (+3.0) of Tomlinson et al. (2002), and thick box represents depleted mantle estimate range (+2.5 to +3.0) of Cousens (2000), both for 2.7 Ga. Symbols are the same as Figure 6.2.

In a study of the 1890 Ma Amisk Group metavolcanic arc rocks of the Flin Flon belt, Stern et al. (1992) found that arc derived rocks have the greatest isotopic variability with ε_{Nd} values ranging from +2.1 to +4.8. The variability in values require these rocks to have contributions from much older light REE-enriched crust and suggests that the mantle source to the arc assemblage was probably oceanic lithosphere within a subduction zone mantle wedge, modified by the addition of fluids and melts (Stern et al., 1992). It was also proposed by Stern et al. (1992) that the Amisk Group metavolcanic arc rocks were formed in a supra-subduction zone environment in which the mantle source probably did not have a unique Nd isotopic composition because of the isotopic heterogeneities and isotopic variations caused by the addition of subduction-related fluids and melts. According to Stern et al. (1992) the lower or more negative the ε_{Nd} values

120

in a dataset, the more contaminated the sample. Highly negative numbers and highly variable data sets are explained as being the result of Archean crust with strong negative ε_{Nd} values being incorporated into the parental magmas (Stern et al., 1992). Even samples that showed positive ε_{Nd} values such as +0.4 and slightly negative numbers such as -0.1, were assumed to have interacted with much older LREE-enriched lithosphere; a characteristic consistent with a continental arc.

Stern et al. (1992) also interpreted the higher amount of calc-alkaline rocks in the Flin Flon belt to represent continental arc assemblages. Although the Flin Flon metavolcanic rocks are of a younger age than the Hamlin Lake rocks, when compared with each other the Hamlin Lake samples also show a variable
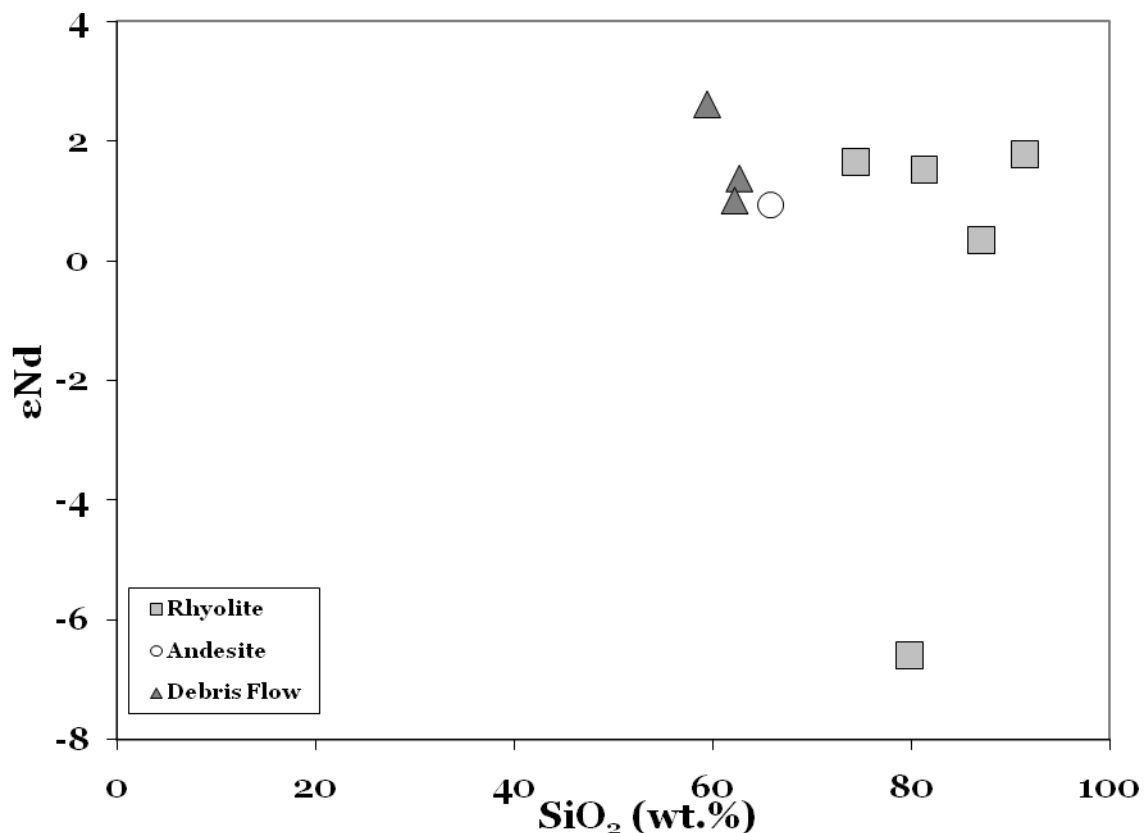
FIGURE 6.4 – A plot of SiO_2 wt. % versus ε_{Nd} demonstrates the difference between AS-05-081 and the remaining samples.

data range of +0.34 to +2.62, which could be the result of crustal interaction with Archean crust as proposed by Stern et al. (1992).

Cousens (2000) looked at a "metarhyolite" of the 2.7 Ga Kam Group and found an ε_{Nd} value of -2.6, with the negative value explained as the result of inheritance of older crustal material. The Chan basalts of the Kam Group showed ε_{Nd} values ranging from +1.4 to +4.0, with the depleted mantle estimated to be between +2.5 and +3.0 at the time, indicating a depleted mantle source (Cousens, 2000). These observations by Cousens (2000) help explain the Hamlin Lake rocks because they too fall within the range of ε_{Nd} values in the Kam Group and suggest that even though they are below average depleted mantle they are most likely slightly contaminated by an older contaminant. Theriault and Tella (1997) interpreted a set of mafic volcanic samples from the 2.66 Ga Rankin Inlet Group with ε_{Nd} values of -1.1, +0.8 and +1.6 as having variable contamination from older crust. They proposed that more evolved ε_{Nd} values may reflect contamination of the mantle source by subduction of terrigenous sediments.

It is clear that some of the Hamlin Lake rocks have undergone contamination and even if the rocks are derived from a mature oceanic arc, it is possible that the continental signature originated from the recycling of older crust within the mantle. If the mantle was heterogeneous it could be that the Hamlin Lake rocks reflect these isotopic variations. In a study of the 3.01–2.83 Ga Obonga Lake Greenstone belt in the western Superior Province, Tomlinson et al. (2002) concluded that a felsic rock having ε_{Nd} value of +0.3 was the result of recycling of older crust within the mantle, or small amounts of older crustal contamination and it was concluded that a mature arc-system with a continental crust component was the source (Tomlinson et al., 2002). At the northwest periphery of the Superior Province, the Assean Lake Crustal Complex is an ancient assembly of rocks, which contains Nd model ages of orthogneiss samples of ~3.5-3.7 Ga, but there are also three samples with model ages older than ~4.0 Ga interpreted as indicating recycling of extremely old crust (Böhm et al., 2003). The single old model age at Hamlin Lake may indicate a similar process but additional data points are required to confirm this.

Cousens (2000) used an ε_{Nd} versus SiO_2 plot to prove the origin of the source of magmas in the 2.7 Ga Kam Group of the Yellowknife Greenstone Belt. When the samples of the Kam Group did not plot together, Cousens (2000) concluded that the samples were inconsistent with a single homogeneous source because of the gaps between samples. When the nine Sm-Nd samples from Hamlin Lake are plotted on the same plot, they plot relatively close to each other, suggesting a single source, except for sample AS-05-081 (Fig. 6.3). Sample AS-05-081 plots much lower than the remaining eight samples suggesting contamination.

6.3 Conclusions

The Sm-Nd isotopic system has become a very powerful tool for identifying and understanding the nature of the crust at times of volcanism and the tectonic settings in which the systems were produced because it remains undisturbed throughout most crustal processes (Theriault and Tella, 1997). The volcanic rocks at Hamlin Lake show subduction signatures, including negative Nb and Ti anomalies, and arc signatures such as enrichment of the LREE compared to HREE and calc-alkaline affinities. The Hamlin Lake area has Sm-Nd values that are indicative of a depleted mantle origin with one sample showing strong contamination. The Hamlin Lake rocks have an isotopic signature that implies variable contamination by older continental material likely as a result of the subduction of continentally derived sediment.

The radiogenic isotope data from the Hamlin Lake area displays characteristics of magmas that have been contaminated by older continental material. Geochemical data from Hamlin Lake is consistent with it being a mature oceanic island arc rather than a continental arc. The majority of the ε_{Nd} data from Hamlin Lake lies close to the calculated values for depleted mantle at 2.7 Ga. Given the lack of geochemical evidence for eruption through continental crust, the trend to less positive values in some samples is best explained by contamination by subducted terrigenous sediment rather than eruption in continental arc. The strongly negative ε_{Nd} for sample AS-05-081 can be

accounted for by the same method, but would require considerably more contaminant or a uniquely older source.

7.1 Introduction

Oxygen isotopic analyses were carried out on 37 samples from the Hamlin Lake area; 17 rhyolites, eight dacites, eight andesites, two pink breccia and two samples of banded iron formation (Fig. 7.1). The samples were analyzed for their whole rock O isotope content to determine the extent of the alteration in the Hamlin Lake area and examine any relationship between $\delta^{18}O$ values and stratigraphy. The oxygen isotope data for the Hamlin Lake suite is shown in Table 7.1.

Oxygen isotopes can be used in VMS districts to better understand chemical changes in rocks caused by hydrothermal fluids and associated variability in fluid temperatures (Brauhart et al., 2000). Delta ^{18}O values are generally positive in rocks and minerals, because they are enriched in ^{18}O relative to VSMOW (Vienna Standard Mean Ocean Water; Faure, 1986). Most silicate rocks have $\delta^{18}O$ values of 5-15‰, but isotopic compositions vary between igneous, sedimentary and metamorphic rocks making it possible to discriminate the origin
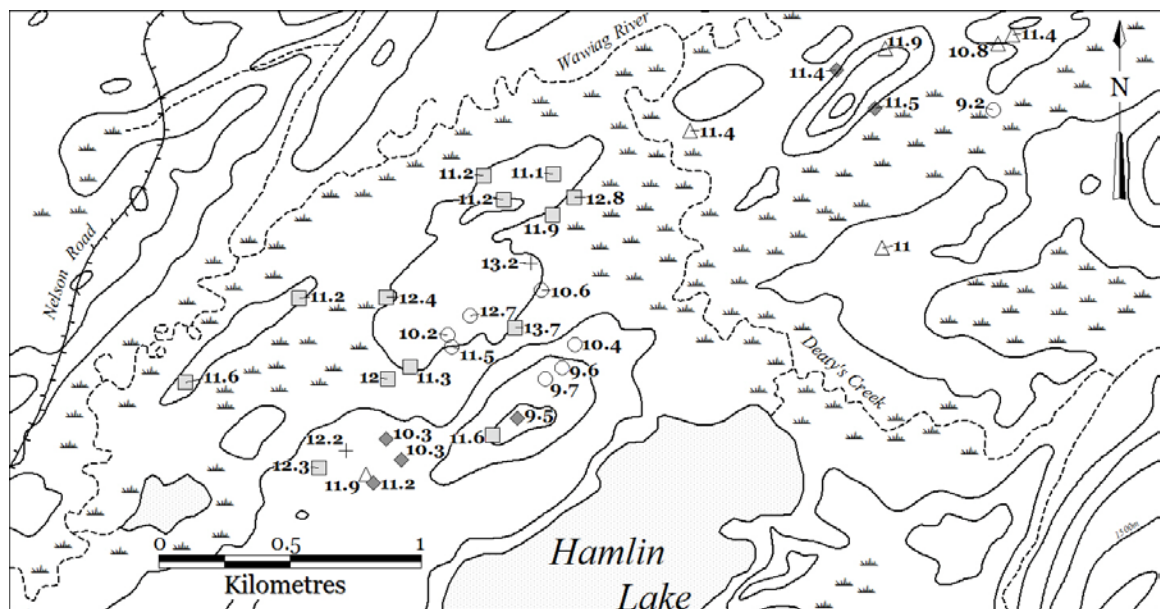
FIGURE 7.1 – A topographic map showing the location of the samples analyzed for oxygen isotopes along with their $\delta^{18}O$ values. (Squares=rhyolites, circles=andesites, triangles=dacites, diamonds=debris flows, stars=pink breccias and crosses=BIF).

TABLE 7.1 – Results of [18]O isotope analyses.

Sample	δ [18]O (‰ VSMOW)	Lithology
AS-06-009	9.2	Andesite
AS-05-064	9.6	Andesite
AS-05-066	9.7	Andesite
AS-05-056	10.2	Andesite
AS-05-086	10.4	Andesite
LR-05-006	10.6	Andesite
AS-05-041	11.5	Andesite
AS-05-053a	12.7	Andesite
AS-05-024b	12.2	BIF
G05-9	13.2	BIF
AS-06-018	10.8	Dacite
OC-327	11.0	Dacite
AS-06-010	11.4	Dacite
AS-06-002	11.4	Dacite
OC-339	11.9	Dacite
AS-05-021	11.9	Dacite
AS-05-004a	7.0	Pink breccia
AS-05-001a	8.4	Pink breccia
G05-15	11.1	Rhyolite
AS-06-005	11.2	Rhyolite
G05-19	11.2	Rhyolite
AS-05-049	11.3	Rhyolite
AS-06-007	11.6	Rhyolite
AS-05-062	11.6	Rhyolite
G05-13	11.9	Rhyolite
OC-159	12.0	Rhyolite
AS-05-012	12.3	Rhyolite
AS-06-011	12.4	Rhyolite
G05-18	12.5	Rhyolite
G05-14	12.8	Rhyolite
LR-05-002	13.7	Rhyolite
AS-05-059	9.5	Debris flow
AS-05-032	10.3	Debris flow
AS-05-034b	10.3	Debris flow
AS-05-018	11.2	Debris flow
OC-336	11.4	Debris flow
OC-332	11.5	Debris flow

of the rocks (Faure, 1986). Epstein and Taylor (1967) showed that quartz has the highest tendency to concentrate ^{18}O followed by dolomite, alkali feldspar, calcite, plagioclase, muscovite, anorthite, pyroxene, hornblende, olivine, garnet, biotite, chlorite, ilmenite and finally magnetite. In general, the $\delta^{18}O$ values of igneous rocks increase with increasing concentration of SiO_2 (Faure, 1986). Faure (1986) stated that the values of $\delta^{18}O$ of igneous rocks and their minerals is determined by among other factors (1) the temperature of crystallization; (2) the $\delta^{18}O$ of the magma; (3) effects of fractional crystallization; and (4) interaction with aqueous solutions.

The ^{18}O composition of water from a single source can be increased or decreased during the evolution of hydrothermal fluids (Ohmoto and Rye, 1974). This is achieved by loss of a vapor phase, by redox reactions and by isotopic exchange with various types of rocks. Ohmoto and Rye (1974) reported that probably the most important mechanism which can affect isotopic compositions of fluids is the oxygen and hydrogen isotope exchange reaction with country rocks. This is supported by the work of Brauhart et al. (2000) who showed that a regional decrease in whole rock oxygen isotope values with depth in the volcanic pile of the Panorama VMS district of Western Australia, was the result of increasing temperature of seawater-rock interaction with depth. The zone of low oxygen isotope values that usually underlie VMS mineralization is interpreted to represent a high temperature discharge zone, where evolved seawater was returned to the paleoseafloor in a convective hydrothermal system (Brauhart et al., 2000).

7.2 Results

The $\delta^{18}O$ data for Hamlin Lake varied for each of the lithologies analyzed (Table 7.1; Fig. 7.1). $\delta^{18}O$ values of the rhyolites varied from 11.1 to 13.7‰, the dacite volcanic rocks from 10.8 to 11.9‰ and the andesite volcanic rocks from 9.2 to 12.7‰. The two BIF samples are 12.2 and 13.2‰ and the two pink breccia samples are 7.0 and 8.4‰. The overlap in the $\delta^{18}O$ values of the different lithologies suggests that there has either been little hydrothermal alteration or that it is pervasive within the scale of the study. Intense selective alteration

would result in low $\delta^{18}O$ because minerals such as quartz and feldspar can be mobilized under such conditions and have the highest ^{18}O absorbing qualities. If a lithology did go through strong alteration, then it would show extremely low $\delta^{18}O$ values, because it would have leached ^{18}O absorbing minerals from the rocks.

When examining the petrographic thin sections that accompanied ten of the samples analyzed for oxygen isotopes, it is clear that some of the samples are more altered than others. The rhyolites are all fine-grained to very fine-grained with sericite contents ranging from 15-35% and quartz ranging from 40-80%. There are relict feldspars in one sample, as well as quartz phenocrysts, replaced by sericite crystals. In one sample, the sericite is associated with veining, but this is not the case in most samples where sericite alteration is pervasive.

The dacite volcanic rocks are very fine-grained with 20-70% sericite and quartz contents of 25-70%. There is also an estimated 5-10% chlorite in thin section, which appears as concentrated clusters of crystals.

In thin section the andesites are very similar in appearance to the rhyolites, except that there appears to be more carbonate alteration in the andesite samples than the rhyolite samples. The calcite crystals are fine-grained and interstitial with the quartz grains, although there are a few larger calcite grains present. There does not appear to be as much sericite alteration affecting the andesites as the rhyolites.

When the petrography is combined with the alteration box plot for the oxygen isotope samples (Fig. 7.2) it is apparent that there are samples, which are strongly altered and samples that are less altered. Chapter 5 discussed the geochemistry of the Hamlin Lake suite including the major and trace elements and their mobility. Of the 37 samples that were analyzed for oxygen isotopes at Hamlin Lake, the most common type of alteration is sericite. Chlorite alteration is present, but it is more abundant in the debris flow samples than the volcanic rocks. When looking closely at the individuals samples, the rhyolite samples that are located outside of the least-altered box were estimated to contain 30-35% sericite. For example, sample AS-05-012 contains approximately 35% sericite in thin section and also has a very high $\delta^{18}O$ value (12.3 ‰). This suggests that high $\delta^{18}O$ values are indicative of higher sericite content and consequently more

intense alteration. Andesite sample AS-05-053 is also found outside the least altered box (Fig. 7.2) near AS-05-012 and also has a high $\delta^{18}O$ value (12.7 ‰), as well as sample AS-05-021, which shows approximately 70% sericite supporting the argument that the Hamlin Lake suite has elevated $\delta^{18}O$ values as a result of alteration.

When looking at plots of $\delta^{18}O$ plotted against CCPI and AI (Fig. 7.3a and 7.3b, respectively), there is no relationship of increasing or decreasing $\delta^{18}O$ with increasing degree of alteration. This suggests that the observed variation in $\delta^{18}O$ has not been disturbed by hydrothermal alteration and can be utilized to investigate the mineralizing system in the Hamlin Lake area.
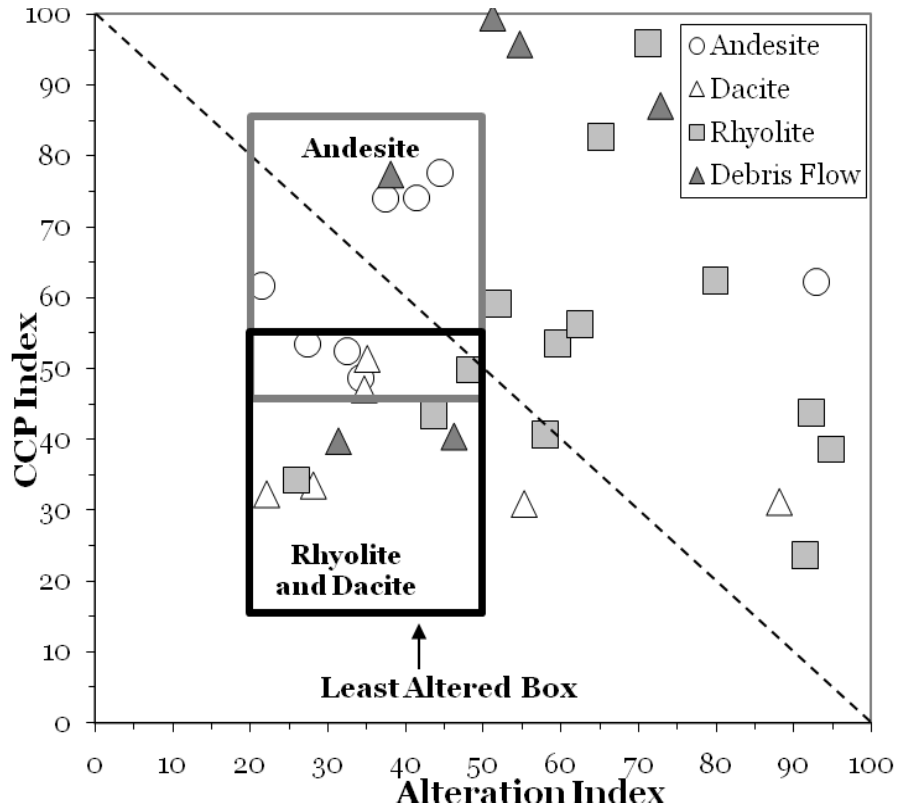
FIGURE 7.2 – An alteration box plot of the 37 samples analyzed for oxygen isotopes.
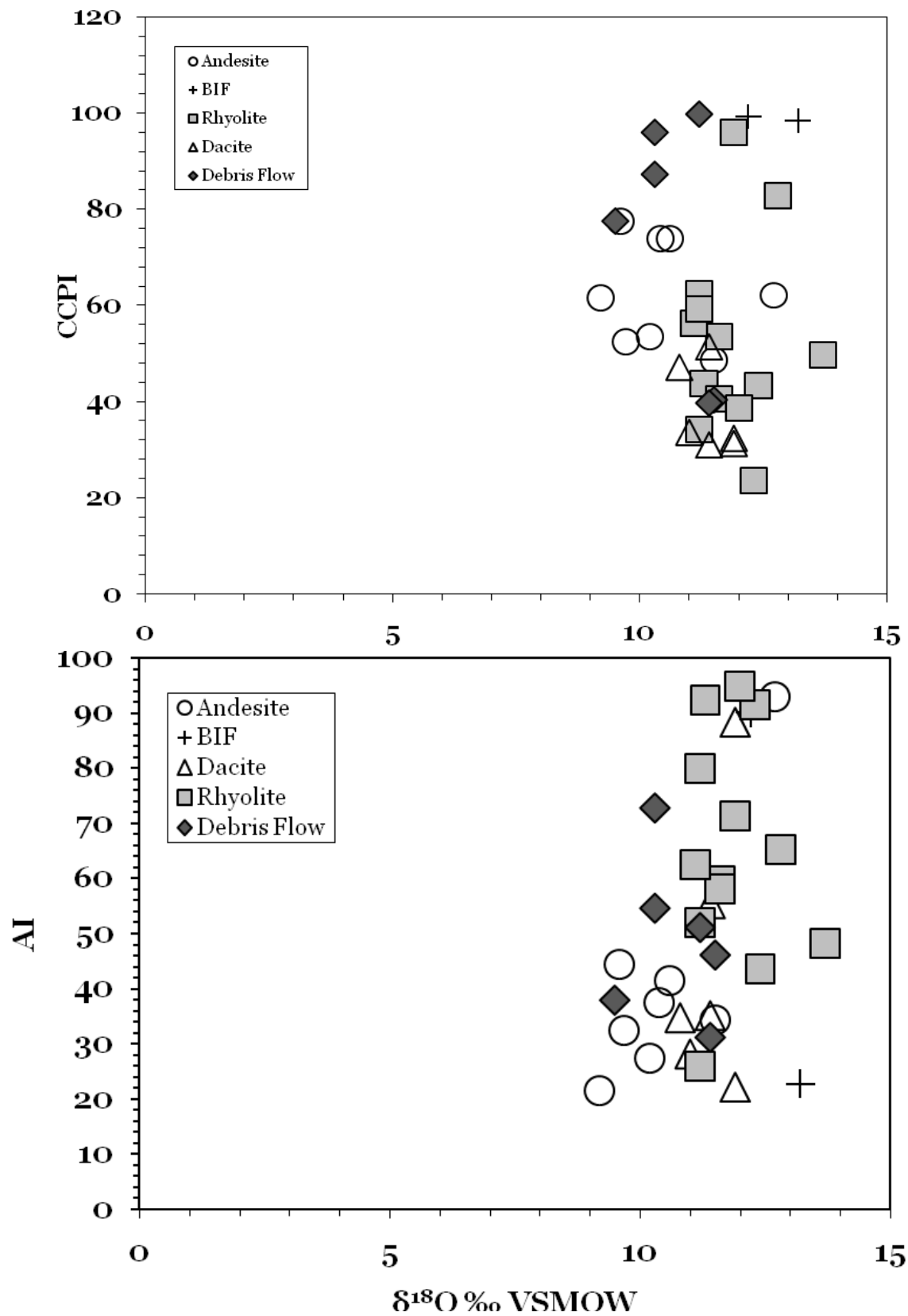
FIGURE 7.3 – Plots of (a) $\delta^{18}O$ versus CCPI and (b) $\delta^{18}O$ versus AI. The lack of a linear relationship indicates that alteration did not affect the $\delta^{18}O$ values.

7.3 Discussion

In a hydrothermal system, like the one that created the alteration seen at Hamlin Lake, rocks become enriched in $\delta^{18}O$ because: (1) water is 90% oxygen by mass volume; and (2) seawater contains more ^{18}O than is in equilibrium with rock at low temperatures and thus "enriches" the rock in recharge areas (Cathles, 1993). Furthermore, the intensity and volume of isotopic alteration can be used to estimate the amount of water-rock interaction and provides a quantitative measure of the potential of the system for massive sulfide mineralization (Cathles, 1993).

In the Abitibi region, the average unaltered $\delta^{18}O$ value of rhyolitic rocks is ~8‰, while for an andesite it is ~6‰ (Beaty et al., 1988). In the absence of unaltered sample at Hamlin Lake it is not unreasonable to assume that isotope values for unaltered volcanic rocks were similar to the Abitibi samples. In the Hamlin Lake region, the average $\delta^{18}O$ value for the rhyolites is ~12‰, while the dacites are ~11‰ and the andesites are ~10‰. This suggests that the rhyolite and andesite volcanic rocks $\delta^{18}O$ values have both been enriched ~4‰ compared to the equivalent unaltered rhyolite and andesite values in the Superior Province. In a study by Barrett et al. (1992) of the Mobrun deposit of the Abitibi region, the average $\delta^{18}O$ value for rhyolite and andesite volcanic rocks was enriched by ~4‰ when compared to fresh rhyolite and andesite volcanic rocks in the Abitibi region. Barrett et al. (1992) determined that a temperature of approximately 250°C is required for the alteration fluids to enrich the samples by ~4‰. This is seen in the Horne mine, which needed ~250°C to enrich the volcanic rocks by 2-4‰ (Barrett et al., 1992). Hoy (1993) observed that temperature models for VMS deposits demonstrate that temperatures of fluids range from a high-temperature (300-350°C) mineralized core outward to lower temperatures (~200°C), distal to the orebodies. The 4‰ increase in the samples at Hamlin Lake may indicate that the hydrothermal fluids that affected the Hamlin Lake area were at the lower end of the range for VMS deposits, which is consistent with other evidence, such as sericite alteration that it represents the distal portion of a hydrothermal system.

An oxygen isotope study by Hoy (1993) compared the bulk-rock $\delta^{18}O$ values of hydrothermally altered lithologies surrounding six VMS deposits,

including Mobrun, Horne, Norbec, Amulet, Ansil and Corbet mines, all found in the Noranda area of the 2.7 Ga Blake River Group in the Abitibi greenstone belt. Hoy (1993) found that $\delta^{18}O$ in samples increased up stratigraphy. This was interpreted to be the result of the fact that alteration zones were comprised of two mineralogically distinct assemblages: the first is volumetrically predominant and made up of a quartz-sericite-albite assemblage, and the second is a chlorite-quartz assemblage, which is volumetrically smaller and usually located in a pipe-shaped zone beneath the sulfide body (Hoy, 1991). Overall, the $\delta^{18}O$ values of a sample depends on the proportions of minerals in a sample and their ^{18}O values (Hoy, 1993), because according to Taylor (1974) ^{18}O isotopes fractionate from $\delta^{18}O_{chlorite} < \delta^{18}O_{sericite} < \delta^{18}O_{albite} < \delta^{18}O_{quartz}$. A chlorite core underlies some of the deposits and is surrounded by quartz-sericite altered volcanic rocks, which Hoy (1993) explained would cause low $\delta^{18}O$ values beneath the ore body and would increase as one moves away from the orebody. Hoy (1993) observed this
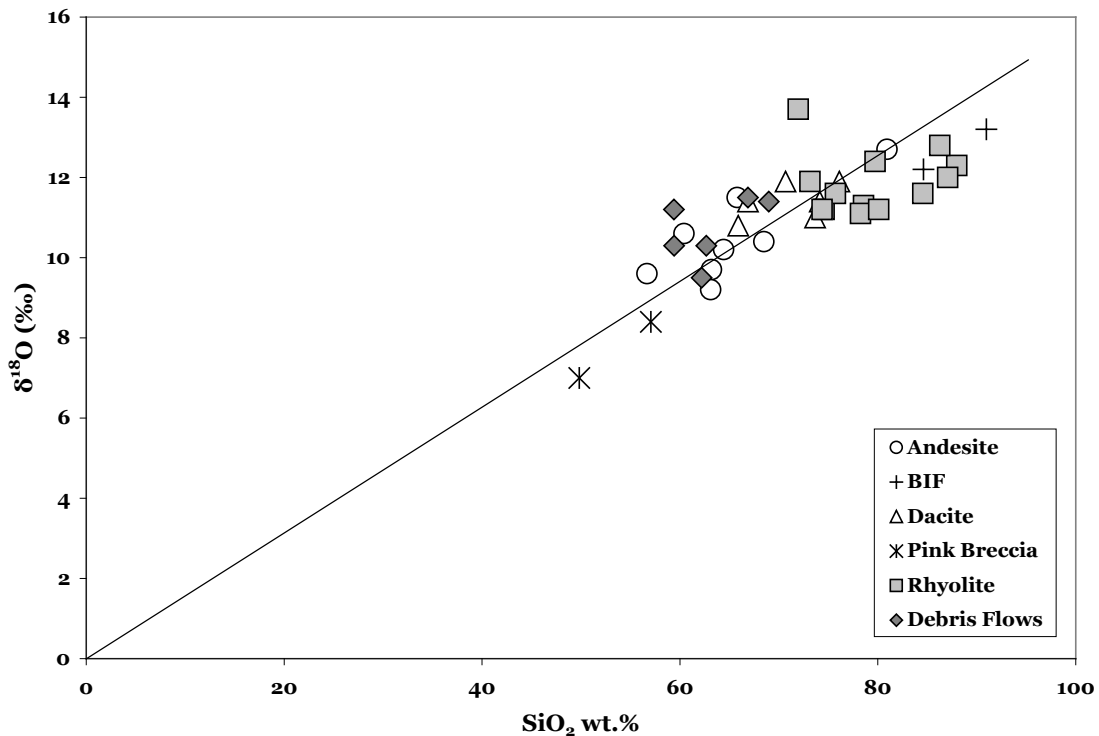
FIGURE 7.4 – A plot of SiO$_2$ wt.% versus $\delta^{18}O$ values showing as SiO$_2$ wt.% increases, so does the $\delta^{18}O$ values.

pattern at the Corbet and Ansil mines with low $\delta^{18}O$ values (2-6‰) around the ore body and an increase in values as one moves away from the deposit (up to 11‰). At the Mobrun deposit there is no distinct lateral variations seen in the $\delta^{18}O$ values, which were attributed to the absence of a defined pipe (Barrett et al., 1992). The lack of a pronounced gradient in $\delta^{18}O$ values at Hamlin Lake is consistent with the absence of any recognized feeder zone.

In the Hamlin Lake area, an area of approximately 4x6 kilometres was sampled. Cathles (1993) noted that even though convective processes tend to concentrate hydrothermal discharge, the area of fluid recharge in a convective system is much greater than the area of discharge. This means that in order to use $\delta^{18}O$ as an exploration tool, an area of at least 10x10 kilometres can prove to be much more useful because $\delta^{18}O$ values often show a gradient pattern in VMS related hydrothermal systems.

To date no massive sulfide deposit has been found at Hamlin Lake and there is no specific area that shows a lower or higher series of $\delta^{18}O$ values to indicate a stringer zone. The lack of sufficient $\delta^{18}O$ patterns does not mean that there is not a massive sulfide zone in the area, but only that the hydrothermal system may have affected a very large area (20x20km) and the scale of this mapping project is not able to cover it fully. Hannington et al. (2003) explained that most VMS districts are not mapped at a large enough scale to include the limits of hydrothermal systems. The low temperature implied by the ^{18}O isotopes at Hamlin Lake suggests it may represent the fringes of a larger VMS system.

CHAPTER 8

DISCUSSION AND CONCLUSIONS

8.1 Introduction

The volcanic suites that are associated with volcanogenic massive sulfide deposits can be difficult to classify because of hydrothermal alteration that is commonly associated with them. Primary textures and minerals are often non-existent as a result of intense alteration, however, with the use of whole-rock geochemistry, stable isotopes and radiogenic isotopes, original rock lithologies and tectonic setting can be recognized.

8.2 VMS Mineralization and Alteration

The massive sulfides found at Hamlin Lake consist of massive pyrite lenses in a fine-grained matrix. The LN7 sulfides are similar in appearance to the debris flows, however, instead of chert clasts, there are pyrite clasts, suggesting that massive sulfide clasts were incorporated in a debris flow upon deposition. This relationship suggests that there may have been a massive sulfide deposit in the vicinity of Hamlin Lake at one point. The LN7 sulfides indicate previous banding of the sulfides before they were deformed and incorporated in the debris flow. The absence of a significant VMS deposit at Hamlin Lake could be because sulfide production was shut off before it was able to accumulate a significant amount of sulfide mineralization. The LN7 sulfides were previously either fragmented and then transported or were formed at proximal hydrothermal vents on a sloped surface and eventually becoming part of a debris flow. Similar observations of sulfides within a debris flow unit were made by Walker and Lentz (2006) at the Flat Landing massive sulfide deposit of the Bathurst mining camp.

The extent of the mineralization at Hamlin Lake consists of the LN7 area where there are other outcrops with minor disseminated pyrite mineralization, but no significant accumulation of sulfides. Walker and Lentz (2006) stated that the absence of a well-defined proximal facies, such as a stringer zone argues for sulfide deposition distal to the vent complex. At Hamlin Lake there is no stringer zone recognized and this has lead to the conclusion that the vent that was

responsible for sulfide deposition in the area is distal to the Hamlin Lake felsic package, but not so far that the LN7 sulfides were not able to be deposited or that the iron formation could not be formed.

The LN7 mineralized area is located in the south eastern portion of the mapping area (Fig.4.1). There is a higher concentration of debris flow outcrops in the area surrounding the LN7 sulfides compared to the other part of Hamlin Lake area that were mapped during this study. The debris flow units contain abundant chlorite, which typically is found below massive sulfides in VMS deposits, as a result of the alteration pipe concentrating chlorite in the main discharge zone (Fig. 1.1; Franklin, 2005). The alteration pipe would normally show high amounts of MgO and/or FeO_T, and K_2O because of chlorite concentrations, but Hamlin Lake does not show elevated average concentration of MgO (~2.34) or K_2O (~1.43) in the debris flow units, suggesting that they are not part of an alteration pipe related to VMS mineralization. However, the lower average MgO contents could also be because it was difficult to separate the chert clasts from the chlorite matrix when submitting samples for analysis and as a result, chert clasts were included in the samples.

When looking at the rest of the units in the area, weak to intense sericite alteration is the most common type of alteration present. Some major elements are interpreted to have been mobile because samples did not show clustering within units on major element plots. Major element mobility is a common observation in the pervasively altered zones found surrounding massive sulfide deposits (Lesher et al., 1986). At Hamlin Lake, the rhyolites show a low Na_2O wt.% compared to K_2O wt.% suggesting that the rhyolites were more intensely altered than any other unit and is typical of sericite alteration in VMS systems. This is consistent with thin section observation. However, in thin section, the average loss on ignition (LOI) values for the rhyolites are low, but the average loss on ignition (LOI) values are lower (1.82) than any other unit, a sign of weak alteration. Both the andesites and dacites, show average Na_2O wt.% greater than K_2O wt.%, indicative of less intense alteration, however, the LOI values on average are 3.78 for the andesites and 2.24 for the dacites, which is a feature typically associated with alteration. It is not obvious why the unit with the most

135

alteration petrographically and geochemically would have the lowest LOI, but it may reflect the primary lithology.

The HFSE elements of Hamlin Lake are generally immobile (REE, Y) in the distal portions, which is common for VMS deposits (Lesher et al., 1986).

Detailed petrography were combined with geochemistry to assess the range of the alteration index (AI) and the chlorite-carbonate-pyrite index (CCPI) values for the weakly to intensely altered volcanic rocks at Hamlin Lake. The least-altered rhyolites have comparable alteration indices to unaltered modern arc rhyolites (AI=30-60 and CCPI=10-40; Gifkins et al., 2005). Even though the least-altered volcanic rocks show variations in their content of REE, the slopes of the patterns stay the same, indicating that the rhyolite rocks are chemically related to the andesite rocks, probably by fractionation (Fig. 5.17). The alteration box plots support earlier observations that the andesites underwent the least amount of alteration followed by the dacites and finally the rhyolites, which were often moderately to intensely altered (Fig. 5.8). On the alteration box plot a least altered box was based on the samples of the rhyolites, dacites and andesites with the highest Na_2O wt.% values, as this represents the least hydrothermal alteration. In the field, the outcrops were small and lenticular and volcanic units were not traceable for any distance, and as a result, neither was alteration. The volcaniclastic units at Hamlin Lake may account for the patchy alteration. Volcaniclastic textures would allow for hydrothermal fluids to pass more easily as the massive, coherent flows have been more porous and permeable allowing for greater fluid/rock interaction. This is the case with the rhyolite unit, because it contains more volcaniclastic material, it may have allowed for more fluids to pass through it.

Oxygen isotopes were analyzed for 39 samples to better constrain the alteration. Although the extent of the alteration system at Hamlin Lake is unknown, it is thought that it is larger than the area that was covered by oxygen isotope sampling. The Hamlin Lake volcanic rocks do exhibit $\delta^{18}O$ differences between the different lithologies, however because outcrops are small, lenticular and not continuous, an obvious alteration halo was not recognized even though one is commonly produced in response to hydrothermal alteration around VMS

deposits. On average, the samples analyzed for oxygen isotopes are 4‰ higher than the average rhyolite, dacite or andesite in the Superior Province (6-8‰; Beaty et al., 1988), which is characteristic of low temperature hydrothermal fluids. The lack of an oxygen isotope halo is caused by an inconsistency of lithology in the area and could reflect a small distal portion of a larger system.

8.3 Tectonic Setting and Volcanology

At Hamlin Lake, primary textures and minerals were affected by hydrothermal alteration consequently. The rhyolites, dacites and andesites were virtually indistinguishable in the field. In contrast, the iron formation and pink breccia units were easy to identify in the field, because they were very distinct from the volcanic units.

Rare primary volcanic textures were identified using a combination of field observations and petrography. This combination allowed for the identification of massive pyroclastic and volcaniclastic units, suggesting a very complex volcanic area regime. Some of the pyroclastic units observed in the Hamlin Lake area show fiamme and lapilli that are diagnostic of explosive activity (Fig. 4.7). Pyroclastic debris and volcaniclastic units show redeposited, subaqueous, pyroclastic debris. These primary pyroclastic flows are diagnostic of and only found in shallow subaqueous flows. The fact that no units were traceable over a long distance or confined to any one area is interpreted to reflect an unstable depositional environment. The assortment of multiple units over a small area may also reflect multiple volcanic centres. The identification of primary pyroclastic units demonstrates that the area was formed in a shallow subaqueous setting because explosive eruptions capable of generating these units are restricted to this environment. Other textures recognized at Hamlin Lake that are indicative of a shallow setting are the presence of silica nodules. These nodules are diagnostic of hot, gas-supported deposition in a shallow setting (McPhie et al., 1993). The sag structure that was found (Fig. 4.14) is also consistent with a subaqueous environment because of deformation of the underlying beds that were deformed in response to clast contact with bedding. All of these features demonstrate that the Hamlin Lake area was produced in a

shallow setting that was not too far away from the volcanic vent or vents, but deep enough that the wave base did not affect the primary textures (1-2 km).

The outcrops at Hamlin Lake display lenticular shapes, which is especially noticeable in the debris flow units. The lenticular shape is interpreted to have been produced in response to deposition on a sloped surface and in turn, an unstable environment. The debris flows were likely shed off a sloped surface and geochemically are associated with the andesites and rhyolites. The abundance of debris flows increase up stratigraphy, which can be explained by an increase in explosive activity. Because the debris flows are concentrated around the mineralized area (Fig. 4.1), it is thought that the increase in explosive activity may have destroyed a massive sulfide deposit that was forming at the vent site. This could explain why there are massive sulfide lenses (thought to originally be sulfide fragments) in the LN7 sulfides. The LN7 sulfides may be the remainder of a massive sulfide deposit in the Hamlin Lake area that was destroyed by explosive volcanic activity.

The banded iron formation found at Hamlin Lake is of the Algoma-type iron formation variety and is commonly found around volcanic or volcaniclastic rocks, and is thought to have formed in arcs or back-arcs, spreading ridges or rift environments (Peter, 2003). The banded iron formation at Hamlin Lake cannot be traced for any distance; however, it helps to understand what environment Hamlin Lake was created in and at what depth. Since the bedding of the iron formations found at Hamlin Lake are not disturbed; they must have been produced below wave base (>0.1 km).

The geochemistry of the volcanic suite can be used to determine the tectonic setting and can also explain with geochemical variations on a plot of Zr (ppm) versus Y (ppm) the andesites and rhyolites are distinct from the dacites. The differences between the andesites and rhyolites and the dacites suggest that there were variable incompatible element abundances in the source magma. Pearce (1982) noted that fractionated calc-alkaline lavas are usually depleted in Zr, Y, Nb and heavy REE, but not Th, U, or the LREE, all of which are observed in the Hamlin Lake volcanic rocks. Barrett and MacLean (1999) noted that variable chemistries seen in different sequences are a result of not only tectonic setting,

138

but also depth of magma generation, fractionation and the amount of interaction with continental crust. All of the volcanic units display negative Nb and Ti anomalies when plotted on a PM plot, indicative of a subduction setting.

Felsic rocks related to VMS systems can be geochemically separated into four different groups with the use of a $[Yb]_{cn}$ versus $[La/Yb]_{cn}$ plot (Lesher et al., 1986). The Hamlin Lake rocks again show similarities between the andesites and rhyolites, but not the dacites when plotted on the $[Yb]_{cn}$ versus $[La/Yb]_{cn}$ plot. The dacites plot within the FI field, the andesites and rhyolites plot within the FII field. Hart et al. (2004) stated that no VMS deposits are hosted by FI felsic volcanic rocks; however, FI felsic volcanic rocks may be present in the same volcanic succession as the deposits. Some FII rhyodacites and rhyolites host VMS deposits, but most are barren. FIII and FIV high silica rhyolites are much less abundant in the rock record, but commonly host VMS deposits, regardless of their age, and FIII rhyolites appear to host many of the largest deposits. The dominance of FII felsics at Hamlin Lake is consistent with the presence of sulfide mineralization even though no deposit has yet been found.

Although there are a lot of petrogenetic models for the formation of felsic magmas involved with VMS deposits, most think that they are the result of fractionation processes in high level magma chambers (Lesher et al., 1986; Hart et al., 2004). It is believed that these high level chambers also provide the heat and/or metals required to generate an ore-forming VMS hydrothermal system. FII, FII and FIV felsic volcanic rocks are thought to be associated with high level magma chambers, whereas FI magmas are thought to have originated from a much deeper source. This can explain the many differences seen geochemically between the dacites and the rhyolites and andesites at Hamlin Lake. If FI magmas are generated from a deeper source and the dacites all fall within the FI field, then it explains why the dacite trace element samples always plot away from the rhyolites and andesites.

The Sm-Nd isotope data for Hamlin Lake also suggests that there were different magma sources and variable contamination. Sm-Nd can identify and help understand the crustal processes that affected volcanic rocks that erupted in the Archean. The δ_{Nd} for depleted mantle is thought to be between +2.5 and +3.0

at 2.7 Ga (Cousens, 2000). The samples of Hamlin Lake fall close to this estimate, except for one sample which shows an ε_{Nd} of -6.59 that is proof of contamination by a much older source. The trend towards lower ε_{Nd} values at Hamlin Lake is consistent with either contamination by continental crust or intrusion of terrigenous sediments introduced into the subduction zone. The absence of other features characteristic of Andean-style subduction zone makes the latter model more likely. A plot of $[Yb]_{cn}$ versus $[La/Yb]_{cn}$ provides further evidence for this when compared to the work of Polat (1999) who separated fields on this particular plot into slab melting TTD's, modern average slab-derived magmas and slab-dehydration post-Archean granitoids. The dacites fall within the average slab-derived magmas field, while the rhyolites and andesites fall within the slab-dehydration field. This suggests that the dacites may have been the result of a slab derived magma and the rhyolites and andesites are derived from a shallower dehydrated slab melt. This can explain the differences in trace element geochemistry between the volcanic units. These observations are consistent with the growth of the Archean continental crust as a subduction-accretion complex along convergent plate margins

Hamlin Lake comprises volcanic and volcaniclastic rocks deposited as debris flows in shallow water depths, possibly from multiple vents. The geochemistry and isotopes indicate the magmas were derived from a sub-arc mantle that had been contaminated by subducted terrigenous sediment derived from older continental crust and erupted in a mature-island arc setting. The alteration and mineralization are consistent with Hamlin Lake having been the distal part of a larger hydrothermal system that may have formed a VMS deposit.

REFERENCES

Bally, A.W., Scotese, C.R. and Ross, M.I. 1989. North America: Plate tectonic setting and tectonic elements; *In* The Geology of North America: An Overview, The geology of North America, Volume A, Geological Society of America, p.1-16.

Barrett, T.J., Cattalani, S., Chartrand, F. and Jones, P., 1991. Massive sulfide deposits of the Noranda area, Quebec. II. The Aldermac mine, Can. J. Earth Sci., vol. 28, p.1301-1327.

Barrett, T.J., Cattalani, S. and MacLean, W.H., 1993a. Volcanic lithogeochemistry and alteration at the Delbridge massive sulfide deposit, Noranda, Quebec, Jour. Geochem. Explor., vol. 48, p.135-173.

Barrett, T.J. and MacLean, W.H., 1991. Chemical, Mass, and Oxygen Isotope Changes During Extreme Hydrothermal Alteration of an Archean Rhyolite, Noranda, Quebec, Economic Geology, vol. 86, p.406-414.

Barrett, T.J. and MacLean, W.H., 1999. Volcanic Sequences, Lithogeochemistry, and Hydrothermal Alteration in Some Bimodal Volcanic-Associated Massive Sulfide Systems, *in* Barrie, C.T. and Hannington, M.D., eds., Volcanic-Associated Massive Sulfide Deposits: Processes and Examples in Modern and Ancient Settings, Reviews in Economic Geology, Vol. 8, p.101-131.

Barrett, T.J., MacLean, W.H. and Areback, H., 2005. The Palaeoproterozoic Krisineberg VMS deposit, Skellefte district, northern Sweden. Part II: chemostratigraphy and alteration, Mineralium Deposita, vol. 40, p.368-395.

Barrett, T.J., MacLean, W.H., Cattalani, S. and Hoy, L., 1993b. Massive sulfide deposits of the Noranda area, Quebec. V. The Corbet mine, Can. J. Earth Sci., vol. 30, p.1934-1954.

Barrett, T.J., MacLean, W.H. and Tennant, S.C., 2001. Volcanic Sequence and Alteration at the Parys Mountain Volcanic-Hosted Massive Sulfide Deposit, Wales, United Kingdom: Applications of Immobile Element Lithogeochemistry, Economic Geology, vol. 96, p.1279-1305.

Barrie, C.T., Ludden, J.N. and Green, T.H., 1993. Geochemistry of Volcanic Rocks Associated with Cu-Zn and Ni-Cu Deposits in the Abitibi Subprovince, Economic Geology, vol. 88, p.1341-1358.

Beaty, D.W., Taylor, H.P. and Coad, P.R., 1988. An Oxygen Isotope Study of the Kidd Creek, Ontario, Volcanogenic Massive Sulfide Deposit: Evidence for a High [18]O Ore Fluid, Economic Geology, vol. 83, p.1-17.

Beaty, D.W. and Taylor, H.P., 1982. Some Petrologic and Oxygen Isotopic Relationships in the Amulet Mine, Noranda, Quebec, and Their Bearing on the Origin of Archean Massive Sulfide Deposits, Economic Geology, vol. 77, p.95-108.

Bédard, J.H., Brouillette, P., Madore, L. and Berclaz, A., 2003. Archaean cratonization and deformation in the northern Superior Province, Canada: an evaluation of plate tectonic versus vertical tectonic models, Precambrian Research, vol. 127, p.61-87.

Böhm, C.O., Heaman, L.M., Stern, R.A., Corkery, M.T. and Creaser, R.A., 2003. Nature of Assean lake ancient crust, Manitoba: a combined SHRIMP-ID-TIMS U-Pb geochronology and Sm-Nd isotope study, Precambrian Research, vol. 126, p.55-94.

Bradshaw, G.D., Tucker, T., Peter, J.M., Paradis, S. and Rowins, S.M., 2001. Geology of the Wolverine polymetallic volcanic-hosted massive sulphide deposit, Finlayson Lake district, Yukon Territory, Canada, in Emond, D.S. and Weston, L.H., eds., Yukon Exploration and Geology 2000: Whitehorse, Exploration and Geological Services Division, Yukon, Indian and Northern Affairs Canada, p.269-287.

Brauhart, C.W., Huston, D.L. and Andrew, A.S., 2000. Oxygen isotope mapping in the Panorama VMS district, Pilbara Craton, Western Australia: applications to estimating temperatures of alteration and to exploration, Mineralium Deposita, vol. 35, p.727-740.

Bridge, D.A., Marr, J.M., Hasimoto, K., Obara, M. and Suzuki, R., 1986, Geology of the Kutcho Creek volcanogenic massive sulphide deposits, northern British Columbia, in Morin, J.A., eds., Mineral deposits of the northern Cordillera: Canadian Institute of Mining and Metallurgy Special Volume 37, p.115.128.

Campbell, I.H, Lesher, C.M., Coad, P., Franklin, J.M., Gorton, M.P. and Thurston, P.C., 1984. Rare-earth element mobility in alteration pipes below massive Cu-Zn sulfide deposits, Chemical Geology, vol. 45, p.181-202.

Card, K.D. and Ciesielski, A., 1986. DNAG#1, Subdivisions of the Superior Province of the Canadian Shield, Geoscience Canada, vol. 13, p.5-13.

Cas, R. and Wright, J., 1991. Subaqueous pyroclastic flows and ignimbrites: an assessment, Bulletin of Volcanology, vol. 53, p.357-380.

Cathles, L.M., 1993. Oxygen Isotope Alteration in the Noranda Mining District, Abitibi Greenstone Belt, Quebec, Economic Geology, Vol.88, p.1483-1511.

Cattell, A., Krogh, T.E. and Arndt, N.T., 1984. Conflicting Sm-Nd whole rock and U-Pb zircon ages for Archean lavas from Newton Township, Abitibi Belt, Ontario, Earth Planet. Sci. Lett., vol. 70, p.280-290.

Cooke, D.L. and Moorhouse, W.W., 1969. Timiskaming Volcanism in the Kirkland Lake area, Ontario, Canada, Canadian Journal of Earth Sciences, vol. 6, p.117-129?

Corfu, F. and Stott, G.M., 1998. Shebandowan greenstone belt, western Superior Province: U-Pb ages, tectonic implications, and correlations, GSA Bulletin, vol. 110, p.1467-1484.

Costa, U.R., Barnett, R.L. and Kerrich, R., 1983. The Mattagami Lake mine Archean Zn-Cu sulfide deposit, Quebec: Hydrothermal coprecipitation of talc and sulfides in a sea-floor brine pool – evidence from geochemistry, $^{18}O/^{16}O$, and mineral chemistry, Economic Geology, vol. 78, p.1144-1203.

Cousens, B.L., 1996. Magmatic evolution of Quaternary mafic magmas at Long Valley Caldera and the Devils Postpile, California: Effects of crustal contamination on lithospheric mantle-derived magmas, Journal of Geophysical Research, vol. 101, p.27673-27689.

Cousens, B.L., 2000. Geochemistry of the Archean Kam Group, Yellowknife Greenstone Belt, Slave Province, Canada, Jour. Geol., vol. 108, p.181-197.

Crawford, A.J., Corbett, K.D. and Everland, J.L., 1992. Geochemistry of the Cambrian Volcanic-Hosted Massive Sulfide-Rich Mount Read Volcanics, Tasmania, and Some Tectonic Implications, Economic Geology, vol. 87, p.597-619.

DePaolo, D.J., 1981. Trace Element and Isotopic Effects of Combined Wallrock Assimilation and Fractional Crystallization, Earth Planet. Sci. Lett., vol. 53, p.189-202.

De Rosen-Spence, A., Provost, G., Dimroth, E., Gochnauer, K. and Owen, V., 1980. Archean Subaqueous Felsic Flows, Rouyn-Noranda, Quebec, Canada, and their Quaternary Equivalents, Precambrian Research, vol. 12, p.43-77.

Downey, W.S., McCutcheon, S.R. and Lentz, D.R., 2006. A Physical Volcanological, Chemostratigraphic, and Petrogenetic Analysis of the Little Falls Member, Tetagouche Group, Bathurst Mining Camp, New Brunswick, Exploration and Mining Geology, vol. 15, p.199-220.

Dickin, A.P., 2005. Radiogenic Isotope Geology; Cambridge University Press, Cambridge, 492p.

Epstein, S. and Taylor, H.P. Jr., 1967. Variation of O^{18}/O^{16} in minerals and rocks: In P.H. Abelson, ed., Researches in Geochemistry, vol. 2, p.29-62. John Wiley, New York, 663p.

Eremin, , N.I., Dergachev, A.L., Sergeeva, N.E. and Pozdnyakova, N.V., 2000. Types of volcanic-hosted massive sulfide deposits: Geology of Ore Deposits, vol. 42, p.160-171.

Faure, G., 1986. Principles of Isotope Geology; John Wiley & Sons, Toronto, 589p.

Franklin, J.M., Gibson, H.L., Jonasson, I.R. and Galley, A.G., 2005. Volcanogenic Massive Sulfide Deposits, Economic Geology 100th Anniversary Volume, p.523-560.

Franklin, J.M., Sangster, D.M. and Lydon, J.W., 1981. Volcanic-associated massive sulfide deposits: Economic Geology 75th Anniversary Volume, p. 485-627.

Giblin, P.E., 1964. Geology of the Burchell lake Area, District of Thunder Bay; Ontario Department of Mines, Geological Report No. 19, 39p.

Gifkins, C., Herrmann, W. and Large, R., 2005. Altered Volcanic Rocks – A guide to description and interpretation: Hobart, Australia, Centre for Ore Deposit and Exploration Studies, University of Tasmania, 275p.

Gifkins, C.C. and Allen, R.L., 2001. Textural and chemical characteristics of diagenetic and hydrothermal alteration in glassy volcanic rocks – examples from the Mount Read Volcanics, Tasmania, Economic Geology, vol.96, p.973-1002.

Gorton, M.O. and Schandl, E.S., 2000. From continents to island arcs: A geochemical index of tectonic setting for arc-related and within-plate felsic to intermediate volcanic rocks, The Canadian Mineralogist, vol.38, p.1065-1073.

Gribble, C.D. and Hall, A.J., 1992. Optical Mineralogy: Principles & practice; University-College London, London, p.302.

Gross, G.A. (1995) Iron-rich sedimentary strata, in Canadian Mineral Deposit Types: A Geological Synopsis, Geological Survey of Canada Economic Geology Report 36, 86p.

Hamilton, P.J., O'Nions, R.K., Evenson, N.M., Bridgwater, D.E. and Aliart, J.H., 1978. Sm-Nd isotopic investigations of Isua supracrustals and implications for mantle evolution, Nature, vol.272, p.41-43.

Hannington, M.D., Barrie, C.T., and Bleeker, W., 1999a. The giant Kidd Creek volcanogenic massive sulfide deposit, western Abitibi subprovince, Canada: Preface and introduction: Economic Geology Monograph 10, p.1-30.

Hannington, M.D., Poulsen, K.H., Thompson, J.F.H., and Sillitoe, R.H., 1999b. Volcanogenic gold in the massive sulfide environment: Reviews in Economic Geology, vol. 8, p.325-356.

Hannington, M.D., Santaguida, F., Kjarsgaard, I.M. and Cathles, L.M., 2003. Regional-scale hydrothermal alteration in the Central Blake River Group, western Abitibi subprovince, Canada: implications for VMS prospectivity, Mineralium Deposita, vol. 38, p.393-422.

Harris, F.R., 1970. Geology of the Moss Lake Area, District of Thunder Bay; Ontario Department of Mines and Northern Affairs, Geological Report 85, 61p.

Hart, T.R., 2007. 9. Project Unit 06-003. Geochronology of the Hamlin and Wye Lakes Area, Shebandowan Greenstone Belt, Thunder Bay District *In* Summary of Field Work and Other Activities 2007, Ontario Geological Survey, Open File Report 6213, p.9-1 to 9-8.

Hart, T.R., Gibson, H.L. and Lesher, C.M., 2004. Trace element geochemistry and petrogenesis of felsic volcanic rocks associated with volcanogenic massive Cu-Zn-Pb sulfide deposits, Economic Geology, vol.99, p.1003-1013.

Hawksworth, C.J., Gallagher, K., Hergt, J.M. and McDermott, F., 1993. Mantle and Slab Contributions in Arc Magmas, Annu. Rev. Earth Planet. Sci., vol. 21, p.175-204.

Hodgkinson, J.M., 1968. Geology of the Kashabowie Area, District of Thunder Bay; Ontario Department of Mines, Geological Report 53, 35p.

Hoffman, , P.F., 1991. On accretion of granite-greenstone terranes. In: Robert, F., Sheahan. P.A., Green, S.B. (Eds). Nuna Conf. Greenstone Gold and Crustal Evolution, Val d' Or. Geol. Assoc. Can., p.32-45.

Hollings, P., Richardson, A., Creaser, R.A. and Franklin, J.M., 2007. Radiogenic isotope characteristics of the Mesoproterozoic intrusive rocks of the Nipigon Embayment, northwestern Ontario, Can. Jour. Earth Sci., vol. 44, p. 1111-1129.

Hollings, P., Wyman, D. and Kerrich, R., 1999. Komatiite-basalt-rhyolite volcanic associations in Northern Superior Province greenstone belts:

significance of plume-arc interaction in the generation of the proto continental Superior Province, Lithos, vol. 46, p.137-161.

Howell, D.G., 1989. Tectonics of suspect terranes---Mountain building and continental growth; Chapman and Hall, London, 232p.

Hoy, Lawrence D., 1993. Regional Evolution of Hydrothermal Fluids in the Noranda District, Quebec: Evidence from $\delta^{18}O$ Values from Volcanogenic Massive Sulfide Deposits, Economic Geology, vol. 88, p.1526-1541.

Huston, D.L. and Taylor, B.E., 1999. Genetic Significance of Oxygen and Hydrogen Isotope Variations at the Kidd Creek Volcanic-Hosted Massive Sulfide Deposit, Ontario Canada, Economic Geology, Monograph 10, p.335-350.

Hutchinson, R.W., 1973. Volcanogenic sulfide deposits and their metallogenic significance, Economic Geology, vol.68, p. 1223-1246.

Jacobsen, S.B., 2003. How Old Is Planet Earth?, Science, vol. 300, p.1513-1514.

Kusky, T.M. and Polat, A., 1999. Growth of granite—greenstone terranes at convergent margins, and stabilization of Archean cratons, Tectonophysics, vol. 305, p.43-73.

Langford, F.F. and Morin, J.A., 1976. The development of the Superior Province of northwestern Ontario by merging island arcs, Amer. Jour. Sci., vol. 276, p.1023-1034.

Large, R.R., Gemmell, J.B., Paulick, H. and Huston D.L., 2001a. The Alteration Box Plot: A Simple Approach to Understanding the Relationship between Alteration Mineralogy and Lithogeochemistry Associated with Volcanic-Hosted Massive Sulfide Deposits, Economic Geology, vol. 96, p.957-971.

Large, R.R., Allen, R.L., Blake, M.D. and Herrmann, W., 2001b. Hydrothermal Alteration and Volatile Element Halos for the Rosebery K Lens Volcanic-Hosted Massive Sulfide Deposit, Western Tasmania, Economic Geology, vol. 96, p.1055-1072.

Large, R.R., McPhie, J., Gemmell, B.J., Herrmann, W. and Davidson, G. 2001c. The Spectrum of Ore Deposit Types, Volcanic Environments, Alteration Halos, and Related Exploration Vectors in Submarine Volcanic Successions: Some examples from Australia, Economic Geology, vol. 96, p.913-938.

Lavigne, Aubut and Scott, 1990. Base metal mineralization the Shebandowan Greenstone Belt; *in* Field Trip Guidebook, 36th Annual Meeting, Institute on Lake Superior Geology, vol. 36, pt.2, p.67-97.

Leistel, J.M., Marcoux, E., Thieblemont, D., Quesada, C., Sanchez, A., Almodovar, G.R., Pascual, E. and Saez, R., 1998. The volcanic-hosted massive sulphide deposits of the Iberian Pyrite Belt: Review and preface to the thematic issue: Mineralium Deposita, vol. 33, p.2-30.

Le Maitre, R.W., Streckeisen, A., Zanettin, B., Le Bas, M.J., Bonin, B., Bateman, G., Bellieni, G., Dudek, A., Efremova, S., Keller, J., Lamere, J., Sabine, P.A., Schmind, R., Sorensen, H. and Woolley, A.R., 2002. Igneous Rocks: A Classification and Glossary of Terms, Recommendations of the International Union of geological Sciences, Subcommission of the Systematics of Igneous Rocks: Cambridge University Press, p.

Lentz, D.R. (eds.), 1994. Alteration and Alteration Processes Associated with Ore-Forming Systems; Geological Association of Canada, Mineral Deposits Division, Short Course Notes, vol. 11, 467p.

Lentz, D.R., 1998. Petrogenetic evolution of felsic volcanic sequences associated with Phanerozoic volcanic-hosted massive sulphide systems: the role of extension geodynamics, Ore Geology Reviews, vol. 12, p.289-327.

Lentz, D.R., 1999. Petrology, Geochemistry, and Oxygen Isotope Interpretation of felsic Volcanic and Related Rocks Hosting the Brunswick 6 and 12 Massive Sulfide Deposits (Brunswick Belt), Bathurst Mining Camp, New Brunswick, Canada, Economic Geology, vol. 94, p.57-86.

Lentz, D.R. and McCutcheon, S.R., 2006. Brunswick No.6 Massive Sulfide Deposit, Bathurst Mining Camp, Northern New Brunswick, Canada: A Synopsis of the Geology and Hydrothermal Alteration System, Exploration and Mining Geology, vol. 15, p.123-156.

Lerouge, C., Deschamps, Y., Joubert, M., Béchu, Fouillac, A.-M. and Castro, J.A., 2001. Regional oxygen isotope systematics of felsic volcanics; a potential exploration tool for volcanogenic massive sulphide deposits in the Iberian Pyrite Belt, Jour. Of Geochem. Explor., vol. 72. p.193-210.

Lesher, C.M., Goodwin, A.M., Campbell, I.H. and Gorton, M.P., 1986. Trace-element geochemistry of ore-associated and barren, felsic metavolcanic rocks in the Superior Province, Canada, Can. J. Earth Sci., vol. 23, p.222-237.

Loren, R.A., 2002. Petrology: the study of igneous, sedimentary and metamorphic rocks; McGraw-Hill, Toronto, p.720.

Lowe, D.R. 1976. Grain Flow and Grain Flow Deposits, Journal of Sediment Petrology, vol. 46, p.188-199.

Maas, R., McCulloch, M.T., Campbell, I.H. and Coad, P.R., 1986. Sm-Nd and Rb-Sr dating of an Archean massive sulfide deposit: Kidd Creek, Ontario, Geology, vol. 14, p.585-588.

MacKenzie, W.S. and Guilford, C., 1980. Atlas of rock-forming minerals in thin section; Longman Scientific & Technical, New York, 98p.

MacLean, W.H. and Barrett, T.J., 1993. Lithogeochemical techniques using immobile elements, Jour. Geochem. Explor., vol. 48, p.109-133.

McPhie, J., Doyle, M. and Allen, R., 1993. Volcanic Textures - A guide to the interpretation of textures in volcanic rocks: Hobart, Australia, Centre for Ore Deposit and Exploration Studies, University of Tasmania, 197p.

Miller, C., Halley, S., Green, G., and Jones, M., 2001. Discovery of the West 45 Voclanic-Hosted Massive Sulfide Deposit Using Oxygen Isotopes and REE Geochemistry, Economic Geology, vol. 96, p.1227-1237.

Nesbitt, B.E., Longstaffe, F.J., Shaw, D.R. and Muehlenbachs, K., 1984. Oxygen Isotope Geochemistry of the Sullivan Massive Sulfide Deposit, Kimberley, British Columbia, Economic Geology, vol. 79, p.933-946.

Ohmoto, H., 1996. Formation of volcanogenic massive sulfide deposits: The Kuroko perspective, Ore Geology Reviews, vol. 10, p.135-177.

Ohmoto, H. and Rye, R.O., 1974. Hydrogen and Oxygen Isotopic Compositions of Fluid Inclusions in the Kuroko Deposits, Japan, Economic Geology, vol. 69, p.947-953.

Othman, D.B., White, W.M. and Patchett, J., 1989. The geochemistry of marine sediments, island arc magma genesis and crust-mantle recycling, Earth Planet. Sci. Lett., vol. 94, p.1-21.

Osmani, I.A., 1997. Geology and mineral potential: Greenwater Lake area, West-Central Shebandowan Greenstone Belt; Ontario Geological Survey, Report 296, 135p.

Osterberg, S.A., Morton, R.L. and Franklin, J.M., 1987. Hydrothermal Alteration and Physical Volcanology of Archean Rocks in the Vicinity of the Headway-Coulee Massive Sulfide Occurrence, Onaman Area, Northwestern Ontario, Economic Geology, vol. 82, p.1505-1520.

Paradis, S., Taylor, B.E., Watkinson, D.H. and Jonasson, I.R., 1993. Oxygen Isotope Zonation and Alteration in the Northern Noranda District, Quebec: Evidence for Hydrothermal Fluid Flow, Economic Geology, vol. 88, p.1512-1525.

Pearce, J.A., 1982. Trace element characteristics of lavas from destructive plate boundaries, *in* Thorpe, R.S., eds., Andesite: Chichester, Wiley, p.525-548.

Percival, J.A., Stern, R.A. and Skulski, T., 2001. Crustal growth through successive arc magmatism: reconnaissance U-Pb SHRIMP data from the northeastern Superior Province, Canada, Precambrian Res., vol. 109, p.203-238.

Peter, J.M., 2003. Ancient iron formations: their genesis and use in the exploration for stratiform base metal sulphide deposits, with examples from the Bathurst Mining Camp, in Lentz, D.R., ed., Geochemistry of Sediments and Sedimentary Rocks: Evolutionary Considerations to Mineral Deposit-Forming Environments: Geological Association of Canada, GeoText 4, p.145-176.

Piercey. S.J., Mortensen, J.K. and Creaser, R.A., 2003. Neodymium isotope geochemistry of felsic volcanic and intrusive rocks from the Yukon-Tanana Terrane in the Finlayson Lake Region, Yukon, Canada, Can. J. Earth Sci., vol. 40, p.77-97.

Piercey, S.J., Paradis, S., Murphy, D.C. and Mortensen, J.K., 2001. Geochemistry and Paleotectonic Setting of Felsic Volcanic Rocks in the Finlayson Lake Volcanic-Hosted Massive Sulfide District, Yukon, Canada, Economic Geology, vol. 96, p.1877-1905.

Polat, A., 1999. Geochemistry of subduction-related mafic to felsic volcanic rocks of the late Archean Wawa greenstone belts, Superior Province, Canada. ARI, vol. 51, p.277-295.

Polat, A and Kerrich, R., 2001. Magnesian andesites, Nb-enriched basalt-andesites, and adakites from late-Archean 2.7 Ga Wawa greenstone belts, Superior Province, Canada: implications for late Archean subduction zone petrogenetic processes, Contrib. Mineral Petrol., vol. 141, p.36-52.

Polat, A., Kerrich, R. and Wyman, D.A., 1998. The late Archean Schreiber-Hemlo and White River-Dayohessarah greenstone belts, Superior Province: collages of oceanic plateaus, oceanic arcs, and subduction-accretion complexes, Tectonophysics, vol. 289, p.295-326.

Polat, A., Li, J., Fryer, B., Kusky, T., Gagnon, J. and Zhang, S., 2006. Geochemical characteristics of the Neoarchean (2800-2700 Ma) Taishan greenstone belt, North China Craton: Evidence for plume-craton interaction, Chemical Geology, vol. 230, p.60-87.

Prior, G.J., Gibson, H.L., Watkinson, D.H., Cook, R.E. and Hannington, M.D., 1999a. Rare Earth and High Field Strength Element Geochemistry of the Kidd Creek Rhyolites, Abitibi Greenstone Belt, Canada: Evidence or

Archean Felsic Volcanism and Massive Sulfide Ore Formation in an Iceland-Style Rift Environment, Economic Geology, Monograph 10, p.457-484.

Prior, G.J., Gibson, H.L., Watkinson, D.H., Cousens, B.L., Cook, R.E. and Barrie, C.T., 1999b. Sm-Nd Isotope Study of Rhyolites from the Kidd Creek Mine Area, Abitibi Subprovince, Canada, Economic Geology, Monograph 10, p.485-496.

Raymond, L.A., 1995. Petrology: The study of Igneous, Sedimentary and Metamorphic rocks, McGraw-Hill, Toronto, 720p.

Richard, P., Shimizu,N. and Allegre, C.J., 1976. $^{143}Nd/^{146}Nd$, a Natural Tracer: an application to oceanic basalts, Earth Planet. Sci. Lett., vol. 31, p.269-278.

Rollison, H. R., 1993. Using Geochemical Data: evaluation, presentation, interpretation; Pearson Education Ltd., England, 352p.

Schandl, E.S. and Gorton, M.P., 2002. Application of high field strength elements to discriminate tectonic settings in VMS environments, Economic Geology, vol. 97, p.629-642.

Schandl, E.S., Gorton, M.P. and Wasteneys, H.A., 1995. Rare Earth Element Geochemistry of the Metamorphosed Volcanogenic Massive Sulfide Deposits of the Manitouwadge Mining Camp, Superior Province, Canada: A Potential Exploration Tool? Economic Geology, vol. 90, p.1217-1236.

Scott, C.R., Mueller, W.U. and Pilote, P., 2002. Physical volcanology, stratigraphy, and lithogeochemistry of an Archean volcanic arc: evolution from plume-related volcanism to arc rifting of SE Abitibi Greenstone Belt, Val d'Or, Canada, Precambrian Research, vol. 115, p.223-260.

Sherlock, R.L. and Michaud, M., 2000. Volcanogenic massive sulfide deposits of Latin America: An overview: Geological Association of Canada Special Publication 2, p.19-46.

Simpson, K., Davies, A., McPhie, J., Cooke, D., Gemmell, B. and Large, R., 2006. Volcanology and Breccias for the Explorationist; Mineral Exploration Roundup 2006.

Smithies, R.H., Champion, D.C. and Cassidy, K.F., 2003. Formation of Earth's early Archaean continental crust, Precambrian Research, vol. 127, p.89-101.

Sol, S., Thomson, C.J., Kendall, J.-M., White, D., VanDecar, J.C. and Asudeh, I., 2002. Seismic tomographic images of the cratonic upper mantle beneath

the Western Superior Province of the Canadian Shield—a remnant Archean slab? Phys. Earth. Planet. Inter., vol. 134, p.53-69.

Stern, R.A., Syme, E.C., Bailes, A.H., Galley, A.G., Thomas, D.J. and Lucas, S.B., 1992. Nd-isotopic stratigraphy of Early Proterozoic Amisk Group metavolcanic rocks from the Flin Flon belt, Manitoba and Saskatchewan; in Radiogenic Age and Isotopic Studies: Report 6; Geological Survey of Canada, Paper 92-2, p.73-84.

Stott, G.M., Corkery, T., Leclair, A., Boily, M. and Percival, J., 2007. A revised terrane map for the Superior Province as interpreted from aeromagnetic data [abstract]; Institute on Lake Superior Geology Proceedings, 53rd Annual Meeting, Lutsen, MN, vol. 53, part1, p.74-75.

Stott, G.M. and Schnieders, B.R., 1983. Gold mineralization in the Shebandowan Belt and its relation to regional deformation patterns; in The Geology of Gold in Ontario, Ontario Geological Survey, Miscellaneous Paper 110, p.181-193.

Sun, S. and McDonough, W.F., 1989. Chemical and isotopic systematic of oceanic basalts: implications for mantle composition and processes; in Magmatism in ocean basins, Geological Society of London, Special Publication No.42, p.313-345.

Taylor, H.P., Jr. and Sheppard, S.M.F., 1986. Igneous rocks: I. Processes of isotope fractionation and stable isotopes: Reviews in Mineralogy, vol. 16, p.227-271.

Thériault, R.J. and Tella, S., 1997. Sm-Nd isotopic studies on mafic volcanic rocks form the Rankin Inlet and Tavani regions, District of Keewatin, Northwest Territories; in Radiogenic and Isotopic Studies: Report 10; Geological Survey of Canada, Current Research 1997-F, p.61-66.

Thompson, A.J.B and Thompson (Eds.), J.F.H., 1996. Atlas of Alteration: A field and petrographic guide to hydrothermal alteration minerals, Mineral Deposits Division-GAC, p.119.

Thurston, P.C., 1991. Geology of Ontario: Introduction; in Geology of Ontario, Ontario Geological Survey, spec. vol. 4, pt.1, p.3-25.

Thurston, P.C., 1991. Archean Geology of Ontario: Introduction; in Geology of Ontario, Ontario Geological Survey, spec. vol. 4, pt.1, p.73-78.

Thurston, P.C., Osmani, I.A. and Stone, D., 1991. Northwestern Superior Province: review and terrane analysis. In: Thurston, P.C., Williams, H.R., Sutcliffe, H.R., Stott, G.M. (Eds). Geology of Ontario. Ont. Geol. Surv., Spec. vol. 4, part 1, p.81-141.

Tomlinson, K.Y., Davis, D.W., Percival, J.A., Hughes, D.J. and Thurston, P.C., 2002. Mafic to felsic magmatism and crustal recycling in the Obonga Lake greenstone belt, western Superior Province: evidence from geochemistry, Nd isotopes and U-Pb geochronology, Precambrian Research, vol. 114, p.295-325.

Tomlinson, K.Y. and Percival, J.A., 2000. Geochemistry and Nd isotopes of granitoids rocks in the Shikag-Garden Lakes area, Ontario: recycled Mesoarchean crust in the central Wabigoon Subprovince; Geological Survey of Canada, Current Research 2000-E12; 11p.

Tomlinson, K.Y., Stott, G.M., Percival, J.A. and Stone, D., 2004. Basement terrane correlations and crustal recycling in the western Superior Province: Nd isotopic character of granitoid and felsic volcanic rocks in the Wabigoon subprovince, N. Ontario, Canada, Precambrian Research, vol. 132, p.245-274.

Walker, J.A. and Lentz, D.R., 2006. The Flat Landing Brook Zn-Pb-Ag Massive Sulfide Deposit, Bathurst Mining Camp, Exploration and Mining Geology, vol. 15, p.221-247.

Whalen, J.B., Percival, J.A., McNicoll, V.J. and Longstaffe, F.J., 2002. A Mainly Crustal Origin for Tonalitic Granitoid Rocks, Superior Province, Canada: Implications for Late Archean Tectonomagmatic Processes, Jour. Petrology, vol. 43, p.1551-1570.

Williams, H.R., 1990. Subprovince accretion tectonics in the south-central Superior Province. Can. J. Earth Sci., vol. 27, p.570-581.

Williams, H.R., Stott, G.M., Heather, K.B., Muir, T.L. and Sage, R.P., 1991. Wawa Subprovince; in Geology of Ontario, Ontario Geological Survey, spec. vol. 4, pt.1, p.485-539.

Winter, L.S., Tosdal, R.M., Franklin, J.M. and Tegart, P., 2004. A reconstructed Cretaceous depositional setting for giant volcanogenic massive sulfide deposits at Tambogrande, northwestern Peru, Special Publication of Society of Economic Geology, vol. 11, p.319-340.

Wyman, D.A., 2000. High-precision exploration geochemistry: applications for volcanogenic massive sulfide deposits, Aust. Jour. Earth Sci., vol. 47, p.861-871.

Wyman, D.A. (eds.), 1996. Trace Element Geochemistry of Volcanic Rocks: Applications for Massive Sulphide Exploration; Geological Association of Canada, Short Course Notes, vol. 12, 402p.

Yamagishi, H., 1987. Studies on the Neogene subaqueous lavas and hyaloclastites in southwest Hokkaido. Rep. Geol. Surv. Hokkaido, vol. 59, p.55-117.

Yamagishi, H. and Dimroth, E. 1985. A comparison of Miocene and Archean rhyolite hyaloclastites: Evidence for a hot and fluid rhyolite lava, Journal of Volcanology and Geothermal Research, vol. 23, p.337-355.

Zengqian H., Zaw, K., Xiaoming, Q., Qingtong, Y., Jinjie, Y., Mingji, X., Deming, F. and Xianke, Y., 2001. Origin of the Gacun Volcanic-Hosted Massive Sulfide Deposit in Sichuan, China: Fluid Inclusion and Oxygen Isotope Evidence, Economic Geology, vol. 96, p.1491-1512.

APPENDIX A

Field Sample Locations

Sample #	Easting	Northing	Lithology	Assay #
AS-05-001a	663184	5372274	Field:Pink Breccia	335501
AS-05-001b	663184	5372274	Field:Pink Breccia	335502
AS-05-001c	663184	5372274	Field:Pink Breccia	335503
AS-05-002	663162	5372245	Field:Pink Breccia	335504
AS-05-003	663096	5372268	Field:Pink Breccia	335505
AS-05-004a	663085	5372258	Field:Pink Breccia (gabbro fragment)	335506
AS-05-004b	663085	5372258	Field:Pink Breccia	335507
AS-05-005	663055	5372214	Field:Pink Breccia (felsic fragments)	335508
AS-05-006	663034	5372213	Field:Pink Breccia(mafic fragments)	335509
AS-05-007	663000	5372192	Field:Pink Breccia	335510
AS-05-008	662497	5372352	Field:Rhyolite	335511
AS-05-009	662477	5372386	Field:Mafic Dike	335512
AS-05-010a	662464	5372394	Field:Quartz-eye Rhyolite; Geochem:Rhyolite	335513
AS-05-010b	662464	5372394	Field:Quartz-eye Rhyolite (with fragments); Geochem:Rhyolite	335514
AS-05-011	662453	5372393	Field:Quartz-eye Rhyolite; Geochem:Rhyolite	335515
AS-05-012	662415	5372411	Field:Quartz-eye Rhyolite; Geochem:Rhyolite	335516
AS-05-013	662412	5372474	Field:Quartz-eye Rhyolite; Geochem:Rhyolite	335517
AS-05-014	662370	5372435	Field:Quartz-eye Rhyolite; Geochem:Rhyolite	335518
AS-05-015	662365	5372476	Field:Quartz-eye Rhyolite; Geochem:Rhyolite	335519
AS-05-016	662310	5372594	Potassically Altered Feldspar Porphyry	335520
AS-05-017	662627	5372346	Field:Mafic Debris Flow; not analyzed	
AS-05-018	662622	5372353	Field:Mafic Debris Flow; Geochem:Rhyolite	335521
AS-05-019	662624	5372360	Field:Mafic Debris Flow; Geochem:Andesite	335522
AS-05-020a	662628	5372359	Chloritized Feldspar Porphyry	335523
AS-05-020b	662628	5372359	Field:Rhyolite; Geochem:Dacite	335524
AS-05-021	662595	5372387	Field:Rhyolite; Geochem:Dacite	335525
AS-05-022	662576	5372442	Field:Rhyolite; Geochem:Andesite	335526
AS-05-023	662576	5372442	Field:Rhyolite; Geochem:Andesite	335527

Sample #	Easting	Northing	Lithology	Assay #
AS-05-024a	662520	5372473	Field:Quartz-eye Rhyolite; Geochem:Rhyolite	335528
AS-05-024b	662520	5372473	Field:Banded Iron Formation; Geochem:BIF	335529
AS-05-025	662483	5372515	Field:Quartz-eye Rhyolite; Geochem:Rhyolite	335530
AS-05-026	662447	5372588	Field:Quartz-eye Rhyolite; Geochem:Rhyolite	335531
AS-05-027	662649	5372346	Field:Rhyolite; Geochem:Andesite	335532
AS-05-028	662649	5372368	Field:Mafic Debris Flow; Geochem:Rhyolite	335533
AS-05-029	662654	5372406	Field:Rhyolite; Geochem:Andesite	335534
AS-05-030	662692	5372402	Field:Mafic Debris Flow; Geochem:Andesite	335535
AS-05-031	662681	5372426	Field:Mafic Debris Flow; Geochem:Rhyolite	335536
AS-05-032	662730	5372440	Field:Mafic Debris Flow; Geochem:Rhyolite	335537
AS-05-033	662623	5372468	Field:Mafic Debris Flow; Geochem:Andesite	335538
AS-05-034a	662660	5372520	Field:Rhyolite; Geochem:Andesite	335539
AS-05-034b	662672	5372520	Field:Felsic Debris Flow; Geochem: Rhyolite	335540
AS-05-034c	662665	5372520	Field:Mafic Debris Flow; Geochem:Rhyolite	335541
AS-05-034d	662670	5372528	Field:Mafic Debris Flow; Geochem:Andesite	335542
AS-05-035	662677	5372565	Field:Rhyolite (crystal tuff); Geochem:Dacite	335543
AS-05-036	663025	5372915	Field:Rhyolite (possible tuff); Geochem:Andesite	335544
AS-05-037	663003	5372917	Field:Rhyolite (crystallized tuff); Geochem:Andesite	335545
AS-05-038	662984	5372895	Field:Mafic Debris Flow/Iron Formation; Geochem:Rhyolite	335546
AS-05-039	662972	5372884	Field:Felsic to Intermediate Rhyolite; Geochem:Andesite	335547
AS-05-040	662963	5372891	Field:Mafic Debris Flow; Geochem:Andesite	335548
AS-05-041	662921	5372870	Field:Mottled/Bleached Rhyolite; Geochem:Andesite	335549
AS-05-042	662870	5372862	Field:Bleached Rhyolite; Geochem:Rhyolite	335550

Sample #	Easting	Northing	Lithology	Assay #
AS-05-043	662867	5372846	Field:Quartz/feldspar-eye Rhyolite; Geochem:Rhyolite	335551
AS-05-044	662858	5372832	Field:Quartz-eye Rhyolite; Field:Rhyolite	335552
AS-05-045	662679	5372769	Field:Rhyolite; Geochem:Rhyolite	335553
AS-05-046a	662704	5372774	Field:Sericitized Rhyolite; Geochem:Rhyolite	335554
AS-05-046b	662704	5372774	Field:Rhyolite; Geochem:Rhyolite	335555
AS-05-047	662732	5372878	Field:Rhyolite; Geochem:Rhyolite	335556
AS-05-048	662743	5372839	Field:Altered Rhyolite; Geochem:Rhyolite	335557
AS-05-049	662763	5372795	Field:Altered Quartz-eye Rhyolite; Geochem:Rhyolite	335558
AS-05-050	662782	5372806	Field:Banded Iron Formation; Geochem:BIF	335559
AS-05-051	662787	5372821	Field:Mafic Debris Flow; Geochem:Rhyolite	335560
AS-05-052	662999	5372992	Field;Felsic Debris Flow; Geochem:Rhyolite	335561
AS-05-053	662993	5372990	Field:Rusty Felsic Rhyolite (cherty); Geochem:Andesite	335562
AS-05-054	662956	5372953	Field:Rhyolite (silicified); Geochem:Rhyolite	335563
AS-05-055	662937	5372937	Field:Rhyolite; Geochem:Andesite	335564
AS-05-056	662764	5372927	Field:Rhyolite; Geochem:Andesite	335565
AS-05-057	662764	5372939	Field:Rhyolite; Geochem:Andesite	335566
AS-05-058	662765	5372950	Field:Rhyolite; Geochem:Rhyolite	335567
AS-05-059	662765	5372962	Field:Mafic Debris Flow; Geochem:Rhyolite	335625
AS-05-060	662766	5372973	Field:Mafic Debris Flow; Geochem: Rhyolite	335626
AS-05-061	662767	5372985	Field:Mafic Debris Flow; Geochem:Andesite	335627
AS-05-062	662767	5372996	Field:Rhyolite (massive); Geochem:Rhyolite	335628
AS-05-063	662768	5373008	Field:Mafic Debris Flow; Geochem:Rhyolite	335629
AS-05-064	662768	5373019	Field:Rhyolite; Geochem:Andesite	335630

Sample #	Easting	Northing	Lithology	Assay #
AS-05-065	662769	5373031	Field:Felsic to Intermediate Volcanics; Geochem:Andesite	335631
AS-05-066	662770	5373042	Field:Intermediate Volcanics; Geochem:Andesite	335632
AS-05-067	662770	5373054	Field:Intermediate Volcanics; Geochem:Andesite	335633
AS-05-068	663170	5372500	Field:Rhyolite; Not analyzed	75384
AS-05-069a	663294	5372620	Field:Rhyolite; Not analyzed	75385
AS-05-069b	663294	5372620	Field:Rhyolite; Not analyzed	75386
AS-05-070	663350	5372598	Field:Rhyolite; Not analyzed	75387
AS-05-071	663565	5372712	Field:Rhyolite; Not analyzed	75388
AS-05-072	663570	5372728	Field:Mafic Volcanics; Not Analyzed	75389
AS-05-072a	663570	5372728	Field:Intermediate Volcanics; Not analyzed	75390
AS-05-073a	663649	5372842	Field:Intermediate Volcanics; Not analyzed	75391
AS-05-073b	663649	5372842	Field:Intermediate Volcanics; Not analyzed	75393
AS-05-074	663050	5372224	Field:Mafic Volcanics; Not analyzed	75392
AS-05-075	663745	5372885	Field:Mafic Volcanics; Not analyzed	75394
AS-05-076	663537	5372996	Field:Intermediate Volcanics; Not analyzed	75395
AS-05-077			Quartz vein	75396
AS-05-078a	664062	5373111	Field:Rhyolite; Geochem:Rhyolite	335606
AS-05-078b	664062	5373111	Field:Rhyolite; Geochem:Rhyolite	335607
AS-05-079a	664081	5373111	Field:Intermediate Volcanics; Geochem:Andesite	335608
AS-05-079b	664081	5373111	Field:Rhyolite; Geochem:Rhyolite	335609
AS-05-080	664114	5373080	Field:Rhyolite; Geochem:Rhyolite	335610
AS-05-081	664160	5373112	Field:Qtz-eye Rhyolite; Geochem:Rhyolite	335611
AS-05-082	664273	5373154	Field:Potassically Altered Quartz-eye Rhyolite; Geochem:Rhyolite	335612
AS-05-083	663375	5372911	Field:Mottled Rhyolite; Geochem:Andesite	335613
AS-05-084	663377	5372905	Field:Rhyolite; Geochem:Andesite	335614

Sample #	Easting	Northing	Lithology	Assay #
AS-05-085	663377	5372886	Field:Massive Rhyolite; Geochem:Andesite	335615
AS-05-086	663393	5372880	Field:Mafic Debris Flow; Geochem:Andesite	335616
AS-05-087	663365	5372600	Field:Rhyolite; Not analyzed	335617
AS-05-088	662999	5372334	Field:Rhyolite; Geochem:Andesite	335634
AS-05-089	663287	5372872	Field:Rhyolite; Geochem:Andesite	335635
AS-05-090	663288	5372851	Field:Rhyolite; Geochem:Andesite	335636
AS-06-001	664143	5373430	Field:Rhyolite; Geochem:Dacite	28301
AS-06-002	663831	5373696	Field:Rhyolite; Geochem:Dacite	28302
AS-06-003	662465	5373077	Field:Rhyolite Lapilli Tuff; Geochem:Andesite	28303
AS-06-004	662467	5373073	Field:Quartz-eye Rhyolite; Geochem:Rhyolite	28304
AS-06-005	662338	5373059	Field:Quartz-eye Rhyolite; Geochem:Rhyolite	28305
AS-06-006	662158	5372988	Field:Quartz-eye Rhyolite; Geochem:Rhyolite	28306
AS-06-007	661905	5372738	Field:Quartz-eye Rhyolite; Geochem:Rhyolite	28307
AS-06-008	662020	5372900	Field:Pink Breccia; Geochem:Andesite	28308
AS-06-009	664990	5373776	Field:Felsic Debris Flow; Geochem:Andesite	28309
AS-06-010	665063	5374063	Field:Rhyolite tuff; Geochem:Dacite	28310
AS-06-011	662672	5373062	Field:Qtz-eye Rhyolite; Geochem:Rhyolite	28311
AS-06-012	662800	5372990	Field:Rhyolite Lapilli Tuff (juv seds?); Geochem:Andesite	28312
AS-06-013	663150	5372615	Field:Chert Clast	28313
AS-06-014	663100	5372562	Field:Chert Clast	28314
AS-06-015	662875	5372830	Field:Mafic Volcanics; Geochem:Rhyolite	28315
AS-06-016	663572	5372720	Field:VMS Sulfides	28316
AS-06-017	662960	5372650	Field:Massive Sulfides	28317
AS-06-018	665008	5374030	Field:Rhyolite; Geochem:Dacite	28318
RM-01	663303	5372834	Field:Rhyolite; Geochem:Andesite	335590

Sample #	Easting	Northing	Lithology	Assay #
RM-02	663286	5372829	Field:Rhyolite; Geochem:Andesite	335591
RM-03a	663775	5372690	Field:Rhyolite; Geochem:Andesite	335592
RM-03b	663775	5372690	Field:Rhyolite; Geochem:Andesite	335593
RM-03c	663387	5372850	Field:Rhyolite; Geochem:Andesite	335594
RM-04	663414	5372975	Field:Rhyolite; Geochem:Andesite	335595
RM-05	663383	5373048	Field:Rhyolite; Geochem:Andesite	335596
RM-06	663487	5372994	Field:Rhyolite; Geochem:Andesite	335597
RM-07a	663256	5372800	Field:Rhyolite; Geochem:Andesite	335598
RM-07b	663256	5372800	Field:Rhyolite; Geochem:Andesite	335599
RM-08	663200	5372796	Field:Rhyolite; Geochem:Andesite	335600
RM-15	663097	5372895	Field:Rhyolite; Geochem:Dacite	335605
LR-05-001	663098	5373004	Field:Rhyolite; Geochem:Andesite	335568
LR-05-002	663164	5372943	Field:Rhyolite; Geochem:Rhyolite	335569
LR-05-003	663196	5372989	Field:Felsic Tuff; Geochem:Andesite	335570
LR-05-004	663217	5373013	Field:Rhyolite; Geochem:Andesite	335571
LR-05-005	663216	5373058	Field:Rhyolite; Geochem:Andesite	335572
LR-05-006	663265	5373087	Field:Rhyolite; Geochem:Andesite	335573
LR-05-007	663082	5372919	Field:Rhyolite; Geochem:Andesite	335574
LR-05-008	663175	5372890	Field:Rhyolite; Geochem:Andesite	335575
G05-7	663127	5373123	Geochem:Rhyolite	335576
G05-9	663225	5373188	Geochem:BIF	335578
G05-10	663188	5373251	Geochem:Rhyolite	335579
G05-11	663114	5373360	Geochem:Rhyolite	335580
G05-12	663247	5373473	Geochem:Rhyolite	335581
G05-13	663308	5373376	Geochem:Rhyolite	335582
G05-14	663391	5373441	Geochem:Rhyolite	335583
G05-15	663309	5373530	Geochem:Rhyolite	335584

Sample #	Easting	Northing	Lithology	Assay #
G05-16	663255	5373611	Geochem:Rhyolite	335585
G05-17	663115	5373643	Geochem:Rhyolite	335586
G05-18	663045	5373526	Geochem:Rhyolite	335587
G05-19	663120	5373434	Geochem:Rhyolite	335588
G05-20	663189	5373360	Geochem:Rhyolite	335589
G05-40	663573	5372647	Field:Pink Breccia; Geochem:Pink Breccia	335486
OC-151	662985	5372386	Field: Felsic Debris Flow; Geochem:Andesite	335406
OC-153	662929	5372433	Field:Cherty Rhyolite; Geochem:Andesite	335408
OC-154b	662921	5372458	Field:Qtz-eye Rhyolite; Geochem:Andesite	335410
OC-156	662823	5372541	Field:Cherty Rhyolite; Geochem:Andesite	335443
OC-159	662679	5372749	Field:Quartz-eye Rhyolite; Geochem:Rhyolite	335412
OC-162	662724	5372806	Field:Quartz-eye Rhyolite; Geochem:Rhyolite	335413
OC-164	662738	5372841	Field:Quartz-eye Rhyolite; Geochem:Rhyolite	335415
OC-165	662694	5372864	Field:Quartz-eye Rhyolite; Geochem:Andesite	335440
OC-168b	662971	5372541	Field:Mafic Debris Flow; Geochem:Andesite	335442
OC-195	662818	5372886	Field:Quartz-eye Rhyolite; Geochem:Rhyolite	335428
OC-202	662663	5373091	Field:Crystal Tuff Rhyolite; Geochem:Andesite	335429
OC-257	663855	5373899	Field:Quartz-eye Rhyolite; Geochem:Dacite	335451
OC-258	663849	5373870	Field: Ash Tuff Rhyolite; Geochem:Dacite	335452
OC-259	663871	5373801	Field:Ash Tuff Rhyolite; Geochem:Dacite	335453
OC-261	663907	5373742	Field:Ash Tuff Rhyolite; Geochem:Dacite	335454
OC-262	663937	5373705	Field:Ash Tuff Rhyolite; Geochem:Dacite	335455
OC-263	664111	5373512	Field:Rhyolite; Geochem:Dacite	335456
OC-264	664113	5373490	Field:Rhyolite; Geochem:Dacite	335457
OC-265	664125	5373496	Field:Cherty Rhyolite; Geochem:Dacite	335458
OC-266	664160	5373434	Field:Felsic Debris Flow; Geochem:Dacite	335459

Sample #	Easting	Northing	Lithology	Assay #
OC-267	664125	5373413	Field:Crystal Tuff; Geochem:Dacite	335460
OC-269	663983	5373934	Field:Ash Tuff Rhyolite; Geochem:Dacite	335461
OC-270	664018	5373912	Field:Ash Tuff Rhyolite; Geochem:Dacite	335462
OC-271	664065	5373836	Field:Ash Tuff Rhyolite; Geochem:Dacite	335463
OC-272	664084	5373820	Field:Ash Tuff Rhyolite; Geochem:Dacite	335464
OC-273	664213	5373708	Field:Ash Tuff Rhyolite; Geochem:Dacite	335465
OC-274	664231	5373716	Field:Ash Tuff Rhyolite; Geochem:Dacite	335466
OC-275	664224	5373668	Field:Ash Tuff Rhyolite; Geochem:Dacite	335467
OC-276	664165	5373271	Field:Ash Tuff Rhyolite; Geochem:Dacite	335468
OC-277	663991	5374007	Field:Ash Tuff Rhyolite; Geochem:Dacite	335469
OC-281	663555	5372794	Field:Felsic Debris Flow; Geochem:Andesite	335473
OC-320	663533	5373005	Field:Rhyolite; Geochem:Andesite	335444
OC-321	663535	5373011	Field:Rhyolite; Geochem:Andesite	335445
OC-322a	663528	5373009	Field:Rhyolite; Geochem:Andesite	335446
OC-323	663514	5373005	Field:Crystal Tuff Rhyolite; Geochem:Andesite	335448
OC-326	664586	5373213	Field:Rhyolite; Geochem:Andesite	335619
OC-327	664565	5373250	Field:Rhyolite; Geochem:Dacite	335620
OC-328	664510	5373324	Field:Rhyolite; Geochem:Andesite	335621
OC-329	664501	5373209	Field:Rhyolite; Geochem:Andesite	335622
OC-332	664538	5373780	Field:Felsic Crystal Tuff; Geochem:Dacite	335487
OC-333	664492	5373842	Field:Felsic Crystal Tuff; Geochem:Dacite	335488
OC-334	664447	5373861	Field:Felsic Crystal Tuff; Geochem:Dacite	335489
OC-335	664418	5373911	Field:Felsic Crystal Tuff; Geochem:Dacite	335490

Sample #	Easting	Northing	Lithology	Assay #
OC-336	664392	5373927	Field:Felsic Crystal Tuff; Geochem:Dacite	335491
OC-337	664322	5374029	Field:Ash Tuff Rhyolite; Geochem:Dacite	335492
OC-338	664501	5374018	Field:Ash Tuff Rhyolite; Geochem:Dacite	335493
OC-339	664577	5374009	Field:Crystal Tuff Rhyolite; Geochem:Dacite	335494
OC-343	664910	5372576	Field:Mafic Volcanics	639420
OC-348	663851	5371844	Field:Granite	
OC-350	663482	5370961	Field:Mafic Volcanics	

APPENDIX B

Whole Rock Geochemistry

Sample Number	AS-05-001a	AS-05-001b	AS-05-001c	AS-05-002
Easting	663184	663184	663184	663162
Northing	5372274	5372274	5372274	5372245
Geochemical Lithology	Pink Breccia	Pink Breccia	Pink Breccia	Pink Breccia
SiO_2	59.62	67.68	68.67	63.88
TiO_2	0.47	0.36	0.31	0.41
Al_2O_3	18.19	16.42	16.19	16.95
Fe_2O_3	5.82	3.68	3.44	4.94
MnO	0.04	0.02	0.02	0.02
MgO	3.05	1.75	1.53	2.52
CaO	4.14	1.94	2.00	3.69
K_2O	3.21	2.63	2.67	2.19
Na_2O	5.28	5.40	5.07	5.24
P_2O_5	0.19	0.12	0.11	0.16
LOI	4.01	2.32	1.84	1.51
Sum	99.80	100.00	99.62	99.50
Mg#	0.54	0.51	0.49	0.53
Ti	2811	2148	1832	2435
P	818	536	489	709
Cr	42	51	61	51
Co	16	9	8	15
Ni	16	14	14	18
Rb	115	93	93	100
Sr	344	260	310	461
Cs	3	1	2	3
Ba	341	380	419	268
Sc				
V	103	75	72	100
Ta	0.52	0.51	0.51	0.51
Nb	3.1	4.1	4.1	4.1
Zr	75	95	91	109
Hf	2.1	3.1	3.1	3.0
Th	2.1	3.1	3.1	2.0
U	0.5	0.6	0.7	0.6
Y	12.0	10.1	7.8	11.0
La	15.4	17.9	15.0	14.2
Ce	32.8	34.2	28.4	29.9
Pr	3.96	3.69	3.06	3.45
Nd	16.15	14.13	11.61	13.61
Sm	3.02	2.35	2.04	2.54
Eu	0.73	0.61	0.51	0.61
Gd	2.71	2.05	1.94	2.34
Tb	0.42	0.31	0.20	0.30
Dy	1.88	1.54	1.22	1.73
Ho	0.42	0.31	0.20	0.41
Er	1.15	1.02	0.71	1.12
Tm	0.10	0.10	0.10	0.10
Yb	0.94	0.72	0.71	1.02
Lu	0.21	0.10	0.10	0.20
Cu	40	49	22	52
Zn	26	19	18	22
Mo	44	11	2	615
Ag	1	1	1	1
Tl	0.52	0.51	0.51	0.51
Pb	5.2	5.1	5.1	5.1
Sn	2.1	1.0	1.0	2.0
Sb				

Sample Number	AS-05-003	AS-05-004a	AS-05-004b	AS-05-005	AS-05-006
Easting	663096	663085	663085	663055	663034
Northing	5372268	5372258	5372258	5372214	5372213
Geochemical Lithology	Pink Breccia	Pink Breccia	Pink Breccia	Pink Breccia	Pink Breccia
SiO_2	61.64	50.91	64.71	71.17	57.74
TiO_2	0.76	1.08	0.74	0.36	0.83
Al_2O_3	16.29	14.36	15.12	14.57	16.81
Fe_2O_3	7.86	13.14	6.02	4.17	8.36
MnO	0.03	0.15	0.03	0.02	0.10
MgO	2.74	7.27	2.25	2.05	5.18
CaO	4.16	8.90	4.32	1.76	7.28
K_2O	3.42	1.91	2.14	3.34	0.73
Na_2O	2.89	2.18	4.47	2.45	2.81
P_2O_5	0.20	0.10	0.21	0.10	0.16
LOI	1.61	2.1	2.42	2.37	3.22
Sum	99.86	100.00	99.72	99.55	99.53
Mg#	0.43	0.55	0.45	0.52	0.58
Ti	4570	6491	4424	2149	4956
P	887	446	895	447	676
Cr	102	92	123	41	124
Co	41	40	18	16	26
Ni	69	68	83	25	91
Rb	151	78	92	127	28
Sr	242	285	211	188	265
Cs	6	4	5	3	1
Ba	546	224	264	709	85
Sc					
V	106	334	104	78	181
Ta	0.71	0.51	0.61	0.61	0.52
Nb	10.2	4.1	8.2	8.2	5.2
Zr	169	74	134	210	118
Hf	5.1	2.0	4.1	6.1	3.1
Th	2.0	1.0	2.0	3.1	1.0
U	0.9	0.5	0.8	0.9	0.5
Y	27.7	29.1	23.3	23.5	18.5
La	15.9	5.3	28.6	17.9	9.9
Ce	35.2	13.2	49.3	38.5	22.0
Pr	4.07	1.84	5.12	4.40	2.58
Nd	16.67	9.09	19.37	18.44	11.57
Sm	3.66	2.76	3.89	3.89	2.58
Eu	1.02	1.02	1.02	0.92	0.83
Gd	4.37	3.78	4.41	4.10	3.10
Tb	0.71	0.72	0.61	0.61	0.52
Dy	4.27	4.70	3.79	3.89	3.10
Ho	0.91	1.02	0.82	0.82	0.62
Er	2.85	3.17	2.36	2.46	1.76
Tm	0.41	0.51	0.31	0.31	0.31
Yb	2.85	2.86	2.15	2.36	1.76
Lu	0.51	0.51	0.31	0.41	0.31
Cu	1392	249	1327	1096	224
Zn	26	44	25	23	37
Mo	79	4	38	12	4
Ag	1	1	1	1	1
Tl	0.51	0.51	0.51	0.51	0.52
Pb	7.1	6.1	5.1	5.1	5.2
Sn	2.0	2.0	2.0	3.1	2.1
Sb					

Sample Number	AS-05-007	AS-05-008	AS-05-010a	AS-05-010b	AS-05-011
Easting	663000	662497	662464	662464	662453
Northing	5372192	5372352	5372394	5372394	5372393
Geochemical Lithology	Pink Breccia	Andesite	Rhyolite	Rhyolite	Rhyolite
SiO_2	58.04	62.25	87.89	83.15	89.17
TiO_2	0.90	0.70	0.15	0.13	0.11
Al_2O_3	15.99	17.39	7.62	6.68	5.93
Fe_2O_3	8.66	6.05	0.97	4.27	1.58
MnO	0.07	0.07	0.02	0.16	0.03
MgO	4.46	3.66	0.42	1.26	0.55
CaO	5.63	4.94	0.37	2.34	0.62
K_2O	2.68	1.39	2.38	0.48	1.66
Na_2O	3.38	3.39	0.15	1.49	0.34
P_2O_5	0.19	0.14	0.02	0.03	0.02
LOI	1.89	3.25	1.32	2.11	1.43
Sum	99.83	100.10	98.75	99.92	99.77
Mg#	0.53	0.57	0.49	0.39	0.43
Ti	5377	4213	911	796	669
P	845	631	88	134	89
Cr	153	93	41	82	41
Co	23	19	1	1	1
Ni	107	76	5	16	5
Rb	121	35	43	11	36
Sr	250	210	15	123	25
Cs	7	2	1	1	1
Ba	242	142	502	119	205
Sc					
V	163	145	6	6	5
Ta	0.51	0.52	0.81	0.61	0.51
Nb	7.1	5.2	9.1	8.2	7.1
Zr	154	136	224	190	164
Hf	5.1	4.1	7.1	6.1	5.1
Th	2.0	2.1	3.0	3.1	2.0
U	0.9	0.5	0.9	0.8	0.6
Y	29.3	18.0	32.1	33.1	27.0
La	20.7	12.8	15.6	20.1	14.1
Ce	44.2	27.1	36.1	43.5	31.0
Pr	5.30	3.10	4.26	5.31	3.86
Nd	22.83	12.61	17.23	21.86	15.62
Sm	4.89	2.69	3.95	5.11	3.55
Eu	1.22	0.83	0.61	0.82	0.51
Gd	5.40	3.10	4.05	5.21	3.75
Tb	0.82	0.52	0.71	0.92	0.71
Dy	4.99	3.00	4.87	5.52	4.26
Ho	1.02	0.62	1.11	1.23	0.91
Er	3.06	1.86	3.85	3.58	2.84
Tm	0.41	0.31	0.61	0.61	0.51
Yb	2.85	1.86	3.95	3.58	2.74
Lu	0.41	0.31	0.61	0.61	0.41
Cu	1458	38	5	17	5
Zn	38	50	21	41	21
Mo	342	2	2	2	2
Ag	1	1	1	1	1
Tl	0.51	0.52	0.51	0.51	0.51
Pb	5.1	5.2	5.1	6.1	5.1
Sn	2.0	1.0	1.0	1.0	1.0
Sb					

Sample Number	AS-05-012	AS-05-013	AS-05-014	AS-05-015	AS-05-016
Easting	662415	662412	662370	662365	662310
Northing	5372411	5372474	5372435	5372476	5372594
Geochemical Lithology	Rhyolite	Rhyolite	Rhyolite	Rhyolite	Andesite
SiO_2	87.44	79.47	78.68	83.30	58.75
TiO_2	0.17	0.24	0.27	0.26	0.71
Al_2O_3	8.95	11.11	12.01	10.86	17.44
Fe_2O_3	0.74	5.62	3.99	2.14	7.90
MnO	0.01	0.14	0.10	0.04	0.14
MgO	0.06	0.66	2.03	0.37	3.47
CaO	0.03	0.10	0.30	0.04	5.86
K_2O	2.37	2.33	1.92	2.58	0.97
Na_2O	0.21	0.32	0.68	0.38	4.63
P_2O_5	0.01	0.02	0.03	0.03	0.13
LOI	1.2	2.01	2.49	1.63	4.53
Sum	99.78	99.61	100.20	100.10	99.37
Mg#	0.15	0.20	0.53	0.27	0.49
Ti	1032	1407	1598	1585	4209
P	44	89	134	133	549
Cr	40	31	41	20	157
Co	1	3	1	1	23
Ni	7	9	5	9	71
Rb	45	54	68	61	22
Sr	52	61	107	48	233
Cs	1	1	1	2	1
Ba	393	350	146	242	213
Sc					
V	5	5	5	5	147
Ta	0.71	0.92	1.03	0.81	0.52
Nb	10.1	12.2	13.3	11.2	5.2
Zr	252	306	348	300	133
Hf	7.1	9.2	10.3	9.1	4.2
Th	3.0	4.1	4.1	4.1	1.0
U	1.0	0.9	0.8	1.1	0.5
Y	41.1	39.0	36.9	32.4	19.2
La	5.3	9.7	15.0	3.7	13.9
Ce	24.3	27.8	39.7	17.2	29.9
Pr	1.62	2.86	4.51	1.12	3.67
Nd	6.78	12.55	18.46	5.08	14.46
Sm	2.43	3.57	4.41	1.83	3.14
Eu	0.61	1.12	0.92	0.51	0.94
Gd	3.85	4.39	5.02	2.74	3.25
Tb	1.01	1.02	1.03	0.71	0.52
Dy	6.68	6.63	6.15	5.29	3.35
Ho	1.52	1.43	1.44	1.22	0.63
Er	4.45	4.59	4.31	3.96	2.10
Tm	0.71	0.71	0.72	0.61	0.31
Yb	4.15	4.69	4.72	4.17	1.89
Lu	0.61	0.71	0.72	0.71	0.31
Cu	10	9	5	5	5
Zn	27	58	83	45	73
Mo	2	2	2	2	2
Ag	1	1	1	1	1
Tl	0.51	0.51	0.51	0.51	0.52
Pb	6.1	5.1	6.2	5.1	5.2
Sn	1.0	1.0	1.0	1.0	1.0
Sb					

Sample Number	AS-05-018	AS-05-019	AS-05-020a	AS-05-020b	AS-05-021
Easting	662622	662624	662628	662628	662595
Northing	5372353	5372360	5372359	5372359	5372387
Geochemical Lithology	Rhyolite	Andesite	Andesite	Dacite	Dacite
SiO_2	67.75	61.33	54.69	79.82	77.70
TiO_2	0.03	0.65	0.76	0.20	0.26
Al_2O_3	1.04	16.07	18.57	11.20	14.69
Fe_2O_3	25.59	7.28	8.70	3.21	1.54
MnO	1.17	0.15	0.22	0.06	0.02
MgO	2.48	4.06	4.32	1.21	0.59
CaO	1.73	5.21	10.27	1.03	0.43
K_2O	0.14	2.72	0.48	2.91	4.45
Na_2O	0.04	2.40	1.80	0.30	0.25
P_2O_5	0.02	0.13	0.19	0.05	0.07
LOI	2.73	6.52	4.14	1.97	2.18
Sum	99.54	99.44	99.98	99.64	100.15
Mg#	0.18	0.55	0.52	0.45	0.46
Ti	185	3849	4565	1223	1532
P	90	560	819	223	312
Cr	41	96	73	41	31
Co	5	24	24	8	5
Ni	14	93	37	20	11
Rb	8	77	10	65	97
Sr	56	173	600	70	47
Cs	1	3		2	3
Ba	76	256	70	409	318
Sc					
V	14	150	193	23	25
Ta	0.51	0.54	0.52	0.51	0.51
Nb	1.0	5.4	4.2	1.0	2.0
Zr	19	127	86	93	114
Hf	1.0	3.2	3.1	2.0	3.1
Th	1.0	1.1	2.1	1.0	1.0
U	0.5	0.5	0.5	0.5	0.5
Y	7.2	17.8	13.4	3.7	3.5
La	3.1	10.2	15.9	7.9	9.3
Ce	5.2	22.2	34.9	15.7	18.5
Pr	0.62	2.78	4.59	1.63	2.25
Nd	2.67	11.34	18.78	6.12	7.87
Sm	0.62	2.46	3.76	1.02	1.33
Eu	0.21	0.75	1.04	0.31	0.31
Gd	0.82	2.78	3.44	0.92	1.12
Tb	0.21	0.43	0.52	0.10	0.10
Dy	0.93	2.89	2.50	0.51	0.61
Ho	0.21	0.64	0.52	0.10	0.10
Er	0.72	1.82	1.36	0.31	0.31
Tm	0.10	0.32	0.21	0.10	0.10
Yb	0.72	1.71	1.25	0.31	0.31
Lu	0.10	0.32	0.21	0.10	0.10
Cu	40	17	8	11	5
Zn	58	93	84	38	24
Mo	2	2	2	2	2
Ag	1	1	1	1	1
Tl	0.51	0.54	0.52	0.51	0.51
Pb	5.1	5.4	7.3	5.1	5.1
Sn	1.0	1.1	1.0	1.0	1.0
Sb					

Sample Number	AS-05-022	AS-05-023	AS-05-024a	AS-05-024b	AS-05-025
Easting	662576	662576	662520	662520	662483
Northing	5372442	5372442	5372473	5372473	5372515
Geochemical Lithology	Andesite	Andesite	Rhyolite	BIF	Rhyolite
SiO_2	61.86	61.48	89.99	85.17	86.33
TiO_2	0.65	0.86	0.15	0.01	0.18
Al_2O_3	16.81	20.10	6.60	0.21	8.58
Fe_2O_3	6.41	7.02	0.93	12.53	1.60
MnO	0.15	0.10	0.01	0.47	0.02
MgO	3.60	3.76	0.17	1.41	0.28
CaO	7.07	1.24	0.05	0.08	0.11
K_2O	1.29	5.06	2.01	0.03	2.78
Na_2O	2.02	0.21	0.07	0.08	0.10
P_2O_5	0.15	0.18	0.01	0.01	0.01
LOI	2.31	4.16	0.93	0.91	1.3
Sum	99.94	99.78	99.86	100.30	99.70
Mg#	0.55	0.54	0.29	0.20	0.28
Ti	3866	5130	908	60	1093
P	670	774	44	44	44
Cr	102	104	61	71	30
Co	19	28	1	1	1
Ni	79	81	13	5	5
Rb	32	106	41	0	54
Sr	222	63	15	1	22
Cs	3	4	1		1
Ba	120	716	265	3	546
Sc					
V	137	182	5	7	5
Ta	0.51	0.52	0.71	0.50	0.81
Nb	5.1	7.3	9.1	1.0	10.1
Zr	133	166	194	16	255
Hf	3.1	4.2	6.1	1.0	8.1
Th	1.0	2.1	3.0	1.0	3.0
U	0.5	0.5	0.8	0.5	1.0
Y	17.8	20.0	32.3	1.8	36.1
La	12.8	12.3	10.5	2.0	14.5
Ce	27.2	28.2	26.7	3.8	35.2
Pr	3.38	3.34	2.93	0.40	4.05
Nd	13.51	13.67	11.31	1.61	16.62
Sm	3.07	3.13	2.73	0.20	4.26
Eu	0.92	0.94	0.50	0.10	0.91
Gd	3.17	3.34	3.53	0.30	4.46
Tb	0.51	0.52	0.71	0.10	0.81
Dy	3.07	3.44	4.85	0.20	5.67
Ho	0.61	0.73	1.11	0.10	1.22
Er	1.84	2.09	3.43	0.20	3.75
Tm	0.31	0.31	0.50	0.10	0.61
Yb	1.84	2.09	3.63	0.20	3.65
Lu	0.31	0.31	0.61	0.10	0.61
Cu	5	31	5	84	5
Zn	74	106	15	43	16
Mo	2	2	2	2	2
Ag	1	1	1	1	1
Tl	0.51	0.52	0.50	0.50	0.51
Pb	5.1	7.3	5.0	5.0	5.1
Sn	1.0	1.0	3.0	2.0	3.0
Sb					

Sample Number	AS-05-026	AS-05-027	AS-05-028	AS-05-029	AS-05-030
Easting	662447	662649	662649	662654	662692
Northing	5372588	5372346	5372368	5372406	5372402
Geochemical Lithology	Rhyolite	Andesite	Rhyolite	Andesite	Andesite
SiO_2	76.81	59.06	66.62	60.77	63.90
TiO_2	0.24	0.68	0.11	0.69	0.66
Al_2O_3	10.96	17.55	4.46	16.24	16.33
Fe_2O_3	4.61	8.43	23.41	8.26	5.90
MnO	0.09	0.25	1.12	0.21	0.15
MgO	1.88	3.70	2.70	4.77	3.43
CaO	1.19	6.69	1.28	4.27	6.26
K_2O	3.03	0.90	0.20	1.62	1.70
Na_2O	1.17	2.54	0.06	3.03	1.55
P_2O_5	0.01	0.20	0.04	0.14	0.14
LOI	2.6	2.77	2.32	3.24	3.46
Sum	99.81	99.26	100.25	99.32	99.28
Mg#	0.47	0.49	0.20	0.56	0.56
Ti	1416	4070	675	4090	3913
P	45	853	179	586	588
Cr	62	103	51	93	93
Co	5	22	5	23	18
Ni	17	91	15	85	76
Rb	96	23	24	36	46
Sr	70	250	5	202	279
Cs	4	1	2	1	2
Ba	538	148	34	200	495
Sc					
V	73	152	14	140	142
Ta	0.82	0.51	0.51	0.52	0.52
Nb	11.3	6.2	4.1	5.2	5.2
Zr	329	136	86	125	124
Hf	10.3	4.1	3.1	4.1	4.1
Th	4.1	2.1	1.0	1.0	1.0
U	1.2	0.5	0.5	0.5	0.5
Y	35.6	20.6	20.0	17.0	18.4
La	22.1	13.8	6.1	18.8	12.2
Ce	50.3	29.3	11.9	38.8	26.4
Pr	5.65	3.39	1.43	4.34	3.11
Nd	23.82	14.20	5.84	17.57	12.54
Sm	5.03	3.09	1.33	3.62	3.00
Eu	0.92	0.93	0.31	1.14	0.73
Gd	5.44	3.50	1.84	3.51	3.00
Tb	0.92	0.51	0.31	0.52	0.52
Dy	5.85	3.19	2.46	2.89	2.90
Ho	1.23	0.72	0.61	0.62	0.62
Er	3.90	2.06	1.95	1.76	1.76
Tm	0.51	0.31	0.31	0.21	0.21
Yb	3.90	1.75	2.05	1.65	1.76
Lu	0.62	0.31	0.41	0.21	0.31
Cu	22	19	18	20	13
Zn	43	57	46	79	57
Mo	2	2	2	2	2
Ag	1	1	1	1	1
Tl	0.51	0.51	0.51	0.52	0.52
Pb	5.1	5.1	5.1	5.2	5.2
Sn	2.1	2.1	2.0	2.1	1.0
Sb					

Sample Number	AS-05-031	AS-05-032	AS-05-033	AS-05-034a	AS-05-034b
Easting	662681	662730	662623	662660	662672
Northing	5372426	5372440	5372468	5372520	5372520
Geochemical Lithology	Rhyolite	Rhyolite	Andesite	Andesite	Rhyolite
SiO_2	75.25	62.00	61.53	61.23	64.74
TiO_2	0.07	0.41	0.61	0.76	0.27
Al_2O_3	1.34	12.02	15.84	18.12	10.00
Fe_2O_3	17.60	18.22	7.01	5.78	17.11
MnO	0.30	0.54	0.14	0.14	1.63
MgO	2.26	2.58	3.94	2.95	2.81
CaO	2.88	1.12	7.47	5.24	2.53
K_2O	0.07	2.34	0.62	4.02	0.58
Na_2O	0.19	0.72	2.68	1.59	0.28
P_2O_5	0.03	0.06	0.17	0.16	0.04
LOI	0.84	4.19	4.82	6.12	3
Sum	99.48	100.10	99.81	99.68	99.81
Mg#	0.22	0.24	0.55	0.53	0.27
Ti	423	2440	3654	4535	1607
P	132	273	734	697	180
Cr	61	63	84	75	21
Co	5	15	18	18	4
Ni	15	28	66	68	9
Rb	5	70	16	83	29
Sr	7	77	256	150	137
Cs	1	2	1	3	7
Ba	13	328	71	329	32
Sc					
V	22	63	124	145	14
Ta	0.50	0.52	0.53	0.53	0.72
Nb	1.0	6.3	5.3	6.4	9.3
Zr	29	158	129	143	227
Hf	1.0	5.2	3.2	4.3	7.2
Th	1.0	3.1	1.1	1.1	3.1
U	0.5	0.7	0.5	0.5	1.0
Y	10.6	24.9	19.8	18.9	37.5
La	4.4	15.4	13.2	12.6	22.3
Ce	8.6	32.7	28.5	27.9	48.1
Pr	1.01	3.86	3.47	3.30	5.98
Nd	4.13	15.45	14.08	13.64	23.51
Sm	1.01	3.24	3.26	2.98	5.36
Eu	0.30	0.83	0.95	1.07	1.34
Gd	1.31	3.34	3.57	3.20	5.88
Tb	0.20	0.63	0.63	0.53	1.03
Dy	1.71	3.97	3.57	3.30	6.29
Ho	0.40	0.83	0.74	0.64	1.34
Er	1.21	2.61	2.00	1.92	4.02
Tm	0.20	0.42	0.32	0.21	0.62
Yb	1.31	2.82	2.10	1.92	3.92
Lu	0.20	0.42	0.32	0.32	0.62
Cu	22	44	34	43	9
Zn	44	64	68	65	99
Mo	2	3	2	2	2
Ag	1	1	1	1	1
Tl	0.50	0.52	0.53	0.53	0.52
Pb	5.0	5.2	5.3	5.3	7.2
Sn	1.0	2.1	1.1	1.1	2.1
Sb					

Sample Number	AS-05-034c	AS-05-034d	AS-05-035	AS-05-036	AS-05-037
Easting	662665	662670	662677	663025	663003
Northing	5372520	5372528	5372565	5372915	5372917
Geochemical Lithology	Rhyolite	Andesite	Dacite	Andesite	Andesite
SiO_2	78.29	71.61	76.27	68.23	59.50
TiO_2	0.37	0.65	0.24	0.82	0.70
Al_2O_3	10.23	14.58	14.86	16.59	15.27
Fe_2O_3	3.55	5.76	1.91	5.25	8.15
MnO	0.18	0.20	0.05	0.08	0.13
MgO	1.74	1.50	0.98	2.74	5.49
CaO	2.39	1.01	1.48	1.81	7.42
K_2O	2.35	4.09	3.91	3.81	1.81
Na_2O	0.79	0.50	0.25	0.50	1.37
P_2O_5	0.11	0.10	0.06	0.18	0.16
LOI	3.15	2.79	2.2	2.98	7.33
Sum	99.61	99.60	99.53	99.54	99.92
Mg#	0.52	0.36	0.53	0.53	0.60
Ti	2229	3886	1410	4882	4205
P	496	449	268	765	706
Cr	62	62	31	402	302
Co	5	8	3	27	33
Ni	13	16	7	155	175
Rb	53	80	63	87	46
Sr	64	64	70	112	240
Cs	2	3	2	3	2
Ba	228	506	619	368	243
Sc					
V	42	96	18	133	155
Ta	0.52	0.62	0.51	0.52	0.54
Nb	6.2	8.2	2.0	7.2	6.5
Zr	146	205	112	144	129
Hf	4.1	6.2	3.1	4.1	3.2
Th	2.1	3.1	1.0	1.0	1.1
U	0.5	0.9	0.5	0.5	0.5
Y	21.4	28.6	3.3	17.5	19.0
La	11.7	18.1	9.3	12.8	12.7
Ce	25.6	39.1	18.9	28.9	28.2
Pr	2.99	4.63	2.05	3.50	3.35
Nd	11.98	18.52	7.36	13.92	13.81
Sm	2.58	4.01	1.23	3.20	3.02
Eu	0.72	1.03	0.31	0.82	0.97
Gd	2.99	4.42	1.12	3.30	3.45
Tb	0.52	0.72	0.10	0.52	0.54
Dy	3.41	4.73	0.51	2.99	3.35
Ho	0.72	1.03	0.10	0.62	0.65
Er	2.17	2.88	0.20	1.75	1.94
Tm	0.31	0.41	0.10	0.21	0.22
Yb	2.27	2.88	0.20	1.65	1.73
Lu	0.41	0.41	0.10	0.31	0.32
Cu	6	6	5	48	54
Zn	45	59	22	65	103
Mo	2	2	2	2	2
Ag	1	1	1	1	1
Tl	0.52	0.51	0.51	0.52	0.54
Pb	5.2	5.1	5.1	5.2	5.4
Sn	1.0	2.1	1.0	1.0	1.1
Sb					

Sample Number	AS-05-038	AS-05-039	AS-05-040	AS-05-041	AS-05-042
Easting	662984	662972	662963	662921	662870
Northing	5372895	5372884	5372891	5372870	5372862
Geochemical Lithology	Rhyolite	Andesite	Andesite	Andesite	Rhyolite
SiO_2	56.91	63.06	51.17	63.01	93.19
TiO_2	0.08	0.68	0.76	0.81	0.09
Al_2O_3	3.76	14.43	19.27	20.07	3.46
Fe_2O_3	34.35	5.59	15.35	4.12	0.87
MnO	0.67	0.13	1.03	0.04	0.03
MgO	2.99	4.80	3.35	2.18	0.43
CaO	1.11	7.54	4.38	4.13	0.84
K_2O	0.06	1.69	0.79	2.08	0.94
Na_2O	0.06	1.93	3.75	3.43	0.15
P_2O_5	0.02	0.15	0.16	0.13	0.01
LOI	1.45	6.21	3.59	3.05	1.27
Sum	99.94	99.98	99.94	99.92	99.49
Mg#	0.16	0.65	0.32	0.54	0.52
Ti	487	4091	4539	4823	547
P	89	651	679	585	44
Cr	20	309	114	103	61
Co	2	28	9	11	2
Ni	9	164	46	31	6
Rb	6	41	15	65	25
Sr	7	247	332	212	24
Cs	1	1	2	2	1
Ba	6	224	165	404	180
Sc					
V	13	147	139	196	5
Ta	0.51	0.53	0.52	0.52	0.51
Nb	3.0	6.4	7.3	7.2	6.1
Zr	75	126	168	168	102
Hf	2.0	3.2	5.2	5.2	3.0
Th	1.0	1.1	2.1	2.1	2.0
U	0.6	0.5	0.5	0.5	0.5
Y	20.1	19.0	28.2	17.9	20.4
La	13.3	13.1	16.8	15.3	11.1
Ce	26.1	29.2	35.0	32.1	23.8
Pr	2.94	3.63	4.15	3.71	2.73
Nd	11.36	14.50	16.91	14.23	11.04
Sm	2.54	2.99	3.73	3.09	2.33
Eu	0.91	0.96	1.45	1.03	0.41
Gd	2.94	3.52	3.94	3.20	2.84
Tb	0.51	0.53	0.73	0.52	0.51
Dy	2.74	3.20	4.36	3.09	3.04
Ho	0.61	0.64	0.93	0.62	0.71
Er	1.93	1.81	2.80	1.86	2.03
Tm	0.30	0.32	0.41	0.21	0.30
Yb	1.93	1.81	2.90	1.75	2.13
Lu	0.30	0.32	0.41	0.31	0.30
Cu	6	31	5	34	8
Zn	96	90	67	75	51
Mo	2	2	2	2	2
Ag	1	1	1	1	1
Tl	0.51	0.53	0.52	0.52	0.51
Pb	5.1	5.3	7.3	5.2	5.1
Sn	1.0	1.1	1.0	1.0	2.0
Sb					

Sample Number	AS-05-043	AS-05-044	AS-05-045	AS-05-046a	AS-05-046b
Easting	662867	662858	662679	662704	662704
Northing	5372846	5372832	5372769	5372774	5372774
Geochemical Lithology	Rhyolite	Rhyolite	Rhyolite	Rhyolite	Rhyolite
SiO_2	87.50	77.32	78.37	84.15	80.47
TiO_2	0.09	0.11	0.22	0.22	0.22
Al_2O_3	5.46	7.88	12.24	11.10	10.98
Fe_2O_3	3.86	9.42	1.79	0.77	3.61
MnO	0.17	0.44	0.04	0.01	0.15
MgO	0.91	2.13	1.24	0.11	0.48
CaO	0.39	1.50	0.91	0.04	0.67
K_2O	0.91	0.35	2.05	3.09	3.09
Na_2O	0.67	0.83	3.11	0.48	0.32
P_2O_5	0.03	0.02	0.03	0.02	0.02
LOI	1.41	2.19	1.46	1.47	2.09
Sum	100.25	99.52	99.69	99.68	99.72
Mg#	0.34	0.33	0.60	0.24	0.23
Ti	547	674	1339	1339	1286
P	133	89	133	89	89
Cr	51	51	41	41	31
Co	1	1	1	1	1
Ni	8	6	6	5	7
Rb	24	13	68	47	66
Sr	51	106	103	27	26
Cs	1	1	2	1	2
Ba	244	161	407	348	408
Sc					
V	5	5	5	5	5
Ta	0.61	0.82	1.12	1.01	0.92
Nb	7.1	11.2	14.2	13.2	13.3
Zr	168	226	364	333	339
Hf	5.1	7.2	11.2	9.1	9.2
Th	3.0	4.1	5.1	4.1	4.1
U	0.7	0.8	1.2	1.2	1.1
Y	27.4	29.9	46.2	51.3	55.9
La	17.4	21.6	29.1	28.0	27.4
Ce	39.4	48.4	65.0	62.9	61.1
Pr	4.87	6.14	8.12	7.71	7.46
Nd	18.87	24.23	32.37	32.58	31.56
Sm	4.06	5.21	6.90	7.51	7.46
Eu	0.81	0.72	1.73	1.52	1.53
Gd	4.77	5.32	7.41	7.82	8.17
Tb	0.81	0.92	1.32	1.42	1.43
Dy	5.07	5.42	7.81	8.63	9.09
Ho	1.01	1.12	1.62	1.83	1.94
Er	2.84	3.27	4.87	5.28	5.92
Tm	0.41	0.51	0.81	0.81	0.92
Yb	2.64	3.17	4.67	5.07	5.72
Lu	0.51	0.51	0.81	0.81	0.92
Cu	5	14	5	5	18
Zn	52	100	45	28	104
Mo	2	2	2	2	2
Ag	1	1	1	1	1
Tl	0.51	0.51	0.51	0.51	0.51
Pb	5.1	6.1	7.1	5.1	5.1
Sn	1.0	2.0	4.1	3.0	4.1
Sb					

Sample Number	AS-05-047	AS-05-048	AS-05-049	AS-05-050	AS-05-051
Easting	662732	662743	662763	662782	662787
Northing	5372878	5372839	5372795	5372806	5372821
Geochemical Lithology	Rhyolite	Rhyolite	Rhyolite	BIF	Rhyolite
SiO_2	77.79	76.59	80.07	91.17	52.61
TiO_2	0.30	0.23	0.20	0.01	0.14
Al_2O_3	12.18	12.00	10.64	0.12	7.28
Fe_2O_3	4.61	2.89	3.45	7.36	27.66
MnO	0.09	0.09	0.10	0.36	1.16
MgO	0.71	0.63	0.44	0.73	4.70
CaO	0.51	2.12	0.06	0.09	5.57
K_2O	3.61	1.88	4.64	0.03	0.79
Na_2O	0.18	3.53	0.37	0.11	0.08
P_2O_5	0.03	0.04	0.03	0.01	0.01
LOI	2.33	2.56	1.35	0.5	5.46
Sum	99.42	99.63	99.58	99.28	98.23
Mg#	0.25	0.32	0.22	0.18	0.27
Ti	1780	1354	1215	60	825
P	134	179	133	44	46
Cr	41	31	51	50	21
Co	1	1	1	1	2
Ni	10	5	5	5	5
Rb	116	48	75	1	39
Sr	41	126	34	1	77
Cs	3	2	2		6
Ba	512	207	734	2	25
Sc					
V	6	5	5	5	5
Ta	1.02	1.03	0.81	0.50	0.74
Nb	14.3	13.3	12.2	1.0	9.5
Zr	350	345	311	1	203
Hf	10.2	9.2	9.1	1.0	6.4
Th	4.1	4.1	4.1	1.0	3.2
U	1.1	1.1	1.0	0.5	0.8
Y	46.1	47.2	45.1	2.8	41.8
La	26.3	27.7	18.5	0.7	22.3
Ce	57.8	61.7	40.3	1.1	48.5
Pr	7.27	7.70	4.76	0.10	5.93
Nd	29.90	31.82	20.07	0.60	24.04
Sm	6.86	7.80	4.97	0.10	5.51
Eu	1.43	1.54	1.12	0.10	0.95
Gd	7.37	8.52	5.68	0.20	6.25
Tb	1.33	1.44	1.12	0.10	1.06
Dy	7.99	8.31	6.99	0.20	6.78
Ho	1.64	1.64	1.52	0.10	1.38
Er	4.81	4.82	4.56	0.10	4.13
Tm	0.72	0.72	0.71	0.10	0.64
Yb	4.51	4.52	4.36	0.10	4.13
Lu	0.82	0.72	0.71	0.10	0.64
Cu	14	5	18	65	186
Zn	97	88	107	65	383
Mo	2	2	2	2	2
Ag	1	1	1	1	1
Tl	0.51	0.51	0.51	0.50	0.53
Pb	5.1	6.2	6.1	5.0	7.4
Sn	3.1	3.1	2.0	1.0	4.2
Sb					

Sample Number	AS-05-052	AS-05-053	AS-05-054	AS-05-055	AS-05-056
Easting	662999	662993	662956	662937	662907
Northing	5372992	5372990	5372953	5372937	5372918
Geochemical Lithology	Rhyolite	Andesite	Rhyolite	Andesite	Andesite
SiO_2	87.22	83.01	90.80	63.79	64.47
TiO_2	0.17	0.34	0.03	0.77	0.74
Al_2O_3	6.79	8.98	3.12	19.11	18.42
Fe_2O_3	2.68	4.24	4.20	6.26	4.24
MnO	0.09	0.04	0.10	0.19	0.09
MgO	0.63	0.44	0.81	1.30	2.14
CaO	0.28	0.03	0.32	3.82	4.87
K_2O	1.82	2.65	0.05	2.34	1.60
Na_2O	0.27	0.21	0.55	2.28	3.27
P_2O_5	0.04	0.07	0.02	0.16	0.15
LOI	1.33	2.2	1	2.7	2.92
Sum	99.92	99.77	99.87	99.43	99.86
Mg#	0.34	0.19	0.30	0.31	0.53
Ti	1033	2023	182	4560	4446
P	177	312	88	673	674
Cr	20	31	20	93	93
Co	3	1	3	7	12
Ni	9	5	5	14	39
Rb	48	62	1	60	45
Sr	22	20	13	215	186
Cs	1	2		2	2
Ba	320	532	18	268	155
Sc					
V	18	70	12	165	147
Ta	0.51	0.51	0.51	0.51	0.52
Nb	4.1	4.1	2.0	6.2	6.2
Zr	96	85	65	146	138
Hf	3.0	2.0	2.0	4.1	4.1
Th	2.0	2.0	1.0	1.0	1.0
U	0.5	0.5	0.5	0.5	0.5
Y	15.5	7.5	13.1	17.4	17.5
La	10.9	3.9	7.6	14.0	13.6
Ce	23.6	7.5	15.7	30.3	29.3
Pr	2.64	0.61	1.72	3.39	3.40
Nd	10.74	2.35	7.37	14.19	14.22
Sm	2.13	0.61	1.52	2.88	3.09
Eu	0.61	0.20	0.30	0.93	0.93
Gd	2.33	0.82	1.72	3.08	3.30
Tb	0.30	0.10	0.20	0.41	0.41
Dy	2.33	1.12	1.82	2.78	2.99
Ho	0.51	0.20	0.40	0.51	0.62
Er	1.52	0.72	1.31	1.75	1.75
Tm	0.20	0.10	0.20	0.21	0.21
Yb	1.42	0.72	1.31	1.54	1.65
Lu	0.20	0.10	0.20	0.21	0.21
Cu	8	25	11	16	42
Zn	34	36	85	77	86
Mo	2	2	2	2	2
Ag	1	1	1	1	1
Tl	0.51	0.51	0.51	0.51	0.52
Pb	5.1	17.4	5.1	9.3	6.2
Sn	1.0	2.0	1.0	2.1	2.1
Sb					

Sample Number	AS-05-057	AS-05-058	AS-05-059	AS-05-060	AS-05-061
Easting	662876	662854	663174	663133	663097
Northing	5372903	5372914	5372598	5372593	5372577
Geochemical Lithology	Andesite	Rhyolite	Rhyolite	Rhyolite	Andesite
SiO_2	65.55	84.19	64.47	63.16	67.98
TiO_2	0.78	0.18	0.56	0.46	0.39
Al_2O_3	19.53	10.19	14.55	12.44	9.76
Fe_2O_3	3.41	1.00	10.25	13.39	14.60
MnO	0.13	0.01	0.45	1.02	0.65
MgO	1.20	0.41	2.56	2.34	2.53
CaO	3.65	0.25	3.37	6.26	2.44
K_2O	5.06	2.07	1.11	0.38	0.55
Na_2O	0.51	1.66	2.61	0.51	1.05
P_2O_5	0.19	0.03	0.07	0.04	0.05
LOI	5.1	1.27	2.58	3.19	3.12
Sum	99.91	99.84	99.10	99.45	98.70
Mg#	0.44	0.47	0.35	0.28	0.28
Ti	4675	1093	3324	2725	2291
P	828	133	314	180	225
Cr	95	10	41	41	52
Co	21	4	11	13	10
Ni	67	7	26	36	26
Rb	105	47	57	26	31
Sr	91	67	219	462	103
Cs	3	1	4	3	6
Ba	620	175	133	79	70
Sc					
V	164	9	73	63	63
Ta	0.53	0.91	0.62	0.62	0.52
Nb	6.3	11.1	7.2	6.2	5.2
Zr	147	289	184	157	121
Hf	4.2	8.1	6.2	5.2	4.1
Th	1.1	4.1	3.1	3.1	2.1
U	0.5	0.9	0.9	0.8	0.5
Y	29.9	39.0	29.4	18.5	17.8
La	16.0	29.4	19.1	16.5	10.5
Ce	36.4	56.0	39.2	34.4	21.7
Pr	4.53	7.09	4.62	4.03	2.48
Nd	20.23	30.39	19.51	16.94	10.53
Sm	4.74	6.38	4.31	3.62	2.27
Eu	1.48	1.42	1.03	1.03	0.72
Gd	5.37	6.58	4.52	3.93	2.48
Tb	0.84	1.01	0.82	0.62	0.52
Dy	5.27	6.48	5.13	4.13	2.89
Ho	0.95	1.32	1.13	0.83	0.72
Er	2.85	4.36	3.49	2.38	2.07
Tm	0.32	0.61	0.51	0.31	0.31
Yb	2.53	4.46	3.49	2.27	2.17
Lu	0.32	0.61	0.51	0.41	0.31
Cu	42	31	63	73	36
Zn	126	41	51	58	84
Mo	2	2	2	2	2
Ag	1	1	1	1	1
Tl	0.53	0.51	0.51	0.52	0.52
Pb	12.6	5.1	5.1	14.5	24.8
Sn	3.2	2.0	1.0	1.0	2.1
Sb					

Sample Number	AS-05-062	AS-05-063	AS-05-064	AS-05-065	AS-05-066
Easting	663079	663007	663345	663310	663280
Northing	5372535	5372541	5372792	5372770	5372750
Geochemical Lithology	Rhyolite	Rhyolite	Andesite	Andesite	Andesite
SiO_2	87.40	67.84	59.69	61.07	64.71
TiO_2	0.11	0.23	0.70	0.72	0.93
Al_2O_3	7.02	6.34	15.02	14.77	16.86
Fe_2O_3	1.58	19.10	8.08	7.01	4.65
MnO	0.03	0.67	0.23	0.17	0.08
MgO	0.79	2.57	6.11	6.16	3.20
CaO	0.99	2.64	5.95	4.79	2.15
K_2O	1.50	0.36	1.06	0.82	0.85
Na_2O	0.56	0.21	3.04	4.34	6.29
P_2O_5	0.02	0.05	0.13	0.14	0.29
LOI	1.46	1.66	3.2	5.45	2.22
Sum	98.23	98.89	98.24	98.35	99.94
Mg#	0.52	0.23	0.62	0.66	0.60
Ti	669	1341	4090	4252	5579
P	89	222	541	601	1250
Cr	41	20	331	318	92
Co	5	8	36	38	20
Ni	15	16	199	211	44
Rb	73	19	39	38	26
Sr	69	69	196	139	215
Cs	4	3	3	5	2
Ba	139	33	128	94	154
Sc					
V	8	26	128	141	127
Ta	0.51	0.51	0.52	0.53	0.61
Nb	6.1	4.1	6.2	6.4	9.2
Zr	162	94	124	122	164
Hf	5.1	3.1	3.1	3.2	5.1
Th	2.0	1.0	1.0	1.1	2.0
U	0.6	0.5	0.5	0.5	0.5
Y	13.9	17.9	15.5	16.3	23.4
La	10.3	9.4	12.4	11.4	16.0
Ce	21.2	18.9	26.9	25.4	35.8
Pr	2.54	2.24	3.20	3.07	4.50
Nd	10.76	9.66	13.95	13.13	19.64
Sm	2.33	2.14	2.79	2.86	4.19
Eu	0.71	0.61	0.93	0.95	1.43
Gd	2.54	2.34	3.10	3.28	4.40
Tb	0.41	0.41	0.52	0.53	0.82
Dy	2.64	2.85	3.10	3.18	4.60
Ho	0.61	0.61	0.62	0.64	0.92
Er	1.62	2.03	1.86	1.91	2.76
Tm	0.20	0.31	0.31	0.32	0.41
Yb	1.52	2.14	1.76	1.91	2.56
Lu	0.20	0.41	0.31	0.32	0.41
Cu	12	27	28	19	55
Zn	178	46	93	76	70
Mo	2	2	2	2	2
Ag	1	1	1	1	1
Tl	0.51	0.51	0.52	0.53	0.51
Pb	102.5	5.1	5.2	5.3	5.1
Sn	4.1	1.0	1.0	1.1	1.0
Sb					

Sample Number	AS-05-067	AS-05-068	AS-05-069a	AS-05-071	AS-05-072
Easting	663251	663170	663294	663565	663570
Northing	5372674	5372500	5372620	5372712	5372728
Geochemical Lithology	Andesite	Not analyzed for trace	Not analyzed for trace elements	Not analyzed for trace	Not analyzed for trace
SiO_2	65.44	41.91	77.06	72.23	62.81
TiO_2	0.60	0.31	0.26	0.36	0.54
Al_2O_3	17.76	8.92	8.47	10.66	12.18
Fe_2O_3	6.66	31.91	6.23	5.57	10.78
MnO	0.07	1.17	0.13	0.05	0.10
MgO	2.07	6.66	1.07	1.48	2.25
CaO	1.78	5.60	2.41	2.04	4.21
K_2O	3.79	3.12	2.93	4.98	5.39
Na_2O	1.77	0.32	1.38	2.56	1.62
P_2O_5	0.04	0.07	0.07	0.08	0.13
LOI	3.53	6.55	1.68	1.67	2.68
Sum	99.06	98.94	98.77	98.77	98.65
Mg#	0.41	0.31	0.27	0.37	0.31
Ti	3543	3193			4572
P	181	430			658
Cr	62	190			378
Co	13	1			44
Ni	30	56			71
Rb	157				
Sr	152				402
Cs	6				
Ba	341	245			398
Sc					
V	94	92			133
Ta	0.73				
Nb	8.3				
Zr	214				
Hf	6.2				
Th	4.1				
U	0.9				
Y	22.3	25.7			41.1
La	14.3				
Ce	29.8				
Pr	3.53				
Nd	14.62				
Sm	3.21				
Eu	0.93				
Gd	3.32				
Tb	0.62				
Dy	3.84				
Ho	0.83				
Er	2.59				
Tm	0.41				
Yb	2.59				
Lu	0.41				
Cu	108	320			3184
Zn	43	294			156
Mo	6	11			73
Ag	1	2			5
Tl	0.52	11.78			8.22
Pb	5.2	31.1			10.3
Sn	1.0	10.7			10.3
Sb					

Sample Number	AS-05-072a	AS-05-073a	AS-05-073b	AS-05-074	AS-05-075
Easting	663570	663649	663649	663050	663745
Northing	5372728	5372842	5372842	5372224	5372885
Geochemical	Not analyzed	Not analyzed	Not analyzed	Not analyzed	Not analyzed
Lithology	for trace	for trace	for trace	for trace	for trace
SiO_2	61.93	62.65	60.35	53.76	51.14
TiO_2	0.49	0.60	0.70	0.75	0.26
Al_2O_3	12.01	15.06	13.33	14.50	7.97
Fe_2O_3	11.97	12.48	8.20	9.37	27.34
MnO	0.10	0.03	0.10	0.11	0.17
MgO	2.10	1.18	6.17	8.06	5.04
CaO	5.14	0.43	3.84	5.29	3.32
K_2O	5.22	4.98	5.45	4.63	4.28
Na_2O	0.94	2.48	1.56	3.32	0.39
P_2O_5	0.11	0.12	0.28	0.20	0.10
LOI	3.43	4.82	2.46	2.67	3.90
Sum	98.62	98.54	98.73	98.67	100.62
Mg#	0.28	0.17	0.62	0.65	0.29
Ti	3990				
P	562				
Cr	334				
Co	9				
Ni	71				
Rb	0				
Sr	413				
Cs					
Ba	356				
Sc					
V	132				
Ta					
Nb					
Zr					
Hf					
Th					
U					
Y	38.3				
La					
Ce					
Pr					
Nd					
Sm					
Eu					
Gd					
Tb					
Dy					
Ho					
Er					
Tm					
Yb					
Lu					
Cu	1748				
Zn	134				
Mo	10				
Ag	3				
Tl	5.18				
Pb	12.4				
Sn	10.4				
Sb					

Sample Number	AS-05-076	AS-05-078a	AS-05-078b	AS-05-079a	AS-05-079b
Easting	663537	664062	664062	664081	664081
Northing	5372996	5373111	5373111	5373111	5373111
Geochemical Lithology	Not analyzed for trace	Rhyolite	Rhyolite	Andesite	Rhyolite
SiO_2	72.12	72.69	72.10	68.61	75.39
TiO_2	0.39	0.50	0.42	0.83	0.39
Al_2O_3	11.79	12.88	11.43	15.14	11.90
Fe_2O_3	6.41	5.03	8.76	4.81	4.18
MnO	0.17	0.05	0.05	0.04	0.02
MgO	3.33	1.44	2.06	1.84	1.45
CaO	1.31	1.71	0.52	3.04	1.22
K_2O	3.85	3.38	3.09	3.49	2.15
Na_2O	0.54	2.22	1.50	2.04	3.23
P_2O_5	0.09	0.09	0.06	0.15	0.07
LOI	3.11	2.17	2.74	2.35	1.81
Sum	100.32	100.10	100.00	99.80	99.99
Mg#	0.53	0.39	0.34	0.46	0.43
Ti	431	3003	2527	4973	2320
P	124	401	269	670	311
Cr	911	61	31	143	41
Co	1	9	8	17	7
Ni	34	18	23	47	14
Rb		124	127	139	97
Sr	36	249	123	251	174
Cs		5	5	5	4
Ba	157	633	333	378	231
Sc		4	4	5	3
V	37	74	52	168	59
Ta		0.61	0.62	0.51	0.71
Nb		9.2	9.3	7.2	10.2
Zr		200	265	145	240
Hf		6.1	7.2	4.1	7.1
Th		3.1	3.1	2.0	3.1
U		0.7	0.9	0.5	0.9
Y		30.2	22.0	23.8	30.9
La		18.0	13.8	13.9	15.7
Ce		40.3	29.6	30.9	33.2
Pr		4.91	3.50	3.79	3.97
Nd		19.11	13.57	15.98	15.89
Sm		4.40	3.19	3.89	4.07
Eu		0.92	0.72	1.13	0.92
Gd		4.50	3.19	3.99	4.18
Tb		0.82	0.62	0.72	0.81
Dy		5.11	3.70	4.30	5.09
Ho		1.02	0.82	0.92	1.02
Er		3.07	2.47	2.46	3.16
Tm		0.41	0.41	0.31	0.51
Yb		2.96	2.67	2.36	3.36
Lu		0.51	0.41	0.31	0.51
Cu	115	229	160	255	207
Zn	67	39	45	32	30
Mo	9	14	47	17	21
Ag	1	1	1	1	1
Tl	7.22	0.51	0.51	0.51	0.51
Pb	36.1	5.1	5.1	5.1	5.1
Sn	10.3	2.0	2.1	1.0	2.0
Sb		0.12	0.10	0.55	0.33

Sample Number	AS-05-080	AS-05-081	AS-05-082	AS-05-083	AS-05-084
Easting	664114	664160	664273	663375	663377
Northing	5373080	5373112	5373154	5372911	5372905
Geochemical Lithology	Rhyolite	Rhyolite	Rhyolite	Andesite	Andesite
SiO_2	80.04	81.36	78.09	64.44	62.17
TiO_2	0.26	0.21	0.20	0.85	1.00
Al_2O_3	11.66	10.36	10.97	14.49	17.37
Fe_2O_3	2.08	2.00	3.52	7.52	5.73
MnO	0.01	0.01	0.04	0.19	0.11
MgO	0.52	0.66	0.59	2.23	2.90
CaO	0.14	0.10	0.99	7.59	6.32
K_2O	2.31	3.15	4.72	0.59	0.82
Na_2O	2.94	2.13	0.85	1.85	3.29
P_2O_5	0.04	0.02	0.02	0.27	0.29
LOI	2.19	1.33	1.51	2.89	2.52
Sum	99.93	99.52	99.90	99.97	99.44
Mg#	0.36	0.42	0.27	0.39	0.53
Ti	1532	1276	1217	5062	5966
P	178	88	89	1168	1254
Cr	31	10	30	82	123
Co	3	2	7	19	45
Ni	5	5	7	40	115
Rb	75	94	108	18	27
Sr	76	56	100	327	244
Cs	1	2	3	1	1
Ba	283	393	1031	146	154
Sc	1	1	2	5	5
V	9	7	6	126	142
Ta	0.92	0.91	0.91	0.62	0.62
Nb	12.3	12.2	12.2	9.3	10.3
Zr	295	277	301	157	185
Hf	9.2	9.1	9.1	4.1	5.1
Th	4.1	4.1	4.1	2.1	2.1
U	1.0	1.0	0.9	0.5	0.5
Y	42.2	50.5	43.6	25.8	28.1
La	14.9	16.8	24.8	17.5	18.1
Ce	33.9	39.9	53.7	38.6	41.7
Pr	4.29	4.66	6.70	4.84	5.23
Nd	17.79	19.46	26.70	19.15	21.65
Sm	4.81	5.17	6.30	4.22	4.92
Eu	0.92	1.11	1.32	1.44	1.33
Gd	5.11	6.18	6.60	4.22	4.92
Tb	1.02	1.32	1.22	0.72	0.82
Dy	7.16	8.92	7.72	4.53	4.82
Ho	1.53	1.82	1.62	0.93	1.03
Er	4.50	5.37	4.67	2.57	2.87
Tm	0.72	0.81	0.71	0.41	0.41
Yb	4.70	5.47	4.77	2.57	2.87
Lu	0.72	0.81	0.71	0.41	0.41
Cu	28	40	71	51	14
Zn	13	15	26	84	82
Mo	3	2	6	2	2
Ag	1	1	1	1	1
Tl	0.51	0.51	0.51	0.51	0.51
Pb	5.1	5.1	5.1	5.1	5.1
Sn	2.0	2.0	2.0	2.1	2.1
Sb	0.05	0.05	0.06	0.09	0.06

Sample Number	AS-05-085	AS-05-086	AS-05-088	AS-05-089	AS-05-090
Easting	663377	663393	662999	663287	663288
Northing	5372886	5372880	5372334	5372872	5372851
Geochemical Lithology	Andesite	Andesite	Andesite	Andesite	Andesite
SiO_2	63.59	77.06	61.88	66.35	58.20
TiO_2	0.88	0.38	0.92	0.83	0.93
Al_2O_3	15.90	9.36	15.64	14.63	17.79
Fe_2O_3	6.62	6.96	8.11	6.52	6.94
MnO	0.15	0.13	0.16	0.12	0.14
MgO	2.73	1.69	3.79	2.55	3.22
CaO	6.18	2.12	5.69	4.88	7.96
K_2O	0.54	1.05	0.61	1.79	1.67
Na_2O	3.15	1.17	2.97	2.09	2.87
P_2O_5	0.27	0.07	0.23	0.24	0.27
LOI	2.48	3.22	3.76	3.8	3.39
Sum	99.37	100.15	98.51	98.85	98.65
Mg#	0.48	0.35	0.51	0.46	0.51
Ti	5226	2292	5423	4925	5525
P	1164	316	998	1044	1175
Cr	103	114	104	83	104
Co	22	14	25	21	23
Ni	50	50	50	46	46
Rb	14	33	22	67	51
Sr	208	116	250	175	299
Cs	1	1	1	3	2
Ba	119	209	133	210	214
Sc	4	4			
V	135	80	25	22	26
Ta	0.62	0.52	0.62	0.62	0.72
Nb	9.2	4.1	9.4	8.3	10.4
Zr	163	91	157	153	171
Hf	4.1	3.1	4.2	4.2	5.2
Th	2.1	1.0	2.1	2.1	2.1
U	0.5	0.5	0.5	0.5	0.6
Y	26.5	11.2	25.2	22.0	26.4
La	16.4	7.6	15.2	13.2	18.5
Ce	38.2	16.3	35.1	30.9	40.8
Pr	4.62	1.86	4.37	3.74	4.97
Nd	18.87	7.34	19.34	16.33	21.75
Sm	4.31	1.65	4.37	3.74	4.66
Eu	1.23	0.52	1.46	1.14	1.55
Gd	4.31	1.55	4.47	3.74	4.97
Tb	0.72	0.31	0.73	0.73	0.83
Dy	4.41	1.76	4.89	4.06	4.97
Ho	0.92	0.41	1.04	0.83	1.04
Er	2.67	1.14	2.81	2.50	3.11
Tm	0.41	0.21	0.42	0.42	0.41
Yb	2.56	1.14	2.70	2.60	3.00
Lu	0.41	0.21	0.42	0.42	0.52
Cu	10	65	35	26	6
Zn	92	52	88	67	86
Mo	2	2	2	2	2
Ag	1	1	1	1	1
Tl	0.51	0.52	0.52	0.52	0.52
Pb	5.1	5.2	5.2	5.2	5.2
Sn	2.1	1.0	2.1	2.1	2.1
Sb	0.07	0.05			

Sample Number	RM-01	RM-02	RM-03a	RM-03b	RM-03c
Easting	663303	663286	663775	663775	663387
Northing	5372834	5372829	5372690	5372690	5372850
Geochemical Lithology	Andesite	Andesite	Andesite	Andesite	Andesite
SiO_2	73.89	62.36	66.31	69.57	61.97
TiO_2	0.78	0.83	0.71	0.54	1.00
Al_2O_3	13.26	15.02	15.89	11.97	16.54
Fe_2O_3	3.19	9.98	6.74	9.04	6.97
MnO	0.05	0.18	0.11	0.37	0.15
MgO	0.96	3.01	3.03	2.17	3.15
CaO	3.25	5.51	3.68	3.17	5.03
K_2O	1.31	1.15	2.84	0.39	0.58
Na_2O	3.12	1.72	0.58	2.67	4.34
P_2O_5	0.20	0.26	0.10	0.10	0.28
LOI	1.3	2.73	3.03	2.55	2.87
Sum	99.56	99.52	99.25	99.94	99.99
Mg#	0.40	0.40	0.50	0.35	0.50
Ti	4677	4931	4205	3261	5987
P	884	1122	450	448	1213
Cr	71	72	21	123	93
Co	10	17	13	9	33
Ni	22	35	27	40	84
Rb	42	32	83	16	15
Sr	160	244	140	194	221
Cs	2	2	2	1	1
Ba	169	229	511	73	157
Sc					
V	83	101	94	81	121
Ta	0.51	0.51	0.52	0.51	0.62
Nb	7.1	7.2	7.2	5.1	9.3
Zr	111	128	166	105	153
Hf	3.0	4.1	5.2	3.1	5.1
Th	1.0	2.1	3.1	2.1	1.0
U	0.5	0.5	0.7	0.5	0.5
Y	17.2	22.9	22.8	12.7	27.5
La	10.9	14.3	15.3	8.4	16.3
Ce	26.0	32.9	34.1	18.5	37.8
Pr	3.34	4.11	4.02	2.26	4.84
Nd	13.98	17.27	15.88	9.03	20.39
Sm	3.04	3.70	3.61	1.85	4.53
Eu	0.91	1.23	0.93	0.72	1.44
Gd	3.14	4.01	3.71	2.05	5.04
Tb	0.51	0.62	0.62	0.31	0.82
Dy	2.94	3.91	3.71	2.15	4.74
Ho	0.61	0.82	0.83	0.41	1.03
Er	1.72	2.36	2.37	1.33	2.68
Tm	0.20	0.31	0.41	0.21	0.41
Yb	1.62	2.36	2.48	1.23	2.68
Lu	0.20	0.31	0.41	0.21	0.41
Cu	18	53	12	11	13
Zn	30	72	68	77	78
Mo	2	2	2	2	2
Ag	1	1	1	1	1
Tl	0.51	0.51	0.52	0.51	0.51
Pb	5.1	5.1	5.2	5.1	5.1
Sn	2.0	2.1	2.1	1.0	1.0
Sb					

Sample Number	RM-04	RM-05	RM-06	RM-07a	RM-07b
Easting	663414	663383	663487	663256	663256
Northing	5372975	5373048	5372994	5372800	5372800
Geochemical Lithology	Andesite	Andesite	Andesite	Andesite	Andesite
SiO_2	63.18	63.54	71.39	63.77	60.79
TiO_2	0.98	0.97	0.40	0.83	0.46
Al_2O_3	16.15	16.48	8.89	15.42	9.37
Fe_2O_3	7.31	6.43	11.74	7.20	16.49
MnO	0.17	0.15	0.37	0.13	0.36
MgO	3.15	2.74	2.54	3.03	4.12
CaO	5.05	5.35	3.28	6.40	7.08
K_2O	0.86	0.82	0.50	0.66	0.92
Na_2O	2.88	3.25	0.84	2.34	0.30
P_2O_5	0.27	0.28	0.04	0.22	0.11
LOI	3.03	2.54	3.26	2.79	3.43
Sum	99.90	99.44	99.65	99.90	99.23
Mg#	0.49	0.48	0.32	0.48	0.36
Ti	5873	5783	2417	4995	2732
P	1170	1209	180	943	497
Cr	124	92	72	82	41
Co	35	35	17	24	27
Ni	85	70	67	43	45
Rb	27	25	17	25	44
Sr	211	227	136	279	140
Cs	2	1	2	1	12
Ba	180	151	62	162	44
Sc					
V	128	126	78	103	81
Ta	0.62	0.62	0.52	0.62	0.52
Nb	9.3	9.2	3.1	8.2	5.2
Zr	152	156	87	144	99
Hf	5.2	5.1	3.1	4.1	3.1
Th	1.0	2.1	1.0	2.1	2.1
U	0.5	0.5	0.5	0.5	0.5
Y	28.7	26.2	10.6	24.9	17.2
La	16.1	16.4	6.8	16.9	11.4
Ce	37.6	38.2	15.3	37.7	24.2
Pr	4.95	4.82	1.76	4.73	2.90
Nd	20.21	20.63	7.34	19.13	12.12
Sm	4.43	4.62	1.55	4.11	2.49
Eu	1.24	1.23	0.52	1.34	0.93
Gd	4.85	4.72	1.65	4.32	2.69
Tb	0.72	0.82	0.31	0.62	0.41
Dy	4.74	4.52	1.65	4.11	2.80
Ho	1.03	0.92	0.41	0.82	0.62
Er	2.89	2.77	1.24	2.47	1.76
Tm	0.41	0.41	0.21	0.31	0.31
Yb	2.78	2.57	1.24	2.37	1.86
Lu	0.41	0.41	0.21	0.41	0.31
Cu	6	24	50	5	165
Zn	85	70	62	142	107
Mo	2	2	5	2	2
Ag	1	1	1	1	1
Tl	0.52	0.51	0.52	0.51	0.52
Pb	5.2	5.1	5.2	5.1	5.2
Sn	2.1	1.0	2.1	2.1	2.1
Sb					

Sample Number	RM-08	RM-15	LR-05-001	LR-05-002	LR-05-003
Easting	663200	663097	663098	663164	663196
Northing	5372796	5372895	5373004	5372943	5372989
Geochemical Lithology	Andesite	Dacite	Andesite	Rhyolite	Andesite
SiO_2	65.70	76.85	58.37	73.30	58.56
TiO_2	0.96	0.28	0.87	0.57	0.84
Al_2O_3	15.32	14.37	19.53	14.95	17.74
Fe_2O_3	5.99	2.29	8.17	2.86	8.79
MnO	0.07	0.02	0.12	0.06	0.11
MgO	2.18	1.23	3.31	1.22	5.85
CaO	5.01	1.33	3.77	2.82	3.00
K_2O	1.49	2.06	2.24	2.71	2.29
Na_2O	2.98	1.50	3.40	1.41	2.62
P_2O_5	0.30	0.06	0.21	0.09	0.19
LOI	1.69	2	4.72	1.93	4.75
Sum	99.58	98.60	99.73	100.20	99.72
Mg#	0.44	0.54	0.47	0.48	0.59
Ti	5733	1652	5223	3423	5036
P	1287	267	916	400	825
Cr	92	31	409	20	284
Co	20	4	34	8	35
Ni	36	6	185	16	170
Rb	51	38	57	64	51
Sr	263	195	232	149	192
Cs	4	2	2	2	2
Ba	230	372	355	358	578
Sc		1			
V	116	32	173	53	170
Ta	0.61	0.51	0.52	0.71	0.53
Nb	9.2	2.0	7.3	8.2	6.3
Zr	148	119	137	216	132
Hf	4.1	3.1	4.2	6.1	3.2
Th	2.0	1.0	2.1	4.1	1.1
U	0.5	0.5	0.5	0.9	0.5
Y	28.3	3.9	21.8	24.9	18.5
La	17.1	13.3	16.1	20.2	12.3
Ce	38.2	25.4	36.9	43.4	27.0
Pr	4.88	2.65	4.41	4.79	3.15
Nd	20.45	9.39	18.05	18.97	13.23
Sm	4.48	1.63	3.57	3.77	2.94
Eu	1.22	0.41	1.26	0.82	0.84
Gd	4.78	1.33	4.09	4.08	3.26
Tb	0.71	0.20	0.63	0.61	0.53
Dy	4.58	0.71	3.99	3.98	3.15
Ho	0.92	0.10	0.73	0.82	0.63
Er	2.85	0.31	2.31	2.55	1.89
Tm	0.41	0.10	0.31	0.31	0.21
Yb	2.85	0.31	2.20	2.45	1.79
Lu	0.41	0.10	0.31	0.31	0.21
Cu	40	5	90	12	62
Zn	70	41	108	52	93
Mo	2	2	2	2	2
Ag	1	1	1	1	1
Tl	0.51	0.51	0.52	0.51	0.53
Pb	5.1	5.1	5.2	5.1	5.3
Sn	1.0	1.0	2.1	2.0	1.1
Sb		0.05			

Sample Number	LR-05-004	LR-05-005	LR-05-006	LR-05-007	LR-05-008
Easting	663217	663216	663265	663082	663175
Northing	5373013	5373058	5373087	5372919	5372890
Geochemical Lithology	Andesite	Andesite	Andesite	Andesite	Andesite
SiO_2	65.49	62.03	64.07	57.79	60.48
TiO_2	0.77	0.65	0.66	0.76	0.70
Al_2O_3	15.83	14.30	14.18	15.94	15.35
Fe_2O_3	6.37	7.42	6.92	9.61	7.89
MnO	0.09	0.13	0.10	0.13	0.10
MgO	2.87	4.39	5.69	8.19	6.17
CaO	2.21	6.15	3.81	3.35	4.18
K_2O	0.60	0.60	0.06	0.73	0.15
Na_2O	5.63	4.16	4.37	3.32	4.79
P_2O_5	0.14	0.17	0.15	0.17	0.19
LOI	3.26	6.75	5.45	6.23	5.79
Sum	99.25	99.24	99.83	99.44	99.99
Mg#	0.50	0.57	0.64	0.65	0.63
Ti	4587	3860	3932	4541	4200
P	587	749	646	745	834
Cr	269	300	296	331	329
Co	32	32	33	41	35
Ni	132	172	176	188	187
Rb	15	13	1	15	2
Sr	220	207	178	270	261
Cs	1			1	
Ba	101	134	17	369	36
Sc					
V	134	124	138	162	146
Ta	0.52	0.54	0.53	0.53	0.53
Nb	6.2	5.4	5.3	5.3	6.4
Zr	122	102	111	117	122
Hf	4.1	3.2	3.2	3.2	3.2
Th	1.0	1.1	1.1	1.1	1.1
U	0.5	0.5	0.5	0.5	0.5
Y	15.3	14.8	16.3	17.9	17.5
La	11.2	11.3	10.6	11.0	12.3
Ce	26.0	24.6	23.1	24.6	27.6
Pr	3.10	2.90	2.64	2.88	3.18
Nd	12.61	12.02	11.53	12.16	13.06
Sm	2.79	2.47	2.33	2.45	2.76
Eu	0.93	0.75	0.74	0.75	0.74
Gd	2.79	2.79	2.64	2.88	2.87
Tb	0.41	0.32	0.42	0.43	0.42
Dy	2.69	2.47	2.54	2.88	2.76
Ho	0.52	0.43	0.53	0.53	0.53
Er	1.55	1.50	1.59	1.81	1.70
Tm	0.21	0.11	0.21	0.21	0.21
Yb	1.45	1.29	1.48	1.71	1.70
Lu	0.21	0.21	0.21	0.21	0.21
Cu	42	46	42	48	68
Zn	82	90	87	115	102
Mo	2	2	2	2	2
Ag	1	1	1	1	1
Tl	0.52	0.54	0.53	0.53	0.53
Pb	5.2	5.4	5.3	5.3	5.3
Sn	1.0	1.1	1.1	1.1	1.1
Sb					

Sample Number	LR-05-021	G05-7	G05-9	G05-10	G05-11
Easting	663057	663127	663225	663188	663114
Northing	5372245	5373123	5373188	5373251	5373360
Geochemical Lithology		Rhyolite	BIF	Rhyolite	Rhyolite
SiO_2	35.41	91.05	93.35	78.35	76.35
TiO_2	0.31	0.05	0.01	0.27	0.28
Al_2O_3	6.77	2.80	0.28	12.58	12.32
Fe_2O_3	52.70	4.65	5.05	2.77	3.72
MnO	0.02	0.14	0.40	0.06	0.07
MgO	1.15	0.93	0.17	0.86	0.71
CaO	0.40	0.05	0.65	0.72	1.28
K_2O	3.01	0.14	0.03	3.74	3.33
Na_2O	0.13	0.17	0.05	0.62	1.91
P_2O_5	0.12	0.01	0.01	0.03	0.02
LOI	17.45	0.94	1.68	2.51	2.63
Sum	100.21	98.96	99.14	98.79	99.37
Mg#	0.05	0.31	0.07	0.41	0.30
Ti	2266	303	61	1599	1663
P	649	44	44	134	90
Cr	344	20	20	10	10
Co	57	1	4	3	1
Ni	272	7	11	33	5
Rb		3	2	111	88
Sr	48	4	21	39	88
Cs				3	4
Ba	65	60	21	427	346
Sc					
V	59	9	10	8	10
Ta		0.50	0.51	1.13	1.13
Nb		4.0	1.0	14.4	15.4
Zr		92	9	348	350
Hf		3.0	1.0	10.3	10.3
Th		1.0	1.0	4.1	5.1
U		0.5	0.5	1.1	1.2
Y	8.5	18.9	3.1	42.9	48.6
La		9.0	1.7	30.4	30.3
Ce		19.2	2.5	67.1	66.5
Pr		2.32	0.20	8.00	8.01
Nd		9.59	1.02	34.48	33.38
Sm		2.12	0.10	7.70	7.19
Eu		0.40	0.10	1.64	1.64
Gd		2.42	0.31	8.41	8.53
Tb		0.30	0.10	1.33	1.34
Dy		2.52	0.31	8.11	8.53
Ho		0.50	0.10	1.54	1.75
Er		1.62	0.20	4.41	5.14
Tm		0.20	0.10	0.62	0.72
Yb		1.51	0.10	4.31	5.03
Lu		0.20	0.10	0.62	0.72
Cu	670	5	9	5	28
Zn	48	100	23	69	119
Mo	59	2	2	2	2
Ag	6	1	1	1	1
Tl	18.16	0.50	0.51	0.51	0.51
Pb	30.3	5.0	5.1	5.1	5.1
Sn	12.1	2.0	1.0	3.1	3.1
Sb					

Sample Number	G05-12	G05-13	G05-14	G05-15	G05-16
Easting	663247	663308	663391	663309	663255
Northing	5373473	5373376	5373441	5373530	5373611
Geochemical Lithology	Rhyolite	Rhyolite	Rhyolite	Rhyolite	Rhyolite
SiO_2	79.64	75.73	87.91	80.80	84.98
TiO_2	0.20	0.16	0.12	0.28	0.21
Al_2O_3	11.39	8.05	5.14	11.48	9.04
Fe_2O_3	3.25	11.06	4.12	2.59	0.87
MnO	0.03	0.45	0.14	0.05	0.02
MgO	0.25	2.95	0.82	1.12	0.13
CaO	0.18	0.98	0.70	0.78	0.44
K_2O	2.01	0.28	0.85	1.87	1.07
Na_2O	3.02	0.32	0.18	1.01	3.20
P_2O_5	0.02	0.02	0.03	0.02	0.03
LOI	1.25	3.33	1.71	2.41	0.81
Sum	99.91	99.94	99.88	99.31	99.92
Mg#	0.15	0.37	0.30	0.49	0.25
Ti	1214	930	732	1659	1269
P	88	90	133	89	132
Cr	10	10	10	10	10
Co	1	16	3	3	1
Ni	5	60	11	34	11
Rb	58	9	21	51	24
Sr	82	26	18	116	69
Cs	2		1	1	1
Ba	286	65	133	331	207
Sc					
V	9	7	5	5	5
Ta	1.11	0.72	0.51	1.02	0.81
Nb	14.2	11.4	5.1	13.3	11.1
Zr	340	244	124	310	232
Hf	10.1	7.2	3.1	10.2	7.1
Th	4.1	3.1	2.0	4.1	3.0
U	1.2	0.7	0.5	1.1	0.9
Y	48.4	36.7	21.1	41.1	38.9
La	25.1	18.8	13.4	12.9	19.8
Ce	56.5	42.5	29.3	33.0	44.1
Pr	6.68	5.07	3.66	3.79	5.54
Nd	27.54	21.21	15.26	15.37	23.39
Sm	6.48	4.86	3.36	4.10	5.44
Eu	1.62	0.93	0.61	0.92	1.21
Gd	7.60	5.59	3.66	5.43	6.25
Tb	1.22	0.93	0.61	1.13	1.01
Dy	8.10	6.31	3.56	7.48	6.45
Ho	1.62	1.34	0.71	1.64	1.41
Er	4.86	4.03	2.14	4.71	4.13
Tm	0.71	0.62	0.31	0.72	0.60
Yb	4.76	4.34	2.14	4.20	3.93
Lu	0.61	0.62	0.31	0.61	0.60
Cu	8	21	5	7	5
Zn	50	145	48	60	21
Mo	2	2	2	2	2
Ag	1	1	1	1	1
Tl	0.51	0.52	0.51	0.51	0.50
Pb	5.1	5.2	5.1	5.1	5.0
Sn	3.0	1.0	2.0	3.1	1.0
Sb					

Sample Number	G05-17	G05-18	G05-19	G05-20	G05-39
Easting	663115	663045	663120	663189	663574
Northing	5373643	5373526	5373434	5373360	5372716
Geochemical Lithology	Rhyolite	Rhyolite	Rhyolite	Rhyolite	Andesite
SiO_2	76.98	81.24	76.21	81.08	53.55
TiO_2	0.22	0.19	0.22	0.24	0.17
Al_2O_3	12.46	10.23	11.99	10.31	9.13
Fe_2O_3	3.74	2.44	5.73	3.31	30.07
MnO	0.06	0.04	0.10	0.09	0.25
MgO	1.38	0.14	0.92	1.34	3.24
CaO	1.28	0.73	0.23	0.63	0.74
K_2O	1.38	1.37	2.05	2.51	2.61
Na_2O	2.46	3.59	2.53	0.48	0.18
P_2O_5	0.03	0.02	0.02	0.01	0.07
LOI	2.52	1.24	1.71	2.26	8.844128996
Sum	99.35	99.90	99.33	100.05	103.27
Mg#	0.45	0.11	0.26	0.47	0.19
Ti	1292	1153	1281	1411	1527
P	134	88	89	45	218
Cr	10	10	10	10	966
Co	4	2	1	1	1
Ni	12	9	6	10	51
Rb	52	26	67	77	
Sr	86	81	54	34	73
Cs	1	1	3	2	
Ba	313	332	263	258	159
Sc					
V	5	5	5	5	23
Ta	1.03	0.81	1.02	0.82	
Nb	14.4	12.2	13.2	12.3	
Zr	325	272	329	277	
Hf	10.3	9.1	10.2	8.2	
Th	4.1	3.0	4.1	4.1	
U	1.1	1.0	1.1	1.0	
Y	50.2	46.0	49.6	35.9	25.2
La	27.4	19.9	23.1	24.5	
Ce	60.8	43.9	50.2	50.7	
Pr	7.70	5.57	6.41	6.65	
Nd	32.42	23.29	27.07	27.73	
Sm	7.59	5.57	6.41	6.34	
Eu	1.54	1.22	1.53	1.33	
Gd	8.31	6.78	7.53	6.96	
Tb	1.44	1.11	1.32	1.13	
Dy	8.72	7.29	8.55	6.55	
Ho	1.85	1.62	1.83	1.33	
Er	5.54	4.86	5.49	3.89	
Tm	0.82	0.71	0.81	0.51	
Yb	5.44	4.56	5.39	3.58	
Lu	0.82	0.71	0.81	0.51	
Cu	6	120	5	5	2359
Zn	125	23	94	105	173
Mo	2	3	2	2	9
Ag	1	1	1	1	3
Tl	0.51	0.51	0.51	0.51	10.94
Pb	5.1	5.1	5.1	5.1	27.3
Sn	3.1	2.0	3.1	3.1	10.9
Sb					

Sample Number	G05-40	OC-151	OC-153	OC-154b	OC-156
Easting	663573	662985	662929	662921	662823
Northing	5372647	5372386	5372433	5372458	5372541
Geochemical Lithology	Pink Breccia	Andesite	Andesite	Andesite	Andesite
SiO_2	75.33	79.84	66.92	67.23	62.38
TiO_2	0.29	0.45	0.87	0.70	0.77
Al_2O_3	13.04	11.61	16.52	15.87	15.57
Fe_2O_3	3.55	1.97	4.81	5.41	6.72
MnO	0.01	0.02	0.14	0.16	0.13
MgO	1.07	1.18	2.18	1.66	4.21
CaO	0.83	1.27	3.14	6.01	4.59
K_2O	4.26	2.43	2.60	2.08	0.81
Na_2O	1.58	1.18	2.69	0.75	4.62
P_2O_5	0.03	0.05	0.12	0.13	0.19
LOI	1.69	1.86	3.19	2.3	2.07
Sum	98.34	99.88	100.00	100.00	99.32
Mg#	0.40	0.57	0.50	0.40	0.58
Ti		2688	5202	4173	4592
P	122	222	541	581	802
Cr	11	41	238	82	327
Co	13	3	48	11	29
Ni	11	11	228	29	182
Rb	41	93	81	54	24
Sr	21	102	253	209	238
Cs	3	2	2	3	2
Ba	886	358	231	264	133
Sc	2				
V	23	36	188	147	151
Ta	1.02	0.61	0.52	0.51	0.51
Nb	12.2	7.1	5.2	5.1	6.1
Zr	351	191	81	138	117
Hf	10.2	5.1	3.1	4.1	3.1
Th	3.9	3.1	1.0	1.0	1.0
U	0.4	0.8	0.5	0.5	0.5
Y	17.3	20.2	18.4	20.5	18.0
La	17.5	10.6	8.4	12.3	12.3
Ce	38.2	22.8	19.7	26.0	27.5
Pr	6.00	2.65	2.58	3.17	3.37
Nd	26.45	10.60	11.16	13.31	13.89
Sm	6.21	2.34	2.58	2.97	3.06
Eu	1.12	0.51	0.83	0.92	0.92
Gd	6.00	2.55	2.89	3.17	3.17
Tb	1.12	0.51	0.52	0.51	0.51
Dy	7.12	3.26	3.10	3.38	3.06
Ho	1.53	0.71	0.62	0.72	0.61
Er	4.58	2.14	1.96	2.15	1.84
Tm	0.71	0.31	0.31	0.31	0.31
Yb	4.78	2.14	1.65	2.15	1.84
Lu	0.81	0.31	0.21	0.31	0.20
Cu	1923	30	58	17	59
Zn	22	31	84	83	66
Mo	4	21	2	2	2
Ag	2	1	1	1	1
Tl	0.51	0.51	0.52	0.51	0.51
Pb	5.1	5.1	5.2	5.1	5.1
Sn	2.0	2.0	1.0	1.0	1.0
Sb	0.07				

Sample Number	OC-159	OC-162	OC-164	OC-165	OC-168b
Easting	662679	662724	662738	662694	662971
Northing	5372749	5372806	5372841	5372864	5372541
Geochemical Lithology	Rhyolite	Rhyolite	Rhyolite	Andesite	Andesite
SiO_2	88.66	85.77	77.48	61.34	55.12
TiO_2	0.16	0.20	0.25	0.94	0.76
Al_2O_3	7.26	8.80	11.71	17.18	18.25
Fe_2O_3	1.32	2.06	2.50	8.29	8.17
MnO	0.01	0.01	0.10	0.18	0.23
MgO	0.16	0.26	0.50	3.31	5.52
CaO	0.04	0.03	2.07	4.29	7.58
K_2O	2.27	2.69	2.04	2.49	1.51
Na_2O	0.09	0.15	3.33	1.84	2.65
P_2O_5	0.02	0.03	0.03	0.13	0.21
LOI	1.11	1.37	2.61	5.6	2.64
Sum	99.37	99.33	99.40	99.51	100.10
Mg#	0.21	0.21	0.30	0.47	0.60
Ti	970	1216	1478	5590	4556
P	88	133	134	555	896
Cr	30	20	21	64	72
Co	1	1	1	16	24
Ni	5	5	5	47	34
Rb	44	59	52	59	53
Sr	14	23	111	125	546
Cs	1	2	2	3	2
Ba	281	386	223	431	317
Sc					
V	16	5	5	229	187
Ta	0.61	0.81	1.03	0.53	0.51
Nb	9.1	10.1	13.4	6.4	4.1
Zr	201	263	322	154	89
Hf	6.1	8.1	9.2	4.2	3.1
Th	3.0	3.0	4.1	2.1	2.1
U	0.7	1.0	1.1	0.5	0.5
Y	30.7	42.9	45.1	20.5	13.4
La	13.3	19.7	27.5	15.0	15.7
Ce	30.0	42.2	62.6	33.6	34.8
Pr	3.74	5.07	7.80	4.03	4.42
Nd	15.78	21.09	32.97	16.32	18.49
Sm	3.84	5.37	7.80	3.50	3.59
Eu	0.81	1.22	1.54	0.95	1.03
Gd	4.25	6.49	8.01	3.28	3.29
Tb	0.81	1.22	1.34	0.53	0.51
Dy	4.85	7.30	8.01	3.39	2.47
Ho	1.11	1.52	1.64	0.74	0.51
Er	3.34	4.77	4.83	2.33	1.34
Tm	0.51	0.71	0.72	0.32	0.21
Yb	3.34	4.66	4.62	2.44	1.23
Lu	0.40	0.71	0.62	0.32	0.10
Cu	5	16	6	25	5
Zn	18	37	71	76	78
Mo	2	2	2	2	2
Ag	1	1	1	1	1
Tl	0.51	0.51	0.51	0.53	0.51
Pb	5.1	5.1	5.1	5.3	5.1
Sn	2.0	3.0	3.1	2.1	1.0
Sb					

Sample Number	OC-195	OC-202	OC-257	OC-258	OC-259
Easting	662818	662663	663855	663849	663871
Northing	5372886	5373091	5373899	5373870	5373801
Geochemical Lithology	Rhyolite	Andesite	Dacite	Dacite	Dacite
SiO_2	88.66	59.07	77.10	75.91	76.25
TiO_2	0.19	0.62	0.23	0.23	0.22
Al_2O_3	6.99	16.26	14.78	14.44	14.46
Fe_2O_3	1.56	7.27	1.39	1.81	1.96
MnO	0.01	0.14	0.01	0.02	0.02
MgO	0.21	5.31	0.44	0.74	0.46
CaO	0.02	6.40	0.59	1.35	1.13
K_2O	2.19	1.49	2.40	1.79	1.80
Na_2O	0.14	3.22	3.03	3.66	3.67
P_2O_5	0.01	0.21	0.03	0.05	0.04
LOI	1.12	7.83	1.87	2.48	2.16
Sum	99.57	99.79	99.44	99.76	99.82
Mg#	0.23	0.62	0.41	0.47	0.34
Ti	1152	3708	1344	1353	1287
P	44	900	133	224	178
Cr	40	239	10	10	10
Co	1	27	1	2	2
Ni	5	95	5	5	5
Rb	48	40	41	32	31
Sr	14	323	159	176	161
Cs	1	2	2	2	2
Ba	446	369	353	329	296
Sc					
V	5	155	9	9	10
Ta	0.61	0.54	0.51	0.51	0.51
Nb	8.1	4.3	1.0	1.0	2.0
Zr	200	99	110	107	106
Hf	6.1	3.3	3.1	3.1	3.1
Th	3.0	3.3	1.0	1.0	1.0
U	0.7	0.9	0.5	0.5	0.5
Y	32.4	12.6	2.8	3.2	3.1
La	20.9	18.0	7.9	10.4	9.9
Ce	46.6	38.8	16.1	20.5	19.6
Pr	5.87	4.77	1.73	2.26	2.15
Nd	24.58	19.10	6.11	7.69	7.56
Sm	5.76	3.47	1.02	1.23	1.12
Eu	1.11	0.98	0.31	0.21	0.31
Gd	6.07	3.04	0.82	1.03	1.02
Tb	1.01	0.43	0.10	0.10	0.10
Dy	5.76	2.17	0.41	0.41	0.51
Ho	1.21	0.43	0.10	0.10	0.10
Er	3.54	1.30	0.20	0.21	0.20
Tm	0.51	0.22	0.10	0.10	0.10
Yb	3.44	1.19	0.20	0.21	0.20
Lu	0.40	0.11	0.10	0.10	0.10
Cu	30	5	6	5	5
Zn	37	124	33	44	45
Mo	2	2	2	2	2
Ag	1	1	1	1	1
Tl	0.51	0.54	0.51	0.51	0.51
Pb	5.1	5.4	9.2	7.2	9.2
Sn	2.0	1.1	1.0	1.0	1.0
Sb					

Sample Number	OC-261	OC-262	OC-263	OC-264	OC-265
Easting	663907	663937	664111	664113	664125
Northing	5373742	5373705	5373512	5373490	5373496
Geochemical Lithology	Dacite	Dacite	Dacite	Dacite	Dacite
SiO_2	76.15	74.99	71.12	68.64	69.28
TiO_2	0.24	0.26	0.39	0.39	0.35
Al_2O_3	14.81	14.64	15.61	16.02	17.07
Fe_2O_3	1.74	1.87	2.58	3.70	3.33
MnO	0.01	0.03	0.03	0.04	0.02
MgO	0.41	0.44	0.85	1.28	1.23
CaO	0.67	0.95	4.27	4.44	2.89
K_2O	2.26	3.44	0.71	0.89	2.43
Na_2O	3.68	3.34	4.36	4.54	3.32
P_2O_5	0.04	0.05	0.08	0.07	0.07
LOI	1.74	1.88	1.14	1.62	1.84
Sum	99.35	99.93	99.70	99.65	99.49
Mg#	0.34	0.34	0.42	0.43	0.45
Ti	1403	1527	2304	2316	2077
P	178	222	353	311	311
Cr	10	10	40	51	41
Co	2	2	6	7	9
Ni	5	5	22	21	22
Rb	37	49	16	19	47
Sr	169	163	445	371	384
Cs	2	2	1	1	3
Ba	320	489	111	169	630
Sc					
V	9	9	46	49	65
Ta	0.51	0.51	0.51	0.51	0.51
Nb	1.0	1.0	1.0	2.0	2.0
Zr	111	105	68	96	100
Hf	3.1	3.1	2.0	3.0	3.1
Th	1.0	1.0	1.0	1.0	1.0
U	0.5	0.5	0.5	0.5	0.5
Y	2.8	3.0	3.7	5.4	5.2
La	10.1	10.4	6.6	8.8	9.6
Ce	20.4	20.6	13.2	18.1	19.1
Pr	2.24	2.24	1.42	2.03	2.14
Nd	7.74	7.95	5.66	7.73	8.15
Sm	1.22	1.22	1.11	1.42	1.53
Eu	0.31	0.31	0.30	0.41	0.51
Gd	1.02	1.02	1.01	1.32	1.32
Tb	0.10	0.10	0.10	0.20	0.20
Dy	0.41	0.41	0.61	0.91	1.02
Ho	0.10	0.10	0.10	0.10	0.20
Er	0.20	0.20	0.40	0.41	0.51
Tm	0.10	0.10	0.10	0.10	0.10
Yb	0.20	0.20	0.30	0.41	0.41
Lu	0.10	0.10	0.10	0.10	0.10
Cu	7	9	13	30	63
Zn	66	46	36	45	52
Mo	2	2	2	2	2
Ag	1	1	1	1	1
Tl	0.51	0.51	0.51	0.51	0.51
Pb	12.2	18.3	20.2	11.2	10.2
Sn	1.0	1.0	1.0	1.0	1.0
Sb					

Sample Number	OC-266	OC-267	OC-269	OC-270	OC-271
Easting	664160	664125	663983	664018	664065
Northing	5373434	5373413	5373934	5373912	5373836
Geochemical Lithology	Dacite	Dacite	Dacite	Dacite	Dacite
SiO_2	72.46	68.35	76.07	76.00	79.16
TiO_2	0.30	0.28	0.16	0.18	0.25
Al_2O_3	15.64	16.12	15.02	15.36	14.17
Fe_2O_3	2.11	3.06	1.85	1.76	1.36
MnO	0.03	0.05	0.01	0.01	0.02
MgO	0.78	1.45	0.26	0.24	0.55
CaO	2.49	4.84	0.97	0.32	0.37
K_2O	1.81	0.76	3.37	2.34	3.46
Na_2O	4.31	4.97	2.25	3.75	0.61
P_2O_5	0.07	0.13	0.04	0.04	0.05
LOI	2.64	2.48	2.27	1.54	2.26
Sum	99.51	99.96	99.89	99.81	99.21
Mg#	0.45	0.51	0.23	0.23	0.47
Ti	1786	1660	982	1096	1472
P	314	582	179	177	223
Cr	41	62	10	10	10
Co	9	8	2	2	2
Ni	23	42	5	11	5
Rb	41	17	50	40	58
Sr	242	467	114	164	124
Cs	2	1	3	3	4
Ba	236	131	455	380	464
Sc					
V	41	49	8	10	9
Ta	0.51	0.51	0.51	0.51	0.51
Nb	2.1	1.0	1.0	2.0	1.0
Zr	92	63	107	119	113
Hf	3.1	2.1	3.1	4.1	3.1
Th	1.0	1.0	1.0	1.0	1.0
U	0.5	0.5	0.5	0.5	0.5
Y	3.5	3.3	2.7	2.8	2.6
La	6.8	6.2	9.6	9.9	8.5
Ce	13.4	12.3	19.0	19.4	16.8
Pr	1.54	1.33	2.05	2.13	1.84
Nd	5.86	5.54	7.47	7.41	6.45
Sm	1.03	1.03	1.13	1.02	0.92
Eu	0.31	0.41	0.31	0.30	0.20
Gd	1.03	0.92	0.92	1.02	0.82
Tb	0.10	0.10	0.10	0.10	0.10
Dy	0.62	0.51	0.41	0.51	0.41
Ho	0.10	0.10	0.10	0.10	0.10
Er	0.31	0.31	0.20	0.20	0.20
Tm	0.10	0.10	0.10	0.10	0.10
Yb	0.31	0.21	0.20	0.30	0.20
Lu	0.10	0.10	0.10	0.10	0.10
Cu	7	14	7	7	5
Zn	35	47	37	52	69
Mo	2	3	2	2	2
Ag	1	1	1	1	1
Tl	0.51	0.51	0.51	0.51	0.51
Pb	7.2	11.3	13.3	12.2	15.3
Sn	1.0	1.0	1.0	1.0	1.0
Sb					

Sample Number	OC-272	OC-273	OC-274	OC-275	OC-276
Easting	664084	664213	664231	664224	664165
Northing	5373820	5373708	5373716	5373668	5373271
Geochemical Lithology	Dacite	Dacite	Dacite	Dacite	Dacite
SiO_2	77.84	69.30	68.41	79.19	78.02
TiO_2	0.24	0.36	0.35	0.29	0.25
Al_2O_3	14.92	15.88	16.99	14.40	14.94
Fe_2O_3	1.21	3.27	2.78	1.32	1.06
MnO	0.01	0.04	0.04	0.01	0.02
MgO	0.30	1.21	0.84	0.45	0.22
CaO	0.79	4.68	4.32	0.39	0.31
K_2O	3.32	1.24	1.78	3.45	3.35
Na_2O	1.33	3.95	4.41	0.45	1.80
P_2O_5	0.04	0.07	0.08	0.05	0.04
LOI	2.29	3.37	3.82	2.19	1.96
Sum	99.95	99.77	100.05	100.10	99.61
Mg#	0.35	0.45	0.40	0.43	0.31
Ti	1411	2172	2119	1716	1468
P	179	316	363	223	178
Cr	10	62	31	10	10
Co	1	7	8	1	1
Ni	5	25	36	5	5
Rb	64	26	38	58	58
Sr	221	410	355	117	127
Cs	3	1	1	3	4
Ba	509	176	262	512	408
Sc					
V	9	45	52	9	10
Ta	0.51	0.52	0.52	0.51	0.51
Nb	2.0	1.0	2.1	2.0	1.0
Zr	120	83	93	111	117
Hf	4.1	2.1	3.1	3.1	4.1
Th	1.0	1.0	1.0	1.0	1.0
U	0.5	0.5	0.5	0.5	0.5
Y	2.9	4.0	4.1	2.9	2.6
La	10.0	7.8	6.7	8.6	8.9
Ce	19.9	15.0	13.5	17.8	18.0
Pr	2.15	1.66	1.56	1.94	1.94
Nd	7.57	6.52	6.03	6.75	7.14
Sm	1.13	1.24	1.04	1.02	1.02
Eu	0.31	0.41	0.42	0.31	0.31
Gd	1.02	1.14	1.14	0.92	0.92
Tb	0.10	0.10	0.10	0.10	0.10
Dy	0.41	0.62	0.62	0.41	0.41
Ho	0.10	0.10	0.10	0.10	0.10
Er	0.20	0.31	0.31	0.20	0.20
Tm	0.10	0.10	0.10	0.10	0.10
Yb	0.20	0.31	0.31	0.20	0.20
Lu	0.10	0.10	0.10	0.10	0.10
Cu	5	22	33	9	7
Zn	23	56	48	59	27
Mo	2	2	2	2	2
Ag	1	1	1	1	1
Tl	0.51	0.52	0.52	0.51	0.51
Pb	10.2	7.2	10.4	12.3	12.2
Sn	1.0	1.0	1.0	1.0	1.0
Sb					

Sample Number	OC-277	OC-281	OC-320	OC-321	OC-322a
Easting	663991	663555	663533	663535	663528
Northing	5374007	5372794	5373005	5373011	5373009
Geochemical Lithology	Dacite	Andesite	Andesite	Andesite	Andesite
SiO_2	75.70	71.61	61.72	76.38	50.45
TiO_2	0.22	0.66	1.39	0.57	0.61
Al_2O_3	15.01	15.39	24.07	13.01	14.17
Fe_2O_3	1.36	2.12	1.31	4.63	25.66
MnO	0.01	0.02	0.02	0.03	1.64
MgO	0.38	1.07	0.44	1.20	6.60
CaO	0.90	1.44	1.85	0.09	0.47
K_2O	1.77	2.90	4.59	3.76	0.05
Na_2O	4.61	4.65	4.25	0.22	0.26
P_2O_5	0.04	0.14	0.34	0.11	0.08
LOI	1.72	2.05	2.46	3.42	6.97
Sum	99.66	99.49	99.43	98.56	100.10
Mg#	0.38	0.53	0.43	0.36	0.36
Ti	1342	3918	8299	3354	3673
P	178	624	1477	452	328
Cr	10	71	390	41	32
Co	2	10	10	87	25
Ni	5	131	71	126	58
Rb	34	90	117	96	1
Sr	194	159	145	28	8
Cs	2	2	4	2	1
Ba	296	295	353	391	6
Sc			4		1
V	9	106	244	47	88
Ta	0.51	0.61	0.72	0.52	0.54
Nb	2.0	8.2	11.3	7.3	7.5
Zr	112	189	185	195	190
Hf	4.1	6.1	5.1	5.2	5.4
Th	1.0	5.1	1.0	2.1	3.2
U	0.5	1.4	0.5	0.7	1.1
Y	2.7	23.9	48.9	17.8	21.5
La	10.0	7.6	21.2	4.9	4.8
Ce	19.9	16.8	48.7	10.3	11.0
Pr	2.14	2.14	6.05	1.14	1.29
Nd	7.53	8.68	25.33	4.45	5.16
Sm	1.22	2.14	6.05	1.24	1.29
Eu	0.31	0.61	1.33	0.41	0.43
Gd	1.02	2.76	6.87	1.45	1.40
Tb	0.10	0.51	1.23	0.41	0.32
Dy	0.41	3.37	7.79	2.69	2.90
Ho	0.10	0.71	1.64	0.62	0.75
Er	0.20	2.45	4.51	1.97	2.90
Tm	0.10	0.31	0.62	0.31	0.54
Yb	0.20	2.55	3.69	2.18	3.87
Lu	0.10	0.41	0.51	0.41	0.64
Cu	50	15	17	193	669
Zn	40	28	34	450	432
Mo	2	14	2	7	2
Ag	1	1	1	1	1
Tl	0.51	0.51	0.51	0.52	0.54
Pb	13.2	9.2	5.1	5.2	5.4
Sn	1.0	1.0	2.1	3.1	1.1
Sb			0.05		0.05

Sample Number	OC-323	OC-326	OC-327	OC-328	OC-329
Easting	663514	664586	664565	664510	664501
Northing	5373005	5373213	5373250	5373324	5373209
Geochemical Lithology	Andesite	Andesite	Dacite	Andesite	Andesite
SiO_2	59.46	58.94	74.92	60.25	43.83
TiO_2	0.42	0.74	0.20	0.89	1.01
Al_2O_3	18.48	16.45	14.52	19.04	21.22
Fe_2O_3	6.34	8.80	2.05	4.12	13.31
MnO	0.22	0.18	0.01	0.18	0.24
MgO	3.50	2.36	0.53	1.20	4.96
CaO	4.98	8.81	2.63	6.54	12.44
K_2O	2.62	0.54	1.80	3.37	1.21
Na_2O	3.83	3.18	3.32	4.40	1.78
P_2O_5	0.15	0.01	0.01	0.01	0.02
LOI	5.46	2.44	1.37	6.2	3.43
Sum	99.81	99.72	99.78	99.32	99.90
Mg#	0.55	0.37	0.36	0.39	0.45
Ti	2537	4425	1216	5307	6022
P	646	45	44	47	90
Cr	42	51	41	107	217
Co	14	45	2	9	29
Ni	26	54	9	31	135
Rb	64	15	39	65	38
Sr	335	212	317	221	325
Cs	2	1	2	2	2
Ba	475	136	241	482	183
Sc	3				
V	103	18	4	18	18
Ta	0.74	0.51	0.51	0.53	0.52
Nb	8.5	7.2	2.0	7.5	7.2
Zr	83	124	99	125	151
Hf	3.2	4.1	3.0	3.2	4.1
Th	2.1	2.1	1.0	2.1	2.1
U	0.8	0.6	0.5	0.5	0.5
Y	11.1	18.0	3.8	17.9	18.4
La	17.6	13.5	9.4	13.4	15.1
Ce	38.2	29.2	18.3	29.7	35.6
Pr	4.55	3.59	2.03	3.63	4.25
Nd	17.77	13.94	7.00	14.29	16.47
Sm	3.17	3.08	1.22	2.88	3.42
Eu	0.74	0.92	0.30	0.85	0.93
Gd	2.86	3.08	1.01	2.77	3.31
Tb	0.42	0.51	0.10	0.43	0.52
Dy	1.90	3.08	0.61	2.88	3.11
Ho	0.32	0.62	0.10	0.64	0.62
Er	1.06	1.85	0.30	1.71	1.97
Tm	0.21	0.31	0.10	0.21	0.31
Yb	1.06	1.85	0.30	1.71	1.97
Lu	0.21	0.31	0.10	0.21	0.31
Cu	6	287	5	10	110
Zn	94	56	16	223	84
Mo	2	2	2	3	8
Ag	1	1	1	1	1
Tl	0.53	0.51	0.51	0.53	0.52
Pb	5.3	16.4	5.1	5.3	5.2
Sn	2.1	2.1	1.0	2.1	2.1
Sb	0.05				

Sample Number	OC-330	OC-332	OC-333	OC-334	OC-335
Easting	664509	664538	664492	664447	664418
Northing	5373165	5373780	5373842	5373861	5373911
Geochemical Lithology	Gabbro	Dacite	Dacite	Dacite	Dacite
SiO_2	50.59	69.50	71.72	73.30	81.00
TiO_2	1.62	0.34	0.27	0.23	0.26
Al_2O_3	13.39	17.78	14.71	13.84	10.74
Fe_2O_3	17.98	2.87	2.56	2.29	2.15
MnO	0.25	0.01	0.02	0.03	0.02
MgO	5.92	1.13	0.91	0.63	0.79
CaO	8.08	2.38	3.93	4.47	1.17
K_2O	0.36	3.21	2.08	1.67	1.20
Na_2O	1.79	2.68	3.73	3.50	2.61
P_2O_5	0.01	0.09	0.06	0.04	0.06
LOI	2.9	3.08	4.11	4.5	1.93
Sum	100.05	99.38	99.39	99.44	98.89
Mg#	0.42	0.47	0.44	0.38	0.45
Ti	9693				
P	45	341	271	262	224
Cr	10	4	11	3	17
Co	55	7	6	6	9
Ni	43	14	13	9	17
Rb	11	4	4	3	2
Sr	175	40	92	125	19
Cs	1	3	3	1	1
Ba	53	367	227	178	149
Sc		1	1	1	1
V	37	46	32	26	30
Ta	0.51	0.52	0.52	0.52	0.51
Nb	6.2	2.1	2.1	1.0	1.0
Zr	117	115	90	73	95
Hf	4.1	3.1	3.1	2.1	3.1
Th	1.0	1.0	1.0	1.0	1.0
U	0.5	0.5	0.5	0.5	0.5
Y	37.5	5.5	4.8	4.0	2.9
La	9.9	9.6	8.1	6.7	5.6
Ce	22.8	19.3	16.1	13.0	11.8
Pr	3.09	2.17	1.77	1.47	1.33
Nd	14.21	8.98	7.41	5.76	5.30
Sm	4.33	1.55	1.46	1.15	0.92
Eu	1.34	0.52	0.42	0.42	0.31
Gd	4.74	1.44	1.15	0.94	0.82
Tb	0.93	0.21	0.21	0.10	0.10
Dy	6.39	1.14	0.94	0.73	0.51
Ho	1.34	0.21	0.21	0.10	0.10
Er	4.02	0.62	0.52	0.42	0.31
Tm	0.62	0.10	0.10	0.10	
Yb	4.02	0.52	0.52	0.31	0.31
Lu	0.62	0.10	0.10	0.10	
Cu	179	28	32	31	37
Zn	83	94	100	45	35
Mo	6	2	2	2	2
Ag	1	1	1	1	1
Tl	0.51	0.52	0.52	0.52	0.51
Pb	5.1	33.0	39.6	5.2	5.1
Sn	1.0	1.0	1.0	1.0	1.0
Sb			0.05		0.09

Sample Number	OC-336	OC-337	OC-338	OC-339	AS-06-001
Easting	664392	664322	664501	664577	664143
Northing	5373927	5374029	5374018	5374009	5373430
Geochemical Lithology	Dacite	Dacite	Dacite	Dacite	Dacite
SiO_2	71.57	71.99	80.35	74.17	71.45
TiO_2	0.30	0.30	0.22	0.26	0.27
Al_2O_3	16.21	15.58	12.14	13.70	14.30
Fe_2O_3	2.53	2.80	0.85	1.98	3.49
MnO	0.02	0.02	0.04	0.03	0.04
MgO	1.31	1.12	0.26	0.59	1.16
CaO	2.20	3.16	1.65	3.76	4.23
K_2O	1.61	1.50	1.99	1.56	0.86
Na_2O	4.20	3.47	2.45	3.82	4.11
P_2O_5	0.05	0.06	0.05	0.13	0.09
LOI	2.91	3.83	2.35	4.01	2.94
Sum	99.37	98.27	98.41	99.38	98.89
Mg#	0.53	0.47	0.40	0.39	0.42
Ti					
P	299	291	236	542	
Cr	10	15	1	11	72
Co	8	8	1	6	7
Ni	26	24	6	10	36
Rb	3	3	3	4	16
Sr	25	35	42	102	452
Cs	2	1	2	2	1
Ba	337	280	332	181	90
Sc	2	2	1	1	
V	39	35	13	31	36
Ta	0.52	0.52	0.51	0.52	0.21
Nb	2.1	2.1	2.0	2.1	1.3
Zr	102	97	68	83	79
Hf	3.1	3.1	2.0	2.1	1.3
Th	1.0	1.0	1.0	1.0	0.5
U	0.5	0.5	0.5	0.5	0.1
Y	4.0	4.3	4.0	4.9	2.9
La	7.7	7.4	5.9	7.6	6.8
Ce	15.7	14.4	11.4	15.0	14.3
Pr	1.75	1.56	1.23	1.77	1.46
Nd	7.21	6.45	5.02	6.98	6.18
Sm	1.34	1.14	0.92	1.35	1.11
Eu	0.52	0.42	0.41	0.52	0.45
Gd	1.13	1.04	0.92	1.25	0.98
Tb	0.21	0.10	0.10	0.21	0.10
Dy	0.72	0.83	0.72	0.94	0.60
Ho	0.10	0.10	0.10	0.21	0.09
Er	0.41	0.42	0.41	0.52	0.30
Tm	0.10	0.10	0.10	0.10	0.03
Yb	0.41	0.42	0.31	0.52	0.28
Lu	0.10	0.10	0.10	0.10	0.03
Cu	19	28	9	22	10
Zn	47	36	17	41	37
Mo	2	2	2	2	2
Ag	1	1	1	1	1
Tl	0.52	0.52	0.51	0.52	0.52
Pb	5.2	5.2	5.1	5.2	5.2
Sn	1.0	1.0	1.0	1.0	1.0
Sb		0.27			

Sample Number	AS-06-002	AS-06-003	AS-06-004	AS-06-005	AS-06-006
Easting	663831	662465	662467	662338	662158
Northing	5373696	5373077	5373073	5373059	5372988
Geochemical Lithology	Dacite	Andesite	Rhyolite	Rhyolite	Rhyolite
SiO_2	76.46	64.05	81.26	78.30	74.28
TiO_2	0.18	0.88	0.19	0.16	0.19
Al_2O_3	14.56	17.98	10.81	11.05	13.88
Fe_2O_3	2.25	5.57	2.44	4.82	4.75
MnO	0.02	0.06	0.02	0.16	0.04
MgO	0.39	2.63	0.79	1.01	2.37
CaO	0.21	3.17	0.37	0.97	0.21
K_2O	3.20	3.73	3.87	3.38	3.51
Na_2O	2.69	1.74	0.22	0.14	0.76
P_2O_5	0.04	0.18	0.03	0.03	0.02
LOI	1.92	5.36	1.96	2.96	2.85
Sum	98.95	98.15	98.65	98.23	98.44
Mg#	0.28	0.51	0.41	0.32	0.52
Ti					
P					
Cr	10	275	20	21	10
Co	1	16	2	2	2
Ni	6	98	15	6	14
Rb	45	66	68	62	80
Sr	81	80	15	50	23
Cs	3	2	2	2	2
Ba	611	242	549	230	317
Sc					
V	5	136	5	5	5
Ta	0.10	0.53	0.92	0.82	1.24
Nb	1.4	6.5	12.0	12.0	14.8
Zr	124	155	322	312	452
Hf	2.4	3.4	8.4	8.1	11.8
Th	0.7	1.4	3.6	3.6	5.0
U	0.2	0.4	1.0	1.0	1.4
Y	1.9	16.7	35.6	43.5	20.9
La	9.3	12.6	17.1	25.5	35.5
Ce	19.6	28.6	40.1	56.4	86.8
Pr	2.03	3.23	4.69	6.83	10.56
Nd	7.65	14.81	21.32	30.73	45.41
Sm	1.00	2.91	4.94	7.33	10.14
Eu	0.34	0.89	0.82	1.22	1.75
Gd	1.06	3.59	5.81	7.31	10.40
Tb	0.08	0.52	0.97	1.22	1.39
Dy	0.45	3.09	6.61	8.08	7.49
Ho	0.07	0.65	1.36	1.61	1.19
Er	0.18	2.05	4.53	5.01	3.01
Tm	0.01	0.25	0.61	0.70	0.40
Yb	0.27	2.12	4.51	4.91	3.54
Lu	0.02	0.26	0.60	0.70	0.50
Cu	5	99	5	8	8
Zn	56	81	84	109	132
Mo	2	3	2	2	2
Ag	1	1	1	1	1
Tl	0.51	0.53	0.51	0.52	0.51
Pb	5.1	5.3	5.1	5.2	5.1
Sn	1.0	1.1	2.0	3.1	4.1
Sb					

Sample Number	AS-06-007	AS-06-008	AS-06-009	AS-06-010	AS-06-011
Easting	661905	662020	664990	665063	662672
Northing	5372738	5372900	5373776	5374063	5373062
Geochemical Lithology	Rhyolite	Andesite	Andesite	Dacite	Rhyolite
SiO_2	78.15	78.57	65.22	69.67	82.46
TiO_2	0.19	0.16	0.66	0.30	0.17
Al_2O_3	11.38	10.61	15.92	17.17	9.76
Fe_2O_3	3.25	3.07	5.97	4.77	2.08
MnO	0.04	0.01	0.12	0.04	0.03
MgO	0.61	0.37	1.63	1.27	0.56
CaO	0.71	0.02	5.63	0.96	1.48
K_2O	3.43	6.97	0.94	1.52	1.83
Na_2O	2.21	0.18	3.79	4.21	1.61
P_2O_5	0.03	0.04	0.10	0.08	0.02
LOI	1.83	1.00	1.69	2.38	2.23
Sum	98.76	98.16	98.58	98.46	98.96
Mg#	0.29	0.21	0.38	0.37	0.37
Ti					
P					
Cr	41	30	234	41	31
Co	2	5	16	10	25
Ni	5	12	57	25	71
Rb	55	71	25	27	39
Sr	35	28	399	280	55
Cs	1	1	3	2	1
Ba	364	842	131	261	336
Sc					
V	5	16	124	32	5
Ta	0.92	0.71	0.41	0.10	0.82
Nb	12.0	8.4	5.4	1.8	11.8
Zr	349	301	129	83	305
Hf	8.8	7.5	2.8	1.6	8.6
Th	3.9	3.7	1.2	0.5	3.9
U	1.0	1.0	0.3	0.1	1.1
Y	43.7	27.8	18.7	2.8	39.3
La	26.9	20.0	11.6	6.4	20.4
Ce	61.9	45.6	27.1	13.2	46.5
Pr	7.36	5.32	3.12	1.48	5.86
Nd	33.72	23.64	14.45	5.84	24.35
Sm	7.38	5.28	3.03	1.01	5.73
Eu	1.37	0.89	0.89	0.36	1.19
Gd	8.19	5.19	3.50	0.95	6.20
Tb	1.24	0.77	0.50	0.09	1.10
Dy	8.12	4.81	3.54	0.72	7.42
Ho	1.59	1.05	0.72	0.11	1.49
Er	5.11	3.52	2.10	0.36	4.80
Tm	0.75	0.50	0.30	0.04	0.69
Yb	4.97	3.67	2.20	0.32	4.71
Lu	0.69	0.55	0.31	0.03	0.61
Cu	6	31	16	22	79
Zn	77	30	59	109	31
Mo	2	4	3	2	2
Ag	1	1	1	1	1
Tl	0.51	0.51	0.51	0.51	0.51
Pb	5.1	13.1	6.1	5.1	5.1
Sn	3.1	3.0	2.0	1.0	2.0
Sb					

Sample Number	AS-06-012	AS-06-013	AS-06-014	AS-06-015	AS-06-016
Easting	662800	663150	663100	662875	663572
Northing	5372990	5372615	5372562	5372830	5372720
Geochemical Lithology	Andesite	Chert Clast	Chert Clast	Rhyolite	Sulfides
SiO_2	58.70	97.33	94.58	54.61	27.43
TiO_2	0.72	0.01	0.02	0.19	0.13
Al_2O_3	15.52	0.62	1.96	12.00	3.73
Fe_2O_3	8.09	1.43	2.17	20.41	67.08
MnO	0.12	0.01	0.01	6.10	0.07
MgO	4.28	0.32	0.37	3.25	1.13
CaO	7.98	0.13	0.36	3.32	0.03
K_2O	1.26	0.04	0.32	0.02	0.25
Na_2O	3.17	0.09	0.20	0.07	0.11
P_2O_5	0.17	0.02	0.02	0.03	0.04
LOI	8.49	0.57	0.37	2.73	22.5
Sum	98.54	98.97	98.30	98.60	98.31
Mg#	0.54	0.33	0.27	0.26	0.04
Ti					
P					
Cr	317	91	50	41	13
Co	30	2	1	1	101
Ni	184	7	6	5	19
Rb	26	3	10	5	9
Sr	158	4	19	24	6
Cs	1	0	0	0	2
Ba	172	8	46	10	32
Sc					
V	128	5	5	5	6
Ta	0.44		0.10	1.34	0.13
Nb	6.6	0.7	1.6	16.2	1.8
Zr	138	20	37	367	70
Hf	3.8	0.5	0.9	11.0	2.1
Th	1.4	0.2	0.4	5.4	1.4
U	0.4	0.1	0.1	1.2	0.4
Y	16.6	2.0	3.0	42.8	11.0
La	12.3	2.0	1.8	21.4	5.7
Ce	27.5	3.7	3.9	46.4	10.8
Pr	3.45	0.47	0.42	5.59	1.30
Nd	13.68	1.71	1.61	21.80	5.19
Sm	2.75	0.39	0.39	5.04	1.27
Eu	0.92	0.09	0.15	0.95	0.21
Gd	3.29	0.44	0.46	5.99	1.34
Tb	0.49	0.06	0.05	1.15	0.27
Dy	3.03	0.43	0.50	8.01	1.80
Ho	0.63	0.08	0.11	1.62	0.39
Er	1.97	0.17	0.38	5.28	1.23
Tm	0.28	0.03	0.05	0.79	0.18
Yb	1.86	0.17	0.39	5.59	1.22
Lu	0.25	0.02	0.06	0.81	0.17
Cu	12	5	5	24	2581
Zn	69	15	16	137	25
Mo	2	2	2	2	10
Ag	1	1	1	1	4
Tl	0.55	0.50	0.50	0.51	0.65
Pb	5.5	5.0	5.0	5.1	14.3
Sn	1.1	1.0	1.0	2.1	1.3
Sb					

Sample Number	AS-06-018	AS-05-001a	AS-05-001c	AS-05-004a	AS-05-004b
Easting	665008	663184	663184	663085	663085
Northing	5374030	5372274	5372274	5372258	5372258
Geochemical Lithology	Dacite	Pink Breccia	Pink Breccia	Pink Breccia	Pink Breccia
SiO_2	68.78	56.96	68.77	51.16	65.41
TiO_2	0.31	0.42	0.30	1.32	0.76
Al_2O_3	17.08	19.94	16.14	14.14	16.25
Fe_2O_3	4.03	6.55	3.18	13.53	4.05
MnO	0.03	0.04	0.02	0.14	0.02
MgO	1.10	3.49	1.61	7.27	1.62
CaO	2.83	2.84	1.88	7.59	3.94
K_2O	2.27	3.78	2.74	2.42	1.39
Na_2O	3.50	5.78	5.23	2.30	6.30
P_2O_5	0.07	0.21	0.12	0.11	0.26
LOI	2.3	2.81	1.66	2.04	1.33
Sum	98.17	101.32	101.53	101.02	101.10
Mg#	0.37	0.54	0.53	0.54	0.47
Ti					
P					
Cr	31	21	39	91	88
Co	6				
Ni	19	14	18	79	85
Rb	53	131	95	113	59
Sr	356	364	276	239	220
Cs	3	3	2	8	3
Ba	360				
Sc		11	6	44	12
V	35	105	68	301	81
Ta	0.10	0.21	0.36	0.28	0.59
Nb	2.0	3.5	4.1	5.0	9.0
Zr	102	86	98	95	171
Hf	2.8	2.3	2.5	2.6	4.2
Th	0.6	2.5	2.9	0.5	1.8
U	0.2	0.7	0.7	0.2	0.7
Y	3.8	11.3	6.8	27.1	21.0
La	8.4	15.2	15.4	5.2	18.4
Ce	17.0	32.9	30.0	14.1	37.0
Pr	1.98	4.20	3.44	2.13	4.36
Nd	7.58	17.27	12.99	10.57	17.29
Sm	1.27	3.31	2.27	3.18	3.67
Eu	0.42	0.95	0.62	1.06	0.96
Gd	1.29	2.56	1.71	4.19	3.81
Tb	0.16	0.37	0.22	0.72	0.59
Dy	0.81	2.15	1.24	4.88	3.76
Ho	0.14	0.43	0.23	1.05	0.77
Er	0.46				
Tm	0.05	0.18	0.10	0.45	0.33
Yb	0.42	1.19	0.69	3.04	2.21
Lu	0.05	0.17	0.10	0.46	0.33
Cu	49				
Zn	33				
Mo	2				
Ag	1				
Tl	0.51				
Pb	5.1	7.3	2.7	6.8	4.7
Sn	1.0				
Sb					

Sample Number	AS-05-012	AS-05-016	AS-05-018	AS-05-020b	AS-05-021
Easting	662415	662310	662622	662628	662595
Northing	5372411	5372594	5372353	5372359	5372387
Geochemical Lithology	Rhyolite	Feldspar Porphyry	Rhyolite	Dacite	Dacite
SiO$_2$	88.06	61.01	61.04	79.51	77.44
TiO$_2$	0.15	0.62	0.04	0.18	0.22
Al$_2$O$_3$	8.36	17.21	1.15	12.30	14.77
Fe$_2$O$_3$	0.62	6.99	30.13	2.40	1.45
MnO	0.00	0.10	1.05	0.04	0.02
MgO	0.18	3.63	3.30	1.02	0.66
CaO	0.04	4.54	3.18	0.53	0.53
K$_2$O	2.38	0.78	0.07	3.71	4.63
Na$_2$O	0.20	4.99	0.04	0.25	0.21
P$_2$O$_5$	0.01	0.13	0.01	0.06	0.06
LOI	1.17	3.33	3.58	1.92	2.21
Sum	101.09	101.21	100.88	101.19	100.11
Mg#	0.39	0.53	0.19	0.48	0.50
Ti					
P					
Cr	8	145	24	16	28
Co					
Ni	26	81	39	13	8
Rb	43	18	2	73	91
Sr	47	298	89	42	42
Cs	1	1	1	2	3
Ba					
Sc	3	22	3	3	3
V	4	123	10	16	18
Ta	0.67	0.36			
Nb	9.4	5.3	1.0	1.2	1.5
Zr	264	142	20	95	115
Hf	6.8	3.4	0.4	2.3	3.0
Th	3.1	1.4	0.2	0.6	0.7
U	1.0	0.3	0.1	0.1	0.2
Y	38.5	16.8	7.4	2.8	2.8
La	3.1	13.8	3.6	7.7	9.1
Ce	15.2	29.6	6.3	16.4	19.4
Pr	1.13	3.50	0.78	1.84	2.19
Nd	4.82	13.80	3.32	6.57	7.94
Sm	1.94	2.94	0.77	1.09	1.32
Eu	0.51	0.84	0.30	0.30	0.33
Gd	3.77	3.01	1.05	0.75	0.90
Tb	0.86	0.48	0.17	0.09	0.11
Dy	6.35	3.00	1.06	0.50	0.57
Ho	1.42	0.62	0.24	0.09	0.10
Er					
Tm	0.62	0.27	0.11	0.04	0.04
Yb	4.01	1.87	0.81	0.28	0.26
Lu	0.59	0.29	0.13	0.04	0.04
Cu					
Zn					
Mo					
Ag					
Tl					
Pb	1.8	4.3	1.1	0.7	0.9
Sn					
Sb					

Sample Number	AS-05-024b	AS-05-028	AS-05-034a	AS-05-034b
Easting	662520	662649	662660	662672
Northing	5372473	5372368	5372520	5372520
Geochemical Lithology	BIF	Rhyolite	Andesite	Rhyolite
SiO_2	86.24	50.07	66.52	60.31
TiO_2	0.03	0.11	0.67	0.23
Al_2O_3	0.25	6.03	17.80	10.16
Fe_2O_3	11.31	35.86	3.10	21.28
MnO	0.45	1.51	0.07	1.99
MgO	1.57	3.96	1.54	3.10
CaO	0.09	2.12	3.46	2.33
K_2O	0.01	0.24	3.85	0.51
Na_2O	0.04	0.08	2.94	0.04
P_2O_5	0.00	0.02	0.04	0.04
LOI	0.27	2.25	3.95	3.22
Sum	99.71	100.03	101.08	100.58
Mg#	0.23	0.20	0.52	0.24
Ti				
P				
Cr	19	28	95	20
Co				
Ni	27	30	58	29
Rb		19	80	28
Sr		6	167	99
Cs		3	3	7
Ba				
Sc	1	5	20	7
V	9	13	116	12
Ta		0.33	0.39	0.64
Nb		4.3	5.7	8.2
Zr	4	133	155	239
Hf	0.1	3.3	3.7	6.2
Th		1.7	1.5	3.6
U		0.5	0.4	1.0
Y	1.3	22.1	14.1	37.9
La	2.4	5.0	7.6	23.0
Ce	5.0	12.1	17.9	51.1
Pr	0.55	1.42	2.29	6.23
Nd	2.09	5.89	9.30	25.49
Sm	0.35	1.46	2.16	5.72
Eu	0.17	0.36	0.82	1.26
Gd	0.32	2.01	2.26	6.09
Tb	0.04	0.41	0.38	0.99
Dy	0.24	3.00	2.44	6.41
Ho	0.05	0.72	0.52	1.37
Er				0.00
Tm	0.03	0.36	0.23	0.63
Yb	0.19	2.52	1.56	4.35
Lu	0.03	0.40	0.24	0.68
Cu				
Zn				
Mo				
Ag				
Tl				
Pb	0.7	1.9	4.2	4.2
Sn				
Sb				

Sample Number	AS-05-035	AS-05-036	AS-05-041	AS-05-048	AS-05-049
Easting	662677	663025	662921	662743	662763
Northing	5372565	5372915	5372870	5372839	5372795
Geochemical Lithology	Dacite	Andesite	Andesite	Rhyolite	Rhyolite
SiO_2	75.38	70.19	66.47	64.02	79.33
TiO_2	0.23	0.70	0.69	0.55	0.17
Al_2O_3	15.51	15.59	18.44	13.43	10.54
Fe_2O_3	1.81	4.91	3.31	8.10	3.95
MnO	0.05	0.08	0.04	0.06	0.14
MgO	0.93	2.58	1.80	4.08	0.63
CaO	1.51	1.59	3.70	4.45	0.07
K_2O	4.34	3.60	1.93	2.61	4.67
Na_2O	0.17	0.58	3.48	2.52	0.47
P_2O_5	0.06	0.18	0.14	0.19	0.02
LOI	2.15	2.89	2.59	3.78	1.42
Sum	101.16	100.70	101.54	100.89	100.93
Mg#	0.53	0.54	0.54	0.53	0.26
Ti					
P					
Cr	14	419	92	88	10
Co					
Ni	7	146	23	104	16
Rb	52	48	56	110	65
Sr	66	86	180	153	28
Cs	2	2	2	7	3
Ba					
Sc	3	12	20	15	3
V	19	150	121	91	3
Ta		0.37	0.41	0.44	0.78
Nb	1.5	6.0	5.8	6.8	10.9
Zr	122	124	153	127	321
Hf	3.2	3.2	3.7	3.1	8.2
Th	0.6	1.2	1.6	1.6	3.8
U	0.1	0.4	0.4	0.7	1.0
Y	2.9	13.7	14.5	18.9	33.3
La	8.0	6.3	12.8	22.1	19.0
Ce	18.1	16.1	27.9	37.6	42.8
Pr	2.08	2.15	3.28	4.00	5.35
Nd	7.57	9.42	13.03	14.58	22.28
Sm	1.29	2.36	2.67	2.84	5.15
Eu	0.35	0.58	0.83	0.78	1.00
Gd	0.87	2.51	2.71	2.98	5.35
Tb	0.11	0.42	0.42	0.49	0.88
Dy	0.57	2.61	2.61	3.25	5.80
Ho	0.10	0.52	0.54	0.70	1.27
Er					
Tm	0.04	0.21	0.24	0.32	0.59
Yb	0.26	1.40	1.63	2.15	4.02
Lu	0.04	0.21	0.25	0.33	0.62
Cu					
Zn					
Mo					
Ag					
Tl					
Pb	1.5	1.4	3.4	3.3	3.2
Sn					
Sb					

Sample Number	AS-05-050	AS-05-053a	AS-05-053b	AS-05-056	AS-05-086
Easting	662782	662993	662993	662907	663393
Northing	5372806	5372990	5372990	5372918	5372880
Geochemical Lithology	BIF	Andesite	Andesite	Andesite	Andesite
SiO_2	91.18	89.30	89.93	65.55	70.55
TiO_2	0.00	0.10	0.14	0.65	0.54
Al_2O_3	0.09	6.52	1.28	17.66	12.64
Fe_2O_3	7.07	1.55	8.03	3.81	7.24
MnO	0.52	0.02	0.02	0.10	0.20
MgO	0.98	0.32	0.17	2.01	2.07
CaO	0.10	0.02	0.04	4.99	3.39
K_2O	0.02	2.08	0.29	1.29	1.20
Na_2O	0.04	0.09	0.06	3.79	2.08
P_2O_5			0.02	0.15	0.10
LOI	0.43	1.44	3.43	2.81	3.34
Sum	101.47	101.33	100.79	101.10	100.42
Mg#	0.23	0.31	0.05	0.54	0.39
Ti					
P					
Cr	14	19	20	24	91
Co					
Ni	19	3	2	17	43
Rb	1	46	6	38	39
Sr	2	13	13	5	184
Cs		2		2	2
Ba					
Sc	1	5	2	19	15
V	4	34	25	115	96
Ta		0.29		0.81	0.35
Nb		2.9	2.3	5.7	5.1
Zr		91	28	147	116
Hf		2.7	0.8	3.6	2.8
Th		1.8	0.6	1.5	1.4
U		0.7	0.2	0.4	0.5
Y	2.7	10.2	4.8	15.4	17.0
La	0.3	1.3	1.7	12.1	11.4
Ce	0.6	3.0	3.9	26.5	26.2
Pr	0.08	0.39	0.49	3.24	3.19
Nd	0.39	1.65	2.01	13.03	12.47
Sm	0.11	0.80	0.52	2.92	2.67
Eu	0.08	0.30	0.13	1.01	0.83
Gd	0.21	1.29	0.55	2.94	2.73
Tb	0.04	0.27	0.11	0.46	0.45
Dy	0.27	1.81	0.77	2.78	2.87
Ho	0.06	0.40	0.18	0.57	0.61
Er					
Tm	0.03	0.19	0.08	0.24	0.29
Yb	0.17	1.35	0.54	1.58	1.94
Lu	0.03	0.23	0.07	0.24	0.29
Cu					
Zn					
Mo					
Ag					
Tl					
Pb	1.0	9.5	11.7	4.8	4.2
Sn					
Sb					

APPENDIX C

Sm-Nd Isotope Analyses

Sample Name	AS-05-081	AS-05-036	OC-159	AS-05-059	AS-05-034b
Geochemical Lithology	Rhyolite	Andesite	Rhyolite	Rhyolite	Debris Flow
Sample Wt. (g)	0.16		0.22	0.16	0.19
Spike Wt. (g)	0.10		0.10	0.10	0.10
$^{146/144}$Nd	0.72		0.72	0.72	0.72
$^{148/144}$Nd	0.38		0.56	0.45	0.38
$^{143/144}$Nd	0.51		0.51	0.51	0.51
$^{143/144}$Nd 2-Sigma	0.00		0.00	0.00	0.00
$^{147/149}$Sm	0.55		0.31	0.39	0.52
$^{152/149}$Sm	0.98		0.55	0.69	0.92
AGE	2700	2700	2700	2700	2700
Nd Alpha Factor	0.00	0.00	0.00	0.00	0.00
Corrected $^{146/144}$Nd	0.72		0.72	0.72	0.72
Corrected $^{148/144}$Nd	0.38		0.57	0.45	0.38
Corrected $^{143/144}$Nd	0.51		0.51	0.51	0.51
Nd (ppm)	27.06	11.88	8.96	18.78	25.26
Error Magnification Factor	2.68		1.74	2.14	2.78
^{143}Nd/^{144}Nd (est)	0.51	0.51	0.51	0.51	0.51
Sm Alpha factor	0.00		0.00	0.00	0.00
Corrected 147/149	0.55		0.31	0.39	0.52
Corrected 152/149	0.98		0.55	0.70	0.93
Total Sm	7.40	2.62	2.14	4.14	5.77
Error Magnification Factor	2.04		1.41	1.57	1.92
^{147}Sm/^{144}Nd	0.17	0.13	0.14	0.13	0.14
^{143}Nd/^{144}Nd init	0.51	0.51	0.51	0.51	0.51
Eps Nd (CHUR)T	-6.59	0.93	0.34	1.01	1.38
Tdm (0.214, 0.513115)	4251	2925	3028	2919	2895

Sample Name	AS-05-010b	G05-19	AS-05-042	AS-05-032
Geochemical Lithology	Rhyolite	Rhyolite	Rhyolite	Debris Flow
Sample Wt. (g)	0.15	0.15	0.26	0.21
Spike Wt. (g)	0.10	0.15	0.10	0.10
$^{146/144}$Nd	0.72	0.72	0.72	0.72
$^{148/144}$Nd	0.42	0.47	0.39	0.41
$^{143/144}$Nd	0.51	0.51	0.51	0.51
$^{143/144}$Nd 2-Sigma	0.00	0.00	0.00	0.00
$^{147/149}$Sm	0.45	0.39	0.49	0.44
$^{152/149}$Sm	0.79	0.69	0.87	0.78
AGE	2700	2700	2700	2700
Nd Alpha Factor	0.00	0.00	0.00	0.00
Corrected $^{146/144}$Nd	0.72	0.72	0.72	0.72
Corrected $^{148/144}$Nd	0.42	0.47	0.39	0.41
Corrected $^{143/144}$Nd	0.51	0.51	0.51	0.51
Nd (ppm)	23.97	27.39	16.91	18.78
Error Magnification Factor	2.37	2.05	2.62	2.46
^{143}Nd/^{144}Nd (est)	0.51	0.51	0.51	0.51
Sm Alpha factor	0.00	0.00	0.00	0.00
Corrected 147/149	0.45	0.39	0.49	0.44
Corrected 152/149	0.80	0.69	0.87	0.78
Total Sm	5.47	6.45	3.81	3.90
Error Magnification Factor	1.71	1.57	1.83	1.69
^{147}Sm/^{144}Nd	0.14	0.14	0.14	0.13
^{143}Nd/^{144}Nd init	0.51	0.51	0.51	0.51
Eps Nd (CHUR)T	1.52	1.65	1.78	2.62
Tdm (0.214, 0.513115)	2881	2878	2851	2761

APPENDIX D

Oxygen Isotope Analyses

Sample	Yield	δ¹⁸O (‰VSMOW)	Lithology
AS-06-009	13.5	9.2	Andesite
AS-05-064	13.9	9.6	Andesite
AS-05-066	13.9	9.7	Andesite
AS-05-056	13.7	10.2	Andesite
AS-05-086	13.8	10.4	Andesite
LR-05-006	14.0	10.6	Andesite
AS-05-041	14.5	11.5	Andesite
AS-05-053a	15.5	12.7	Andesite
AS-05-024b	14.7	12.2	BIF
G05-9	14.9	13.2	BIF
AS-06-018	14.4	10.8	Dacite
OC-327	14.6	11.0	Dacite
AS-06-010	14.4	11.4	Dacite
AS-06-002	14.7	11.4	Dacite
OC-339	14.5	11.9	Dacite
AS-05-021	14.2	11.9	Dacite
AS-05-004a	13.2	7.0	Pink Breccia
AS-05-001a	13.7	8.4	Pink Breccia
G05-15	14.9	11.1	Rhyolite
AS-06-005	14.6	11.2	Rhyolite
G05-19	14.8	11.2	Rhyolite
AS-05-049	14.7	11.3	Rhyolite
AS-06-007	14.5	11.6	Rhyolite
AS-05-062	15.1	11.6	Rhyolite
G05-13	15.2	11.9	Rhyolite
OC-159	14.6	12.0	Rhyolite
AS-05-012	15.3	12.3	Rhyolite
AS-06-011	14.9	12.4	Rhyolite
G05-18	15.0	12.5	Rhyolite
G05-14	14.9	12.8	Rhyolite
LR-05-002	14.3	13.7	Rhyolite
AS-05-059	13.6	9.5	Debris Flow
AS-05-032	13.2	10.3	Debris Flow
AS-05-034b	12.9	10.3	Debris Flow
AS-05-018	11.8	11.2	Debris Flow
OC-336	14.5	11.4	Debris Flow
OC-332	13.8	11.5	Debris Flow